SISSA

International School for Advanced Studies

PhD course in Statistical Physics

VII cycle

Academic Year 2015/2016

Aspects of localization in disordered many-body quantum systems

Thesis submitted for the degree of

Doctor Philosophiae

Candidate:

Valentina Ros

Supervisors:

Markus Müller and Antonello Scardicchio

Abstract

For a quantum system to be permanently out-of-equilibrium, some non-trivial mechanism must be at play, to counteract the general tendency of entropy increase and flow toward equilibration. Among the possible ways to protect a system against local thermalization, the phenomenon of localization induced by quenched disorder appears to be one of the most promising. Although the problem of localization was introduced almost sixty years ago, its many-body version is still partly unresolved, despite the recent theoretical effort to tackle it. In this thesis we address a few aspects of the localized phase, mainly focusing on the interacting case. A large part of the thesis is devoted to investigating the underlying "integrable" structure of many-body localized systems, i.e., the existence of non-trivial conservation laws that prevent ergodicity and thermalization. In particular, we show that such conserved operators can be explicitly constructed by dressing perturbatively the non-interacting conserved quantities, in a procedure that converges when scattering processes are weak enough. This is reminiscent of the quasiparticle theory in Fermi liquids, although in the disordered case the construction extends to the full many-body energy spectrum, and it results in operators that are *exactly* conserved. As an example of how to use the constructive recipe for the conserved quantities, we compute the long-time limit of an order parameter for the MBL phase in antiferromagnetic spin systems. Similar analytical tools as the ones exploited for the construction of the conserved operators are then applied to the problem of the stability of single-particle localization with respect to the coupling to a finite bath. In this context, we identify a quantum-Zeno-type effect, whereby the bath unexpectedly enhances the particle's localization. In the final part of the thesis, we discuss several mechanisms by which thermal fluctuations may influence the spatial localization of excitations in interacting many-body states.

Contents

Introduction

Disorder in condensed matter systems is not only abundant and often unavoidable: it is also the primary source of a rich phenomenology, expecially in quantum mechanical problems of randomly scattered and interfering matter waves. In his seminal work of 1958 [10], P. W. Anderson made this intuition concrete by incorporating the randomness as a key ingredient in the theoretical modeling of a quantum system, following the principle that "*a random system is to be treated not as just a dirty regular one, but in a fundamentally different way*" [11]. His prediction of the suppression of transport, then called "localization", laid the foundations for the theory of quantum dynamics in a strongly-disordered environment. Its implications go far beyond the realm of solid state physics, as the occurrence of localization challenges the basic assumptions underlying the theory of equilibration and thermalization in isolated quantum many-body systems.

Motivated by the problem of energy transport in spin systems, Anderson formulated in [10] a tight-binding model of a single particle moving in a stochastic potential landscape, and argued for the suppression of the particle's diffusion at sufficiently strong disorder. In the single-particle setting, the absence of dc transport is encoded in the *exponential decay* in real space of the eigenfunctions. This implies that initial wave packets with compact support remain confined in the vicinity of the initial support at any later time: even when the system's energy is large enough to overcome the surrounding potential barriers, the '*quantum random walker*' is localized by the random environment. The effect of disorder is particularly dramatic in low dimensionality ($d \leq 2$), where for arbitrarily weak strength of the randomness the full set of single-particle eigenstates is exponentially localized and the system is insulating [3]. In $d \geq 3$, as the strength of the disorder is weakened, a transition occurs: localization survives in the eigenstates at the edges of the energy spectrum, while states in the middle of the energy band become delocalized in space. A disorder-dependent critical energy (called "mobility edge") appears within the spectrum, separating the energies corresponding to localized and delocalized states. The *Anderson transition* has dynamical signatures: transport coefficients are exactly zero if all the eigenstates are localized (or, at $T = 0$, if the Fermi level belongs to the localized region of the spectrum), while they are finite (albeit possibly small) at any finite temperature in presence of delocalized portions of the spectrum.

The suppression of transport is a signature of the coherence of the scattering processes of the particle on the surrounding impurities. As such, it is spoiled by fluctuations (e.g. lattice vibrations) that restore transport by allowing transitions between eigenstates localized in different regions of space. The non-trivial statement following from Anderson's

work is that "*the model itself provides no such reservoirs and permits no transport, in spite of its large size and random character*" [10]. Whether the same statement remains true even in the presence of interactions between the constituent degrees of freedom is a question of theoretical interest and practical relevance, which motivated the search for the so called *Many-Body Localized (MBL) phase* [63].

The problem of localization for many-body systems was first addressed systematically in [72, 20], where it was shown that the fermionic single-particle localized phase is perturbatively stable with respect to the addition of weak interactions. The exponential tails emerge in this case in the correlations of the density operators on individual many-body eigenstates, which are exponentially decaying in the distance between the operators themselves, implying the vanishing of the diffusion constant [20]. The perturbative analysis has gained support from subsequent numerical works revealing signatures of a localized phase even in the large interaction regime, provided that the randomness is sufficiently large [132, 21, 134, 108]. Traces of MBL have been found in various one-dimensional fermionic systems on a lattice and in disordered spin chains: they are encoded in both the properties of the many-body eigenstates and energies (such as the area-law scaling of the bipartite entanglement entropy and the Poissonian level statistics) and in dynamical features such as the logarithmic growth in time of the entanglement entropy of a time evolved product state.

These features of MBL systems are in sharp contrast with the conventional scenario for *thermalization* of an isolated, extensive quantum system. The latter assumes that the environment of any small subsystem of the macroscopic body acts as a thermal bath with which the subsystem can exchange particles and energy, and which leads to the eventual thermalization of the subsystems, independently of its initial state. In MBL systems, due to the suppression of transport over large scales, some *local memory* of the initial condition is retained for arbitrarily large times. Thus, they violate the standard assumption behind quantum thermodynamics, namely the ergodicity of the quantum dynamics in the presence of interactions. MBL disordered systems, despite being thermodynamically large, interacting and at finite excitation energy densities, fail to equilibrate through their own dynamics and remain *permanently out-of-equilibrium*. As such, they open interesting possibilities for: (i) the storage of quantum information, that can be locally manipulated and retrieved [152] (ii) the protection of topological order at finite temperature, or the realization of long-range order and finite temperature phase transitions in $d = 1$, that would be forbidden by the equilibrium statistical mechanics [136, 81, 35].

The authors of [72, 20] predicted an *extensive* mobility edge separating the lower-energy localized many-body eigenstates from the extended, higher-energy ones. The extensivity of the mobility edge entails that the dynamical transition occurs at a finite temperature $T_c > 0$ (related to the critical energy by the standard thermodynamical relation), below which the scattering processes are unable to restore the diffusive transport of the densities associated to the global conserved quantities (energy, spin, particle number etc), and thermalization is hindered. While the possibility of extensive mobility edges is debated [49], there is a relatively broad consensus in the community regarding the existence, for lattice models with bounded energy density, of a strong-disordered phase in

which the *entire spectrum* is MBL. This has been proved [86] for a disordered spin chain under a reasonable assumption, and its signatures have been detected experimentally in artificial quantum systems with tunable interactions and disorder [151, 158].

At given energy density, as the disorder is weakened a phase transition occurs, marked by the sharp change in the structure of the individual eigenstates, that become delocalized and develop extensive entanglement entropy. The transition has only *dynamical signatures*: transport is restored, and with it thermalization. Lying outside the realm of equilibrium statistical mechanics, this transition poses fundamental questions concerning its properties and nature, that are the subject of ongoing research.

Structure of the thesis

Most of the content of this thesis concerns the analysis of the localized phase: the latter is amenable to analytical treatment, since perturbative methods are controlled in the regime of strong disorder. The thesis is structured as follows: in the introductory chapter, the notion of localization is recalled, together with the perturbative arguments for its stability in the weakly interacting regime. The phenomenology of Many-Body Localized systems is discussed, and interpreted in the light of their emergent integrability. Some aspects of the dynamical transition to the delocalized, thermal phase are also briefly discussed. In the core of the thesis, my original achievements are reported.

- In Chapter 2, I present a recipe to construct the conserved quantities for a system of interacting fermions on a disordered lattice. The operators are built in terms of an expansion in a local operator basis, which is argued to converge in a regime of parameters corresponding to weak interactions among the fermions. The structure of the resulting operators is argued to imply the suppression of transport.
- In Chapter 3, I exploit the recipe for the explicit construction of the conserved charges to compute the long-time limit of the remanent magnetization of an antiferromagnetic quantum spin chain. The latter is proposed to be an order parameter of the MBL phase, that is readily accessible by experiments in magnets.
- In Chapter 4, I address some aspects related to the stability of localization with respect to the coupling to additional degrees of freedom, focusing on the problem of a localized single particle coupled to a finite bath. I discuss the occurrence of a "quantum Zeno effect" in the strong coupling regime, in which repeated "measurements" of the particle by the bath are responsible for the enhancement of localization.
- The above results are derived within a perturbative treatment, exploiting an approximation dubbed "forward approximation" whose nature and accuracy I analyze in Chapter 5.
- The final chapter contains a discussion on mechanisms by which thermal fluctuations may enhance the mobility of individual excitations in interacting systems, and proposes some analytical schemes to address them.

The Chapters 2 to 6 are based on the following publications:

1. V. Ros, M. Müller, A. Scardicchio, *Integrals of motion in the Many-Body Localized phase*, Nucl. Phys. B 891 (2015), pp. 420-465, and Nucl. Phys. B 900 (2015), pp. 446-448.
2. V. Ros, M. Müller, *Remanent magnetization: signature of Many-Body Localization in quantum antiferromagnets*, arXiv:1608.06225.
3. D. Huse, R. Nandkishore, F. Pietracaprina, V. Ros, A. Scardicchio, *Localized systems coupled to small baths: From Anderson to Zeno*, Phys. Rev. B 92 (2015), pp. 014203-014214.
4. F. Pietracaprina, V. Ros, A. Scardicchio, *The forward approximation as a mean field approximation for the Anderson and Many Body Localization transitions*, Phys. Rev. B 93 (2016), pp. 054201-054216.
5. V. Ros, M. Müller, *Temperature-dependent effects on effective mobility edges*, in preparation.

1 How disorder breaks quantum ergodicity: Many-Body Localization

The chapter is structured as follows: In Sec. 1.1 we discuss how ergodicity breaking has been probed experimentally in interacting, disordered systems; the experimental results provide an intuitive idea of the phenomenon of MBL and of its diagnostics. In Sec. 1.2, we discuss in more detail the criteria for localization and their implications. This discussion is carried on assuming that no mobility edge is present, i.e. that the *full* many-body spectrum is localized, irrespectively of the energy density. This possibility can be realized in disordered systems in discrete space, e.g. spin chains or fermions on a lattice having a finite number of energy bands: in this case, the parameters can be chosen in such a way that the putative transition temperature is larger than the bandwidth, thus ensuring that the full spectrum is localized. Under this hypothesis, the features of MBL systems can be explained assuming the existence of a complete set of approximately local integrals of motion, as we discuss in Sec. 1.3. In Sec. 1.4 we recall the perturbative arguments for the existence and stability of the localized phase, which represent the main tool to treat this phase analytically. We conclude the chapter by briefly commenting on the breakdown of localization and on the disorder-driven dynamical phase transition from an MBL state to an ergodic, diffusive and thermalizing one (Sec. 1.5).

1.1 Quenching disordered systems: the emerging picture

The most direct dynamical protocols probing quantum ergodicity breaking feature isolated systems that are initialized in a state with a well-defined local structure, and that are shown to remain localized (in their time evolution) in states resembling their initial condition.

For disordered systems, protocols of this sort have been realized in [27, 148], where a non-interacting Bose-Einstein condensate is prepared (via trapping) in a confined region of space, and subsequently let evolve (releasing the trap) in a random potential generated with a laser speckle pattern [27] or in a quasi-disordered optical lattice [148]; the density profile at later times is shown to be localized around the region where the condensate was trapped at $t = 0$, with exponential tails departing from the localization center, see Fig. 1.1.

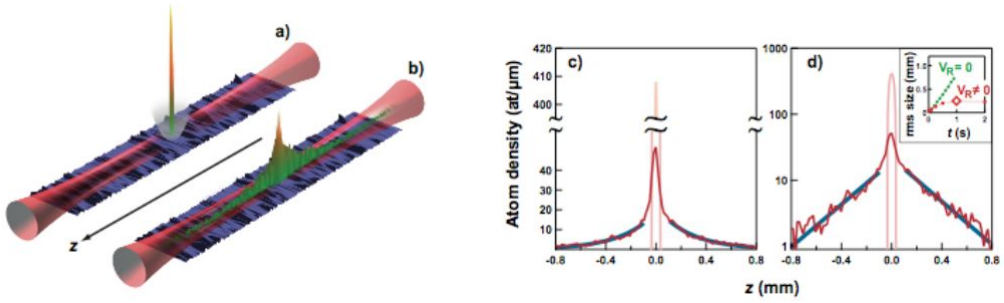

(a) (b)

Figure 1.1: (a) Pictorial representation of the protocol realized in [27]: a small BEC is formed in a trap, and a weak disordered optical potential is superimposed. When the trap is switched off, the BEC starts expanding and then localizes, as observed by direct imaging of the fluorescence of the atoms irradiated by a resonant probe. (b) Density profile of the localized BEC, one second after release, in linear or semi-logarithmic coordinates. Figures taken from Ref. [27]

The same rationale is behind the more recent experiments probing localization in systems of interacting cold atoms and trapped ions [151, 158, 40]. In [151], a one-dimensional interacting Aubry-André model is realized with ultra-cold fermions in an optical lattice Λ. The model has the Hamiltonian

$$H_{AA} = -J \sum_{i\in\Lambda,\sigma} \left(c^\dagger_{i,\sigma} c_{i+1,\sigma} + c^\dagger_{i+1,\sigma} c_{i,\sigma} \right) + \Delta \sum_{i\in\Lambda,\sigma} \cos\left(2\pi\beta i + \phi\right) n_{i,\sigma} + U \sum_{i\in\Lambda} n_{i,\uparrow} n_{i,\downarrow}, \tag{1.1}$$

where $c_{i,\sigma}, c^\dagger_{i,\sigma}$ are annihilation and creation operators of a fermion with spin $\sigma = \{\uparrow,\downarrow\}$ at a site $i \in \Lambda$, $n_{i,\sigma} = c^\dagger_{i,\sigma} c_{i,\sigma}$ is the local density, β is the incommensurable ratio between the periodicities of the two lattices that are superimposed to realize the quasi-disordered potential, and ϕ is a phase offset. A quench-protocol is realized: the system is prepared in a density wave $|\psi_0\rangle$ with only the even sites occupied, which is a highly-excited eigenstate of (1.1) with $J = 0$. Subsequently, the system is let evolve with the dynamics given by (1.1). For strong fluctuations in the potential, i.e. for sufficiently large Δ/J, the time-evolved pure state is found to retain the density pattern of $|\psi_0\rangle$: the imbalance between the occupation of even and odd sites, defined as

$$\mathcal{I}(t) = \frac{2}{|\Lambda|} \sum_{i\in\Lambda} (-1)^i \langle\psi_0|n_i(t)|\psi_0\rangle, \tag{1.2}$$

does not decay to zero but rather relaxes to a finite value, see Fig. 1.2 (a).

A conceptually analogous protocol is realized in [158] with a system of trapped ions subject to optical dipolar forces, which is described by an effective long-range transverse

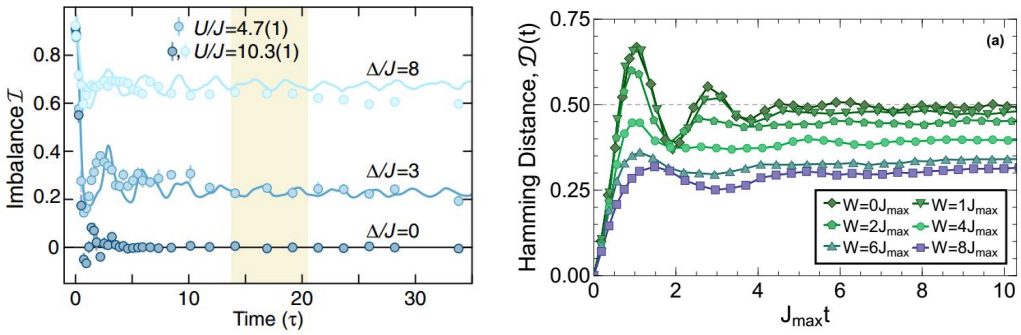

(a) (b)

Figure 1.2: (a) Imbalance defined in Eq. (1.2) as a function of time measured in units of J^{-1}, for different values of disorder Δ, cfr. (1.1). The circles are experimental points obtained averaging over six realizations of disorder, while the continuous lines are DMRG calculations. The figure is taken from Ref. [151]. (b) Hamming distance defined in Eq. (1.4) as a function of time measured in units of J_{max}^{-1}, for different values of disorder. The figure is taken from Ref. [158]

field Ising model with Hamiltonian

$$H_{LRI} = \sum_{i<j\in\Lambda} J_{ij}\sigma_i^x\sigma_j^x + \frac{B}{2}\sum_{i\in\Lambda}\sigma_i^z + \sum_{i\in\Lambda}\frac{D_i}{2}\sigma_i^z \tag{1.3}$$

where σ_i^κ, $\kappa \in \{x, y, z\}$ are Pauli matrices, $D_i \in [-W, W]$ independent random local fields extracted from a uniform distribution, and $J_{ij} \propto J_{max}/|i-j|^\alpha$ with $\alpha > 1$ ($\alpha \approx 1.13$ in [158]). In this setting, the system is initialized in a Néel ordered state $|\psi_0\rangle = |\uparrow\downarrow\uparrow\cdots\rangle$ analogous to the density wave in the fermionic case, and the normalized Hamming distance is measured,

$$\mathcal{D}(t) = \frac{1}{2} - \frac{1}{2|\Lambda|}\sum_{i\in\Lambda}(-1)^i\langle\psi_0|\sigma_i^z(t)|\psi_0\rangle, \tag{1.4}$$

with similar outcomes as for the imbalance, see Fig. 1.2 (b).

Another, similar protocol has been implemented in [40] in two dimensions, by tracking the time evolution of an initially prepared density domain wall for interacting bosons in a disordered optical lattice. Signatures of localization have been observed away from the strongly-disordered regime, being encoded in the fact that the domain wall configuration does not completely melt for very long time scales.

The results summarized in Fig. 1.2 are interpreted as the experimental proof of the existence of a Many-Body Localized phase at sufficiently strong disorder, whose main features are the following:

(i) *The transport of conserved quantities is suppressed:* the fermions (or spin excitations) do not move but remain frozen in their initial location for very long time scales.

The detailed spatial pattern of the particle-density (or the spin-density) of the initial state is not spoiled by the dynamics;

(ii) *Relaxation occurs, toward a state preserving memory of the initial condition:* the imbalance and Hamming distance *do* relax to a stationary value, which is, however, incompatible with ergodicity, in the sense that the system retains *local* memory of its initial condition;

(iii) *Quantum thermalization fails:* thermalization requires that out-of-equilibrium initial conditions evolve toward states that are independent of their detailed local structure, being characterized only by few parameters (temperature, chemical potential etc.) conjugated to the macroscopic conserved quantities. More precisely, an isolated quantum system initialized in a pure state $|\psi\rangle$ is said to thermalize whenever, given an (arbitrary) decomposition into a *finite* subsystem A and the remainder A^C, the reduced density matrix associated to A:

$$\rho_A(t) = \mathrm{Tr}_{A^C}\left(|\psi(t)\rangle\langle\psi(t)|\right) \tag{1.5}$$

converges for $t \to \infty$ to the equilibrium reduced density matrix

$$\rho_A^{(eq)}(T) = \frac{1}{Z(T)}\mathrm{Tr}_{A^C}\left(e^{-H/k_BT}\right). \tag{1.6}$$

H is the system's Hamiltonian and T is the temperature, defined by $\langle\psi|H|\psi\rangle = \mathrm{Tr}\left(H\rho^{(eq)}(T)\right)$ (for simplicity, we are assuming that the energy is the only conserved quantity in the system). The convergence is understood as

$$\lim_{t\to\infty}\lim_{|\Lambda|\to\infty}\mathrm{Tr}\left(\mathrm{O}\,\rho_A(t)\right) = \mathrm{Tr}\left(\mathrm{O}\,\rho_A^{(eq)}(T)\right), \tag{1.7}$$

for any *local* observable O supported in the subsystem A. The condition (1.7) assumes that the number of degrees of freedom in A is kept finite in the thermodynamic limit, and that the latter is taken *before* the infinite time limit, to avoid quantum revivals and recurrence phenomena. It is manifestly violated in the above experimental realizations, where the expectation values of the single-site occupation numbers $n_{i,\sigma}$ or spin operators σ_i^z do not relax to their thermal value (which would be zero given the choice of the initial state) but remain close to the initial values ± 1.

The picture emerging from the experimental realizations contrasts with the expected scenario for the dynamics of an interacting quantum system following a quantum quench. The latter predicts that, as the quench is performed, the excitations start spreading through the system in such a way that their cumulative effect on single sites results in an effective averaging process: the information stored in each site becomes infinitely diluted across the lattice as time progresses, and the system reaches a local steady state [41, 19]. The condition (1.7) formalizes this picture, as it states that the information on the initial condition (which is preserved by the quantum dynamics due to its unitarity) is encoded into global observables, and cannot be recovered by means of local measurements

restricted to the subsystem A. On the contrary, MBL systems initialized in a strongly out-of-equilibrium condition relax toward a non-equilibrium stationary state which preserves the information on the initial condition at each site: the dynamics is not ergodic, despite the system being thermodynamically large, interacting and at finite energy density.

This gives an intuitive notion of what is meant by Many-Body Localization. It is however fair to say that a precise, comprising definition of MBL has not yet been formulated, and the equivalence of the many existing definitions has not yet been established. In the following section, we present a more detailed discussion of the features that are commonly interpreted as signatures of this phenomenon.

1.2 Many-Body Localization: a multifaceted phenomenology

We begin by introducing the main theoretical models in which localization has been argued to occur. The notion of localization was first introduced in [10] for the so-called "Anderson model" of a quantum random walker in random environment, with Hilbert space $l^2(\Lambda)$ (with Λ a d-dimensional lattice), and Hamiltonian

$$H_{\text{And}} = \sum_{a\in\Lambda} \epsilon_a c_a^\dagger c_a + \sum_{\langle a,b\rangle} V_{ab}\left(c_a^\dagger c_b + c_b^\dagger c_a\right) \equiv H_{\text{And}}^{(0)} + V_{\text{And}}. \tag{1.8}$$

In (1.8), $\langle a,b\rangle$ denote the edges in Λ, V_{And} is the kinetic term (customarily called the "hopping term"), and ϵ_a are independent random variables defining a stochastic process indexed by the sites $a \in \Lambda$. Following [10], the choices $V_{ab} = V$ and $\epsilon_a \in [-W/2, W/2]$ are conventionally made. Due to the presence of the static randomness, (1.8) corresponds to a whole family of stochastic Hamiltonians, one for each realization of the random landscape. The problem has thus to be formulated within a statistical framework, through statements concerning the *typical properties* of the family, that are realized with probability one with respect to the probability measure generated by the stochastic potential.

Anderson's approach was extended to the many-body setting in [20, 72] for fermionic Hamiltonians of the form

$$H_{\text{int}} = H_{\text{And}} + U = \sum_\alpha E_\alpha n_\alpha + \frac{1}{2}\sum_{\alpha\beta,\gamma\delta} U_{\alpha\beta,\gamma\delta} c_\alpha^\dagger c_\beta^\dagger c_\gamma c_\delta, \tag{1.9}$$

where α labels the single-particle states, i.e., the eigenstates of the quadratic part (1.8). Subsequently, starting from [132], the occurrence of a localized phase in disordered spin chains was investigated numerically by studying the features of eigenstates. The prototypical model exploited in the numerics is the XXZ spin chain in random fields,

$$H_{\text{XXZ}} = \sum_{a\in\Lambda}\left[J\left(\sigma_a^x\sigma_{a+1}^x + \sigma_a^y\sigma_{a+1}^y\right) + J_z\sigma_a^z\sigma_{a+1}^z + h_a\sigma_a^z\right] = \sum_{a\in\Lambda} H_a, \tag{1.10}$$

with $h_a \in [-W/2, W/2]$, which is equivalent to a model of interacting fermions in a disordered potential through the Jordan-Wigner transformation [93]. More recently, rigorous results on the existence of the MBL phase have been derived in [86] for the

chain:

$$H_{\text{Imb}} = \sum_{a\in\Lambda} \left(h_a \sigma_a^z + J_a \sigma_a^z \sigma_{a+1}^z + \gamma \Gamma_a \sigma_a^x \right) = H_0 \left(\{\sigma_a^z\} \right) + \gamma V \left(\{\sigma_a^x\} \right) \tag{1.11}$$

with random couplings h_a, Γ_a, J_a bounded by 1 and γ assumed to be small.

In the following, we present a list of the main features which emerge from the theoretical analysis of the above models in the localized regime, that have been explored either numerically (for systems in $d = 1$) or by means of perturbative arguments (in any d). We begin with the original formulation given in [10].

1.2.1 Infinite decay time of local excitations: Anderson's criterion

In its most direct formulation, localization corresponds to the fact that a degree of freedom placed at $t = 0$ in a site $a \in \Lambda$ remains in the nearby region of space up to infinite time: The local state $|a\rangle \in l^2(\Lambda)$ associated to the site a has *infinite decay time*.

This feature is captured by the long-time behavior of the survival probability amplitude,

$$\mathcal{A}(t) = \theta(t) \langle a | e^{-iHt} | a \rangle = \frac{i}{2\pi} \int_{\mathcal{B}} dz e^{-izt} G_{aa}(z) = \frac{i}{2\pi} \int_{\mathcal{B}} dz \frac{e^{-izt}}{z - \epsilon_a - S_a(z)}, \tag{1.12}$$

with $\mathcal{B} = \{z : \Im z = \eta > 0\}$. In (1.12), the survival probability is given in terms of the diagonal matrix elements of the resolvent operator:

$$G_{aa}(z) = \langle a | \frac{1}{z - H} | a \rangle \equiv \frac{1}{z - \epsilon_a - S_a(z)}, \tag{1.13}$$

where $S_a(z)$ is the local self energy at site a and $z = E + i\eta$. The functions $G_{aa}(z), S_a(z)$ are analytic in the upper half complex plane, and thus admit the integral representations

$$\begin{aligned} G_{aa}(z) &= \int_{E_0}^{\infty} dE' \, \frac{\mathscr{A}_a(E')}{z - E'}, \\ S_a(z) &= \int_{E_0}^{\infty} dE' \, \frac{\Gamma_a(E')}{z - E'}, \end{aligned} \tag{1.14}$$

where E_0 is the ground state energy of (1.8), $\mathscr{A}_a(E)$ is the local density of states (or spectral function) and $\Gamma_a(E) > 0$ is also a measure defined on the real line. For finite $|\Lambda|$, the functions (1.14) have isolated poles on the real axis, as it holds

$$\begin{aligned} \mathscr{A}_a(E) &= \sum_{\alpha} |\langle \phi_\alpha | a \rangle|^2 \delta(E - E_\alpha), \\ \Gamma_a(E) &= \sum_{\alpha} |\langle a | V^{(a)} | \tilde{\phi}_\alpha \rangle|^2 \delta\left(E - \tilde{E}_\alpha \right), \end{aligned} \tag{1.15}$$

where $|\phi_\alpha\rangle$ are the eigenstates of H_{And} with energy E_α, while $|\tilde{\phi}_\alpha\rangle$ are the eigenstates of the modified Hamiltonian $\tilde{H}^{(a)} = H - V^{(a)}$ obtained removing the terms $V^{(a)}$ connecting

the site a to its neighboring ones in the lattice [57].

The long-time behavior of $\mathcal{A}(t)$ depends on whether the isolated poles of $G_{aa}(z)$ coalesce into a branch cut in the thermodynamic limit, that is to say that $\mathscr{A}_a(E)$ and $\Gamma_a(E)$ become continuous in that limit. In this case, $\Gamma_a(E)$ gives the width of the spectral function $\mathscr{A}_a(E)$,

$$\mathscr{A}_a(E) = \frac{1}{\pi} \frac{\Gamma_a(E)}{(E - \epsilon_a - \Re S_a(E))^2 + (\Gamma_a(E))^2}, \tag{1.16}$$

as it follows from the fact that $\Gamma_a(E) = -\Im S_a(E)$ (using the Sokhotski-Plemelj theorem together with (1.13)). A finite width of the spectral function implies that the survival probability (1.12) is exponentially damped, with a decay rate that is functionally related to $\Gamma_a(E)$ [1]. Thus, the only possibility for localization is that no branch cut develops in the thermodynamic limit, meaning that $\mathscr{A}_a(E), \Gamma_a(E)$ remain singular functions of the form (1.15), i.e., measures concentrated on a countable set of points. In this case, the integral (1.12) is contributed only by the residua of the poles of $G_{aa}(z)$, each of which is multiplied by an oscillating phase: the survival probability remains finite for $t \to \infty$, and the local state $|a\rangle$ does not decay. This corresponds to H_{And} having "pure point" spectrum[2]: an instance of this is given by the trivially localized limit $V = 0$.

Localization is therefore encoded in the (non-)regularity of $\mathscr{A}_a(E), \Gamma_a(E)$. The latter are however random objects, whose detailed structure is washed out if an average over disorder is performed (the average over the position of poles reproduces a continuous function). As pointed out in [10], the two scenarios discussed above can be distinguished within a statistical framework by inspecting the scaling of the full probability distribution of $\Im S_a(E + i\eta)$ in the limit $\eta \to 0$. Indeed, when $\Gamma_a(E)$ is a continuous function in the thermodynamic limit for almost all disorder realizations (with $\Gamma_a(E) = -\lim_{\eta\to 0} \Im S_a(E + i\eta)$), its distribution is regular for $\eta \to 0$. If instead $\Gamma_a(E)$ is singular, of the form (1.15), for finite η the function $\Im S_a(E + i\eta)$ is a sum of Lorentzians of width η centered at random points; for a fixed E, with probability close to one $\Im S_a(E + i\eta)$ is of order η,

[1] This is easily seen in the following way: In presence of a cut, the integral (1.12) needs to be performed analytically continuing $G_{aa}(z)$ to the second Riemann sheet, where

$$S_a(z) \to S_a^{II}(z) = \int_{E_0}^{\infty} dE' \, \frac{\Gamma_a(E')}{z - E'} - 2\pi i \Gamma_a(z). \tag{1.17}$$

In the second Riemann sheet, the integrand in (1.12) exhibits an additional pole (or poles) $z_<$ satisfying $z_< - \epsilon_a - S_a^{II}(z_<) = 0$. The residue associated to this pole contains an exponentially decaying factor with rate $\gamma = -\Im z_< = -\Im S_a^{II}(z_<)$.

[2] A rigorous version of this argument relating the spectral properties of H_{And} with the occurrence of bound states is given by the RAGE (Ruelle, Amrein, Georgescu and Enss) theorem [43]. The theorem exploits the fact that pure point spectrum implies the existence of a complete set of proper eigenstates (i.e., states belonging to the Hilbert space $|\phi_\alpha\rangle \in l^2(\Lambda)$): the decay (in space) of the eigenstates (that ensures that they are normalizable) suffices to prove that

$$\lim_{L\to\infty} \sup_{t\geq 0} \left(\sum_{x \notin C_L} |\langle x|e^{-itH}|a\rangle|^2 \right) = 0, \tag{1.18}$$

for any $a \in \Lambda$ and C_L a cube of side L centered at the origin of Λ.

being of the order of V^2/η only if E is within a Lorentzian, which occurs with vanishing probability $\sim \eta/W$. Thus, in the limit $\eta \to 0$ the distribution of $\Im S_a(E+i\eta)$ becomes singular, peaked at zero. As a result, localization occurs at a given energy E whenever

$$\lim_{\eta\to 0}\lim_{|\Lambda|\to\infty} \mathbb{P}\left(-\Im S_a(E+i\eta)>0\right)=0, \tag{1.19}$$

where the probability is over the disorder realizations. This criterion for localization is recast in [10] as a problem of convergence of the perturbative expansion for $S_a(E)$ around the trivially localized limit $V=0$, see Sec. 1.4.

1.2.2 Accounting for scattering processes: Anderson's argument revisited

The arguments in favor of MBL given in [20, 72] are formulated in the same vein as Anderson's original approach, in terms of the scattering rate $\Gamma_\alpha(\epsilon,t)$ associated to the quasiparticle excitations of the model (1.9). Following [20] we set

$$\Gamma_\alpha(\epsilon,t) = -\Im S^R_\alpha(\epsilon,t), \tag{1.20}$$

where

$$S^R_\alpha(\epsilon,t) = \int d\tau e^{i\epsilon\tau}\, S^R_\alpha\left(t-\frac{\tau}{2},t+\frac{\tau}{2}\right) \tag{1.21}$$

is the Wigner transform of the retarded self energy associated to the one-body Green function

$$G^R_\alpha(t_1,t_2) = -i\theta(t_1-t_2)\langle\left\{c_\alpha(t_1),c^\dagger_\alpha(t_2)\right\}\rangle, \tag{1.22}$$

the quantum average in (1.22) being taken over a density matrix that has to be determined as a solution of the quantum Boltzmann equation. The thermodynamic limit is assumed, as well as an infinitesimal coupling b to a thermal bath, playing the same role as η in the single-particle case. In full analogy with the single particle case, the criterion for Many-Body Localization reads

$$\lim_{b\to 0}\lim_{|\Lambda|\to\infty} \mathbb{P}\left(\Gamma_\alpha(\epsilon)>0\right)=0. \tag{1.23}$$

In both [20, 72], this condition is rephrased in terms of the convergence in probability of the diagrammatic expansion for $\Gamma_\alpha(\epsilon)$. The perturbation theory is controlled by the ratio U/δ_ξ between the two relevant energy scales of the Hamiltonian (1.9), that are: (1) the average energy gap between the single particle states whose localization centers lie within the same "localization volume", i.e., a volume of the size of the localization length ξ in (1.28),

$$\delta_\xi = \frac{1}{\nu\xi^d} \tag{1.24}$$

with ν the density of states, and (2) the typical value U of the interaction matrix elements.

The latter defines the dimensionless constant:

$$\lambda = U\,\nu\xi^d \tag{1.25}$$

measuring the strength of the interaction.

The dynamical implications of (1.23) are best understood by looking at the quantum Boltzmann equation (cfr. Eq. (57) in [20]). The scattering rate Γ_α enters in the collision integral, governing the relaxation of the expectation value of the local occupations $n_\alpha(\epsilon, t)$ of the single-particle energy levels. Its singular dependence on ϵ in the thermodynamic limit, when the coupling to the bath is sent to zero, indicates that the irreversible evolution of the local occupation toward their thermal equilibrium values is hindered. This suggests that in the absence of an external reservoir the system fails to act as a heat bath for itself, as is however required for (1.7) to hold.

1.2.3 MBL as absence of dc transport

The criterion (1.19) implies that local states $|a\rangle$ are bound states: this is known as "spectral localization". Stronger statements, referred to as "dynamical localization", can be rigorously proved in the one-body setting. They correspond to the following bound holding almost surely for some constants $C, \xi > 0$:

$$\sup_{t\geq 0} |\langle a|e^{-iHt}|b\rangle| < Ce^{-|a-b|/\xi}. \tag{1.26}$$

This implies that localized initial conditions $|a\rangle$ have, with probability one, uniformly in time bounded moments of all orders $q > 0$,

$$\sup_{t\geq 0} \left(\sum_x |x|^{2q} |\langle x|e^{-iHt}|a\rangle|^2 \right) < \infty. \tag{1.27}$$

This rules out the possibility of transport, in particular of diffusive transport (which is however expected in the weak disorder regime for $d \geq 3$).

Eq. (1.26) is rigorously proved exploiting the fingerprint of localized disordered systems, that is, the presence of exponential tails, cfr. Fig.1.1. In particular, the eigenstates envelopes satisfy

$$|\phi_\alpha(a)| \sim A_\alpha \exp\left(-\frac{|a - r_\alpha|}{\xi_\alpha}\right), \tag{1.28}$$

where r_α is the localization center of ϕ_α and ξ_α its localization length. Exponential bounds can be derived on either the local matrix elements of the resolvent [65], or on their fractional moments [5] or on the eigenstates correlators [85]. The derivation of these bounds is partly based on perturbative arguments, and it casts the reasoning of [10] into a rigorous analytic framework.

Arguments for the vanishing of the diffusion constant are given also for the many-body

case [20, 72]; similarly to the single particle case, they rely on the exponential spatial decay of the correlations of the local density operators $\rho(r)$ on the exact many-body eigenstates $|E_n\rangle$:

$$\mathcal{L}^{\rho}_{nm}(r) = \sum_{r'} \langle E_n|\rho(r')|E_m\rangle\langle E_m|\rho(r'+r)|E_n\rangle \lesssim \exp\left(-\frac{|r|}{\xi(E)}\right), \tag{1.29}$$

where $E_n \approx E_m \approx E$. We present a variant of these arguments in Sec. 1.3.2. Besides being evident in the experimental realizations discussed in Sec. 1.1, the absence of diffusion has been addressed numerically by analyzing the dc conductivity [18, 22] and the dynamical correlation functions in the infinite-time limit [134, 103]. Note that for charged particles, a vanishing diffusion constant corresponds to a vanishing electrical conductivity, given the Einstein relation which relates linearly the two quantities.

1.2.4 MBL as Anderson localization in Fock-space

It is evident from (1.28) that the localized eigenstates of (1.8) are effectively (up to exponentially small errors) a linear combination of a finite number of local eigenstates of $H^{(0)}_{\text{And}}$, the ones lying within a compact region of size ξ_α around r_α: each state ϕ_α can thus be considered as a weak deformation of an eigenstate of $H^{(0)}_{\text{And}}$ centered at r_α. A useful indicator capturing this spatial structure is the inverse participation ratio (IPR):

$$\text{IPR} = \sum_{a\in\Lambda} |\langle\phi_\alpha|a\rangle|^4, \tag{1.30}$$

which is proportional to $1/\xi^d$ for exponentially localized eigenstates, while it tends to zero as $|\Lambda|^{-1}$ in the delocalized phase [3].

In the interacting case, this intuition translates into the statement that many-body eigenstates are weak deformations of the eigenstates of the non-interacting Hamiltonian, either Fock states in (1.9) or "classical basis states" (product states in the basis of the σ^z_a) in (1.10). This is consistent with the picture, proposed in the seminal work [9], of MBL as Anderson localization "in Fock space", i.e., in an abstract graph whose sites correspond to the non-interacting eigenstates and whose geometry is determined by the interactions.

Several eigenstate features corroborate this picture. The expectation values of the local observables commuting with the non-interacting Hamiltonian (the single-particle occupation numbers n_α or local spin operators σ^z_i) are shown to be close to ±1 also on MBL eigenstates [134]. This has been proved in [86] for the model (1.11), for which it is shown that:

$$\mathbb{E}\left[\sum_n |\langle E_n|\sigma^z_a|E_n\rangle|\right] = 1 - O(\gamma^\kappa), \tag{1.31}$$

[3] Since the IPR equals the infinite-time averaged probability that a particle initialized at site a returns to the same site, its finite value implies that (1.12) does not decay to zero as $t \to \infty$.

where $\kappa > 0$, the average is over the disorder, and $|E_n\rangle$ are the many-body eigenstates. The IPR of classical states in the basis of the eigenstates of (1.10) considered in [46] suggests that the classical states are a superposition of "small" number of many-body eigenstates, which scales exponentially with $|\Lambda|$ but slower[4] than the dimension of the many-body Hilbert space $\mathcal{N} = 2^{|\Lambda|}$. A similar diagnostic is the participation entropy analyzed in [108].

1.2.5 MBL as area-law entanglement in highly excited states

The scenario according to which MBL eigenstates are a weak deformation of the non-interacting ones [21] entails that, similarly to the Fock states, the excited eigenstates $|E_n\rangle$ have low entanglement. For $1d$ systems, this is captured by the bipartite eigenstate entanglement entropy S, which is obtained splitting the system into a left half L and a right half R, and tracing out the degrees of freedom corresponding to one of the halves:

$$S = -\mathrm{Tr}\left(\rho_R \log_2 \rho_R\right) \tag{1.32}$$

with

$$\rho_R = \mathrm{Tr}_L\left(|E_n\rangle\langle E_n|\right). \tag{1.33}$$

It is shown in [21, 108, 101] that S does not scale with system size but obeys an area-law, see Fig. 1.3.

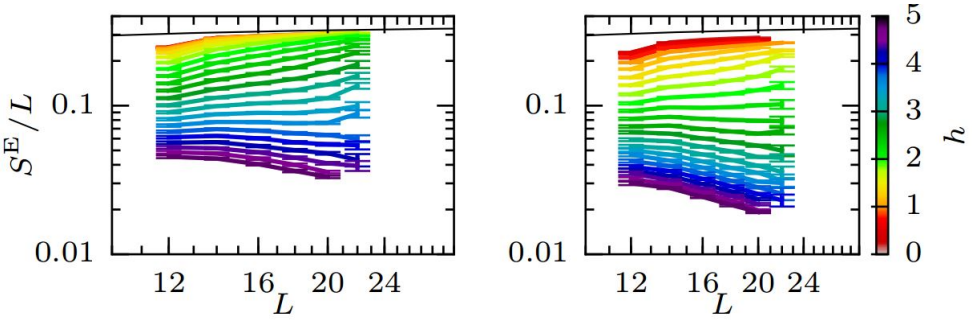

Figure 1.3: Numerical data for the bipartite entanglement entropy (1.32) for the Hamiltonian (1.10) with $J = J_z = 1$ and $h_a \in [-h, h]$, as a function of system size L for different disorder strengths in the middle of the spectrum (left) and in the upper part (right). For strong disorder, S/L decreases signaling area-law. The figure is taken from [108]

This is a typical property of the ground state of gapped Hamiltonians, which in the MBL case extends to the whole spectrum. It is a remarkable feature, as it implies that MBL eigenstates of extensive energy can be efficiently represented via Density-Matrix-RG or

[4] In the many-body case, the analogue of (5.20) decays to zero with the system size in both the localized and delocalized phase: while in the delocalized phase the decay is expected to be as fast as $\mathcal{N}^{-1}$, the MBL phase is characterized by a slower decay. To sharply distinguish between the two phases, the authors of [20] considered the IPR of single-particle excitations on top of the many-body eigenstates, in the basis of the many-body eigenstates themselves. The latter decays to zero in the delocalized phase, while it remains finite whenever MBL occurs.

Matrix Product States [177, 64, 97] and Tensor Networks [34]. Moreover, it allows to access to the dynamical properties in the MBL phase adapting computational approaches originally designed for the ground-state physics; a paradigmatic example is the Strong Disorder Renormalization Group (SDRG) scheme, which was developed in [45, 60, 83] to capture the low-temperature thermodynamical properties of random magnets, and has been recently exploited to characterize the MBL phase by either constructing approximate many-body eigenstates [136] or by describing the dynamical evolution of initial product states [172, 173].

1.2.6 MBL as violation of the Eigenstate Thermalization Hypothesis

A further aspect of the lack of thermalization in the MBL phase is the inherent incompatibility of the structure of the eigenstates with the Eigenstate Thermalization Hypothesis (ETH). The ETH is a scenario furnishing a microscopic justification for thermalization, going back to [90] and later developed in [52, 161, 147] (see Sec.(7.2) in [69] for a comprehensive historical review). It states that the individual eigenstates $|E_n\rangle$ of a thermalizing Hamiltonian locally reproduce the canonical ensembles, that is to say that (1.7) is true with $\rho_A = \mathrm{Tr}_{A^C}\left(|E_n\rangle\langle E_n|\right)$.

In [162] the ETH is formulated as the conjecture that that the diagonal matrix elements of (few-body) observables O on the individual eigenstates are smooth functions of the eigenstate energy, being approximately constant in each energy shell and equal to their microcanonical value. More precisely, it is postulated that

$$\langle E_n|\mathrm{O}|E_m\rangle = \delta_{nm}\overline{\mathrm{O}}(E) + e^{-S(E)/2} f(E,\omega) R_{nm}, \tag{1.34}$$

where $E = (E_n + E_m)/2$ is the mean energy, $\omega = E_n - E_m$, $\overline{\mathrm{O}}(E)$ is the thermal expectation value, $S(E)$ the microcanonical entropy, $f(E,\omega)$ a spectral function that depends smoothly on its arguments, and R_{nm} a random variable with zero mean and unit variance, that in [162] is assumed to be Gaussian distributed [5]. The ansatz (1.34) guarantees that any initial condition reaches a stationary state that is locally thermal at $t \to \infty$, up to corrections that are exponentially small in the system size.

The picture underlying (1.34) is that the eigenstates of thermalizing quantum systems are locally indistinguishable, and "as random as possible" subject to the global energy constraint. This contrasts with the Fock space localization picture discussed in Sec. 1.2.4, that entails that MBL eigenstates in the same energy shell are all locally distinguishable and non-thermal: the expectation values of the local observables (such as n_α or σ_i^z) are

[5] This assumption is made since the system considered in [162] has a classically chaotic counterpart and thus Berry's conjecture is expected to apply (i.e., the eigenstates in the bulk of the spectrum are expected to be a superposition of plane waves with random phases and random Gaussian amplitudes [24]). This feature is, however, non generic, and recently shown to be false for a one-dimensional disordered spin chain in its delocalized, thermalizing phase [107], for which (i) the exponential decay with system size of the off-diagonal matrix elements exhibits a power law correction, and (ii) the fluctuations of R_{nm} are non-Gaussian. This is consistent with the anomalous transport properties observed numerically in this class of systems [15, 109, 4, 94], characterized by a disorder-dependent dynamical exponent vanishing in the MBL phase.

far from their equilibrium value, they strongly fluctuate between states that are close in energy [106], thus allowing to distinguish them. ETH is also incompatible with the area-law scaling of the bipartite entanglement satisfied by MBL eigenstates, as it requires that the entanglement equals to the thermal equilibrium entropy of the subsystem, that scales with the number of it degrees of freedom. This dichotomy has been exploited to pinpoint the phase diagram of disordered systems by probing the violation of ETH in individual eigenstates, obtained from the exact diagonalization of finite samples.

1.2.7 MBL as absence of level repulsion

Starting from the earlier works [23, 12], the statistics of the energy levels of finite disordered samples has been extensively exploited to detect MBL [33, 132, 42]. In particular, the average value $\langle r \rangle$ of the dimensionless ratio $r_n = \min(\delta_n, \delta_{n+1})/\max(\delta_n, \delta_{n+1})$, where $\delta_n = E_{n+1} - E_n$ is the spacing between consecutive eigenvalues, has been used as an indicator of the absence of level repulsion in the MBL phase (signaled by the fact that $\langle r \rangle \to 0.39$ approaches the theoretical value associated to the Poisson distribution as the systems size is increased [108]).

The absence of level repulsion is interpreted as a signature of "integrability" [25], as opposed to the level repulsion exhibited by the random matrix universality classes, commonly regarded as the hallmark of quantum chaos [28, 137, 163]. Its connection with localization is rather intuitive in the single particle case: the exponential decay of the eigenfunctions (1.28) implies that disjoint, distant regions of space are essentially uncorrelated and create almost independent eigenvalues, that are described by a Poisson point process. This statements is rigorously proved for the Anderson model [116] on the basis of the Minami estimate, which bounds the probability of occurrence of two eigenvalues (of the finite volume Hamiltonian) in a small energy interval. By contrast, extended states imply that distant regions have mutual influence, and thus create some repulsion between energy levels [117].

The same intuitive picture is expected to hold for MBL systems, in view of the localization in Fock space that implies that states that are nearby in energy are typically localized far apart in Fock space and do not interact (in the sense that the off-diagonal matrix elements of local operators between such states are exponentially small, thus suggesting that no mixing occurs). On the other hand, the ansatz (1.34) points toward level repulsion, as it posits that the off-diagonal matrix elements of local operators are typically much larger than the level spacing $\omega_{min} \sim \exp(-S(E))$.

1.2.8 MBL as slow growth of entanglement

The above discussion indicates that in the localized phase, the structure of eigenstates is not significantly altered by the interactions: the main features of non-interacting localized states (low entanglement of eigenstates, non-thermal expectation values of local observables etc.) extend to the many-body case. This raises the question of whether the effect of interactions is negligible altogether. This is not the case, as signatures of

the interactions can be traced in the real-time dynamics of the bipartite entanglement entropy $S(t)$, obtained from (1.32), substituting $|E_n\rangle$ in (1.33) with the time-evolved pure state $|\psi(t)\rangle$ of the entire system.

Numerical simulations have been performed for disordered spin chains initialized in a weakly-entangled/product state [39, 178, 17]; after an initial fast growth dominated by the direct nearest-neighbor interactions across the cut (until times of the order of the inverse interaction coupling), $S(t)$ exhibits a slow, *logarithmic growth*, which is expected to continue indefinitely for an infinite system. For finite systems, $S(t)$ saturates to a value that depends on the initial state only [128, 154], which is extensive but nevertheless smaller than the one expected in the thermal regime.

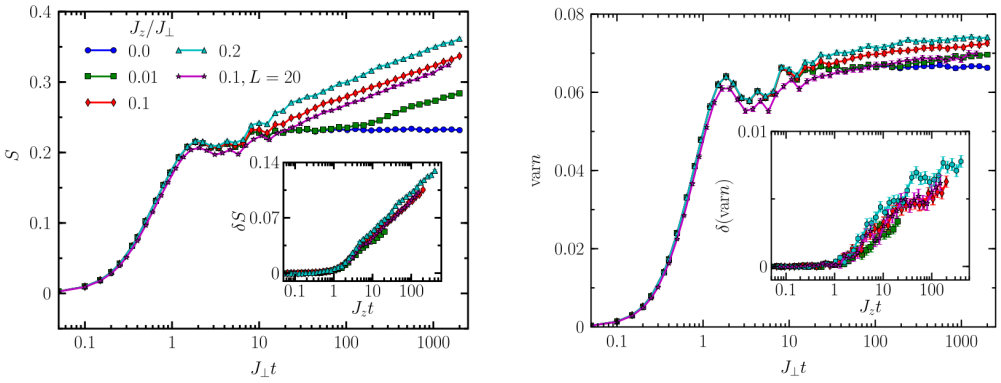

(a) (b)

Figure 1.4: (a) Unbounded growth of the bipartite entanglement after a quench starting from a site-factorized σ^z eigenstate of the Hamiltonian (1.10) with $J = J_\perp$, $h_a \in [-5, 5]$, $L = 10$ and different interaction strengths J_z. The inset shows the same data with a rescaled time axis and subtracted $J_z = 0$ values. (b) Growth of the particle number fluctuations of a half chain after the quench. The behavior is qualitatively different than the entanglement entropy: the interactions do enhance the particle number fluctuations, but while there are signs of a logarithmic growth as for the entanglement, this growth slows down with time. Figures taken from Ref. [17]

The logarithmic scaling is a peculiar feature of the MBL phase [6], that allows one to distinguish it from the non-interacting localized phase, where local disturbances propagate only to the scale of the localization length ξ and $S(t)$ saturates to a finite value independent of the system size.

The unbounded growth of $S(t)$ is nevertheless compatible with the suppression of transport, see Fig. 1.4. It is ascribed to the *interaction-induced dephasing* between the eigenstates involved in the decomposition of the initial product state. The same mechanism is at the root of other distinguishing dynamical features of MBL systems, such as: (i) the power-law decay in time of the response to a (properly designed) spin-echo protocol [152], (ii) the power-law relaxation (toward non-thermal values) of the expectation

[6] As opposed to the linear growth in clean integrable or non-integrable systems [32, 98] and to the sub-ballistic growth in disordered, delocalized systems close to the MBL phase [109, 174].

value of local observables after a quench [155], (iii) the suppression, with respect to the non-interacting case, of the revival rates of single-site observables [170], (iv) the power law decay of the average two-sites entanglement [82]. It indicates that the interactions, despite being unable to restore the diffusive transport of the global conserved charge and to induce thermalization, are nevertheless responsible for a slow propagation of quantum correlations over the entire system.

1.2.9 On the distinctions between the various characterizations of MBL

As it emerges from the above summary, the MBL phase has been characterized either by probing the dynamical properties of the system, or by focusing on the structure of the many-body eigenstates. These two approaches are in principle not equivalent. The first route leads to the original definition of MBL as an insulating phase in which the dc transport of the global conserved quantities is completely suppressed [72, 20]. The suppression of transport is certainly a key feature of localized systems, which distinguishes them from other systems in which the full ergodicity in phase space breaks down, such as systems with spontaneously broken symmetries, one-dimensional integrable systems (see Sec. 1.3.3) or spin glasses, in which the thermal conductivity remains finite. However, this characterization is not exhaustive in the following sense: first, it is known that in one dimension the diffusion constant is zero also in (part of) the delocalized phase, where thermalization is nevertheless restored via a sub-diffusive transport, see Sec. 1.5.2. Secondly, a notion of localization has been defined also for periodically driven systems [139, 138, 44, 1], for which there are no conserved quantities and thus no meaningful dc transport can be defined. In this case, MBL is understood in the sense discussed in Secs. 1.2.6, 1.2.7. On the other hand, the characterization of this phase in terms of the violation of the ETH may also be restrictive, an obvious reason being that the ETH is only a sufficient and not a necessary condition for thermalization (defined in Eq. (1.7)). Moreover, while localization (as well as thermalization in the sense of (1.7)) is a statement about the long-time limit of thermodynamically large systems (see Sec. 1.2.1), the ETH ansatz determines the stationary behavior of finite-size samples. It is possible for a system to have eigenstates satisfying ETH at any finite size, but to have a relaxation time which diverges exponentially with the system size, in such a way that transport and thermalization are hindered in the thermodynamic limit [38].

Keeping these distinctions in mind, we illustrate in the following section how the *full* set of diagnostics of the MBL phase can be justified by means of phenomenological models involving conserved quantities. This suggests that the "emergent integrability" of MBL systems might be considered as a comprehensive characterization of this phase.

1.3 Quasilocal integrals of motion: a unifying framework

MBL systems challenge the basic assumption underlying the statistical description of quantum systems in their long-time limit, that is that scattering processes at finite energy density restore ergodicity. It is a common expectation that the failure of ergodicity in closed, interacting systems is related to some sort of integrability. In fact, the behavior of

MBL systems points toward the existence of an extensive number of conservation laws that strongly constrain the quantum dynamics, preventing transport and thermalization. This expectation has been made concrete in [153, 80, 166], where it has been suggested that MBL Hamiltonians are non-linear functionals of a complete set of conserved operators I_α of the form

$$H_{diag} = h_0 + \sum_\alpha h_\alpha \, I_\alpha + \sum_{\alpha,\beta} h_{\alpha\beta} \, I_\alpha I_\beta + \sum_{\alpha,\beta,\gamma} h_{\alpha\beta\gamma} \, I_\alpha I_\beta I_\gamma + \cdots , \tag{1.35}$$

where the dots stand for higher order products. The I_α, also referred to as "l-bits", are expected to be functionally independent (meaning that each conserved operator cannot be expressed as a function of the others) and mutually commuting. The set is complete in the sense that every many-body eigenstate can be labeled in a unique way with the eigenvalues of the I_α.

While the expansion (1.35) is to some extent generic (in particular, to determine H_{diag} it is necessary to specify a number of coefficients which scales with the size of the Hilbert space [121]), the fingerprint of localization is the "*quasilocality*" of the I_α. The notion of quasilocality extends, at the operator level, the structure of the single-particle eigenstates: similarly to (1.28), the operator norm of I_α is expected to decay exponentially away from a region of typical size ξ_{op} centered in a given point R_α. Precisely, let

$$I_\alpha = \sum_{\mathcal{I}} \mathcal{A}^{(\alpha)}_{\mathcal{I}} \, \mathcal{O}_{\mathcal{I}} \tag{1.36}$$

be the expansion of I_α in a basis of local operators $\mathcal{O}_{\mathcal{I}}$ labeled by $\mathcal{I}$. For the spin chains (1.10) and (1.11), a suitable basis is made by the tensor products of local spin operators $\sigma^{\alpha_1}_{i_1} \otimes \cdots \otimes \sigma^{\alpha_n}_{i_n}$ with $\alpha = \{x, y, z\}$, while in the fermionic case (1.9) the normal-ordered tensor products of creation and annihilation operators of single-particle states can be considered, see Sec. 2.1.1. Let $S(\mathcal{I})$ denote the "support" of $\mathcal{O}_{\mathcal{I}}$, i.e., the set of points/local degrees of freedom on which the operators acts non-trivially. Quasilocality entails that

$$|\mathcal{A}^{(\alpha)}_{\mathcal{I}}| \lesssim C_\alpha \exp\left(- \frac{d\,[R_\alpha, S(\mathcal{I})]}{\xi_{op}} \right), \tag{1.37}$$

where $d\,[R_\alpha, S(\mathcal{I})]$ is the distance between R_α and the furthest degree of freedom in $S(\mathcal{I})$. This has to be understood as a statement about the typical decay of the coefficients -with respect to the realization of the randomness.

This spatial structure implies that the expansion (1.35) is not structureless: the typical value of the coefficients $h_{\alpha\beta\ldots}$ is expected to decay exponentially in the distance between the localization centers of the corresponding operators, on the scale [7] ξ_{op}. This is a key ingredient for MBL: the interactions between the I_α induce dephasing, which occurs over

[7] The length scale ξ_{op} is presumably not the same length scale governing the decay of the correlations of local observables in individual eigenstates, cfr. Eq. (1.29). The latter is expected to exhibit a dependence on the energy, which is generated since not all the terms in the expansion (1.36) survive when projected onto specific eigenstates: the coefficients of the surviving terms set the eigenstate-dependent length-scale $\xi(E)$.

a broad range of time scales due to the exponential [8] structure.

The phenomenological models in [153, 80, 166] assume two additional features for the conserved quantity, namely that (i) the I_α have binary spectrum, and thus can be considered as effective spins (or occupation number) operators, and (ii) the full spin (or fermionic) algebra can be constructed, with ladder operators $I_\alpha^\pm$. This follows straightforwardly from the construction in [86], see Sec. 2.3, where the conserved quantities of the chain (1.11) are obtained from the Pauli operators σ_a^z by means of a unitary rotation $\mathcal{U}$, $I_\alpha = \mathcal{U}^\dagger \sigma_a^z \mathcal{U}$ and $I_\alpha^\pm = \mathcal{U}^\dagger \sigma_a^\pm \mathcal{U}$, that obviously preserves the spectrum and the commutation relations. Additionally, the operators I_α are expected to be a weak deformation of the local degrees of freedom that are conserved by the non-interacting part of the Hamiltonian, either n_α for (1.9) or σ_a^z for (1.10). This is implicit in all the constructions of conserved quantities proposed in the literature.

1.3.1 The key dynamical feature: dephasing without dissipation

Following [155], we discuss the dynamics given by the model (1.35), which consists in dephasing processes involving the elementary excitations I_α. We assume that I_α is an effective spin, with spectrum $\mathrm{spec}(I_\alpha) = \{i_\alpha\} = \{\pm 1\}$, and denote with $|+\rangle_\alpha$ and $|-\rangle_\alpha$ the corresponding eigenstates. Dephasing refers to the suppression of the off-diagonal matrix elements of the reduced density matrix associated to a given subsystem, which reflects the loss of coherence due to the interaction with the surrounding degrees of freedom. When the subsystem is a single $I_{\overline{\alpha}}$ degree of freedom, the suppression is power law in time; this is most easily shown considering an initial state that is a product state in the I_α basis, parametrized as

$$|\psi\rangle = \otimes_{\alpha=1}^{N} \left(A_{\alpha,+}|+\rangle_\alpha + A_{\alpha,-}|-\rangle_\alpha \right). \tag{1.38}$$

The reduced density matrix associated to one $I_{\overline{\alpha}}$ operator reads

$$\rho_{\overline{\alpha}}(t) = \begin{pmatrix} |A_{\overline{\alpha},+}|^2 & A^*_{\overline{\alpha},-} A_{\overline{\alpha},+} \sum_{I'} P_{I'} e^{i(E_+(I')-E_-(I'))t} \\ A_{\overline{\alpha},-} A^*_{\overline{\alpha},+} \sum_{I'} P_{I'} e^{-i(E_+(I')-E_-(I'))t} & |A_{\overline{\alpha},-}|^2 \end{pmatrix}, \tag{1.39}$$

where I' is a configurations of all other I_α effective spins except $I_{\overline{\alpha}}$, $P_{I'} = \prod_{\alpha \neq \overline{a}} |A_{\alpha,i'_\alpha}|^2$ its probability in the state (1.38) and:

$$E_1(I') = h_{\overline{\alpha}} + \sum_{\alpha \neq \overline{\alpha}} h_{\overline{\alpha}\alpha} i'_\alpha + \sum_{\alpha,\beta \neq \overline{\alpha}} h_{\overline{\alpha}\alpha\beta} i'_\alpha i'_\beta + \cdots . \tag{1.40}$$

The terms in (1.40) which contain quantum numbers i'_α of operators I_α localized at maximal distance $d = d(\alpha, \overline{\alpha})$ form $I_{\overline{\alpha}}$ decay as $\sim H_0\, e^{-d/\xi_{op}}$ with H_0 some typical energy scale. This exponential decay implies that degrees of freedom dephase on a sequence of

[8] In the non interacting limit (i.e., in the fermionic language, when the Hamiltonian is quadratic), the Hamiltonian is a *linear* functional $H = \sum_\alpha E_\alpha n_\alpha$ of the conserved operators, that are the occupation numbers n_α of the single-particle eigenstates.

time scales depending on their distance from $I_{\overline{\alpha}}$: at a given time t, the phases in (1.39) that are effectively randomized correspond to those d for which $H_0 e^{-d/\xi_{op}}\ t \gtrsim 1$, and thus only the degrees of freedom at distance

$$d(t) \sim \xi_{op} \log(H_0 t) \tag{1.41}$$

have dephased. For any t, we can thus split

$$E_+(I') = E_+^{\leq d(t)}(I') + E_+^{>d(t)}(I'), \tag{1.42}$$

where $E_+^{>d(t)}(I')$ depends only on quantum numbers i'_α of operators localized at distance $d(\alpha, \overline{\alpha}) > d(t)$. Under the assumption that the $P_{I'}$ are all approximately equal ($A_{\alpha,-} \simeq A_{\alpha,+} \simeq 1/\sqrt{2}$), it holds:

$$\sum_{I'} P_{I'} e^{i(E_+(I')-E_-(I'))t} \sim \frac{1}{2^{|\Lambda|}} \sum_{\substack{i'_\alpha=\pm 1 \\ \alpha: d(\alpha,\overline{\alpha})>d(t)}} e^{2iE_+^{>d(t)}(I')} \left[\sum_{\substack{i'_\beta=\pm 1 \\ \beta: d(\beta,\overline{\alpha})\leq d(t)}} e^{2iE_+^{\leq d(t)}(I')} \right]. \tag{1.43}$$

The sum in square brackets in (1.43) is a sum over $N(t) \sim 2^{2d(t)}$ random numbers of zero mean, which decays as $(N(t))^{-1/2}$; thus

$$[\rho_{\overline{\alpha}}(t)]_{12} \sim \frac{1}{\sqrt{N(t)}} \sim \left(\frac{1}{H_0 t}\right)^{C\xi_{op}}, \tag{1.44}$$

with $C = \log 2$. It follows that the expectation values of the $I_\alpha^\pm$ on the time evolved (1.38) decay as a power law; the same holds true (with different C) for a generic initial state, and for the operator-strings

$$\Pi_{\vec{\alpha}}^{\vec{z}} = I_{\alpha_1}^{z_1} I_{\alpha_2}^{z_2} \cdots I_{\alpha_n}^{z_n}, \tag{1.45}$$

with $\vec{\alpha} = (\alpha_1 \cdots \alpha_n)$, $\vec{z} = (z_1 \cdots z_n)$, $z_i \in \{+, -, 1\}$ and $I_\alpha^1 \equiv I_\alpha$, containing *at least* a pair of $I_\alpha^\pm$ terms [155]. Note that the diagonal matrix elements in (1.39) are time independent, as it follows from the fact that the I_α are constants of motion.

We reviewed this discussion in view of the fact that the scaling (1.41) plays an important role in understanding the peculiar dynamical features of MBL systems, as it appears in the following section.

1.3.2 A comprehensive characterization of MBL

We now discuss how the MBL features recalled in Sec. 1.2 follow from the existence of quasilocal conserved operators with exponentially decaying mutual interactions.

(i) *Suppression of transport:* we report the argument given in [149]. The Kubo formula for the DC conductivity σ at inverse temperature β associated to a local current

density J_r reads:

$$\mathrm{Re}[\sigma(\omega\to 0)] = \frac{\pi\beta}{\Omega}\sum_{r'r}\sum_{m,m'}\frac{e^{-\beta E_{m'}}}{\mathcal{Z}}\langle m'|J_{r'+r}|m\rangle\langle m|J_{r'}|m'\rangle\ \delta_\eta\left(E_{m'}-E_m\right), \tag{1.46}$$

where Ω is the system's volume, $\mathcal{Z}$ is the partition function, $|m\rangle$ the system's eigenstates and $\delta_\eta(x) = \pi^{-1}\eta/(x^2+\eta^2)$ a regularized δ-function. Let us first consider a complete set of strictly local conserved quantities, acting on degrees of freedom that belong to a compact spatial region with finite diameter ζ. Since the set is complete, for any pair m, m' there is a $\tilde{I}$ such that $\tilde{I}|m\rangle = \tilde{I}_m|m\rangle$ and $\tilde{I}|m'\rangle = \tilde{I}_{m'}|m'\rangle$ and $\tilde{I}_{m'} \neq \tilde{I}_m$. For a strictly local current operator and $r > \zeta$, one of the two current matrix elements

$$\langle m'|J_{r'}|m\rangle = \frac{\langle m'|\left[J_{r'},\tilde{I}\right]|m\rangle}{\left(\tilde{I}_m-\tilde{I}_{m'}\right)}, \quad \langle m'|J_{r'+r}|m\rangle = \frac{\langle m'|\left[J_{r'+r},\tilde{I}\right]|m\rangle}{\left(\tilde{I}_m-\tilde{I}_{m'}\right)} \tag{1.47}$$

is exactly zero: in Eq. (1.46) the sum over r is restricted to $r \lesssim \zeta$. Furthermore, for any m the sum over m' is restricted to a finite set, since $J_{r'}|m\rangle$ can differ only in a finite number ($\leq \exp(c\zeta^d)$, with $c = O(1)$) of integrals of motion from $|m\rangle$. Thus, in the thermodynamic limit, when $\eta \to 0$, the contribution to the δ-function vanishes with probability one, and $\mathrm{Re}[\sigma(\omega=0)] = 0$ [9].

For quasilocal conserved quantities, the matrix elements $\langle m'|J_{r'}|m\rangle$ are not exactly zero also for those eigenstates for which $\tilde{I}$ is supported at distance $x\zeta$ from r': they are exponentially small in x. Since there are also exponentially many states m, m' which satisfy these criteria, some energy differences $E_m - E'_m$ in (1.46) become exponentially small. The competition between the matrix elements and the energy denominators is however dominated by the exponential decay of the matrix elements with probability one: this is the key statement that guarantees the existence of quasilocal I_α (see the following chapter). It follows that the conductivity remains zero when quasilocality is properly taken into account.

(ii) *Low entanglement in eigenstates:* all the eigenstates of (1.35) are product states of the approximately-local quantities I_α: their bipartite entanglement entropy is area-law, as the bipartition only affects the I_α that are localized in the vicinity of the cut.

(iii) *Ergodicity breaking and violation of ETH:* as in ordinary integrable systems, the locality of the conserved quantities implies that local memory of the initial condition is preserved at any time, thus preventing thermalization in the sense of (1.7). Moreover, since the many-body eigenstates are simultaneous eigenstates of operators that are weak deformations of the n_α (or σ^z_a), the expectation value of the latter operators does not depart significantly from ± 1: it is non-thermal and it fluctuates

[9] Note that the potentially singular term from $m = m'$ does not contribute because $\langle m|J_r|m\rangle = 0$ by time reversal invariance.

significantly between states that are close in energy, since such states might differ by the eigenvalues of integrals of motion having large overlap with n_α (or σ^z_α).

(iv) *Absence of level repulsion:* The absence of level repulsion arises because adjacent states in the spectrum typically differ by an extensive number of eigenvalues of the I_α: they are unable to hybridize and thus do not repel at the scale of the mean level spacing.

(v) *Slow growth of entanglement:* the logarithmic growth of the bipartite entanglement entropy $S(t)$ follows from the relation (1.41), which determines the number of degrees of freedom in the left-half of the system that have entangled with the right-half at time t [79, 154]. A Lieb-Robinson bound[10] with a logarithmic lightcone has been derived in [99] under a stronger assumption of quasilocality of the conserved quantities, formulated in terms of averages rather than in probability, i.e., requiring that

$$\mathbb{E}\left[\|[I_\alpha, \mathrm{O}]\|\right] \leq e^{-x/\xi}||\mathrm{O}|| \tag{1.48}$$

for a constant ξ and any operator O whose support is at distance x from the localization center of I_α. The bound implies that the growth of the bipartite entanglement entropy is at most logarithmic.

(vi) *Power law decay of expectation values:* Consider an operator O with *finite support* (i.e., a functional of a finite number of Pauli or fermionic operators); expanded in the basis of the $I_\alpha, I^\pm_\alpha$ it reads

$$\mathrm{O} = \sum_{\vec{\alpha}} \mathcal{C}_{\vec{\alpha}}\ (I_{\alpha_1} I_{\alpha_2} \cdots I_{\alpha_n}) + \sum_{\vec{\alpha},\vec{z}} \mathcal{B}_{\vec{\alpha},\vec{z}}\, \Pi^{\vec{z}}_{\vec{\alpha}} = \overline{\mathrm{O}} + \mathrm{O}_{osc}, \tag{1.49}$$

where $\Pi^{\vec{z}}_{\vec{\alpha}}$ defined in (1.45), and thus O_{osc}, contain $I^\pm_\alpha$ terms, while

$$\overline{\mathrm{O}} = \lim_{T\to\infty} \frac{1}{T}\int_0^T \mathrm{O}(t)\, dt = \sum_{\vec{\alpha}} \mathcal{C}_{\vec{\alpha}}\ (I_{\alpha_1} I_{\alpha_2} \cdots I_{\alpha_n}) \tag{1.50}$$

commutes with (1.35). Due to the quasilocality of the I_α and the locality of O, the coefficients $\mathcal{C}_{\vec{\alpha}}$ have themselves an exponentially decaying structure. Let $|\psi\rangle = \sum_I A_I\, |I\rangle$ be an initial state expanded in the basis of simultaneous eigenstates $|I\rangle$ of the I_α. The arguments in Sec. 1.3.1 imply that the second term in

$$\langle\psi(t)|\mathrm{O}|\psi(t)\rangle = \sum_I |A_I|^2 \langle I|\overline{\mathrm{O}}|I\rangle + \sum_{I,J} A_I A^*_J e^{i(E_J - E_I)t} \langle J|\mathrm{O}_{osc}|I\rangle \tag{1.51}$$

decays as a power law in time, due to the randomization of the relative phases in the eigenstates decomposition. The expectation value (1.51) thus exhibits a power law relaxation to the constant, non-thermal value $\sum_I |A_I|^2 \langle I|\overline{\mathrm{O}}|I\rangle$.

[10] The Lieb-Robinson bounds limit the speed at which the information propagates under the dynamics given by quantum many-body systems with local interactions. They state that an effective "speed of light" exists, defining an effective "lightcone", such that correlations outside the lightcone are exponentially suppressed in their distance [104].

These considerations suggest that the existence of quasilocal integrals of motion may be considered as a fundamental defining property of Many-Body Localization. Note that also the scenario mentioned in Sec. 1.2.9, involving systems that are MBL in the thermodynamic limit but nevertheless satisfy the ETH at any finite size, can be justified by assuming the existence of a set of quasi-local operators ("l^*-bits" in the language of [38]) that are *approximately* conserved at any finite size, such that their commutator with the finite size Hamiltonian is not exactly zero but vanishes exponentially in the system size.

1.3.3 The role of disorder: a robust integrability

We have argued above that the quantum ergodicity breaking in MBL systems can be explained in terms of an "emergent integrability". Of course, quantum ergodicity breaking is not an exclusive feature of disordered systems: extensive sets of commuting local conserved quantities exist in "ordinary" integrable systems, by which we mean systems satisfying the Yang-Baxter relations [164, 125]. However, there are two essential differences: (1) while ordinary integrability is not robust with respect to arbitrary local perturbations, the fact that an extensive set of quasilocal operators exists in the MBL phase remains true when the MBL system is perturbed locally (although the detailed structure of the I_α might change); (2) the spatial structure of the conserved quantities differs in the two cases, with relevant implications for the transport properties of the systems.

Ordinary integrable systems are characterized by the fact that arbitrary multi-particle scattering process can be factorized in terms of subsequent two-particle scattering events; the Yang-Baxter relations constraint the two-particle scattering matrix in a way that encodes this factorization. Given this structure, an extensive set of integrals of motion I_k can be systematically constructed[11] as derivatives of a generating function,

$$O_k = \frac{\partial^k}{\partial^k u} \log T(u)\Big|_{u=0}, \tag{1.52}$$

where $T(u)$ is a member of a one parameter family of commuting transfer matrices $T(u)$. The commutativity $[T(u), T(u')] = 0$ is guaranteed by the validity of the Yang-Baxter equations. Since the Hamiltonian is itself a member of the commuting family, $O_1 = H$, it follows that all other operators are conserved.

The logarithm in (1.52) guarantees [110] that the operators O_k are "extensive local conserved charges", where local means that they are sums over all lattice sites of densities having compact support (this is the same notion of locality that applies to the Hamiltonian itself)[12]. Thus, the expansion of an operator O_k involves the full set of local, physical

[11] Despite its compact formulation, this recipe turns out to be often computationally impractical: the spectral properties of integrable systems are thus usually obtained by means of alternative methods, such as Bethe Ansatz techniques.

[12] Conserved charges satisfying a weaker notion of locality (also dubbed "quasilocality") have been introduced for clean integrable systems as well [84]; however, the notion of quasilocality in that context is different with respect to the one expressed in (1.37), and it refers to the fact that the density is quasilocal,

degrees of freedom. In contrast, quasilocal operators in MBL are well-approximated (in norm) by their truncation to finite volumes of size ξ_{op}: the truncation itself is approximately conserved, as it commutes with the Hamiltonian up to exponentially small errors. This exponential decay is the exclusive feature of disordered systems, resulting from the local separation of scales produced by the randomness (as it appears in the perturbative setting, see Sec. 1.4.4). As argued in 1.3.2(i), it is this structure that implies the vanishing of the diffusion coefficient, as opposed to the efficient transport in clean integrable systems [112, 165, 181, 180].

For MBL systems, no Yang-Baxter-based recipe such as (1.52) is available; this raises the question of which is the best recipe to construct the conserved quantities, which optimizes the locality of the resulting operators. Their exponential localization suggests that any such recipe should build the I_α as local deformations of the local, physical degrees of freedom: this idea is at the root of the perturbative construction discussed in the following chapter.

1.4 The mechanism for localization: perturbative arguments

In this section, we review the perturbative arguments developed in [10, 20, 72] to argue for the existence of the localized phase and its stability with respect to weak scattering processes. The perturbative treatment illustrates the main mechanism by which the quenched disorder generates localization: hopping (or scattering) processes are typically associated to large energy mismatches, and thus they are suppressed being typically off-shell, that appear as large denominators in the perturbation theory, guaranteeing its convergence. In reviewing these arguments, we comment on the role of rare fluctuations of the randomness giving rise to resonances, and introduce an approximation scheme (which we refer to as the "forward approximation") that is exploited throughout the following chapters.

1.4.1 Anderson's logic: the relevant divergences signaling delocalization

Anderson's argument for single-particle localization relies on the perturbative expansion for the local self energy in (1.13),

$$S_a(z) = \sum_{\text{loops}(a)} V_{as_n} \prod_{i=1}^{n} \frac{V_{s_i s_{i-1}}}{z - \epsilon_{s_i}}, \tag{1.53}$$

where the sum is over all the loops $l = (s_0 = a, s_1, \cdots, s_{n+1} = a)$ in Λ that include the site a only as a starting and ending point, the weight of each loop being the product of "locators" $V_{ij}(z - \epsilon_i)^{-1}$. The expansion is derived from the perturbative series for the

rather than the conserved quantity itself.

propagator

$$G_{ba}(z) = \frac{1}{z-\epsilon_a}\left[\delta_{ab} + \frac{V_{ba}}{z-\epsilon_b} + \sum_c \frac{V_{bc}}{z-\epsilon_b}\frac{V_{ca}}{z-\epsilon_c} + \cdots\right] = \frac{1}{z-\epsilon_a}\sum_{\text{paths}(a,b)}\prod_{i=1}^{n}\frac{V_{s_i s_{i-1}}}{z-\epsilon_{s_i}}, \tag{1.54}$$

obtained by means of iteration of the operator identity:

$$G(z) = \frac{1}{z-H_{\text{And}}^{(0)}} + \frac{1}{z-H_{\text{And}}^{(0)}}V_{\text{And}}\frac{1}{z-H_{\text{And}}} = G_0(z) + G_0(z)\; V_{\text{And}}\; G(z). \tag{1.55}$$

Due to the boundedness of the spectrum of H_{And}, the series converges at least for $\Im z = \eta$ sufficiently large. As pointed out by Anderson, the convergence of the expansion (1.53) when approaching the real axis implies localization, as the criterion (1.19) holds true at any finite order in perturbation theory with probability one. To lowest order in V_{And}, for instance, the distribution of the random variable

$$\Im S_a^{(1)}(E+i\eta) = -\eta\sum_{c\neq a}\frac{|V_{ac}|^2}{(E-\epsilon_c)^2+\eta^2} \tag{1.56}$$

is heavy-tailed, with a typical value which is finite for η finite, but goes to zero with $\eta \to 0$. Since this argument extends to any order in V, it follows that the violation of (1.19) requires that the full perturbative series diverges, in such a way that the analysis order-by-order in V_{And} becomes meaningless. The problem has thus to be addressed directly in the thermodynamic limit, sending $\eta \to 0$ only once the limit $|\Lambda| \to \infty$ is performed; the two limits do not commute, as in problems in which spontaneous symmetry breaking occurs.

The issue of convergence has, however, to be addressed properly, as divergent subsequences in (1.53) appear almost surely, while they *do not* necessarily signal delocalization. These divergences are generated by the *repetition* of large factors that are present almost surely in (1.53) for z sufficiently close the real axis. For instance, a large factor appears to lowest order in the hopping whenever there are two neighboring resonant fields $\epsilon_a \approx \epsilon_b$, so that for $E \sim \epsilon_a$ and η small

$$\left|\frac{V_{ab}}{E+i\eta-\epsilon_a}\frac{V_{bc}}{E+i\eta-\epsilon_b}\right| > 1. \tag{1.57}$$

Since the sum (1.53) contains all possible paths bouncing back and forth between the sites a and b, which contribute with arbitrarily large powers of the factor (1.57), the expansion diverges at $\eta \to 0$.

This divergence signals that a local resonance occurs between the two almost degenerate eigenstates of $H_{\text{And}}^{(0)}$ localized at a, b, whose accidental degeneracy is lifted by the hopping, that hybridizes the local degrees of freedom in a non-perturbative way. In the localized phase, resonances are present, but remain typically confined within a finite region of space of the size of the localization length, which defines the length scale over which the

local degrees of freedom hybridize. At larger scales in the localized phase, resonances become sufficiently rare for the perturbation theory to be asymptotically well defined. On the contrary, delocalization is signaled by the fact that large resonant segments

$$\left| \frac{V_{i_1 k_{n-1}}}{z-\epsilon_{i_1}} \cdots \frac{V_{k_1 i_n}}{z-\epsilon_{k_1}} \frac{V_{i_n i_{n-1}}}{z-\epsilon_{i_n}} \cdots \frac{V_{i_2 i_1}}{z-\epsilon_{i_2}} \right| > 1 \tag{1.58}$$

appear at arbitrarily large n. This means that the hopping keeps mixing degrees of freedom at large distance, producing extended eigenstates.

1.4.2 Local resummations and "renormalized" perturbation theory

Divergences such as the one discussed above can be cured by means of a resummation of the subsequence containing all higher powers of the resonant term. For instance, in the case of the first order resonance (1.57), one considers the set of all loops that reach site b (from some other site c in the lattice), repeatedly jump back and forth the sites a, b, and eventually leave site b jumping to some other site d. Resumming the corresponding weights one obtains:

$$\frac{V_{db}}{z-\epsilon_d}\left[1+\frac{V_{ba}}{z-\epsilon_b}\frac{V_{ab}}{z-\epsilon_a}+\left(\frac{V_{ba}}{z-\epsilon_b}\frac{V_{ab}}{z-\epsilon_a}\right)^2+\cdots\right]\frac{V_{bc}}{z-\epsilon_b}\cdots=\frac{V_{db}}{z-\epsilon_d}\left[\frac{V_{bc}}{z-\epsilon_b-\frac{|V_{ba}|^2}{z-\epsilon_a}}\right]\cdots \tag{1.59}$$

The correction in the denominator (1.59) is exactly the self energy that one would get at site b solving exactly the two level system made out of the sites a, b. Thus, this resummation is equivalent to a local exact diagonalization (see Sec. 3.2.4 for an example at the operator level).

The resummations can be carried on systematically at any order, resulting in an expansion over *self-avoiding* loops, abbreviated as sloops(a):

$$S_a(z)=\sum_{\text{sloops}(a)}\omega_{sl}=\sum_{n=0}^{\infty}\left[\sum_{\text{sloops}(a;n)}\omega_{sl}\right]\equiv\sum_{n=0}^{\infty}s_a^{(n)}(z), \tag{1.60}$$

where $s_a^{(n)}(z)$ sums the contributions of all loops of length n. The weight of a loop $sl=(a,j_1,j_2,\cdots,a)$, with $j_l\neq j_k$ for $l\neq k$, equals

$$\omega_{sl}=V_{aj_n}\frac{V_{j_n j_{n-1}}}{z-\epsilon_{j_n}-S_{j_n}^{(a,\cdots,j_{n-1})}(z)}\cdots\frac{V_{j_2 j_1}}{z-\epsilon_{j_2}-S_{j_2}^{(a,j_1)}(z)}\frac{V_{j_1 a}}{z-\epsilon_{j_1}-S_{j_1}^{(a)}(z)}, \tag{1.61}$$

where $S_d^{(a,b,c)}$ is the sum over all loops starting and ending in d, never visiting d again nor any of the sites a, b, c, of loop weights of the form (1.53). This "renormalized" expansion is obtained as for (1.59): consider (1.61), and consider the set of all paths in (1.53) hopping to a site j_1, going back to it arbitrarily many times, and sharing the subsequent history once they leave site j_1. For $\Im z$ large enough, the sum over all possible loops

around j_1 (never going back to site a) converges. Its resummation $S^{(a)}_{j_1}(z)$ is the self-energy correction in (1.61); this step is iterated for every site along the loop. Finally, the self-energy corrections can themselves be expanded in terms of self-avoiding loops performing an analogous resummation.

The above manipulation can be safely performed for $\Im z$ large enough. Localization occurs in the regime of parameters in which (1.60) is still convergent for $\Im z = \eta \to 0$. This in turn requires that the expansion of each self-energy correction in the denominators is itself convergent in this limit. The whole procedure can be thought of as a self-consistent argument: the resummation is performed assuming that resonances do not proliferate in space at arbitrary distance, in such a way that the series for the self-energy corrections converges when approaching the real axis. Then, the convergence of the renormalized series for $S_a(z)$ is analyzed, to check self-consistently the assumption.

1.4.3 Closing the equations: the Bethe lattice case

The random variable (1.60) is difficult to treat probabilistically due to the statistical correlations between the self-energy corrections appearing in the denominators. For instance, the terms $S^{(a)}_{j_1}(z)$ for the various sites j_1 that are nearest neighbors of a contain the same local random fields, since even if the site a is removed, there are still loops surrounding each j_1 which contain some other j_1'. This type of correlations is absent in lattices having a tree structure such as the Bethe lattice: in that case, the expansion (1.60) simplifies substantially, as the only loops around site a that are self-avoiding are the ones of the form $sl = (a, j_1, a)$ with j_1 a nearest neighbor of site a. This implies

$$S_a(z) = \sum_{j=1}^{K+1} \frac{V_{aj}^2}{z - \epsilon_j - S_j^{(a)}(z)} \equiv \sum_{j:\langle j,a\rangle} \frac{V_{aj}^2}{z - \epsilon_j - \Sigma_j^{\text{cav}}(z)}, \tag{1.62}$$

where j labels the sites that are nearest neighbors of site a, and $K+1$ is the connectivity of the lattice. In (1.62), $\Sigma_j^{\text{cav}}(z)$ is a cavity self-energy, i.e., it is the local self energy at the vertex of the sub-tree rooted in j, obtained from the Bethe lattice once the site a is removed. It satisfies the recursion:

$$\Sigma_j^{\text{cav}}(z) = \sum_{l=1}^{K} \frac{V_{jl}^2}{z - \epsilon_l - \Sigma_l^{\text{cav}}(z)}. \tag{1.63}$$

The variables $\Sigma_l^{\text{cav}}(z)$ in (1.62) are independent for $l \neq l'$, and equally distributed in the thermodynamic limit. Thus, (1.63) is a self-consistency equation for their distribution. In particular, for $z = E + i\eta$,

$$\Gamma_j(z) = \sum_{l=1}^{K} \frac{V_{jl}^2}{(E - \epsilon_l - \Re\Sigma_l^{\text{cav}}(z))^2 + (\eta + \Gamma_l(z))^2} \left[\eta + \Gamma_l(z)\right], \tag{1.64}$$

where $\Gamma_j(z) = -\Im\Sigma_j^{\text{cav}}(z)$, and a similar equation holds for $\Re\Sigma_j^{\text{cav}}(z)$. Exactly at $\eta = 0$, (1.64) admits as a solution a distribution supported on the real axis, $\Im\Sigma_j^{\text{cav}}(z) = 0$. In

the localized phase, this solution is stable with respect to the perturbation $E \to E + i\eta$, meaning that the self-consistent distribution of $\Sigma^{\text{cav}}(E + i\eta)$ converges to a distribution supported on the real axis as $\eta \to 0$, cfr. (1.19). The analysis of the stability of this solution is performed in [2, 6], where an exact criterion for localization is obtained by linearizing (1.64) around $\Im\Sigma^{\text{cav}} = 0$. In [6], the criterion is derived iterating the linearized equation, which yields

$$\Gamma_j(z) = \left(\sum_{\text{paths: } j \to \partial L} \prod_{i=1}^{L} \left[\frac{V_{s_{i-1}s_i}}{E - \epsilon_{s_i} - \Re\Sigma^{\text{cav}}_{s_i}(z)} \right]^2 \right) \Gamma_{s_L}(z), \tag{1.65}$$

where the sum is over all paths $(s_0 = j, s_1, \cdots, s_L)$ from site j to any of the K^L sites $s_L \in \partial L$ at distance L. The stability requires the typical value of the sum in brackets in (1.65) to decay exponentially with L as $\eta \to 0$. Intuitively, this corresponds to the fact that the susceptibility of local levels in the bulk with respect to an infinitesimal coupling to a bath at the boundary sites $s_L \in \partial L$ (inducing a broadening Γ_{s_L} of the local levels) decays to zero in the thermodynamic limit, implying that the effect of the infinitesimal bath at the boundary does not "propagate" to the bulk[13]. In the approximation in which the real parts of the self energies are neglected, this decay condition yields the criterion:

$$\frac{2eVK}{W} \log\left(\frac{W}{2V}\right) < 1, \tag{1.66}$$

for $E = 0$ and $V_{ab} \equiv V$. The same critical condition is found in the framework developed in [2] setting $\Re\Sigma^{\text{cav}} \equiv 0$ (i.e., imposing its distribution to be a delta function in zero), and in [9] with a calculation on the probability of resonances similar to the one reported in the following section.

1.4.4 Finite d and the forward approximation

In [10, 168], the convergence radius of the perturbative expansion is estimated by computing the probability that (1.60) is dominated by a convergent geometric series, i.e. that there exists a $z < 1$ such that:

$$P_{a,N} \equiv \mathbb{P}\left(\forall n > N, |s_a^{(n)}(E)| < z^n\right) \overset{N\to\infty}{\longrightarrow} 1. \tag{1.67}$$

This is done within the forward approximation, which consists in neglecting the self-energy corrections in (1.61). As a consequence, the weight of each loop reduces to a product of independent random variables, as the original loop weights in (1.53); in fact, this approximation amounts to restricting the sum (1.53) to only the loops that are self-avoiding, neglecting the loops that go back to already-visited sites (hence the term "forward").

[13] More rigorously, it is proved in [6] that the exponential increase with L of the typical value of the sum in (1.65) implies a violation of a tightness condition of the distribution of the imaginary part of the cavity propagators, implying that the hypothesis that $\Im\Sigma^{\text{cav}} = 0$ is inconsistent.

Exponential bounds of the form (1.67) are expected to hold if the fluctuations of the random fields ϵ_i are large ($W \gg V$), as typically $V/\epsilon_i \sim V/W$, and thus the typical value of each loop weight scales as $(V/W)^n$. In particular, resonances of the form (1.57),(1.58) are rare, due to the local separation of scales produced by the uncorrelated randomness. Indeed, since the probability that two instances ϵ_i, ϵ_j both lie within the same interval $[E-\delta, E+\delta]$ is of order $O(\delta^2/W^2)$, for small δ a large portion of the lattice needs to be sampled to find two such local fields. The corresponding sites are typically at a distance $R(\delta)$ which is large, with an effective coupling that is exponentially suppressed in this distance, $\sim V\exp(-R(\delta)/\xi)$: in the localized phase, typically $\delta > V\exp(-R(\delta)/\xi)$ and the pair is not resonant. On the contrary, inspecting the potential locally in space, one shall typically find $|\epsilon_i - \epsilon_j| \sim W$, i.e., local energy mismatches of $O(W)$ are generated by the quenched disorder.

This reasoning holds for typical values of single loop weights. The probabilistic statement (1.67) requires, however, to control the rare instances of the disorder giving rise to atypically large path weights, containing resonant segments, as such rare instances dominate the sum over loops of a given length. This means that the large deviations of the path weights have to be determined. For products of independent random variables, this can be easily obtained from the corresponding generating function. We briefly recall how the calculation of (1.67) is performed, as it bears some similarities with the one performed in the many-body case in the next chapter.

Consider $E = 0$ and $V_{ab} \equiv V$: for uniformly distributed local fields $\epsilon_a \in [-W/2, W/2]$, setting

$$|\omega_{sl}| = V \prod_{i=1}^{n} \frac{V}{|z - \epsilon_{j_i}|} \equiv V \left(\frac{2V}{W}\right)^n w_n, \tag{1.68}$$

one finds that the distribution of w_n equals

$$P_{w_n}(w) = \frac{(\log w)^{n-1}}{(n-1)! w^2}. \tag{1.69}$$

Thus, the weight of each loop has a fat-tailed distribution. In finite dimensions, the number of self-avoiding loops of length n scales exponentially with n, approximately as $\sim \kappa^n$ for some constant $\kappa = \kappa(d)$ depending on the dimensionality. Different loops are statistically correlated, due to their partial overlap in space. Assuming that these correlations are negligible, the distribution of $s_a^{(n)}(z)$ in (1.60) is obtained exploiting the fact that, due to the fat-tails of the distribution, the sum over the loops is dominated by the maximal term:

$$\begin{aligned} P\left(|s_a^{(n)}(z)| < z^n\right) &\approx P\left(\max_{\text{sloops}(a;n)} |\omega_{sl}| < z^n\right) \approx \left[P\left(|\omega_{sl}| < z^n\right)\right]^{K^n} \\ &\approx \exp\left[-K^n \log P\left(|\omega_{sl}| > z^n\right)\right]. \end{aligned} \tag{1.70}$$

Approximating

$$P\left(|\omega_{sl}| > z^n\right) = \int_{(Wz/2V)^n}^{\infty} d\omega\, P_{\omega_n}(\omega) \approx P_{\omega_n}\left(\frac{Wz}{2V}\right), \tag{1.71}$$

the probability in (1.67) is estimated to be

$$P_{a,N} \approx \prod_{n=N}^{\infty}\left(1 - \exp\left[-\left(\frac{2eV\kappa(d)}{Wz}\log\left(\frac{Wz}{2V}\right)\right)^n O(n^{-\frac{1}{2}})\right]\right). \tag{1.72}$$

Imposing the limiting condition (1.67) for $z \to 1$, one recovers the condition (1.66) with $K \to \kappa(d)$.

A criterion of the form (1.66) is found whenever the distribution of fat-tailed variables of the form (1.68) is sampled exponentially-many times; it originates in the competition between two exponentials in (1.70): the growth of the number of terms and the decay of the large deviation probability of each individual term; it states that the transition occurs when the maximal value obtained in the sampling is of order $O(1)$. Analogous results are recovered throughout the following chapters: they are derived in different settings, under the common assumption that the correlations between the random variables can be neglected, in such a way that an independent sampling can be performed. We analyze the validity of this assumption in Chapter 5.

The condition (1.66) is termed the "upper limit condition" in [10], as it overestimates the critical value of W/V at which the transition to the delocalized phase occurs. The reason for this is that the forward approximation exploited to derive (1.66) overestimates the effect of small denominators: indeed, suppose that the site j_2 in a self avoiding loop $i \to j_1 \to j_2 \cdots$ is resonant at the given energy, $V/|E - \epsilon_{j_2}| \gg 1$. Then, the locator corresponding to the previous site j_1 along the self-avoiding path has a huge self energy correction, since $S^{(i)}_{j_1}$ contains a factor

$$S^{(i)}_{j_1}(E) = V_{j_1 j_2}\frac{1}{E - \epsilon_{j_2}}V_{j_2 j_1} + \cdots. \tag{1.73}$$

The weight of the loop is thus

$$V_{ij_1}\frac{1}{E - \epsilon_{j_1} - \frac{V^2_{j_1 j_2}}{E-\epsilon_{j_2}} + \cdots}V_{j_1 j_2}\frac{1}{E - \epsilon_{j_2} - \cdots}, \tag{1.74}$$

so that for $E - \epsilon_{j_2} \to 0$ the divergence of the second locator is compensated by the divergence of the self-energy in the first locator. Small denominators essentially neutralize themselves by introducing enormous self-energies for the neighboring sites which then appear as very large denominators: the forward approximation misses this effect. The local resummations discussed in Sec. 1.4.2 thus enhance the convergence as compared to the naive perturbative expansion in the forward approximation. In single particle localization problems on the Bethe lattice with large connectivity, it is known that the critical hopping is increased by a factor $e/2$ [2, 14].

1.4.5 The many-body problem: a self-consistent approach

We now discuss the generalization of the above arguments to the many-body case. In [20], the scattering rate $\Gamma_\alpha(\epsilon)$ in (1.20) is obtained within the "imaginary Self-Consistent Born Approximation" (imSCBA). The SCBA resums a subset of diagrams of the perturbative expansion for the many-body self energies, and results in a self-consistent equation for $\Gamma_\alpha(\epsilon)$ having a structure similar to (1.64):

$$\Gamma_\alpha(\epsilon) = b + \pi \sum_{\beta,\gamma,\delta} |V_{\alpha\beta,\gamma\delta}|^2 \int d\epsilon' d\omega \, \mathscr{A}_\beta(\epsilon') \mathscr{A}_\gamma(\epsilon'+\omega) \mathscr{A}_\delta(\epsilon-\omega) \mathcal{F}\left(n_\beta, n_\gamma, n_\delta\right). \quad (1.75)$$

In (1.75), b is the infinitesimal coupling to the bath, $\mathcal{F}\left(n_\beta, n_\gamma, n_\delta\right) = n_\beta(1-n_\gamma)(1-n_\delta) + (1-n_\beta)n_\gamma n_\delta$ and $\mathscr{A}_\alpha(\epsilon)$ is the many-body spectral function

$$\mathscr{A}_\alpha(\epsilon) \approx \frac{1}{\pi} \frac{\Gamma_\alpha(\epsilon)}{(\epsilon - E_\alpha)^2 + \Gamma_\alpha^2(\epsilon)}, \quad (1.76)$$

defined from the retarded Green function (1.22) in an analogous way as (1.13). Note that in (1.76) the real part of the self-energy is neglected: hence the term "imaginary" in imSCBA.

In full analogy with the Bethe lattice case, the stability of the solution $\Gamma_\alpha(\epsilon) = 0$ with respect to the infinitesimal coupling to the bath is analyzed, by iterating the linearized version of (1.75). Note however that in the many-body case, the equation (1.75) is a closed equation for the scattering rate at *fixed* occupations n_α (we neglected the functional dependence of Γ_α on $\{n_\alpha\}$ in the notation). The time-evolution of the occupations is given by the Boltzmann equation; to address the localized regime, the authors of [20] perform the average in (1.22) over the subset of non-interacting Fock states (on which $n_\alpha = \pm 1$) at a fixed energy density E. The latter is parametrized in terms of a temperature T, which corresponds to the typical energy range over which the single particle excitations contributing to the Fock state are distributed [14]. In the many-body case, the stability analysis requires to estimate the typical size of the sum of all scattering amplitudes generated by the iteration of (1.75), at any given order in the interaction. This is done in [72, 20], where it is argued that the stability breaks down at a critical value of temperature (and not of the intensive energy ϵ of the excitation) that is estimated to be:

$$\frac{T_c}{\delta_\xi} = \frac{C}{\lambda \log(1/\lambda)}, \quad (1.77)$$

where δ_ξ, λ are defined in Eqs. (1.24), (1.25). Not surprisingly, the self-consistent approximation produces an estimate of the Bethe lattice form (1.66), with an effective connectivity $K_{\text{eff}} = T/\delta_\xi$ and the interaction strength replacing the hopping strength.

The analysis in [72, 20] is to some extent analogous to the evaluation of probabilistic

[14] Reasoning as in [73], one might estimate this energy scale by saying that in typical Fock states with energy E above the ground state, the energy is split among $N_E \sim (E/\Delta)^{1/2}$ excitations, where this estimate is done accounting for Fermi statistics ($E \sim \sum_{k=1}^{N_E} k\,\Delta \sim \Delta N_E^2$, with Δ the average level spacing between single-particle levels). Thus, each excitation has a characteristic energy of the order of $T \sim E/N_E \sim (E\Delta)^{\frac{1}{2}}$.

bounds on the sum over path weights in Anderson's single-particle treatment. A similar calculation is performed in the following chapter, when estimating the convergence of the perturbation theory for conserved quantities. In particular, the SCBA generates self-energy diagrams corresponding to decay processes where the number of quasiparticles produced in the final state is maximized, thus maximizing the phase space available for the decay: the same class of diagrams in considered in Sec. 2.2.2. They appear naturally in that framework (that is formulated in the language of an effective single-particle problem) as the terms corresponding to self-avoiding paths in a lattice whose sites correspond to Fock states. This connects with Anderson's upper limit approximation recalled above.

In the many body case, however, the validity of the approximations under which (1.77) is derived is a more subtle issue. It is argued in [49] that the prediction of a transition at a finite temperature is a feature of the ImSCBA, which is unstable with respect to the reinstatement of those scattering processes neglected in this approximation. Moreover, the treatments in [72] and [20] (as well as the one discussed in the following chapter) do not account for the phenomenon of spectral diffusion, which has been recently argued to enhance delocalization [30], reducing substantially the estimated critical temperature (1.77). We discuss in more details these caveats in Secs. 1.5.1, 2.4 and 2.2.6(D), respectively.

1.4.6 The breakdown of perturbation theory: what does it imply?

In the following chapters, we provide estimates for the boundary of stability of the localized phase based on perturbative arguments. A word of caution is however in place. Anderson's criterion for localization, as well as its extension to the many-body case, are *sufficient* but not necessary for localization. In other words, the breakdown of perturbation theory does not necessarily entail delocalization. This is clear in the single particle case, where the system's behavior for large hopping depends on dimensionality: in $d \geq 3$ the divergence of perturbation theory signals a transition to delocalization, whereas in one or two dimensions it only indicates a crossover to a *weakly localized* phase, in which localization emerges due to the destructive interference among the trajectories of the "quantum random walker" that return to the origin, whose amplitudes sum up coherently in the quantum case.

A phenomenological description of the role of dimensionality in the single particle case is given within the scaling theory of localization developed in [3], which we briefly recall. The essential ingredient is the Thouless dimensionless conductance $g(L)$, introduced in [55] to characterize disordered samples of size L and defined as $g(L) = \delta E(L)/\Delta(L)$, with $\Delta(L) = 1/\nu L^d$ the mean spacing between the energy levels in the sample, and $\delta E(L)$ the typical variation $|\delta^2 E_\alpha/\delta\phi^2|$ of the eigenvalues E_α when replacing the periodic boundary conditions by twisted ones. The energy scale $\delta E(L)$ characterizes the sensitivity of the finite system to perturbations at the boundary: it is exponentially decaying for localized systems with $L \gtrsim \xi$, while it equals $\delta E(L) = \hbar D/L^2 = E_{Th}$ in the diffusive regime, with D the diffusion constant. E_{Th} is the so called Thouless energy, defined as the inverse of the typical time required by a perturbation to diffuse through the sample. The theory in [3] is based on the one-parameter-scaling hypothesis, that assumes that

$g(L)$ is *the only* relevant scaling parameter at the transition [15]. This translates into the continuous relation:

$$\frac{d\log g(L)}{d\log L} = \beta(g(L)), \tag{1.78}$$

where the sign of the scaling function β determines the asymptotic transport properties in the infinite volume limit. Although the full function β is unknown, its qualitative behavior is obtained extrapolating from the asymptotic behavior at large g ($\beta(g) = d-2-c/g$) and small g ($\beta(g) \sim \log(g)$), assuming a continuous and monotone function. This, together with the fact that the quantum "weak localization" corrections to the mean-free-path-expression for the conductivity are negative (meaning $c > 0$) [102], suffices to determine that the lower critical dimension for the Anderson transition is $d = 2$: for $d \leq 2$, $\beta(g)$ remains always smaller than zero, implying that the system is asymptotically insulating for any value of disorder and no fixed point $\beta(g_c) = 0$ is present.

1.5 The many-body dynamical phase transition

As follows from the perturbative treatment, the stability of the localized phase is guaranteed by the rareness of resonances: the local degrees of freedom that are strongly hybridized by the interactions (or hopping) form a dilute set in space, as the typical energy differences associated to local rearrangements are large for strong randomness. As the disorder is decreased, the local degrees of freedom start hybridizing at any length scale and resonances proliferate in space, producing eigenstates that are delocalized (in real space or in Fock space). As a consequence, the MBL phase becomes unstable and a disorder-driven transition to delocalization occurs. In the perturbative setting, this is signaled by the divergence of the perturbative expansion around the trivially local limit.

Not much is known about this dynamical phase transition. On one hand, since the numerical techniques exploited to understand the localized phase rely on the weakly-entangled structure of the MBL eigenstates, they are inadequate to tackle the transition. On the other hand, a suitable theoretical framework has not yet been developed. In this section, we report the main debated issues concerning the many-body localization-to-delocalization transition, together with a short review of the results that have emerged from the theoretical analysis and of the methods with which they have been obtained.

1.5.1 The finite temperature *crossover*?

In the perturbative framework, the transition to many-body delocalization occurs at a critical value of disorder (or interaction) which depends on the energy density of the system and thus on its effective temperature, see Eq. (1.77). In other words, for a fixed value of the parameters in the Hamiltonian, an extensive mobility edge $\mathcal{E}_c$ is predicted within the spectrum. It separates the localized many-body eigenstates for which (1.29)

[15] It is assumed that when merging b^d cubes of size L, the conductance of the resulting sample of size bL is a function of the conductance of each block only, $g(bL) = f(b, g(L))$, with no additional separate dependence on the energy, disorder or length L.

holds true and the transport coefficients vanish, from the ones in which the correlations do not decay exponentially and transport is recovered. The fact that $\mathcal{E}_c$ scales with the volume implies[16] that a "finite-temperature metal to insulator transition" occurs, with the conductivity vanishing exactly at the critical temperature T_c, see Fig. 6.2(a). Signatures of mobility edges have been found in exact diagonalization studies of small systems, see Fig. 6.2(b).

The scenario of the finite temperature transition has been questioned in Ref. [49]: there it is argued that the assumption of coexistence of both MBL and delocalized eigenstates at the same values of disorder and interactions is inconsistent, thus ruling out the possibility of a transition driven by changes in the thermodynamic variables (the temperature T or the chemical potential μ). As a consequence, MBL as a function of temperature is "all or none": either all eigenstates are localized and the "integrability" picture of Sec. 1.3 holds true (the latter entails that *each* single eigenstate is a product state in the basis of conserved operators, and thus it is many-body localized), or none of them is and the systems is thermalizing at any temperature. In light of this argument, the numerical evidence for a mobility edge in Fig. 6.2(b) should be interpreted as a finite size effect, the transition line being actually a crossover line.

The main idea behind the argument in [49] is that for delocalization to occur it is not necessary that the whole system is excited at energy densities larger than the putative mobility edge. Rather, rare spontaneous *local* fluctuations in the energy density, termed "bubbles" in [49], are sufficient to restore transport and thermalization, as they can move resonantly through the system and act as a mobile bath. The inconsistency of the coexistence is argued by the following steps: if an ergodic phase exists at high temperature, typical states at lower temperature will contain a finite density of such bubbles, due to local thermal fluctuations. Bubbles can appear at any location in space with finite probability. For resonant spots that are sufficiently large to admit an ETH, random-matrix-like description, it can be argued that (1) bubbles are mobile: the set of configurations corresponding to states with bubbles located in different positions constitute a resonant sub-graph in Hilbert space, and (2) the hybridization is robust with respect to couplings to configurations that do not belong to the sub-graph: bubbles do not diffuse and loose their extra energy in the environment, as the latter is in the supposed MBL phase and thus cannot transport the extra energy to infinity. Since the many-body eigenfunctions hybridize essentially all configurations which are resonantly connected, it

[16] If indeed on the eigenstates $|\psi_n\rangle$ with $E_n < \mathcal{E}_c$ the conductivity within the state is zero, $\sigma(E_n) = 0$, then a saddle point estimate gives:

$$\sigma(T) = \sum_n \frac{e^{-\frac{E_n}{k_B T}}}{\mathcal{Z}(T)} \sigma(E_n) \approx \frac{\int_{\mathcal{E}_c}^{\infty} dE\, e^{S(E) - \frac{E}{k_B T}} \sigma(E)}{\int_{E_0}^{\infty} dE\, e^{S(E) - \frac{E}{k_B T}}} = \begin{cases} \sigma(\tilde{E}(T)) & \text{if } \tilde{E}(T) > \mathcal{E}_c \\ \propto \exp\left[-\frac{\mathcal{E}_c - \tilde{E}(T)}{k_B T}\right] & \text{if } \tilde{E}(T) < \mathcal{E}_c, \end{cases} \tag{1.79}$$

where $\tilde{E}(T)$ solves

$$\left.\frac{\partial S(E)}{\partial E}\right|_{E=\tilde{E}(T)} = \frac{1}{k_B T}. \tag{1.80}$$

Since the difference $\mathcal{E}_c - \tilde{E}(T)$ scales with the system's volume, it diverges in the thermodynamic limit, implying that $\sigma(T) = 0$ for all $T < T_c$ with T_c the temperature corresponding to $\mathcal{E}_c$.

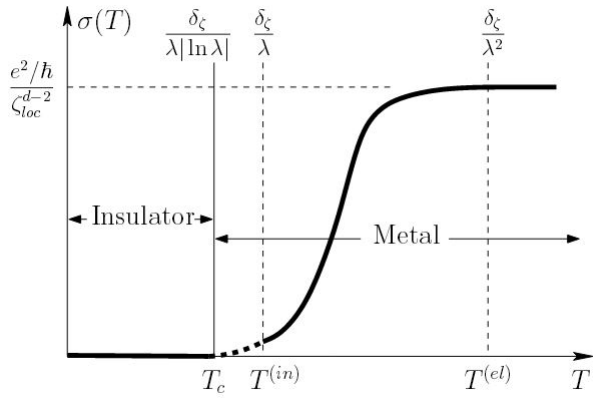

(a)

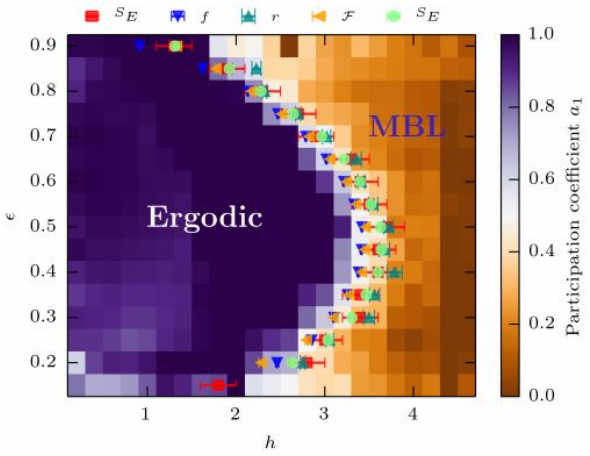

(b)

Figure 1.5: (a) Schematic temperature dependence of the dc conductivity as predicted in [20] for a fermionic Hamiltonian (1.9). Below the critical temperature given in (1.77), the conductivity is exactly zero. (b) Mobility edge obtained numerically in [108] for the Hamiltonian (1.10) with $J = J_z = 1$, $W/2 = h$ and ϵ the energy density. The various symbols correspond to different diagnostics, see [108]. The figures are taken from Refs. [20] and [108].

follows that the latter are delocalized: the putative localized phase at low temperature is destroyed. A similar argument implies that no genuine localization exists in disorder-free systems [48].

This "bubble" argument rules out the possibility of mobility edges in the many-body case, which are claimed to disappear as long as one goes beyond the level of approximation discussed in Sec. 1.4.5. However, it is fully consistent with the existence of an MBL phase at sufficiently strong disorder, in which conserved quantities exist. We investigate this issue further in Sec. 2.4: there, we reformulate the problem in the language of the conserved operators, and illustrate how the scenario of delocalization driven by bubbles

cannot be captured within our approximate treatment.

1.5.2 Diverging lengths, local discontinuities: the nature of the transition?

Method and diagnostics. To date, most of the works addressing the transition resort to exact diagonalization of one dimensional models of limited size [134, 108, 101, 15, 105], or to phenomenological RG-like procedures [174, 140]. The RG scheme in [174] operates on a coarse-grained model made of a sequence of blocks i of varying length, each one being characterized by a single parameter $g_i = \Gamma_i/\Delta_i$, defined as the ratio between an "inverse time of entanglement spreading" across the block Γ_i, and the local level spacing Δ_i. The parameter g_i is analogous to the Thouless conductance identified in [3] as the relevant scaling variable for single-particle localization, see Sec. 1.4.6. Blocks are merged and assigned an insulating ($g \ll 1$) or conducting ($g \gg 1$) character according to RG rules that have a phenomenological justification. The block parameters g_i are not derived from a microscopic model (although the distribution of similar parameters can be computed with exact diagonalization [156] and in principle used as an input for the RG), and no intermediate behavior $g_i \sim 1$ is allowed. Another framework has been developed in [140] to construct the percolating resonant network driving the transition, by progressively merging resonant clusters at larger and larger scales; the method captures only the collective many-body resonances that are "factorizable" into resonances at larger energy (and shorter length) scales, and assumes that these are the relevant ones driving the transition. Both methods are restricted to the case $d = 1$.

Among the quantities that have been more intensively studied, the entanglement entropy in eigenstates plays a central role. Its density $s = S_A/L_A^d$ (with A a region of linear dimension L_A, $S_A = -\mathrm{Tr}\,(\rho_A \log_2 \rho_A)$, $\rho_A = \mathrm{Tr}_{A^c}\,(|E_n\rangle\langle E_n|)$ and $|E_n\rangle$ a many-body eigenstate) is a natural order parameter for the dynamical transition, as it changes sharply from zero in the MBL phase to a finite value in the delocalized phase. Its full distribution has been studied numerically [106, 105]. In particular, the variance (in the case of $L_A = L/2$) is a useful indicator, as it peaks at the transition [101]; similarly, the total correlations in the diagonal ensemble emerging from the dephasing of an initial product state also peak at the transition [70].

Some results. With the above methods, the following results have been obtained:

- On the delocalized side of the transition, a finite-size scaling analysis has been performed on the variance of the eigenstates entanglement entropy [101, 108], see Fig. 1.6. The resulting collapse is interpreted as an indication of the fact that the transition is continuous, characterized by a divergent length scale $\xi \sim \delta^{-\nu}$ with δ measuring the distance to the critical point. Finite-size scaling has been performed also within the RG description, on the typical value of the scaling variable $\langle \log g(l) \rangle$ [174], and on the size of the longest resonant clusters [140]. Different results are obtained for the critical exponent: $\nu \approx 3$ is obtained within the RG, while $\nu \approx 1$ is obtained from exact diagonalization. The latter exponent violates the Harris bound $\nu > 2/d$, with d the spatial dimension [37].

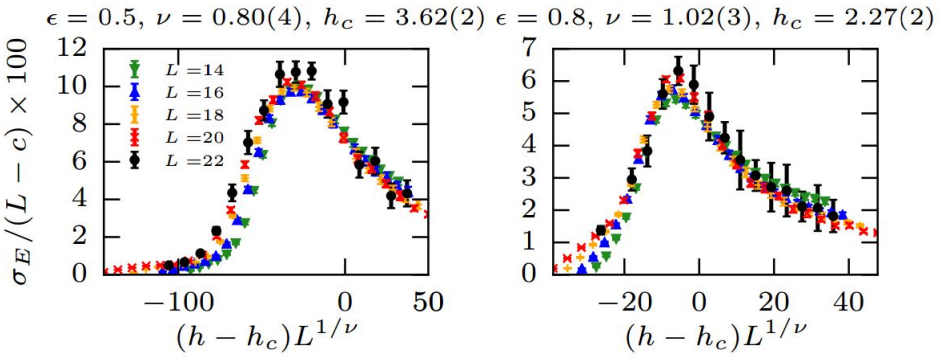

Figure 1.6: Finite-size scaling of the standard deviation σ_E of the bipartite entanglement entropy per site S/L in the middle of the spectrum (left) and in the upper part (right), for the Hamiltonian (1.10) with $J = J_z = 1$ and $h_a \in [-h, h]$. The standard deviation displays a peak at the transition [101]; a scaling of the form $\sigma_E = (L-c)g\left[L^{\frac{1}{\nu}}(h-h_c)\right]$ is assumed. The figures are taken from Ref. [108]

- Under the assumption that the transition is continuous and characterized by a unique divergent length scale $\xi \sim \delta^{-\nu}$, it is proved in [74] that for a sub-region of size $L_A \ll \xi, L$, S_A should exhibit thermal, volume-law behavior in the quantum critical regime. This holds true, provided that S_A is a scaling function of ξ/L_A only and that it varies continuously at the transition. The continuity hypothesis for S_A has been recently questioned in [96], where it is argued that the entanglement entropy of local sub-regions is discontinuous at the transition in the limit $L \to \infty$. This is in line with numerical results showing sub-thermal entanglement entropy in the quantum critical regime [101, 108, 53, 105].

- In the thermal phase in $d = 1$ close to the transition, transport is found to be sub-diffusive [16, 4, 179, 94], and the entanglement spreading sub-ballistic [109, 174]. The RG treatment also gives a length-time scaling that is power-law $l \sim t^{1/z}$ with a continuously disorder-dependent exponent $z(w)$ that equals 2 deep in the thermal phase, where transport is diffusive, it increases with disorder and it presumably diverges in a universal way $z \sim (w - w_c)^{-\zeta}$ at the transition to the MBL phase, where the logarithmic scaling sets in.

- The numerical method in [53] working directly in the thermodynamic limit produces an estimate of the critical value of disorder that is higher than the ones obtained from finite size studies. This indicates that the latter tend to overestimate the extent of the MBL phase, and that the MBL phase would actually become unstable at smaller disorder but only at much longer length scales than the ones accessible with exact diagonalization.

These results suggest the following picture for the dynamical transition in $d = 1$: delocalization occurs as an instability of the localized phase, generated by a sparse[17] network

[17] For the effective model discussed in [140], the scaling function Ξ associated to the length ξ_{loc} of the

of delocalized, entangled regions that suffice to thermalize the whole system in the thermodynamic limit [96]. In the thermal phase nearby the transition, the instability appears only at long length scales, while small systems look localized; the slowing down of transport and of the entanglement spreading is ascribed to the presence of the locally insulating regions within the thermal phase, which are rare but (in one dimension) obstruct transport. These "Griffiths effects" occur also in the localized phase in the vicinity of the transition, where rare thermal region dominate the low-frequency behavior of the ac conductivity [4, 71].

1.5.3 The role of dimensionality: MBL above $d = 1$?

While the role of dimensionality is understood in the single particle case, see Sec. 1.4.6, the same is not true for the many-body case. The numerical works are confined to $d = 1$ for computational reasons; on the other hand, the approximate perturbative arguments were made for arbitrary dimensions d. However, the role of dimensionality seems crucial when going beyond the perturbative regime: the proof in [86] makes explicit use of the fact that $d = 1$, which appears to be a necessary requirement for the full construction to hold, see Sec. 2.3. A similar line of arguments leads to the conclusion that MBL might be unstable with respect to the insertion of low-disordered regions in $d \geq 2$ [47]. Also in [38] it is argued that the conserved quantities are unstableto the coupling to a thermal boundary in $d \geq 2$. On the other hand, signatures of localization have been measured on experimental time scales, as reported in Sec. 1.1.

maximally extended resonant cluster, $\xi_{loc} \sim L\Xi\left((W - W_c)L^{1/\nu}\right)$, has a value at criticality ($\Xi(0) \approx 10^{-2}$) that is much smaller than the one of ordinary percolation ($\Xi(0) \approx 0.5$). This suggests that the cluster of resonating degrees of freedom is sparse at the transition.

2 Dressing occupation numbers: the Fermi insulator

The goal of this chapter is to show that exactly conserved operators $\hat{n}_\alpha$ can be constructed for a fermionic Hamiltonian of the form

$$H = \sum_\alpha E_\alpha n_\alpha + \sum_{\alpha,\beta,\gamma,\delta} U_{\alpha\beta,\gamma\delta}\, c^\dagger_\alpha c^\dagger_\beta c_\gamma c_\delta. \tag{2.1}$$

The $\hat{n}_\alpha$ are obtained form a perturbative dressing of the non-interacting number operators n_α. They can be chosen to have binary spectrum $\{0,1\}$ and to form a complete set, so that (2.4) can be rewritten in terms of these occupation numbers as

$$H = \sum_\alpha H_\alpha \hat{n}_\alpha + \frac{1}{2}\sum_{\alpha\neq\beta} H_{\alpha,\beta}\, \hat{n}_\alpha \hat{n}_\beta + \dots . \tag{2.2}$$

The expression (2.2) is an exact quasi-particle energy functional, which determines the energy of any quasi-particle as a function of the occupations of all others: it thus defines an "interacting Fermi insulator".

The chapter is structured as follows: In Sec. 2.1 we summarize the logic of the construction and the main technical problems addressed. In Sec. 2.2, we give the details of the construction and discuss the convergence of the operator expansion for the $\hat{n}_\alpha$. This is done within some approximations, and relaxing the hypothesis on the binarity of the spectrum. In Sec.2.3, we discuss how the approximations we make can be lifted, comparing our perturbative construction with the mathematically rigorous treatment of Ref. [85]. Finally, in Sec. 2.4 we address the problem of the divergence of the operator expansion as the transition to delocalization is approached, connecting to the debate on the existence of many-body mobility edges shortly described in the previous chapter.

2.1 Construction of exact quasiparticles: a road map

We consider a fermionic Hamiltonian on a lattice Λ,

$$H = \sum_{i\in\Lambda} c^\dagger_i \left[-\frac{1}{2m}\Delta^{(\Lambda)} + V_{\rm dis}(i)\right] c_i + \frac{1}{2}\frac{\lambda}{\nu a^d}\sum_{i,j\in\Lambda} c^\dagger_i c^\dagger_j\, u(i-j)\, c_j c_i, \tag{2.3}$$

where $\Delta^{(\Lambda)}$ is the lattice Laplacian, $V_{\rm dis}$ is a random disordered potential, a the lattice constant, ν the single-particle density of states, and $u(i-j)$ a dimensionless, normalized, short-ranged interaction kernel. The disorder potential is chosen such that the single particle part of the Hamiltonian possesses only fully localized wave-functions ϕ_α with energies E_α, $\alpha = 1, ..., |\Lambda|$. We define the model on a lattice in order to have a finite bandwidth of the single particle problem, that we denote with $\mathcal{W}$, $E_\alpha \in [-\mathcal{W}/2, \mathcal{W}/2]$. This allows us to discuss the perturbation theory at the operator level (in a sense, it allows us to take a meaningful limit of infinite temperature). In the basis of single particle eigenstates, (2.3) reads

$$H = \sum_\alpha E_\alpha n_\alpha + \frac{\lambda}{\nu a^d} \sum_{\alpha<\beta,\gamma<\delta} u_{\alpha\beta,\gamma\delta}\, c^\dagger_\alpha c^\dagger_\beta c_\gamma c_\delta \equiv H_0 + U, \tag{2.4}$$

where some ordering "$<$" between the single particle indices is assumed, and the interactions are antisymmetrized $u_{\alpha\beta,\gamma\delta} = u_{\beta\alpha,\delta\gamma} = -u_{\beta\alpha,\gamma\delta}$.

2.1.1 The perturbative series and its local divergences

In the absence of interactions, the occupation numbers n_α are mutually commuting, conserved quantities. Their quasilocality follows directly from the spatial localization of the single particle wave-functions ϕ_α: the operator $c^\dagger_i c_j$ contributes to the operator expansion:

$$n_\alpha = \sum_{i,j} \phi^*_\alpha(i)\phi_\alpha(j) c^\dagger_i c_j \tag{2.5}$$

with a weight which decays exponentially in the distance between its support (the sites i, j) and the localization center r_α of ϕ_α. By truncating the sum (2.5) to terms with support only within a neighborhood of $m\xi$ of r_α, one obtains an operator whose commutator with the Hamiltonian vanishes up to exponentially small terms. As $m \to \infty$ the operator rapidly converges (in the operator norm) to the conserved n_α.

We aim at constructing an extensive set of $|\Lambda|$ operators $\hat{n}_\alpha$ that are quasilocal, complete and conserved by the *full* interacting Hamiltonian (2.4),

$$[\hat{n}_\alpha, H] = 0. \tag{2.6}$$

$\hat{n}_\alpha$ can be sought as an element of the space C of particle-conserving operators on the Hilbert space, and without loss of generality we may require it to be Hermitian. Since the spectrum of the many-body system is almost surely non-degenerate, it follows that such conserved quantities also satisfy $[\hat{n}_\alpha, \hat{n}_\beta] = 0$. Their mutual commutativity implies that the $\hat{n}_\alpha$ form a commutative algebra: the choice of a basis spanning this algebra is not at all unique, as it will appear clear in the following.

When attempting to construct $\hat{n}_\alpha$ perturbatively, it is natural to consider the formal

expansion

$$\hat{n}_\alpha = n_\alpha + \sum_{n\geq 1} \lambda^n \Delta\hat{n}_\alpha^{(n)}, \tag{2.7}$$

where $\Delta\hat{n}_\alpha^{(n)}$ is determined recursively from $\Delta\hat{n}_\alpha^{(n-1)}$, as the solution of

$$\left[U, \Delta\hat{n}_\alpha^{(n-1)}\right] + \left[H_0, \Delta\hat{n}_\alpha^{(n)}\right] = 0. \tag{2.8}$$

We define two relevant operator subspaces: the kernel K of the linear map $\mathrm{Ad}_{H_0}(X) = [H_0, X]$ defined for $X \in C$, and its image, $O = \mathrm{Ad}_{H_0}(C)$. The latter is the orthogonal complement of K with respect to the inner product of operators, $\langle A, B\rangle = \mathrm{Tr}[A^\dagger B]$, $C = K \oplus O$. K is spanned by all possible products of n_α's, while O is spanned by the normally ordered operators

$$\mathcal{O}_{\mathcal{I},\mathcal{J}} = \prod_{\beta\in\mathcal{I}} c_\beta^\dagger \prod_{\gamma\in\mathcal{J}} c_\gamma \quad \mathcal{I} \neq \mathcal{J}, \tag{2.9}$$

where $\mathcal{I} = (\beta_1, \cdots, \beta_N)$ and $\mathcal{J} = (\gamma_1, \cdots, \gamma_N)$ are sets of indices labeling the single particle states, and the same ordering "$<$" as previously is chosen for the indices β, γ. Let us discuss the existence and uniqueness of the solution of (2.8).

Existence. The equation (2.8) can be solved for $\Delta\hat{n}_\alpha^{(n)}$ provided that the commutator with H_0 can be inverted. This requires that at any order n, $\left[U, \Delta\hat{n}_\alpha^{n-1}\right] \in O$; equivalently, $x(\Psi_0) := \langle\Psi_0|[U, \Delta\hat{n}_\alpha^{(n-1)}]|\Psi_0\rangle = 0$ for every eigenstate Ψ_0 of H_0. This is true for time-reversal symmetric Hamiltonians having real matrix elements in the basis of single particle eigenstates: indeed, at any stage of perturbation theory $\Delta\hat{n}_\alpha^{(n-1)}$ has real coefficients in the occupation number basis: thus, $x(\Psi_0)$ is real. On the other hand, from the anti-Hermiticity of $[U, \Delta\hat{n}_\alpha^{(n-1)}]$ it follows that $x(\Psi_0)$ is purely imaginary, and thus it vanishes indeed.

Uniqueness and binarity. Of course, the conservation equation determines $\Delta\hat{n}_\alpha^{(n)}$ up to arbitrary terms belonging to K. Denoting the latter with $\Delta K_\alpha^{(n)}$, we may formally write

$$\Delta\hat{n}_\alpha^{(n)} = i \lim_{\eta\to 0} \int_0^\infty d\tau e^{-\eta\tau} e^{iH_0\tau} \left[U, \Delta\hat{n}_\alpha^{(n-1)}\right] e^{-iH_0\tau} + \Delta K_\alpha^{(n)} \equiv \Delta J_\alpha^{(n)} + \Delta K_\alpha^{(n)}, \tag{2.10}$$

where $\Delta J_\alpha^{(n)}$ belongs to O. We claim that at any order, $\Delta K_\alpha^{(n)}$ can be *uniquely* fixed in terms of the $\Delta\hat{n}_\alpha^{(m)}$ with $m < n$ imposing the binarity of the spectrum, i.e. $\hat{n}_\alpha^2 = \hat{n}_\alpha$. The result reads

$$\Delta K_\alpha^{(n)} = (1 - 2n_\alpha) \left[\sum_{m=1}^{n-1} \Delta\hat{n}_\alpha^{(m)} \Delta\hat{n}_\alpha^{(n-m)} + \left\{ n_\alpha - \frac{1}{2}, \Delta J_\alpha^{(n)} \right\} \right]. \tag{2.11}$$

Thus, the perturbation theory uniquely defines[1] a set of number operators. We report the derivation of (2.11) in Appendix 2.A.

Let us now address the problem of quasilocality. Despite the perturbative equations are solvable at any finite order, the resulting series (2.7) is affected by the same "trivial" divergences as Anderson's perturbation theory for the self energies, Sec. 1.4.1. Rare resonances between almost degenerate Fock states produce terms with a large norm that, even if rare, appear repeatedly in (2.7), at any order in λ. An example of these repetitions is given in the following.

Suppose that at order n the series expansion contains the term $J_n \equiv \mathcal{J}_n O c_\alpha$, where $O = c^\dagger_{i_1} \cdots c^\dagger_{i_m} c_{j_1} \cdots c_{j_{m-1}}$ is a string of operators with $i, j \neq \{\alpha, \beta, \gamma, \delta\}$. The amplitude $\mathcal{J}_n = O(\lambda^n)$ contains the energy denominator:

$$\mathcal{J}_n \propto \left(\sum_{k=1}^{m} E_{i_k} - \sum_{k=1}^{m-1} E_{j_k} - E_\alpha \right)^{-1} \equiv (\Delta\mathcal{E})^{-1}, \tag{2.12}$$

which we assume to be atypically small. One then easily finds a subsequence of the series (2.7), which contains arbitrarily high powers of the small denominator. Indeed, let us restrict the interaction U to the term $U_{\alpha\beta,\gamma\delta} \left(c^\dagger_\alpha c^\dagger_\beta c_\gamma c_\delta + h.c. \right)$ with $U_{\alpha\beta,\gamma\delta} = \lambda u_{\alpha\beta,\gamma\delta}/(\nu a^d)$; higher order terms in the perturbative expansion are obtained by subsequent application of (2.10) to J_n; this produces:

$$\begin{aligned}
J_{n+1} &\equiv \mathcal{J}_n \frac{U_{\alpha\beta,\gamma\delta}}{\Delta\mathcal{E} + \mathcal{E}_{\alpha\beta,\gamma\delta}} \; O c^\dagger_\beta c_\gamma c_\delta \equiv \mathcal{J}_{n+1} \; O c^\dagger_\beta c_\gamma c_\delta, \\
J_{n+2} &\equiv -\mathcal{J}_{n+1} \frac{U_{\alpha\beta,\gamma\delta}}{\Delta\mathcal{E}} \; O \left(n_\beta (1-n_\gamma)(1-n_\delta) + (1-n_\beta) n_\gamma n_\delta \right) c_\alpha, \\
J_{n+3} &\equiv \mathcal{J}_{n+1} \left[\frac{U_{\alpha\beta,\gamma\delta}}{\Delta\mathcal{E}} \, \frac{U_{\alpha\beta,\gamma\delta}}{\Delta\mathcal{E} + \mathcal{E}_{\alpha\beta,\gamma\delta}} \right] O c^\dagger_\beta c_\gamma c_\delta,
\end{aligned} \tag{2.13}$$

with $\mathcal{E}_{\alpha\beta,\gamma\delta} = E_\alpha + E_\beta - E_\gamma - E_\delta$. By iteration of this procedure, a sub-sequence of operators containing arbitrarily high powers of $(\Delta\mathcal{E})^{-1}$ is generated, preventing the convergence of the series if the term in brackets is larger than 1. Divergences of this kind have to be properly re-summed for the series expansion to make sense. For example, all terms multiplying $O c^\dagger_\beta c_\gamma c_\delta$ re-sum into a self-energy correction of the denominator in the first line of (2.13):

$$J \equiv \mathcal{J}_n \left[\frac{U_{\alpha\beta,\gamma\delta}}{(\Delta\mathcal{E} + \mathcal{E}_{\alpha\beta,\gamma\delta}) - \frac{U^2_{\alpha\beta,\gamma\delta}}{\Delta\mathcal{E}}} \right] O c^\dagger_\beta c_\gamma c_\delta \equiv \mathcal{J} \; O c^\dagger_\beta c_\gamma c_\delta. \tag{2.14}$$

[1] Note that it is not obvious from the outset that this simple perturbative scheme should work and produce a local operator. Indeed, we are applying the perturbation theory to an extensive set of operators which are all null eigenvectors of $\mathrm{Ad}_{H_0}(\cdot)$. In principle one should use degenerate perturbation theory for all these operators simultaneously, which could turn out to require a non-local change of basis. In the remaining of the chapter it is shown, however, that this is not the case.

The term in square brackets in (2.14) contains a very large self energy correction $U^2_{\alpha\beta,\gamma\delta}/\Delta\mathcal{E}$, which compensates the divergence in $\mathcal{J}_n$ when $\Delta\mathcal{E} \to 0$.

As in the single particle case, it is necessary to implement systematically the resummation of repeated terms. To do this at the operator level, it turns out to be convenient to drop the terms $\Delta K^{(n)}_\alpha$ in (2.10), thus defining a new set of operators $\hat{n}_\alpha \to I_\alpha$ such that $I_\alpha - n_\alpha \in O$. Such operators admit the expansion:

$$I_\alpha = n_\alpha + \sum_{N\geq 1} \sum_{\substack{\mathcal{I}\neq\mathcal{J} \\ |\mathcal{I}|=N=|\mathcal{J}|}} \mathcal{A}^{(\alpha)}_{\mathcal{I},\mathcal{J}} \left(\mathcal{O}_{\mathcal{I},\mathcal{J}} + \mathcal{O}^\dagger_{\mathcal{I},\mathcal{J}} \right), \tag{2.15}$$

where $\mathcal{O}_{\mathcal{I},\mathcal{J}}$ is defined in (2.9). The operator expansion (2.15) is non-generic due to the constraint $\mathcal{I} \neq \mathcal{J}$ which guarantees that $I_\alpha - n_\alpha$ is in the subspace O. The above perturbative reasoning guarantees that (2.15) is a consistent ansatz for the conserved quantities, whose coefficients are uniquely determined *just* by imposing $[H, I_\alpha] = 0$. Note that (2.15) should no longer be seen an expansion in λ, but rather as an expansion in the support on which the operators $\mathcal{O}_{\mathcal{I},\mathcal{J}}$ act. In particular, even though motivated by perturbative considerations, in any finite system the above ansatz uniquely determines a conserved operator even if perturbation theory does not converge: in that case I_α is defined as the finite (possibly exponentially large) sum (2.15) whose coefficients are solved by imposing $[H, I_\alpha] = 0$. In a delocalized regime, the operator will have support on the whole system.

The choice (2.15) allows us to reformulate the problem within a single-particle setting, and to implement the set of approximations discussed in Sec. 1.4.1. The drawback of the above ansatz is that it does not define an operator with binary spectrum. We expect however that the convergence of the operator expansion still holds in a non-trivial regime of parameters, also once the missing terms (necessary to impose the binarity) are reinstated[2]. In the following section, we summarize the logic followed to argue that (2.15) converges in the thermodynamic limit, to a quasilocal operator. The technical details are postponed to Sec. 2.2.

2.1.2 Arguing for convergence: main logical steps

The coefficients in (2.15) depend on the interaction strength λ, and approach zero as $\lambda \to 0$. The goal is to argue that for sufficiently small λ the expansion converges in probability, that is, for any $\epsilon > 0$:

$$\lim_{R\to\infty} \mathbb{P}\left(\sum_{\substack{\mathcal{I}\neq\mathcal{J} \\ r(\mathcal{I},\mathcal{J})>R}} |\mathcal{A}^{(\alpha)}_{\mathcal{I},\mathcal{J}}| < \epsilon \right) = 1, \tag{2.16}$$

[2]In a sense, if the expansion (2.15) converges, it can be appropriately normalized to impose $I^2_\alpha = I_\alpha$.

where $r(\mathcal{I},\mathcal{J}) = \max_{\beta\in\mathcal{I}\cup\mathcal{J}}|r_\alpha - r_\beta|$ is the maximal distance between the localization center r_α of the state α and any of the states β that are acted upon by the operator $\mathcal{O}_{\mathcal{I},\mathcal{J}}$. This ensures that the series defining the operator I_α converges almost surely (since $||\mathcal{O}_{\mathcal{I},\mathcal{J}}|| = 1$ for all $\mathcal{I},\mathcal{J}$), and that the resulting operator I_α is quasi-local in the sense of 1.37.

The arguments for the convergence of (2.15) are at the same level of approximation as the ones in [10, 9, 20, 72]. They rely on a mapping to an equivalent single-particle problem, obtained imposing $[I_\alpha, H] = 0$ and interpreting the resulting linear constraints for the amplitudes $\mathcal{A}^{(\alpha)}_{\mathcal{I},\mathcal{J}}$ as the equations for a single particle hopping on a disordered "operator lattice" with sites labeled by the Fock indices $(\mathcal{I},\mathcal{J})$. In particular, the exponential decay of the coefficients of $\mathcal{O}_{\mathcal{I},\mathcal{J}}$ corresponds to the localization of the particle on the lattice, in analogy with the non-interacting case (2.5). In turn, the delocalization of the particle corresponds to the divergence of the operator expansion (2.15). The non-interacting limit is recovered when the particle is fully localized at the site (α,α).

The localization in the operator lattice is argued within a forward approximation, which boils down to replacing each amplitude in (2.15) with its lowest order expansion in the strength of the interaction λ. The approximation is controlled by the largeness of the parameter giving the connectivity of the operator lattice,

$$\mathcal{K} = 4\frac{\mathcal{W}}{\delta_\xi}, \tag{2.17}$$

with $\mathcal{W}$ the bandwidth of the quadratic part of (2.4), and δ_ξ is the average level spacing within a localization volume, defined in (1.24). As a consequence of the forward approximation, the amplitudes in (2.15) can be written as a sum over self-avoiding paths in the operator lattice, cfr. (2.32), in analogy with the Anderson problem. Moreover, within this approximation the number of sites in the lattice at distance N form the site (α,α) grows exponentially with N, as $\mathcal{K}^N$. Thus, a setting similar to the one of single particle problems on the Bethe lattice is recovered: one expects a transition to occur, due to the competition between the exponential growth of the number of sites at a distance N from the root, and the exponential decay of the weights of the self avoiding paths of length N. At variance with the Bethe lattice, however, in the operator lattice there are typically many self-avoiding paths leading to a given site (and plenty of loops, see Fig. 2.1). In particular, the number of paths connecting the root (α,α) to a given site scales *factorially* with their length. This factorial must be compensated in order to recover the exponential scaling required for the transition. We argue that the compensation occurs, as the self-avoiding paths have strongly correlated weights which partially cancel among each others (see also the observation in Sec. 2.1.2 in [20], and the discussion in [73] in the zero-dimensional setting). We develop a systematic way to deal with this "problem of the factorials", exploiting a diagrammatic representation of the scattering processes associated to each path and explicitly showing the cancellations, see Sec. 2.2.3. This leads to the introduction of "effective paths", whose weight is the result of the resummation of the weights of strongly correlated self-avoiding paths.

Once the exponential scaling of the number of (effective) paths is recovered, the estimate

of (2.16) requires to address the following two issues:

I1: The computation of the large deviation probability of individual path or effective path weights. This must account for the correlation of the energy denominators of the locators in a single path, that is present in the many-body even within the forward approximation. This is discussed in Sec. 2.2.4.

I2: The estimate of the total number of effective paths of a given length. This requires to evaluate the number of distinct scattering processes leading to a given final configuration in operator space. This computation is reported in Sec. 2.2.5.

Combining these results, we obtain an estimate for the critical value of the interactions λ_c' at which the integrals I_α become non-local almost surely. The estimate is of the form $\lambda_c' \propto 1/\mathcal{K}\log\mathcal{K}$, cfr. Eq. (2.93). Although it can not be logically excluded that λ_c' is smaller than the λ_c at which delocalization occurs (since it might be possible to find for $\lambda_c' < \lambda < \lambda_c$ a prescription for conserved quantities that leads to more local operators than the one given by (2.15)), we believe that the two values cannot be distinguished within the approximations made. Hence, we use the notation λ_c indistinctly for both critical values, and interpret λ_c' as an estimate of the boundary of stability of the MBL phase, holding at infinite temperature (see Sec. 2.2.6).

2.2 Construction of exact quasiparticles: details

In the following section, we discuss in detail how the program outlined in the previous section is implemented.

2.2.1 An Anderson problem in operator space

A. Details of the model: relevant parameters and energy scales

Since the detailed features of (2.4) are not relevant for our analysis, we coarse grain the model, reducing it to an array of coupled quantum dots of size of the order of the single-particle localization length ξ, which we refer to as localization volumina[3]. We set the matrix elements $u_{\alpha\beta,\gamma\delta}$ to be non-zero only if the corresponding single-particle states have localization center in the same volume or in adjacent ones: this accounts for the locality of the interactions. Moreover, since the matrix elements decrease rather rapidly when the energy difference between involved levels exceeds δ_ξ, we take $u_{\alpha\beta,\gamma\delta}$ to be non-zero only if

$$|E_\alpha - E_\delta|, |E_\beta - E_\gamma| \lesssim \delta_\xi \quad \text{or} \quad |E_\alpha - E_\gamma|, |E_\beta - E_\delta| \lesssim \delta_\xi. \tag{2.18}$$

[3]The coarse-grained model that we consider differs from the one in [20], where the single particle Hamiltonian is diagonalized separately in each localization volume, the inelastic scattering processes are restricted to single-particle states within the same volume, and the volumina are coupled by the hopping terms (elastic processes).

In this case, we sets

$$u_{\alpha\beta,\gamma\delta} = \nu a^d \, \delta_\xi \, \eta_{\alpha\beta,\gamma\delta} \tag{2.19}$$

where $\eta_{\alpha\beta,\gamma\delta}$ is a uniform variable in $[-1,1]$. Correlations between the single-particle energies E_α are neglected.

We assume that $\xi \gg a$. This condition ensures that a large number

$$N_{\rm loc} = \frac{\mathcal{W}}{\delta_\xi} = \mathcal{W}\nu\xi^d \tag{2.20}$$

of single particle wave-functions overlap significantly in space: this will provide the large parameter (2.17) of our analysis. The latter counts the number of scattering process of a particle (hole) α to a 3-particle-hole state (β,γ,δ) satisfying the constraint of locality, together with (2.18): for fixed α, one out of (β,γ,δ) equals any of the closest energy levels above or below α in the local spectrum, while the remaining pair can be chosen in $2N_{\rm loc}$ different ways.

The largeness of $\mathcal{K}$ justifies the approximation that we make, of neglecting terms $u_{\alpha\beta,\gamma\delta}$ where two or more indices are identical, as the phase space associated to these scattering processes is suppressed[4] by a factor $1/\mathcal{K}$. These terms are a priori accounted for in [20], where the basis of Hartree-Fock orbitals is considered instead of ϕ_α; however, they are ultimately neglected also in that work, when performing the statistical analysis of diagrams. Our choice of the basis ϕ_α is made as it allows us to work in full generality in the operator space, while HF orbitals depend on the non-interacting occupation numbers, i.e., they depend on the many-body state on top of which the single particle excitations are considered.

B. The mapping to a single-particle problem

In this section we present the equations defining $\mathcal{A}_{\mathcal{I},\mathcal{J}}$ in (2.15). To illustrate the procedure, we first discuss the non-interacting case and then proceed with the interacting problem.

Warm up: the non-interacting case. Consider a non-interacting Anderson Hamiltonian (1.8) with $V_{ab} = V$, together with the quadratic ansatz

$$I_k = n_k + \sum_{i<j} \mathcal{A}^{(k)}_{ij} \left(c_i^\dagger c_j + c_j^\dagger c_i \right), \tag{2.21}$$

[4]Indeed, for a scattering $\alpha \to \beta$ with the simultaneous creation of (γ,α), both γ and β are almost fixed by (2.18). For a scattering $\alpha \to \beta$ from a particle γ which remains in place, the following argument holds: if this is to be a resonant contribution, one needs the energy increment $\Delta\mathcal{E}$ of the vertex to be $|\Delta\mathcal{E}| = |E_\alpha - E_\beta| \lesssim \delta_\xi/\mathcal{K}$. In a scattering where γ switches to a neighboring state δ, with $|E_\gamma - E_\delta| \sim \delta_\xi$, one can optimize α,β among the $\mathcal{K}$ different choices, such as to make $\Delta\mathcal{E}$ of order $\delta_\xi/\mathcal{K}$. However, if γ remains in place, the optimum over the $\mathcal{K}$ choices for α,β will yield a parametrically bigger $\Delta\mathcal{E} = E_\alpha - E_\beta$, because of the repulsion between the neighboring levels α,β. Therefore such processes are systematically much less resonant than processes involving four distinct levels.

Imposing $[H, I_k] = 0$ and setting

$$\mathcal{A}_{ii}^{(k)} \equiv \delta_{k,i}, \tag{2.22}$$

we obtain the set of linear equations for $\mathcal{A}_{ij}^{(k)}$ with $i \neq j$:

$$(\epsilon_i - \epsilon_j)\mathcal{A}_{ij}^{(k)} - V\left(\mathcal{A}_{i-1j}^{(k)} + \mathcal{A}_{i+1j}^{(k)} - \mathcal{A}_{ij-1}^{(k)} - \mathcal{A}_{ij+1}^{(k)}\right) = 0. \tag{2.23}$$

In view of these equations, we re-interpret $\mathcal{A}_{ij}^{(k)}$ as the wave-function amplitudes of a particle on a square lattice with sites (i, j), and correlated on-site disorder $\mathcal{E}_{i,j} = \epsilon_i - \epsilon_j$, subject to the constraint (2.22). An explicit expression for them can be given in terms of the eigenfunctions ϕ_α as:

$$\mathcal{A}_{ij}^{(k)} = \sum_\alpha \omega_\alpha^k \phi_\alpha(i)\phi_\alpha(j), \tag{2.24}$$

where the ω_α^k have to be determined from the constraint

$$\sum_\alpha \omega_\alpha^k [\phi_\alpha(i)]^2 = \delta_{k,i}. \tag{2.25}$$

Again, the exponential decay of the amplitudes (2.24) in $|i - j|$ follows from the localization in space of the ϕ_α. It implies the convergence of the expansion (2.21) to a quasilocal operator I_k (that differs from the particle number operators n_α in (2.5), as it can be easily seen from the fact that (2.21) does not contain any diagonal terms $i = j \neq k$).

The many-body case. Let us go back to the interacting case. To deal with large index sets, we introduce the following notation: for any index set $\mathcal{X} = (x_1 \cdots x_N)$, we define diagonal coefficients as zero, except if $\mathcal{X} = \{\alpha\}$:

$$\mathcal{A}_{\mathcal{X},\mathcal{X}}^{(\alpha)} \equiv \delta_{\mathcal{X},\{\alpha\}}. \tag{2.26}$$

Moreover, for any l, m (with $l < m$) and any single particle labels γ, δ (with $\gamma < \delta$), we define the index sets:

$$\begin{aligned} \mathcal{X}_l &\equiv (x_1 \cdots \cancel{x_l} \cdots x_N), \\ \mathcal{X}_{lm}^{\gamma} &\equiv (\gamma\ x_1 \cdots \cancel{x_l} \cdots \cancel{x_m} \cdots x_N), \\ \mathcal{X}_{lm}^{\gamma\delta} &\equiv (\gamma\ \delta\ x_1 \cdots \cancel{x_l} \cdots \cancel{x_m} \cdots x_N). \end{aligned} \tag{2.27}$$

In general, the set $\mathcal{X}_{\dots}^{\dots}$ is obtained from $\mathcal{X}$ by eliminating the indices in the subscript and appending the ones in the superscript on the left. The resulting sets are thus not ordered;

let $\sigma[\cdot]$ denote the sign of the permutation which orders the set, and set:

$$\begin{aligned} s[\mathcal{X}_l] &\equiv l, \\ s\left[\mathcal{X}^{\gamma}_{lm}\right] &\equiv l+m+\sigma\left[\mathcal{X}^{\gamma}_{lm}\right], \\ s\left[\mathcal{X}^{\gamma\delta}_{lm}\right] &\equiv l+m+\sigma\left[\mathcal{X}^{\gamma\delta}_{lm}\right]. \end{aligned} \tag{2.28}$$

Finally, for index sets with $|\mathcal{Y}| = |\mathcal{Z}|$ we define the modified amplitudes:

$$\tilde{\mathcal{A}}^{(\alpha)}_{\mathcal{Y},\mathcal{Z}} \equiv (-1)^{s[\mathcal{Y}]+s[\mathcal{Z}]}\mathcal{A}^{(\alpha)}_{\mathcal{Y},\mathcal{Z}}\,. \tag{2.29}$$

With this notation, the condition $[H, I_\alpha] = 0$ is equivalent to the following set of linear equations for $\mathcal{A}^{(\alpha)}_{\mathcal{I},\mathcal{J}}$:

$$\begin{aligned} 0 = &\left(\sum_{n=1}^{N}\frac{E_{\alpha_n}-E_{\beta_n}}{\delta_\xi}\right)\mathcal{A}^{(\alpha)}_{\mathcal{I},\mathcal{J}} + \\ &+\lambda\sum_{\substack{l,m=1\\ l<m}}^{N}\left[\sum_{\gamma<\delta}\left(\eta_{\alpha_l\alpha_m,\gamma\delta}\tilde{\mathcal{A}}^{(\alpha)}_{\mathcal{I}^{\gamma\delta}_{lm},\mathcal{J}} - \eta_{\gamma\delta,\beta_l\beta_m}\tilde{\mathcal{A}}^{(\alpha)}_{\mathcal{I},\mathcal{J}^{\gamma\delta}_{lm}}\right)\right] + \\ &+\lambda\sum_{\substack{l,m=1\\ l<m}}^{N}\sum_{n=1}^{N}(-1)^{N+1}\left[\sum_{\gamma}\left(\eta_{\alpha_l\alpha_m,\gamma\beta_n}\tilde{\mathcal{A}}^{(\alpha)}_{\mathcal{I}^{\gamma}_{lm},\mathcal{J}_n} - \eta_{\gamma\alpha_n,\beta_l\beta_m}\tilde{\mathcal{A}}^{(\alpha)}_{\mathcal{I}_n,\mathcal{J}^{\gamma}_{lm}}\right)\right], \end{aligned} \tag{2.30}$$

where $(\mathcal{I},\mathcal{J}) = (\alpha_1\cdots\alpha_N, \beta_1\cdots\beta_N)$ and $\mathcal{I}\neq\mathcal{J}$. The diagonal coefficients appearing on the right-hand side are defined in (2.26).

Similarly as in the single-particle example, Eq. (2.30) can be thought of as a hopping problem for a single particle on a lattice with sites given by the Fock indices $(\mathcal{I},\mathcal{J})$ and local, correlated disorder

$$\mathcal{E}_{\mathcal{I},\mathcal{J}} = \sum_{n=1}^{N}(E_{\alpha_n}-E_{\beta_n}). \tag{2.31}$$

The hopping is provided by the interaction U, see Fig. 2.1a. The non-interacting limit corresponds to the wave-function $\mathcal{A}^{(\alpha)}$ being completely localized on the site $(\mathcal{I},\mathcal{J}) = (\alpha,\alpha)$. The requirement of convergence of the operator expansion (2.15) can thus be interpreted as a localization condition for the hopping problem on the disordered lattice of Fock indices.

C. A lattice with a hierarchical structure

The lattice geometry, as determined by the interactions, is rather complicated. However, Eqs. (2.30) have a clear hierarchical structure: the equation for index sets $\mathcal{I},\mathcal{J}$ of length N are coupled only to amplitudes with index sets of equal or shorter length. Therefore,

the sites can be organized into generations, according to the length of their index sets (this structure was first highlighted in [9] when analyzing the quasiparticle decay in a zero-dimensional quantum dot). Hopping is possible only within the same generation (second term in (2.30)) or between consecutive ones (third term in (2.30)). In the latter case, the hopping is unidirectional, and thus the hopping problem is non-Hermitian.

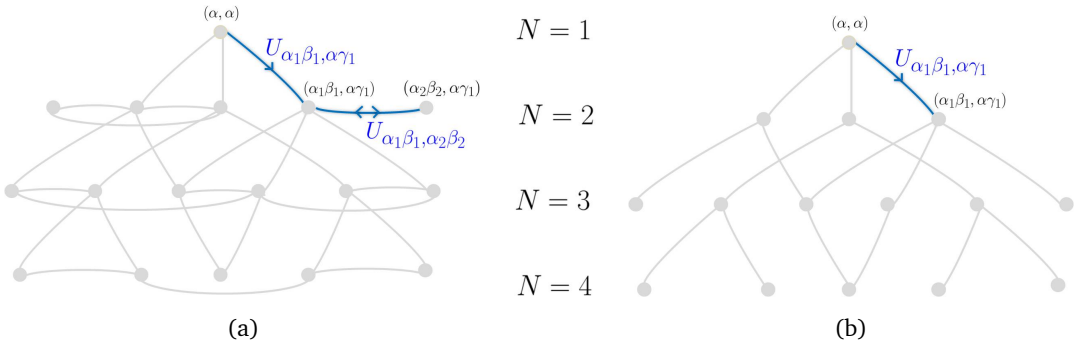

(a) (b)

Figure 2.1: Structure of the operator lattice before (a) and after (b) making the forward approximation. Vertices correspond to Fock indices $(\mathcal{I},\mathcal{J})$; links are drawn between index pairs, which are connected by the interaction U, that is, if the pairs appear simultaneously in at least one of the Eqs. (2.30).

The connectivity of the lattice is a fluctuating variable, determined by the restrictions in energy 2.18 and space (the states involved need to be in the same or in an adjacent localization volume) of the matrix elements $u_{\alpha\beta,\gamma\delta}$. A crucial feature for the following analysis is the different scaling of the *inter*- and *intra*-generation connectivity. Hoppings from a site $(\mathcal{I},\mathcal{J})$ in generation N to a site $(\mathcal{I}',\mathcal{J}')$ in generation $N+1$ requires a particle (or hole) in a state α to scatter to the closest energy level γ above or below α in the single particle spectrum (due to (2.18)), while another particle-hole pair of adjacent levels (β,δ) is created. The number of Fock states $(\mathcal{I}',\mathcal{J}')$ accessible from $(\mathcal{I},\mathcal{J})$ via the decay of a given quasiparticle α is thus of the order of $\sim 4N_{\rm loc}$, i.e. of the connectivity (2.17). In contrast, hoppings from $(\mathcal{I},\mathcal{J})$ to a site of the same generation correspond to processes where each member of a pair of particles (or holes) scatter to one of the two closest energy levels: there are 4 possible final states to which a given pair can decay.

2.2.2 The forward approximation

If $\mathcal{K}$ is large, the number of decay processes of a single particle (or hole) α leading to a site in the following generation is much larger than the one staying in the same generation. This motivates the approximation of neglecting the hopping within the same generation, i.e., of neglecting the second term in (2.30), that we refer to as the forward approximation. Its consequences are the following:

(i) The structure of the lattice simplifies substantially, as some sites that are connected to (α,α) only through inter-generation hoppings are eliminated (the corresponding amplitudes in (2.15) approximated to zero). As pointed out in Sec. 2.1.2, the

resulting simplified lattice, see Fig. 2.1, resembles a Bethe lattice due to the exponential scaling $\sim \mathcal{K}^N$ of the number of sites with their generation N. However, at variance with the Bethe lattice and similarly to the finite dimensional case, there are plenty of loops.

(ii) Once the second term in (2.30) is dropped, the equations for the amplitudes on the retained sites become recursive equations for increasing generations, with initial condition $\mathcal{A}^{(\alpha)}_{\alpha,\alpha} = 1$; this allows one to derive a closed expression for the amplitude at the sites $(\mathcal{I}, \mathcal{J})$ as a sum over all directed, self-avoiding paths from the root (α, α) to the given site:

$$\mathcal{A}^{(\alpha)}_{\mathcal{I},\mathcal{J}} = \sum_{\substack{\text{directed paths} \\ (\alpha,\alpha)\to(\mathcal{I},\mathcal{J})}} (-1)^{\sigma_{\text{path}}} \prod_{i=1}^{N-1} \frac{\lambda\, \eta_{\alpha_i\beta_i,\gamma_i\delta_i}\, \delta_\xi}{\sum_{k=1}^{i} \mathcal{E}_{\alpha_k\beta_k,\gamma_k\delta_k}} \equiv \sum_{\substack{\text{directed paths} \\ (\alpha,\alpha)\to(\mathcal{I},\mathcal{J})}} \omega^{(N)}_{\text{path}}, \quad (2.32)$$

where the factor $(-1)^{\sigma_{\text{path}}}$ takes into account the global fermionic sign associated with the path, arising from the sign factors in (2.30). The expression (2.32) for $\mathcal{A}^{(\alpha)}_{\mathcal{I},\mathcal{J}}$ is of order λ^{N-1}, that is, the lowest possible order in λ for amplitudes of operators involving $2N$ particle-hole indices, as at least $N-1$ interactions are needed to create the corresponding excitations. Thus, the forward approximation amounts to setting to zero, for any N, any term in (2.15) that is of $O(\lambda^N)$ or smaller.

(iii) Within this approximation, the convergence (2.16) is controlled by the generation number N. Indeed, since the amplitudes $\mathcal{A}^{(\alpha)}_{\mathcal{I},\mathcal{J}}$ are of order λ^{N-1} and the interaction is local, the indices satisfy $r(\mathcal{I}, \mathcal{J}) \leq N\xi$: amplitudes involving single particle states sufficiently far away from the localization center α must belong to sufficiently high generations. Thus, (2.16) can be restated as

$$\lim_{N^*\to\infty} \mathbb{P}\left(\sum_{N>N^*} \sum_{\substack{\mathcal{I}\neq\mathcal{J} \\ |\mathcal{I}|=N=|\mathcal{J}|}} \left| A^{(\alpha)}_{\mathcal{I},\mathcal{J}} \right| < \epsilon \right) = 1 \quad (2.33)$$

for arbitrary $\epsilon > 0$. A sufficient condition for (2.33) to hold is that for some $z < 1$ and for N^* sufficiently big:

$$\mathbb{P}\left(\forall N > N^*, \sum_{\substack{\mathcal{I}\neq\mathcal{J} \\ |\mathcal{I}|=N=|\mathcal{J}|}} \left| A^{(\alpha)}_{\mathcal{I},\mathcal{J}} \right| < z^{N-1} \right) = 1 - \zeta(N^*) \quad (2.34)$$

with

$$\lim_{N^*\to\infty} \zeta(N^*) = 0. \quad (2.35)$$

This condition implies the quasilocality of the operators I_α within the forward approximation, as it implies that the first appearance of operators $c_\beta, c^\dagger_\beta$'s in I_α,

with $|r_\beta - r_\alpha| \approx N\xi$ and $N \gg 1$, is with high probability exponentially small in N. The constant $z = \exp(1/\xi_{mb})$ in (2.34) defines a length scale ξ_{mb}, such that truncating the expansion at that scale yields operators that are conserved up to exponentially small corrections: this scale is a localization length pertaining to the interacting problem. The critical value at which the expansion diverges is recovered for $z \to 1$.

The forward approximation simplifies considerably the setting in which to address the convergence of the perturbative expansion. However, it is not free of subtleties. In the following subsections, we derive our main results within this approximate scheme, and postpone to Secs. 2.2.6 and 2.4 the discussion on the caveats related to the approximations made, and on the possible effects produced whenever the neglected terms are taken into account.

2.2.3 Solving the "problem of the factorials"

In this section, we address the problem of the loops formed by highly correlated paths in the operator lattice obtained in the forward approximation. To better understand the nature of the problem, it is useful to consider the diagrammatic representation of the paths shown in Fig. 2.2.

Each path is of length N is associated to an *ordered graph* with N vertices, having two main branches representing the decay of the operators c_α and $c_\alpha^\dagger$ of the initial operator n_α. Self-avoiding paths on the lattice translate into graphs having the geometry of a tree, with a root and N nodes corresponding to the creation of particle-hole pairs. The intermediate states of the graph correspond to the sites $(\mathcal{I}, \mathcal{J})$ along the path in the operator lattice, their energy being $\mathcal{E}_{\mathcal{I},\mathcal{J}}$ in (2.31). The order of the sites along the path fixes the order of the interaction vertices in the graph. The problem of the factorials arises as to each fixed set of N scattering processes, there exist a multiplicity of graphs corresponding to the different order in which the scattering processes occur: each such graph has a different amplitude, as the weights of the paths (2.32) depends on the order in which the interactions occur due to the structure of the energy denominators.

This suggests to introduce a distinction between *graphs* and *diagrams*. Graphs differing only in the ordering of vertices (while sharing the same geometry and labeling of the legs) are grouped into *diagrams* d. An example of graphs belonging to the same diagram is shown in Fig. 2.3: the three paths connecting the state $(\mathcal{I}, \mathcal{J}) = (\alpha_2\beta_2\beta_1\alpha_3, \gamma_2\gamma_1\delta_3\gamma_3)$ to the root (α, α) involve the same interaction matrix elements. The corresponding amplitudes are obviously highly correlated among each others, as they involve the same energies, and strong cancellations between them occur: in the example of Fig. 2.3, the

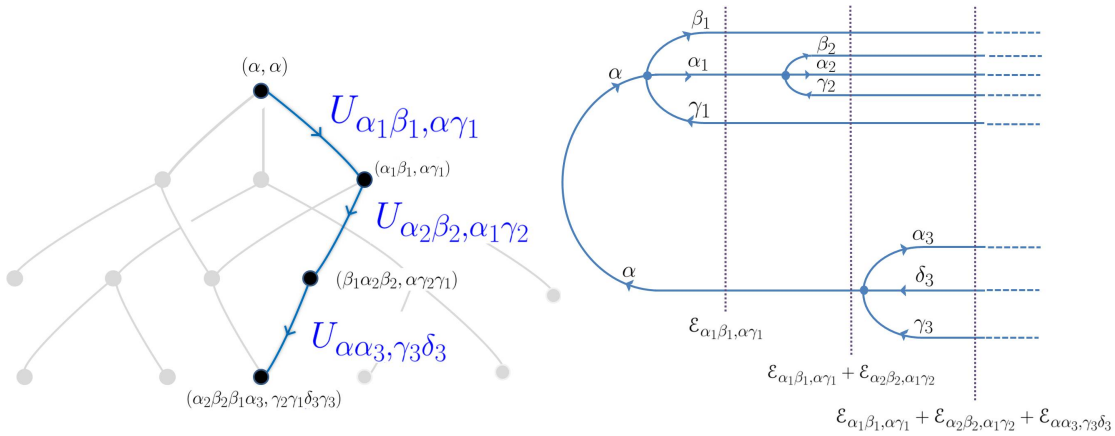

Figure 2.2: Self-avoiding path in the operator lattice and associated ordered scattering graph. The sites $(\mathcal{I},\mathcal{J})$ along the path correspond to the intermediate states of the graph, indicated by dashed lines. Hoppings on the lattice correspond to vertices $U_{\alpha_1\alpha_2,\beta_1\beta_2}$ in the graph. The energy $\mathcal{E}_{\mathcal{I},\mathcal{J}}$ of an intermediate state is the sum of the energy differences $\mathcal{E}_{\alpha_1\alpha_2,\beta_1\beta_2}=E_{\alpha_1}+E_{\alpha_2}-E_{\beta_1}-E_{\beta_2}$ associated with all preceding scatterings. The three excitations emanating from a vertex are associated to the outgoing legs as follows: the excitation with energy level adjacent to the incoming one is associated with the central leg. The upper and lower leg correspond to the particle and the hole, respectively, of the additionally created pair. The condition (2.18) requires them to have an energy difference of the order of δ_ξ.

sum of the energy denominators [5] satisfies

$$\Sigma \equiv \frac{1}{\mathcal{E}_1(\mathcal{E}_1+\mathcal{E}_2)(\mathcal{E}_1+\mathcal{E}_2+\mathcal{E}_3)}+\frac{1}{\mathcal{E}_1(\mathcal{E}_1+\mathcal{E}_3)(\mathcal{E}_1+\mathcal{E}_2+\mathcal{E}_3)} + \frac{1}{\mathcal{E}_3(\mathcal{E}_3+\mathcal{E}_1)(\mathcal{E}_3+\mathcal{E}_1+\mathcal{E}_2)}=\frac{1}{\mathcal{E}_3}\frac{1}{\mathcal{E}_1(\mathcal{E}_1+\mathcal{E}_2)}, \tag{2.36}$$

where $\mathcal{E}_i$ is the energy difference between out- and in-going states at the vertex i. Thus, the sum can be written as a single term $\tilde{\omega}_\Gamma$ that is the product of two weights of the form (2.32), describing the independent decay of the particle $c^\dagger_\alpha$ and the hole c_α respectively:

$$\frac{\tilde{\omega}_\Gamma}{(\lambda\delta_\xi)^3}\equiv\frac{\eta_3}{\mathcal{E}_3}\frac{\eta_1\eta_2}{\mathcal{E}_1(\mathcal{E}_1+\mathcal{E}_2)}, \tag{2.37}$$

where η_i is the random variable associated the vertex i. This is the simplest example of a cancellation between path weights: we refer to $\tilde{\omega}_\Gamma$ as the weight of the 'effective path' associated to the diagram, and we denote it by Γ.

[5] The global sign of amplitudes of tree-like diagrams without loops does not depend on the order in which the interactions act. This is because the associated four-fermion interaction terms mutually commute, which implies that the signs arising from eventually bringing the operators into the normal order are the same for all vertex orders. This justifies the fact that amplitudes are summed keeping fixed the same relative sign.

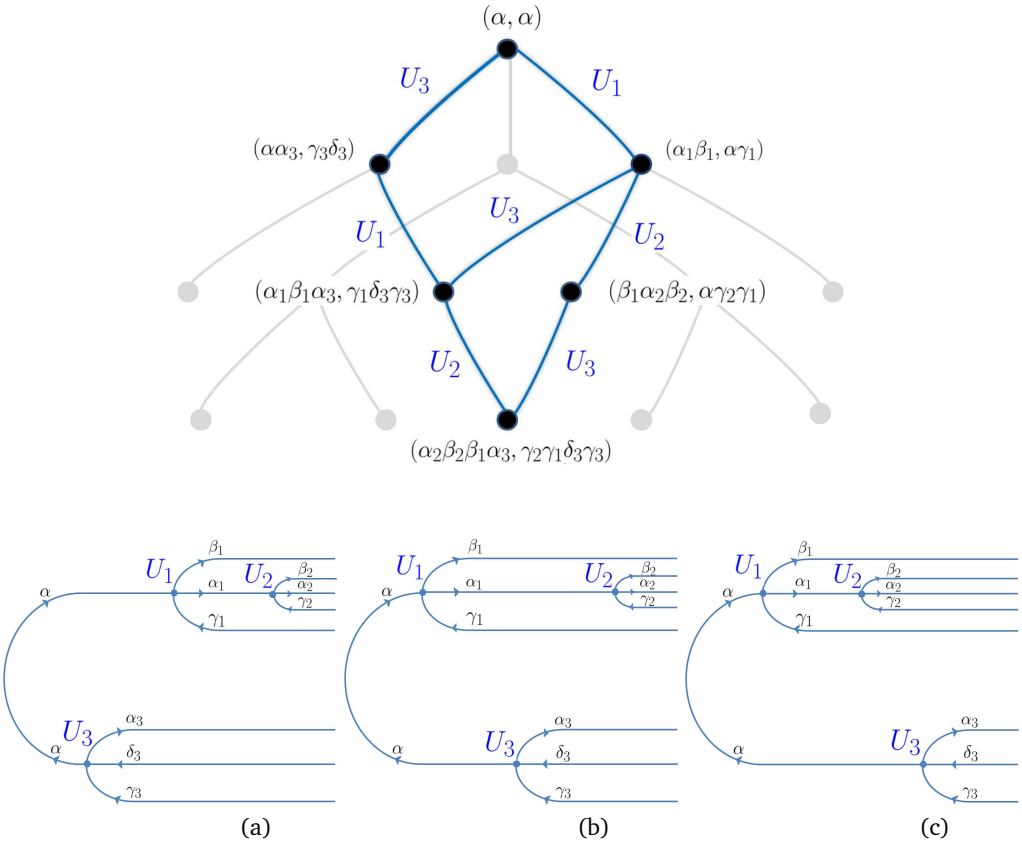

Figure 2.3: Loops in the many-body lattice corresponding to different processes with the same final state, and the corresponding ordered graphs. The graphs differ only in the order in which the interactions U_1, U_2, U_3 act. The weights of such paths are strongly correlated: they are all proportional to the same product of matrix elements, $U_1U_2U_3$, and have highly correlated denominators. The sum over all these ordered graphs constitutes a diagram.

Correlated paths exist for all diagrams with *branchings* (i.e., vertices where more than one of the outgoing excitations undergo further scattering): the order of the subsequent interactions on different branches can be permuted. This corresponds to different paths on the lattice and different ordered graphs, respectively. We argue that resummations of the kind (2.37) can always be performed, in such a way that to each diagram a number of effective paths can be associated, that is much smaller than the number of paths (or graphs) belonging to the diagram. We discuss this considering diagrams whose topology has increasing degree of complexity.

Singly branched diagrams. It can easily be checked by induction that the factorization (2.36) generalizes to an arbitrary number of interactions in diagrams whose only branch is the one between the particle and holes $c^\dagger_\alpha, c_\alpha$. The sum over all path

weights factorizes into the product of the amplitudes associated to the independent decays of the particle $c_\alpha^\dagger$ and the hole c_α, as in (2.37).

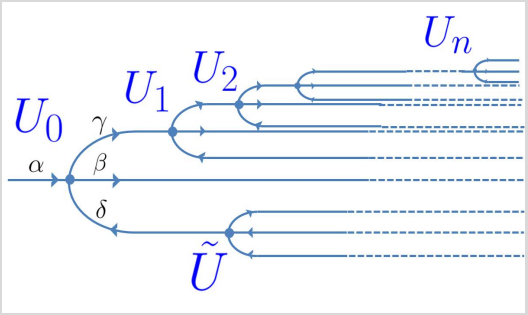

Figure 2.4: Branched decay of a single particle.

Multiply branched diagrams. Let us now discuss further branchings in the sub-diagrams describing the independent decays of the particle $c_\alpha^\dagger$ and the hole c_α. Consider a multi-branched decay of the single particle $c_\alpha^\dagger$, as shown in Fig. 2.4. There the particles γ and δ, which are produced in the first scattering, decay further through n vertices $U_{i=1,\dots,n}$, and the vertex $\tilde{U}$, respectively. The possible orderings of this diagram correspond to $n+1$ correlated paths, which differ by the relative position of the vertex $\tilde{U}$ with respect to the U_i. Their sum,

$$\begin{aligned}\Sigma' =& \frac{1}{\mathcal{E}_0(\mathcal{E}_0+\tilde{\mathcal{E}})(\mathcal{E}_0+\tilde{\mathcal{E}}+\mathcal{E}_1)\cdots(\mathcal{E}_0+\tilde{\mathcal{E}}+\cdots+\mathcal{E}_n)}+ \\ & \frac{1}{\mathcal{E}_0(\mathcal{E}_0+\mathcal{E}_1)(\mathcal{E}_0+\mathcal{E}_1+\tilde{\mathcal{E}})\cdots(\mathcal{E}_0+\mathcal{E}_1\cdots+\mathcal{E}_n)}+\cdots+ \\ & \frac{1}{\mathcal{E}_0(\mathcal{E}_0+\mathcal{E}_1)(\mathcal{E}_0+\mathcal{E}_1+\mathcal{E}_2)\cdots(\mathcal{E}_0+\mathcal{E}_1\cdots+\tilde{\mathcal{E}})},\end{aligned} \tag{2.38}$$

does not simply factorize, but it can nevertheless be written in compact form through an integral representation,

$$\Sigma' = \lim_{\epsilon\to 0}\int \frac{d\omega_1 d\omega_2 \delta\left(\omega_1+\omega_2-\mathcal{E}_0\right)}{\omega_1^-(\omega_1^-+\tilde{\mathcal{E}})\cdot\omega_2^-(\omega_2^-+\mathcal{E}_1)\cdots(\omega_2^-+\mathcal{E}_1+\cdots+\mathcal{E}_n)}, \tag{2.39}$$

where $\omega_i^- = \omega_i - i\epsilon$. Indeed, the sum Σ' (multiplied by the matrix elements of the correspondent vertices) must be equal to the retarded Green function associated to the independent, parallel decay of the particle γ and the hole δ, computed in the forward scattering approximation and at energy $\mathcal{E}_0$. For loop-free graphs like the one of Fig. 2.4, the decay processes of the particle γ and the hole δ are independent. In the time domain, the Green function of their joint decay is the product of the individual Green functions, which leads to the convolution (2.39) in frequency space.

The expression (2.39) for a branched diagram is a random variable, whose probability distribution is hard to analyze. However, the analytic structure of the integrand can be exploited to rewrite Σ' as a sum over a much smaller number of terms than the number of orderings in Eq. (2.38). After performing the integral over ω_2 in Eq. (2.39), we find a number of poles in the complex plane of ω_1. Using the residue theorem, we can write (2.39) as the sum over residues of the poles in the half plane, which contains less poles. In the particular example considered, closing the contour on the upper half plane yields the algebraic identity:

$$\Sigma' = \frac{1}{\tilde{\mathcal{E}}} \frac{1}{\mathcal{E}_0(\mathcal{E}_0+\mathcal{E}_1)(\mathcal{E}_0+\mathcal{E}_1+\mathcal{E}_2)\cdots(\mathcal{E}_0+\mathcal{E}_1+\cdots+\mathcal{E}_n)} - \frac{1}{\tilde{\mathcal{E}}} \frac{1}{(\mathcal{E}_0+\tilde{\mathcal{E}})(\mathcal{E}_0+\tilde{\mathcal{E}}+\mathcal{E}_1)(\mathcal{E}_0+\tilde{\mathcal{E}}+\mathcal{E}_1+\mathcal{E}_2)\cdots(\mathcal{E}_0+\tilde{\mathcal{E}}+\mathcal{E}_1+\cdots+\mathcal{E}_n)}. \tag{2.40}$$

For the considered sub-diagram, the sum over all the $n+1$ orderings of vertices is reduced to the sum of only two 'effective path' weights, whose denominators have a similar structure as the denominators in the original path weight (2.32).

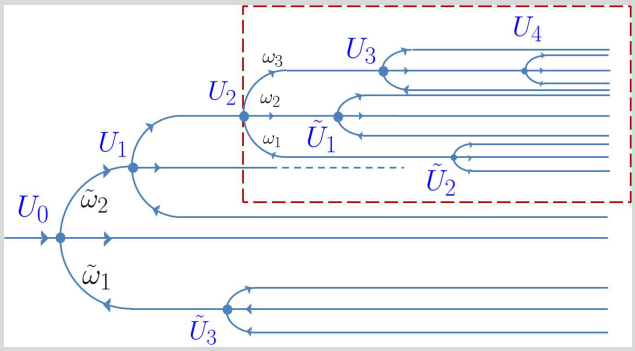

Figure 2.5: A diagram with multiple branchings.

General branched diagrams. A convolution formula analogous to Eq. (2.39) can be written for any branched diagram: to each branching one associates an integral of the form (2.39) with one auxiliary frequency per decaying branch, as well as an energy conserving δ-function for the vertex. Then one eliminates the δ-functions by integrating over the frequency variable, that occurs most often in the denominators. Using the residue theorem, the remaining integrals can be carried out, and the sum over all orderings of a diagram with fixed geometry can be expressed as a much smaller sum of weights of effective paths.

As a further example, we give the explicit expression for the effective path weights associated to diagrams with the geometry of Fig. 2.5. For fixed indices on all segments, there are 105 different orderings of the interactions.[a] Their sum has the

integral representation:

$$I_0\left(\{U\}\right) = \lim_{\epsilon\to 0}\int \frac{d\tilde{\omega}_1 d\tilde{\omega}_2\ \delta\left(\tilde{\omega}_1+\tilde{\omega}_2-\mathcal{E}_0\right)}{\tilde{\omega}_1^-(\tilde{\omega}_1^-+\tilde{\mathcal{E}}_3)\tilde{\omega}_2^-(\tilde{\omega}_2^-+\mathcal{E}_1)} I_1\left(\omega=\tilde{\omega}_2+\mathcal{E}_1+\mathcal{E}_2\right), \tag{2.41}$$

where $\omega_i^- \equiv \omega_i - i\epsilon$, and $I_1\left(\omega\right)$ is the integral representation of the sum of all the weights of the subdiagram in the dashed frame, with incoming energy ω:

$$I_1\left(\omega\right) = \int \frac{d\omega_1 d\omega_2 d\omega_3\ \delta\left(\omega_1+\omega_2+\omega_3-\omega\right)}{\omega_1^-(\omega_1^-+\tilde{\mathcal{E}}_2)\omega_2^-(\omega_2^-+\tilde{\mathcal{E}}_1)\omega_3^-(\omega_3^-+\mathcal{E}_3)(\omega_3^-+\mathcal{E}_3+\mathcal{E}_4)}. \tag{2.42}$$

By means of the residue theorem, I_0 can be rewritten as the sum over only 8 effective path weights:

$$\begin{aligned} I_0\left(\{U\}\right) = &\frac{1}{\tilde{\mathcal{E}}_3}\frac{1}{\mathcal{E}_0(\mathcal{E}_0+\mathcal{E}_1)} I_1(\mathcal{E}_0+\mathcal{E}_1+\mathcal{E}_1) \\ &-\frac{1}{\tilde{\mathcal{E}}_3}\frac{1}{(\tilde{\mathcal{E}}_3+\mathcal{E}_0)(\tilde{\mathcal{E}}_3+\mathcal{E}_0+\mathcal{E}_1)} I_1(\tilde{\mathcal{E}}_3+\mathcal{E}_0+\mathcal{E}_1+\mathcal{E}_1) \end{aligned} \tag{2.43}$$

with:

$$I_1(\omega) = \frac{1}{\tilde{\mathcal{E}}_1\tilde{\mathcal{E}}_2}\left[f(\omega) - f(\omega+\tilde{\mathcal{E}}_1) - f(\omega+\tilde{\mathcal{E}}_2) + f(\omega+\tilde{\mathcal{E}}_1+\tilde{\mathcal{E}}_2)\right] \tag{2.44}$$

and:

$$f(X) = \frac{1}{X(X+\mathcal{E}_3)(X+\mathcal{E}_3+\mathcal{E}_4)}. \tag{2.45}$$

Note that as a function of the $\mathcal{E}_i$ and $\tilde{\mathcal{E}}_i$, I_0 has poles only due to denominators which involve the incoming energy $\mathcal{E}_0$, while I_0 remains regular as any of the $\tilde{\mathcal{E}}_i \to 0$, due to cancellations among different terms.

[a] The interactions in the red dashed frame can be ordered in 15 different ways, for each of which the interaction $\tilde{U}_3$ can be placed in 7 different positions.

This reasoning illustrates how to systematically perform the resummation of correlated paths, generating a set of effective paths for each diagram d. Denoting with $\mathcal{D}_{\mathcal{I},\mathcal{J}}$ the set of all diagrams d with final state $\mathcal{I},\mathcal{J}$, and with $\mathcal{P}(d)$ the set of effective path weights $\tilde{\omega}_\Gamma$ associated to each d, we may write:

$$\mathcal{A}^{(\alpha)}_{\mathcal{I},\mathcal{J}} = \sum_{d\in\mathcal{D}_{\mathcal{I},\mathcal{J}}}\left(\sum_{\Gamma\in\mathcal{P}(d)}\tilde{\omega}_\Gamma\right) \equiv \sum_{d\in\mathcal{D}_{\mathcal{I},\mathcal{J}}} S(d). \tag{2.46}$$

The fact that the procedure described in this section suffices to solve the problem of the factorials, meaning that the factorially-large number of self-avoiding paths reduces to a

number of effective paths $|\mathcal{P}(d)|$ that is only *exponential* in N, is shown to be true in Sec. 2.2.5.

We now come to the solution of the technical issues listed in Sec. 2.1.2, which is necessary in order to estimate the probability distribution of (2.46) for the computation (2.34). This is done in the following two sections.

2.2.4 Issue 1: Large deviations of effective paths

In this section, we compute the large deviations of the path weights, asymptotically in their length N. As we shall argue in Sec. 2.2.6, the large deviations of operator amplitudes (2.46) are essentially determined by the large deviations of effective path weights. The weight of any effective path is the products of two terms, describing the decay of $c_\alpha^\dagger$ and c_α, respectively. In each of those terms, (cf. (2.40) and (2.43)), the functional dependence on the $\mathcal{E}_i$ is similar to that in the original path weights (2.32). We thus compute the large deviations of the latter, and subsequently argue that general effective paths behave essentially identically.

Because of the energy restrictions (2.18) the energy differences $\mathcal{E}_{\alpha\beta,\gamma\delta}/\delta_\xi$ are random variables of order $O(1)$. For simplicity, we take them as independent Gaussian random variables with zero mean and unit variance. The denominators in (2.32) are partial sums of such energies, and we may write:

$$|\omega_{\text{path}}| = \prod_{i=1}^{N-1} \frac{\lambda|\eta_{\alpha_i\beta_i,\gamma_i\delta_i}|}{|s_i|}, \tag{2.47}$$

where $s_i = (\mathcal{E}_1 + \cdots + \mathcal{E}_i)/\delta_\xi$, with $\mathcal{E}_i \equiv \mathcal{E}_{\alpha_i\beta_i,\gamma_i\delta_i}$. Since rare events occur because small denominators are produced, we characterize the distribution of the product of denominators. The numerator behaves as $\sim (\lambda\eta_{\text{typ}})^{N-1}$, with $\eta_{\text{typ}} = \exp[\langle \log|\eta|\rangle] = 1/e$, and we neglect the Gaussian fluctuations of its logarithm.

The distribution function $P_N(y)$ of

$$Y_N \equiv -\sum_{i=1}^{N} \log|s_i| \tag{2.48}$$

can be obtained from its generating function,

$$G_N(k) \equiv \mathbb{E}\left[e^{-kY_N}\right], \tag{2.49}$$

by inverse Laplace transform,

$$P_N(y) = \frac{1}{2\pi i}\int_{\mathcal{B}} e^{yk} G_N(k) dk, \tag{2.50}$$

where $\mathcal{B}$ is the Bromwich path in the complex k-plane. In the present case, the relevant y

scales linearly with N, and thus we define $\tilde{y} = y/N$, and

$$P_N(N\tilde{y}) = \frac{1}{2\pi i}\int_{\mathcal{B}} e^{N\phi_N} dk, \tag{2.51}$$

where the function

$$\phi_N(\tilde{y},k) = \tilde{y}k + \frac{\log G_N(k)}{N} \overset{N\to\infty}{\to} \phi(\tilde{y},k) \tag{2.52}$$

has a well-defined limit, $\phi(\tilde{y},k)$, for large N. In the following, we compute (2.51) with a saddle point calculation, assuming $N \gg 1$.

As we derive in Appendix 2.B, it holds:

$$\phi(\tilde{y},k) = \tilde{y}k + \log\left[\Gamma\left(\frac{k+1}{2}\right) + \sqrt{2\pi}\delta\lambda(k)\right] - \frac{1}{2}\log 2\pi. \tag{2.53}$$

In the saddle point calculation, the contour in (2.51) has to be deformed to pass parallel to the imaginary axis through $k^* = k^*(\tilde{y})$, which satisfies:

$$\begin{aligned}\tilde{y} &= -\frac{d}{dk}\left[\lim_{N\to\infty}\frac{\log G_N(k)}{N}\right]_{k=k^*(\tilde{y})} = -\frac{d}{dk}\left\{\log\left[\Gamma\left(\frac{1+k}{2}\right) + \sqrt{2\pi}\delta\lambda(k)\right]\right\}_{k=k^*(\tilde{y})} \\ &= -\left\{\frac{1}{2}\psi^{(0)}\left(\frac{1+k}{2}\right)\left[1 + \frac{\sqrt{2\pi}\delta\lambda(k)}{\Gamma\left(\frac{1+k}{2}\right)}\right]^{-1} + \frac{\sqrt{2\pi}\delta\lambda'(k)}{\Gamma\left(\frac{1+k}{2}\right) + \sqrt{2\pi}\delta\lambda(k)}\right\}_{k=k^*(\tilde{y})},\end{aligned} \tag{2.54}$$

where $\psi^{(0)}(x) \equiv d\log[\Gamma(x)]/dx$.

As we shall see in Sec. 2.2.6, in the case of parametrically small interaction strength λ (which is relevant for large connectivity $\mathcal{K}$), we can restrict our attention to $\tilde{y} \gg 1$. For large values of $\tilde{y}$, the saddle point tends to $k^* \to -1$. To isolate the singularity in $k = -1$ we use the Laurent expansion of $\psi^{(0)}(x)$ around $x = 0$:

$$\psi^{(0)}\left(\frac{1+k}{2}\right) = -\frac{2}{k+1} - \gamma + \frac{\pi^2}{12}(k+1) + O((k+1)^3), \tag{2.55}$$

where γ is the Euler constant. This allows us to recast (2.54) in the following form:

$$\tilde{y} = \frac{1}{k^*+1} + Q(k^*+1). \tag{2.56}$$

Here, $Q(\cdot)$ is an analytic function with expansion:

$$Q(x) = \frac{\gamma}{2} - \frac{\pi^2}{18}x + O(x^2). \tag{2.57}$$

This yields the equation

$$1+k^*=\frac{1}{\tilde{y}}\left(1-\frac{Q(k^*+1)}{\tilde{y}}\right)^{-1}, \tag{2.58}$$

which can be solved by iteration as an expansion in $1/\tilde{y}$:

$$1+k^*(\tilde{y})=\frac{1}{\tilde{y}}+\frac{\gamma}{2}\frac{1}{\tilde{y}^2}+\left(\frac{\gamma^2}{4}-\frac{\pi^2}{18}\right)\frac{1}{\tilde{y}^3}+\ O\left(\frac{1}{\tilde{y}^4}\right). \tag{2.59}$$

Expanding (2.53) in powers of $k+1$ and substituting (2.59) we find:

$$\phi(\tilde{y},k^*(\tilde{y}))=-\tilde{y}+\log\tilde{y}-\frac{1}{2}\log\left(\frac{\pi}{2e^2}\right)-\frac{\gamma}{2\tilde{y}}+\frac{1}{8}\left(\frac{5\pi^2}{18}-\gamma^2\right)\frac{1}{\tilde{y}^2}+\ O\left(\frac{1}{\tilde{y}^3}\right). \tag{2.60}$$

Finally, within the saddle point approximation to Eq. (2.50), for $\tilde{y}\gg 1$ we obtain

$$P_N\left(-\log\left[\prod_{i=1}^{N}\frac{1}{|s_i|}\right]=N\tilde{y}\right)=C(\tilde{y},N)\left(\frac{2e}{\sqrt{2\pi}}\right)^N\tilde{y}^N e^{-N\mathcal{F}(\tilde{y})}\left[1+\frac{1}{N}\right], \tag{2.61}$$

where

$$\mathcal{F}(\tilde{y})=\tilde{y}+\frac{\gamma}{2\tilde{y}}-\frac{1}{8}\left(\frac{5\pi^2}{18}-\gamma^2\right)\frac{1}{\tilde{y}^2}+\ O\left(\frac{1}{\tilde{y}^3}\right). \tag{2.62}$$

The prefactor

$$C(\tilde{y},N)=\left(\frac{1}{2\pi N\phi_N''(k^*(\tilde{y}))}\right)^{\frac{1}{2}}\frac{c(k^*(\tilde{y}))}{\lambda_{\max}(k^*(\tilde{y}))} \tag{2.63}$$

yields only logarithmic corrections to the exponent.

When restricting to the linear term in (2.62), the large deviation statistics for the correlated denominators coincides with that of *independent*, identically distributed Gaussian energy denominators. Indeed, from Eqs. (2.127) and (2.128) it follows that to leading order in $k+1$ the exponential growth of G_N is almost equal to that of the generating function $g_N(k)=\left[2^{\frac{k+1}{2}}\Gamma\left(\frac{k+1}{2}\right)/\sqrt{2\pi}\right]^N$ associated with products of N independent Gaussian denominators with unit variance. For $\tilde{y}\gg 1$, the tail of the distribution is determined by the residue of the pole of the generation function at $k=-1$, which is identical in the two cases. Repeating the above derivation of large deviations for independent denominators with generating function $g_N(k)$, one finds that it differs from (2.61) at order $O\left(1/\tilde{y}\right)$: the tails for correlated denominators are suppressed by a factor $\exp\left(-N\frac{\log 2}{2}\frac{1}{\tilde{y}}\right)$. The correction $\delta\lambda(k)$ in (2.129) contributes to (2.62) only at order $O\left(1/\tilde{y}^2\right)$.

Physically, this result can be understood as follows: by restricting to $\tilde{y}\gg 1$, we are

concentrating on very rare realizations of Y_N. Those are insensitive to the details in the structure of the denominators. Indeed, atypically big values of objects like $\left(\prod_{i=1}^{N} s_i\right)^{-1}$ arise from restraining the random walk $(s_1, \cdots, s_N)$ to the vicinity of the origin. This boils down to computing the probability that s_i is small *conditioned* on the fact that s_{i-1} was small. To leading order in the typical smallness of such denominators, one obtains the same result as by minimizing N denominators independently. The leading correction with respect to the case of iid denominators consists in a small suppression of the tail, since it is slightly less probable to encounter small denominators, when they are correlated.

The above reasoning can be extended to more general weights $\tilde{\omega}_\Gamma$, associated with effective paths. Indeed, the corresponding denominators are still products of single energies or partial sums (see Eq. (2.40) or Eq. (2.43). In the limit of very large deviations ($\tilde{y} \gg 1$) they all share the same tail distribution (2.61), the only relevant parameter being the total number N of denominators. Therefore, approximating the numerator in $\tilde{\omega}_\Gamma$ with its typical value $(\lambda \eta_{\rm typ})^N$ and using (2.61), we finally obtain:

$$\mathbb{P}\left(\frac{\log|\tilde{\omega}_\Gamma|}{N} = \tilde{x} + \log \lambda \eta_{\rm typ}\right) \approx C(\tilde{x}, N) \left(\frac{2e}{\sqrt{2\pi}}\right)^N \tilde{x}^N e^{-N\mathcal{F}(\tilde{x})}, \tag{2.64}$$

with $\mathcal{F}$ given in (2.62).

2.2.5 Issue 2: how many terms are we summing on?

In this section, we estimate the total number of effective paths of length N, which we denote with:

$$\mathcal{N}_N = \sum_{\substack{\mathcal{I}\neq\mathcal{J} \\ |\mathcal{I}|=N=|\mathcal{J}|}} \sum_{d\in\mathcal{D}_{\mathcal{I},\mathcal{J}}} \mathcal{P}(d). \tag{2.65}$$

We do this in two steps: as a first step, we estimate the number of *diagrams* at a given order N, that we denote with $N_{\rm diag}$. Each diagram d is associated to a certain number $|\mathcal{P}(d)|$ of effective paths, which depends on the structure of the diagram. In the second step, we compute an upper bound on this number, that we denote with $\overline{|\mathcal{P}|}$.

Counting the number of diagrams with a given final state $(\mathcal{I}, \mathcal{J}) = (\alpha_1 \cdots \alpha_N, \beta_1 \cdots \beta_N)$ is complicated due to the locality, which imposes constraints on the geometry of the diagrams. Indeed, the localization centers $r_{\alpha_i}, r_{\beta_i}$ of the single particle indices in the final state $(\mathcal{I}, \mathcal{J}) = (\alpha_1 \cdots \alpha_N, \beta_1 \cdots \beta_N)$ are distributed over a certain number of localization volumina of size ξ around r_α, with a given number of single particle indices per localization volume. Due to the energy restrictions (2.18), particles and holes belonging to the same localization volume are organized in pairs: members of a pair are produced in the same scattering process, and have an energy difference of order δ_ξ. Only particle-hole pairs in nearby localization volumina can be involved in the same interaction vertex: this is what imposes the constraints on the geometry. For example, consider the case of spatial dimension $d = 1$ and consider states $(\mathcal{I}, \mathcal{J})$ having only one particle-hole pair per

localization length: necessarily, they must be associated to diagrams with no branchings in the decays of $c_\alpha^\dagger$ and c_α, since the particle-hole pairs must be created in a fixed order dictated by their spatial sequence, and thus no permutation is possible. In contrast, final states with several pairs per localization length can be reached by a variety of diagrams.

We estimate N_{diag} by computing a lower and an upper bound on it. The lower bound is obtained focusing on a subclass of diagrams, corresponding to scattering processes with a "necklace structure", in which the particle-hole pairs are created in a sequence of n groups of $m_{i=1,\dots,n}$ pairs, each group belonging to a single localization length. We estimate the number of diagrams with this structure, that we denote with $N_{\text{diag}}^{\text{neck}}$. The counting is similar to the one in Ref. [72]: however, in this calculation we include diagrams corresponding to final states with a non-uniform density of particle and hole indices per localization length, which have a larger abundance. An upper bound on N_{diag} is easily obtained dropping any constraint on the geometry due to locality. Combining these results, we obtain the estimate given in Eqs. (2.81), (2.82).

A. How many diagrams? A lower bound

This section is splitted into two parts: in the first one, we consider a fixed sequence of $m_{i=1,\dots,n}$ and we count all possible diagram with necklace structure characterized by this sequence. In the second part, we sum over all possible sequences $m_{i=1,\dots,n}$ in order to get the total number of necklace diagrams.

Constructing necklace diagrams. Consider a sequence of $m_{i=1,\dots,n}$. Each m_i is bounded by the maximal number of particle-hole pairs per localization volume ($N_{\text{loc}} = \mathcal{K}/4$), and $\sum_{i=1}^n m_i = N$. Due to locality, pairs belonging to the $i-$th and $(i+1)-$th group belong to neighboring localization volumina in real space; pairs belonging to different groups $i, j \neq \{i-1, i+1\}$ might belong to the same localization volume. We construct the possible diagrams corresponding to a fixed sequence $m_{i=1,\dots,n}$ in two steps: first, for every group i we build all possible sub-diagrams with final indices corresponding to the indices of the m_i pairs, as illustrated in Fig. 2.6. Then, we connect sub-diagrams of neighboring groups by a single scattering vertex.

A central ingredient for this step is the number of all possible geometries of diagrams with m interactions in a given localization volume, see Fig. 2.6, that we denote by $\mathcal{T}_m$ and determine in Appendix 2.C, the result being:

$$\mathcal{T}_n = \frac{3^{\frac{3}{2}+3n}}{\pi} \frac{\Gamma\left(n+\frac{2}{3}\right)\Gamma\left(n+\frac{4}{3}\right)}{\Gamma\left(2n+3\right)} \sim \frac{3}{4}\sqrt{\frac{3}{\pi}}\frac{1}{n^{\frac{3}{2}}}\left(\frac{27}{4}\right)^n . \tag{2.66}$$

Following the reasonings explained in Fig. 2.6, we find the number of necklace diagrams associated with fixed groups of m_i pairs to be

$$n_{\text{neck}} = \prod_{i=1}^{n} \left[m_i 2^{m_i} m_i! \mathcal{T}_{m_i}\right] . \tag{2.67}$$

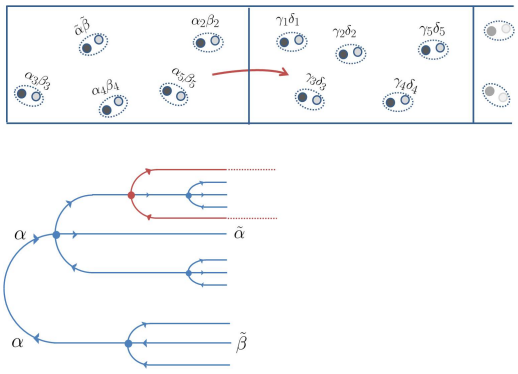

(a) The m_1 pairs of the first group belong to the localization volume containing the localization center r_α, with one pair ($\tilde{\alpha}\tilde{\beta}$ in the Figure) with energies close to ϵ_α. The remaining m_1 pairs ($m_1 - 1$ in the same volume and one in the adjacent volume) are produced in m_1 scatterings organized in diagrams with all possible geometries ($\mathcal{T}_{m_1}$ of them). For each geometry, a factor m_1 comes from the choice of the vertex (red in the Figure) that produces a pair in the subsequent localization volume.

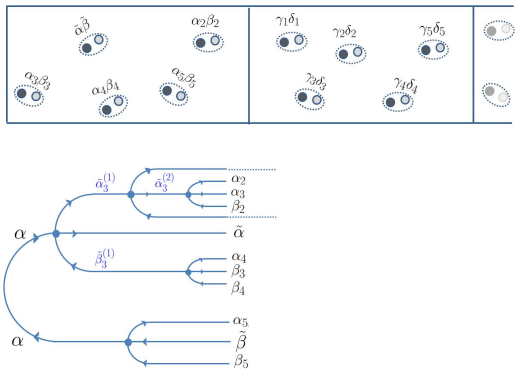

(b) The indices of the remaining $m_1 - 1$ pairs in the localization volume are assigned to the legs. This fixes all labels up to the internal legs. For the first localization volume, the possible internal indices satisfying the energy restrictions are 2^{m_1-2}, α being fixed.

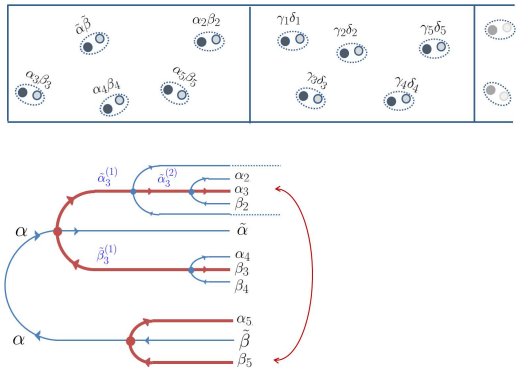

(c) For a fixed geometry and a set of final labels, the permutation of assignments of labels to the legs gives rise to an independent diagram with the same final state, since the matrix elements of the interactions change. There are $(m_1 - 1)!$ such permutations (the pair $\tilde{\alpha}\tilde{\beta}$ is fixed). When legs are permuted, the corresponding internal indices must change as well in order to satisfy the energy restriction of the interactions (in the Figure, $\tilde{\alpha}_3^{(i)} \to \tilde{\alpha}_5^{(i)}$ and $\tilde{\beta}_3^{(i)} \to \tilde{\beta}_5^{(i)}$).

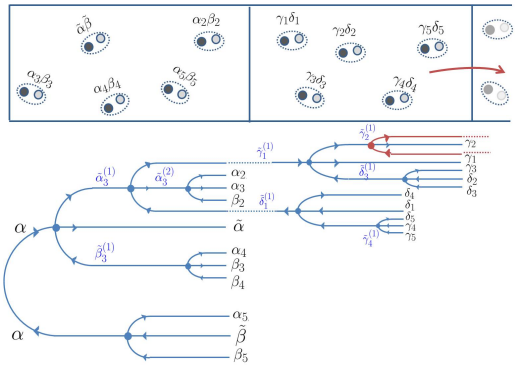

(d) Diagrams corresponding to the decay processes in the adjacent localization volume are attached to a pair of legs selected in (a). Again, m_2 interactions occur on two branches, in a total of $\mathcal{T}_{m_2}$ possible distinct geometries. There are m_2 choices to select the pair of legs to which to attach the next subdiagram. For any of the $m_2!$ labelings of the remaining external legs, there are two choices for each internal index, corresponding to whether the incoming particle scatters up or down in energy. In total there are $m_2 2^{m_2} m_2! \mathcal{T}_{m_2}$ different diagrams associated to this group of pairs. The same counting holds true for the subsequent groups.

Figure 2.6: Construction of the diagrams representing the decay of groups of m_i particle-hole pairs, where members of the same group belong to the same localization volume. The diagrams are constructed by connecting sub-diagrams describing the decay of each single group of pairs. We restrict the combinatorics to only one scattering vertex connecting the sub-diagrams of different groups.

The origin of the various factors is explained in detail in Fig. 2.6: the factor m_i counts the number of pairs which are created subsequently to the first pair entering the volume associated to the group i. One of those m_i pairs belongs to the adjacent localization volume and creates the subsequent cascade of pair creations there. The second factor describes the choice of two levels (the level closest in energy above or below) to which an incoming quasiparticle may scatter at a vertex. The factorial term comes from the choice of assigning the m_i pairs to the final legs of a given tree diagram in the localization volume of group i.

We now count the number of possible diagrams having this structure of m_i. Consider first the case in which only a single group i of pairs occupies a given localization volume. The number of choices of $\{m_i\}$ particle-hole pairs is given by

$$n_s(\{m_i\},\mathcal{K}) \equiv \prod_{i=1}^{n} 2^{m_i} \binom{N_{\text{loc}} - m_i}{m_i} = \prod_{i=1}^{n} \left[2^{m_i} \binom{\mathcal{K}/4 - m_i}{m_i} \right]. \tag{2.68}$$

Indeed, a configuration of m_i pairs of (disjoint) adjacent levels, and the remaining $N_{\text{loc}} - 2m_i$ untouched levels in the same localization volume form a set of $N_{\text{loc}} - m_i$ objects, out of which m_i are pairs. This explains the binomial factor. For each pair, one can choose how to assign the two levels to particle and hole, respectively. This yields the factor 2^{m_i}.

As we will see below, the relevant m_i are of order $O(1) \ll \mathcal{K}$. We therefore approximate:

$$\binom{\mathcal{K}/4 - m_i}{m_i} \approx \frac{(\mathcal{K}/4)^{m_i}}{m_i!}. \tag{2.69}$$

Note that the necklace structure will in general fold back and forth in real space, such that several groups will get to lie in the same volume. Nevertheless, the above approximation remains good as long as the total number of pairs created in a given localization volume is significantly smaller than $\mathcal{K}$.

Counting necklace diagrams. Combining Eqs. (2.67-2.69), the total number of necklace diagrams is:

$$N_{\text{diag}}^{\text{neck}} \approx \sum_{\{m_i\}|\sum_i m_i = N} \frac{1}{2} \prod_{i=1}^{n} [2\mathcal{K}^{m_i} m_i \mathcal{T}_{m_i}]. \tag{2.70}$$

The factors of 2 arise due to freedom of each group to scatter to the left or the right of the preceding group as long as there is still significant phase space in the corresponding localization volumina. The correction due to the finiteness of $\mathcal{K} \gg 1$ is small and was thus neglected.

We now determine the distribution of group sizes $\{m_i\}$ which dominates the sum (2.70),

writing

$$\begin{aligned} N_{\text{diag}}^{\text{neck}} &\approx \frac{1}{2} \sum_{\{m_i\}|\sum_i m_i = N} \prod_i 2\mathcal{K}^{m_i} m_i \mathcal{T}_{m_i} = \frac{\mathcal{K}^N}{2} \sum_{\{m_i\}|\sum_i m_i = N} \prod_i 2 m_i \mathcal{T}_{m_i} \\ &= \frac{\mathcal{K}^N}{2} \sum_{\{n_m\}|\sum_m m n_m = N} \binom{\sum_m n_m}{n_1, n_2, ..., n_m} \prod_m (2m\mathcal{T}_m)^{n_m}, \end{aligned} \tag{2.71}$$

where $n_m = \sum_i \delta_{m,m_i}$ is the number of groups i with m pairs. For the relevant m's, $n_m \sim N \gg 1$; therefore, at large N the sum (2.71) is dominated by the saddle point over the n_m. Imposing the constraint $\sum_m m n_m = N$ with a Lagrange multiplier μ yields the saddle point equations:

$$\mu m = -\log(n_m) + \log(\sum_m n_m) + \log(2m\mathcal{T}_m), \tag{2.72}$$

and thus

$$\frac{n_m}{\sum_{m'} n_{m'}} = 2m\mathcal{T}_m e^{-\mu m}. \tag{2.73}$$

The Lagrange multiplier μ is fixed by the constraint:

$$1 = \sum_m 2m\mathcal{T}_m e^{-\mu m} = -2\frac{d}{d\mu}[\mathcal{T}(x = e^{-\mu})], \tag{2.74}$$

with $\mathcal{T}(x) = \sum_m \mathcal{T}_m x^m = [T(x)]^2$, where $T(x)$ is defined in (2.135). The solution of Eq. (2.74) is:

$$e^{-\mu} = 0.0941. \tag{2.75}$$

The saddle point solution can thus be written as

$$\frac{n_m}{N} = Am\mathcal{T}_m e^{-\mu m}, \tag{2.76}$$

where $1/A = d^2/d\mu^2[T(x = e^{-\mu})^2] = 1/0.778$, as follows from the constraint $\sum_m m n_m = N$. The resulting values for n_m/N are shown in Fig. 2.7a. The probability that a given pair is created in a scattering process involving a total of m pairs in the same localization volume is plotted in Fig. 2.7b. We see that most pairs are created together with a few more pairs within the same localization volume.

Plugging (2.76) into the saddle point for $N_{\text{diag}}^{\text{neck}}$, we find the number of diagrams to grow like

$$N_{\text{diag}}^{\text{neck}} \approx (\mathcal{K}e^{\mu})^N \approx (10.6\,\mathcal{K})^N. \tag{2.77}$$

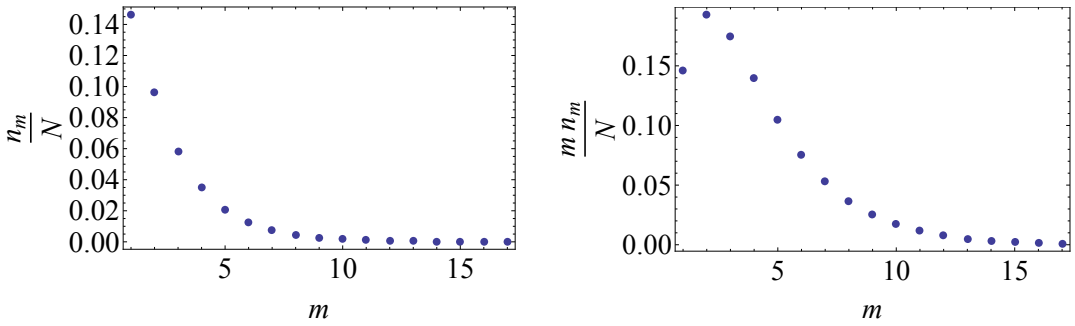

Figure 2.7: The plot (a) shows the distribution of the number n_m/N of groups of m particle-hole pairs in necklace diagrams dominating $\mathcal{N}_N$. The plot (b) shows the probability mn_m/N that a given pair belongs to a group containing m pairs.

A comment: the spatial structure of the dominating processes. Following the above reasoning we find that in the restricted set of necklace diagrams the optimal distribution of group sizes m_i's is peaked at values of order $O(1)$, but still clearly larger than one. Upon folding of the necklace, the number of pairs per localization volume will become even more significantly larger than 1. Thus we see that multiple scattering processes within a localization volume significantly enhance the delocalization tendency. This shows that the many-body problem is genuinely different from an effective one-body problem, in which a simple excitation would propagate nearly ballistically, by shedding one particle-hole excitation in every localization volume. This might have implications for localization in higher dimensions (if any), as it suggests that the necklace-type diagrams are diffusing back and forth a lot. This contrasts with the model in [20], where the hopping strength between adjacent volumina was assumed to be parametrically smaller than λ, which favored the particle-hole creation cascade to fully explore a localization volume before moving on to the next volume. The latter led to conjecture a critical exponent for the localization length in higher dimensions by relating the decay processes of single particle excitations to self-avoiding random walks. This scenario hardly holds in our model, as the optimal processes are not of this kind.

B. How many diagrams? An upper bound

An upper bound on N_{diag} can be easily obtained realizing that all possible diagrams consist in all geometrically possible labellings of trees of size N. The number of trees grows as $(27/4)^N$. For each label one has roughly $3\mathcal{K}$ possibilities, as the pair must lie in a localization volume adjacent to or identical with the one of the pair preceding it on the tree. This yields the simple upper bound

$$N_{\text{diag}} < (3 \cdot \frac{27}{4}\mathcal{K})^N \approx (20.25\,\mathcal{K})^N, \tag{2.78}$$

which yields a growth factor which is only about a factor of 2 bigger than the much more conservative estimate (2.77).

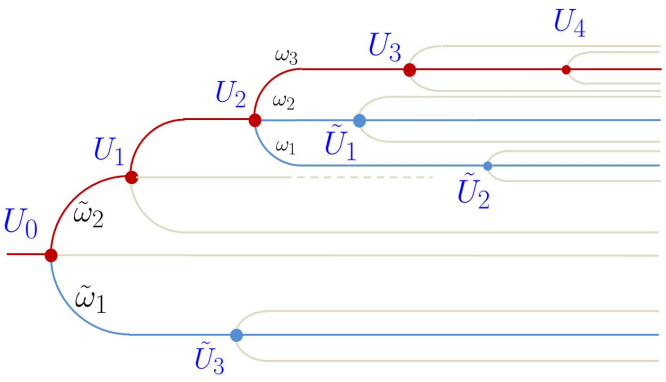

Figure 2.8: Diagram with colored branches. The branches with maximal and minimal (equal to zero) number of interactions along them are colored in red and gray, respectively. In this case, the three branches that remain after eliminating the red one contribute 2 residua each. The total number of effective paths is obtained by multiplying these numbers, which gives $2^3 = 8$.

C. How many effective paths for each diagram?

The minimal number of effective paths associated to a diagram d equals to the product of the number of residua of any of the performed integrals in the representation (2.39) and analogous. This number can be determined from the structure of the diagram using the following rules:

1. eliminate the final leaves which are not associated to auxiliary frequencies, since they do not contribute with poles in the integral representation (Fig. 2.8 represents the diagram of Fig. 2.5, with these eliminated branches colored in gray);

2. determine the directed path (branch) with the maximal number of interactions along it (red one in Fig. 2.8), and eliminate the auxiliary frequencies along this path integrating the corresponding δ-functions;

3. all remaining branches contribute one more residua than interactions along the branch.

To obtain an upper bound on $|\mathcal{P}(d)|$, we compute the minimal number of effective paths associated to diagrams d_{max} with a maximally branched geometry, see Fig. 2.9. The maximally branched diagram consists of two regular rooted trees with $L(N) \equiv \log(N+1)/\log 3$ generations. Since the weights of the two sub-diagrams factorize, we need to count only the effective paths associated to one of them, and square this number. We therefore consider one sub-diagram, and organize its branches according to the number of interactions along it (in Fig. 2.9b, branches with the same number of interactions have the same color). The number l of interactions along a branch ranges from 1 to $L(N) - 1$. There are $2 \cdot 3^{L(N)-1-l}$ branches with l interactions; each of them

contributes with $(l+1)$ residua, yielding a total number of

$$\prod_{l=1}^{L(N)-1}(l+1)^{2\cdot 3^{L(N)-1-l}} = \exp\left(3^{L(N)}\sum_{k=1}^{\infty}\frac{2\log k}{3^k} - \frac{2}{3}\sum_{k=0}^{\infty}\frac{\log\left(k+L(N)+1\right)}{3^k}\right) \tag{2.79}$$

terms. Using that $2\sum_{k=1}^{\infty}3^{-k}\log(k) = 0.29$, one finds that the minimal number of effective paths for diagrams with this geometry, which is the square of the above, scales as:

$$\overline{|\mathcal{P}|} = \exp\left[0.58\,N + o(N)\right]. \tag{2.80}$$

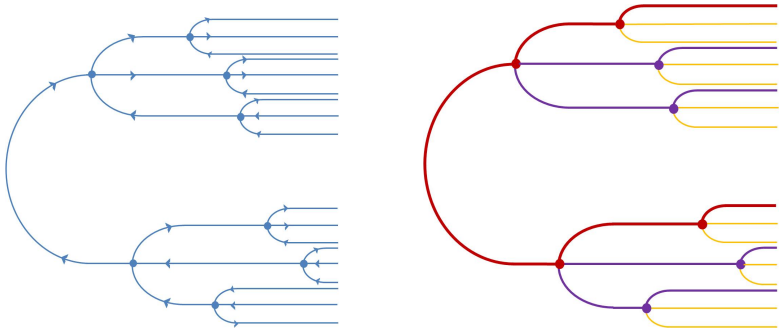

(a) (b)

Figure 2.9: (a) Diagram with the maximal possible number of branchings. (b) Branches with the same number of interactions are drawn with the same color.

D. Total number of effective paths of a given length

The total number of effective paths $\mathcal{N}_N$ is the sum over all diagrams with N interactions of the number of effective paths associated to each diagram, $|\mathcal{P}(d)|$. Approximating the latter with (2.80) and using $e^{\alpha} \approx e^{0.58} = 1.79$ together with (2.77) and (2.78), we find

$$\mathcal{N}_N \approx (C\,\mathcal{K})^N, \tag{2.81}$$

with

$$18.97 < C < 36.25. \tag{2.82}$$

2.2.6 The regime of stability of the perturbative construction

With the elements given in Secs. 2.2.4 and 2.2.5, we are in the position to estimate the left hand side of (2.34). We begin by arguing that, among all the effective paths in (2.46), only very few ones dominate the sum. Based on this hypothesis, we estimate the convergence radius of the perturbation theory for operator. Finally, we comment of the

weak convergence of the operator expansion.

A. Domination by rare, large effective paths

We argue that (2.46) is a random variable with fat tail, dominated by the single effective path with maximal weight contributing to it,

$$\mathcal{A}^{(\alpha)}_{\mathcal{I},\mathcal{J}} \approx \max_{d\in\mathcal{D}_{\mathcal{I},\mathcal{J}}} \left(\max_{\Gamma\in\mathcal{P}(d)} \tilde{\omega}_\Gamma \right) \approx \max_{\Gamma:(\alpha,\alpha)\to(\mathcal{I},\mathcal{J})} \tilde{\omega}_\Gamma. \tag{2.83}$$

It follows from (2.64) that the $\tilde{\omega}_\Gamma$ are random variables with fat-tailed distributions. The effective paths associated to a diagram $d \in \mathcal{D}_{\mathcal{I},\mathcal{J}}$ all involve the same set of energies in their denominators, and are thus correlated. We expect however that the tail of the distribution of their sum, $S(d)$ in (2.46), is similar to the tail distribution of a single effective path, since in the case of a large deviation, $S(d)$ is very likely to be dominated by the effective path with the biggest weight.

Indeed, consider a rare set of energies $\mathcal{E}_i$, which produces an atypically large value of $S(d)$. There is typically one single effective path for which all denominators become simultaneously small, while the combination of energies in the denominators of other effective paths are very likely to be suboptimal for a fraction of the denominators. Therefore, with high probability, $S(d)$ will approximately be equal to the maximum over all effective paths weights: $S(d) \approx \max_{\Gamma\in\mathcal{P}(d)} \tilde{\omega}_\Gamma$. The set of energies $\mathcal{E}_i$ that optimize distinct effective paths are typically different, and thus these rare events can be approximated as being independent from each other. Hence, the tail of the distribution of $S(d)$ is enhanced with respect to the tail of a single path weight by a factor $|\mathcal{P}(d)|$.

This reasoning requires a word of caution: inspecting the explicit examples of Eq. (2.40) or Eq. (2.43), one can see that there exist energy realizations for which cancellations occur between effective paths with significant weight. This happens when the single path weights are individually big, but $\tilde{\mathcal{E}}$ is much smaller than all the other energy variables $\mathcal{E}_i$, which leads to a cancellation between effective paths. However, such configurations require an atypically small $\tilde{\mathcal{E}}$ and do not occur with significant probability. Therefore the suppression of the tail distribution due to such effects is hardly relevant.

Correlations between effective path weights of different diagrams are even weaker than those above, since they share at most a fraction of all $\mathcal{E}_i$. Therefore we may approximate rare deviations of $S(d)$ and $S(d')$ as independent if $d \neq d'$. Given that the $S(d)$ are themselves fat-tailed random variables, the sum over diagrams is dominated by the largest term, and so is (2.46). As a consequence, we obtain the approximation

$$P(\mathcal{A}^{(\alpha)}_{\mathcal{I},\mathcal{J}} = a) \approx |\mathcal{D}_{\mathcal{I},\mathcal{J}}|\overline{\mathcal{P}(d)}P(\tilde{\omega}_\Gamma = a) \approx \mathcal{N}_N P(\tilde{\omega}_\Gamma = a), \tag{2.84}$$

where $\overline{\mathcal{P}(d)}$ is an average number of effective paths contributing to a diagram, which we replaced with $\overline{|\mathcal{P}|}$ computed in (2.80).

B. Putting everything together: the convergence radius

Similarly to the effective path weights of different diagrams, also the amplitudes $\mathcal{A}^{(\alpha)}_{\mathcal{I},\mathcal{J}}$ associated to different sites $\mathcal{I},\mathcal{J}$ are weakly correlated, and we treat them as independent random variables. Let us now consider the probability in (2.34):

$$\mathbb{P}\left(\forall N>N^*,\ \sum_{\substack{\mathcal{I}\neq\mathcal{J}\\ |\mathcal{I}|=N+1=|\mathcal{J}|}}\left|\mathcal{A}^{(\alpha)}_{\mathcal{I},\mathcal{J}}\right|<z^N\right)\approx\prod_{N>N^*}\mathbb{P}\left(\sum_{\substack{\mathcal{I}\neq\mathcal{J}\\ |\mathcal{I}|=N+1=|\mathcal{J}|}}\left|\mathcal{A}^{(\alpha)}_{\mathcal{I},\mathcal{J}}\right|<z^N\right). \tag{2.85}$$

Here we approximated the probability to satisfy the condition at each generation to be independent from the previous generations. As follows from (2.84) and from the fact that the effective paths $\tilde{\omega}_\Gamma$ have fat tails, the amplitudes $\mathcal{A}^{(\alpha)}_{\mathcal{I},\mathcal{J}}$ have themselves a fat-tailed distribution. Their sum is therefore dominated by the maximal amplitude, and each factor on the right hand side (2.85) can be computed as:

$$\begin{aligned}\mathbb{P}\left(\max_{\substack{\mathcal{I}\neq\mathcal{J}\\ |\mathcal{I}|=N+1=|\mathcal{J}|}}|\mathcal{A}^{(\alpha)}_{\mathcal{I},\mathcal{J}}|<z^N\right)&=\prod_{\substack{\mathcal{I}\neq\mathcal{J}\\ |\mathcal{I}|=N+1=|\mathcal{J}|}}\left(1-\mathbb{P}\left(|\mathcal{A}^{(\alpha)}_{\mathcal{I},\mathcal{J}}|>z^N\right)\right)\\ &\approx\exp\left(-\sum_{\substack{\mathcal{I}\neq\mathcal{J}\\ |\mathcal{I}|=N+1=|\mathcal{J}|}}\mathbb{P}\left(|\mathcal{A}^{(\alpha)}_{\mathcal{I},\mathcal{J}}|>z^N\right)\right).\end{aligned} \tag{2.86}$$

Using (2.84), the exponent in (2.86) is re-written as:

$$\sum_{\substack{\mathcal{I}\neq\mathcal{J}\\ |\mathcal{I}|=N+1=|\mathcal{J}|}}\mathbb{P}\left(\left|\mathcal{A}^{(\alpha)}_{\mathcal{I},\mathcal{J}}\right|>z^N\right)\approx\mathcal{N}_N\mathbb{P}\left(|\tilde{\omega}_\Gamma|>z^N\right). \tag{2.87}$$

In (2.87), the competition between two exponential terms is recovered. The probability in (2.87) is a large deviation probability: indeed, the weights $\tilde{\omega}_\Gamma$ of effective paths are of order $O\left(\lambda^N\right)$: in order for $\tilde{\omega}_\Gamma$ to be bigger than z^N (with z arbitrarily close to 1), this decay factor must be compensated by an atypical smallness of the energy denominators. Using (2.64), we estimate:

$$\mathbb{P}\left(|\tilde{\omega}_\Gamma|>z^N\right)\approx\left(\frac{2e}{\sqrt{2\pi}}\right)^N\int_{\log\left(\frac{z}{\lambda\eta_{\rm typ}}\right)}^{\infty}C(\tilde{x},N)\tilde{x}^Ne^{-N\mathcal{F}(\tilde{x})}d\tilde{x}. \tag{2.88}$$

Note that the large deviation result applies since $\tilde{x}\geq\log\left(\frac{z}{\lambda\eta_{\rm typ}}\right)\gg 1$. Approximating the integral with the value of the integrand at the extremum, setting $z=1$ and neglecting

sub-exponential terms in N we obtain:

$$\mathbb{P}\left(|\tilde{\omega}_\Gamma| > 1\right) \approx \left(\frac{2e}{\sqrt{2\pi}} \log\left(\frac{1}{\lambda\eta_{\rm typ}}\right)\right)^N e^{-N\left[\log\left(\frac{1}{\lambda\eta_{\rm typ}}\right)+O\left(1/\log\left(\frac{1}{\lambda\eta_{\rm typ}}\right)\right)\right]}. \tag{2.89}$$

Substitution of (2.89) and (2.81) into (2.87) yields:

$$\sum_{\substack{\mathcal{I}\neq\mathcal{J}\\ |\mathcal{I}|=N+1=|\mathcal{J}|}} \mathbb{P}\left(\left|\mathcal{A}^{(\alpha)}_{\mathcal{I},\mathcal{J}}\right| > 1\right) \simeq \exp\left[N\log\mathcal{G}(\lambda,\mathcal{K}) + o(N)\right], \tag{2.90}$$

with

$$\mathcal{G}(\lambda,\mathcal{K}) = \frac{2e\,C\eta_{\rm typ}}{\sqrt{2\pi}}\lambda\mathcal{K}\log\left(\frac{1}{\lambda\eta_{\rm typ}}\right). \tag{2.91}$$

Taking into account (2.85) and (2.86), we finally obtain:

$$\mathbb{P}\left(\forall N > N^*, \sum_{\substack{\mathcal{I}\neq\mathcal{J}\\ |\mathcal{I}|=N+1=|\mathcal{J}|}} \left|\mathcal{A}^{(\alpha)}_{\mathcal{I},\mathcal{J}}\right| < 1\right) = \prod_{N>N^*} \exp\left[-e^{N\log\mathcal{G}(\lambda,\mathcal{K})+o(N)}\right]. \tag{2.92}$$

If $\mathcal{G}(\lambda,\mathcal{K}) < 1$, then, for N^* sufficiently big, each of the factors in (2.92) is arbitrarily close to 1. Therefore, their product converges to 1 in the limit $N^* \to \infty$ (see also [168] for a similar reasoning). This allows us to conclude that, for all values of λ for which $\mathcal{G}(\lambda,\mathcal{K}) < 1$ holds, (2.34) holds, too, and the series in operator space (2.15) converges to a quasi-local operator. In this regime, the excitation of the single particle level α, localized at r_α, is very unlikely to create a distant disturbance at r_β with large $L = |r_\beta - r_\alpha|$, its probability tending to zero exponentially as $L \to \infty$: there is no diffusion at small λ. The critical value for λ is given by $\mathcal{G}(\lambda_c,\mathcal{K}) = 1$. For large $\mathcal{K}$ and using $\eta_{\rm typ} = 1/e$, we get:

$$\lambda_c = \frac{\sqrt{2\pi}}{C\ 2e}\frac{1}{\mathcal{K}\log\mathcal{K}}. \tag{2.93}$$

For $\lambda < \lambda_c$, the operator series (2.15) converges in norm to an operator that is quasilocal. The delocalization threshold (2.93) looks identical to the critical ratio between hopping and disorder strength for a single particle problem on a Bethe lattice with effective connectivity $\mathcal{K}_{\rm eff} = (C/\sqrt{2\pi})\mathcal{K}$, which is a significantly larger than the connectivity associated with each vertex, $\mathcal{K}$. This reflects the fact that in the many-body problem the same final state can be reached with many different decay processes. The results are nevertheless similar, because both problems are dominated by very few resonant paths, whereby the large local connectivity in the many-body problem ensures that different resonant paths are likely to be uncorrelated, even if they lead to the same final state.

C. Acting on the Hilbert space: Fermi-blocking and temperature dependence

The above construction is carried on at the operator level: no assumption about the occupation of the single-particle energy levels or about the position of the Fermi level E_F is made. The convergence of the series in operator norm entails localization in whatever state the system is. When acting on some many-body states, however, the constructed operators get annihilated when attempting to create particles on occupied states or holes on already empty states. This translates into a reduction of the phase space associated to the decay processes, which in turns implies that the connectivity $\mathcal{K}$ is reduced to an effective connectivity $\mathcal{K}_{\rm eff}$, whose typical value depends both on the average energy density of the states E_a and the average filling fraction of the band. This might increase the convergence of the perturbative expansion.

In an infinite temperature state, and at a filling fraction ν_F each particle-hole creation operator has a chance to annihilate the state with probability $1-\nu_F(1-\nu_F)$, or, in other words, only a fraction of $[\nu_F(1-\nu_F)]^N$ of all operators will not annihilate a typical infinite temperature state. This reduces the connectivity to $\mathcal{K}_{\rm eff}\sim\nu_F(1-\nu_F)\mathcal{K}$. Similar considerations apply to finite temperature: it is not difficult to see that if we use typical values for occupation numbers as given by the Fermi distribution (without assuming the underlying states to be thermal), repeating the above considerations at finite temperature $T\ll E_F$ we obtain $\mathcal{K}_{\rm eff}\sim T/\delta_\xi$. Substitution into (2.93) gives an estimate of the boundary of stability of the MBL phase that is consistent with the one in [20] (and its extension to infinite temperature [16]). This is not surprising, as the class of diagrams that are statistically analyzed is the same: the paths jumping from generation to generation in the operator lattice, selected by the forward approximation, correspond to many-body processes where at each vertex an additional particle-hole pair is created. The same type of processes are retained within the imSCBA, see Sec. 1.4.5. Thus, the same estimate for the critical temperature is recovered. The reason why this result is not in contradiction with the scenario discussed in Sec. 1.5.1 is that the above considerations hold true only within the forward approximation, as discussed in Sec. 2.4.

D. A critical assessment of the approximations made

The explicit estimate (2.93) is the result of a series of approximate steps; let us briefly comment on the legitimacy of the approximations made. The main simplification that we have performed consists in neglecting the second term of Eq. (2.30). This is a controlled approximation whenever the operator sites $(\mathcal{I},\mathcal{J})$ have a density of Fock indices per localization volume that is much smaller than the maximally possible $\sim\mathcal{K}/\xi^d$. However, some subtleties arise at sufficiently high orders in perturbation theory, where operators with a high density of indices per localization volume appear. The reason is that the transitions from a given $(\mathcal{I},\mathcal{J})$ that are due to the second term of Eq. (2.30) can involve any pair of particles or holes in the same localization volume: for operators with a high density of indices per localization volume, those transitions can be as numerous as the third class of terms in Eq. (2.30). We expect that these neglected terms produce a shift in the estimate of the critical threshold (2.93), but do not spoil the norm convergence of the operator expansion at finite but small enough λ (as it follows also from the rigorous

results summarized in Sec. 2.3). However, their impact on the weak convergence of the expansion projected on typical many-body states is more delicate. The neglected terms have indeed the potential to invalidate the statement on the occurrence of a finite temperature transition: we illustrate how in Sec. 2.4.

An additional source of approximation was introduced in Sec. 2.2.1. It corresponds to the fact that the shifts in the single-particle energy levels generated by the diagonal Hartree-terms are neglected. The latter are however relevant, as recently observed in [30]; indeed, they are responsible for the rearrangement of the energy levels within a localization volume, once a new particle-hole excitation is created in the volume. Even at weak interactions the rearrangements are rapidly so important that previously resonantly coupled configurations are driven out of resonance, while new pairs of configurations can become resonantly coupled. The latter do not need to involve the hopping of particles that have previously moved, however, in contrast to the framework of previous analyses. This phenomenon of *spectral diffusion* [31, 76] should be appropriately taken into account when estimating the number of resonant channels by which an excitation can decay: in essence, at any step of the decay process, for a further decay to occur to the next localization volume it is sufficient that at least *one* of the particle-hole pairs belonging to the localization volume of the newly created pair can undergo a resonant transition. The above estimates are instead performed requiring that the newly created pair itself can decay resonantly: this underestimates the number of decay channels available. It is expected that the spectral diffusion, if appropriately taken into account, leads to a reduction of the critical interaction strength (2.93) by a factor $\mathcal{K}^{-a}$ with $a > 0$. Similarly, the critical temperature obtained accounting for this effect [30] is parametrically smaller than (1.77).

2.3 Beyond perturbation theory: the rigorous arguments for MBL

The condition (2.34) states that the probability of collective, high-order resonances between *unperturbed* degrees of freedom decays exponentially in the number of degrees of freedom involved, thus indicating that resonances do not proliferate asymptotically in the perturbation theory (and thus, within the forward approximation, asymptotically in space). A rigorous proof of localization should control resonances at any length scale, taking into account the renormalization of the energies due to resonant transitions occurring at the shorter scale and lower perturbative orders. This program has been carried out rigorously in [86] for the random spin chain (1.11), with a "multi-scale" approach that is reminiscent of the proof of localization in the single-particle case [100, 65]. In this section, we compare the treatment in [86] with our perturbative approach; this illustrates how the approximations performed within our treatment can be lifted. In Appendix 2.D, we shortly comment on the relation between our construction and the alternative recipe to build the conserved quantities proposed in [36].

The reasoning in [86] is based on the construction of a unitary operator $\mathcal{U}$ which brings

the Hamiltonian into a diagonal form in the $\{\sigma_i^z\}$ basis,

$$H' = \mathcal{U} H \mathcal{U}^\dagger = f\left(\{\sigma_i^z\}\right) = h_0 + \sum_i h_i \sigma_i^z + \sum_{i,j} h_{ij} \sigma_i^z \sigma_j^z + \cdots . \tag{2.94}$$

Quasilocality means that its generator A, $\mathcal{U} = e^A$, is quasilocal almost everywhere, up to a collection of rare regions where $\mathcal{U}$ is far from the identity. The quasilocality of $\mathcal{U}$ is rephrased in terms of bounds on the expectation values of the local observables σ_i^z on the many-body eigenstates, see Eq. (1.31). Operators with compact support are deformed by $\mathcal{U}$ into quasilocal operators: an extensive set of quasilocal conserved charges is thus simply given by

$$I_k = \mathcal{U}^\dagger \sigma_k^z \mathcal{U}, \tag{2.95}$$

and it follows from (2.94) that $H = f\left(\{I_k\}\right)$.

The construction of $\mathcal{U}$ is performed within an iterative scheme, $\mathcal{U} = \lim_{n\to\infty} U_n \cdots U_1$, running over a sequence of length scales L_n exponentially increasing with n. Any rotation U_n is chosen so as to eliminate the off-diagonal couplings obtained at the n-th step Hamiltonian ($H^{(n-1)} = U_{n-1} H^{(n-2)} U_{n-1}^\dagger$, where $H^{(0)} = H$) that are of order $O(\gamma^{L_n})$: it implements perturbation theory in the regions where the latter is controlled, and exact diagonalization in resonant regions of size of the order of L_n. The generator of the rotation admits an expansion over *graphs* with a random amplitude (similarly to the expansion over paths in the perturbative construction), whose statistical distribution has to be controlled. It is proved that at any scale, the resonant transitions are rare enough not to spoil the exponential decay inherent in the perturbation theory. The proof relies on an assumption of "limited level attraction" for the energy levels of the many-body Hamiltonian restricted to arbitrary finite volumes of size n, which requires that

$$P\left(\min_{\alpha\neq\beta} |E_\alpha - E_\beta| < \delta\right) < \delta^\nu C^n \tag{2.96}$$

for some positive ν, C and any $\delta > 0$, and α, β labeling the eigenvalues.

We briefly comment on how the expansion over graphs emerges within this context; when it is possible, we make comparisons with the content of Sec. 2.2.

The perturbative framework. The construction is based on an iterative scheme to diagonalize Hamiltonians $H = H_0 + \gamma V$ ($H_0 = \sum_\sigma E_\sigma |\sigma\rangle\langle\sigma|$ being the diagonal part, V the off-diagonal one and γ the small parameter controlling the convergence of the procedure) by means of consecutive rotations. At any step n of this general scheme, a rotation $\tilde{U}_n$ is fixed by imposing a constraint on its generator $\tilde{A}^{(n)}$. At first order, the operator $\tilde{U}_1 H \tilde{U}_1^\dagger$ is diagonal up to $O(\gamma^2)$ provided that $\tilde{A}^{(1)}$ satisfies

$$\left[\tilde{A}^{(1)}, H_0\right] = -\gamma V. \tag{2.97}$$

This requires the following matrix elements of $\tilde{A}^{(1)}$ in the basis of H_0:

$$\langle\sigma|\tilde{A}^{(1)}|\sigma'\rangle = \frac{\gamma}{E_\sigma - E_{\sigma'}}\langle\sigma|V|\sigma'\rangle. \tag{2.98}$$

For the Hamiltonian (1.11), one has

$$\tilde{A}^{(1)} = -\gamma \sum_{i\in\Lambda}\sum_{\rho,\tau=\pm1} \frac{\Gamma_i}{h_i + 2\tau J_i + 2\rho J_{i-1}} \left(\frac{1+\rho\sigma^z_{i-1}}{2}\right) i\sigma^y_i \left(\frac{1+\tau\sigma^z_{i+1}}{2}\right) = \sum_i \tilde{A}^{(1)}(i). \tag{2.99}$$

As an effect of the partial rotation, higher-order interaction terms are generated, that couple classical spin configurations differing by an arbitrarily large number of single spin flips:

$$e^{\tilde{A}^{(1)}} H e^{-\tilde{A}^{(1)}} = H_0 + \sum_{n=1}^{\infty} \frac{\mathrm{Ad}^n_{\tilde{A}^{(1)}}}{n!}\left\{\frac{n}{n+1}V\right\}. \tag{2.100}$$

In the absence of resonances, the newly generated couplings fulfill exponential bounds that guarantee the convergence of the transformed Hamiltonian and encode its quasilocality. The commutators

$$\mathrm{Ad}^n_{\tilde{A}^{(1)}}\{V\} = \gamma \sum_{i_1,\cdots i_n,i_0} \left[\tilde{A}^{(1)}(i_n), \left[\tilde{A}^{(1)}(i_{n-1}), ..., \left[\tilde{A}^{(1)}(i_1), \sigma^x_{i_0}\right]\right]\right] = H_0 + \tilde{V}^{(1)} \tag{2.101}$$

are nonzero only for sequences of sites $i_1, \cdots i_n, i_0$ that are adjacent in space, meaning that i_p must be nearest neighbor of at least one among the $i_0, i_1, \cdots, i_{p-1}$ for all $1 \le p \le n$ (this local structure is analogous to the one we exploit in the computation in Sec. 3.2). Any ordered sequence of operators $\tilde{A}^{(1)}(j_1)\tilde{A}^{(1)}(j_2)...V(j_p)...\tilde{A}^{(1)}(j_n)$ resulting from the expansion of (2.101) is associated to a graph g: the matrix elements of $\tilde{V}^{(1)}$ in the basis $|\sigma\rangle$ can thus be expanded as a sum over graphs, the amplitude of each graph being the product of factors of the form $\gamma/\delta E$ with δE some energy denominator, as in (2.32).

In the absence of resonances, i.e., if the energy denominators are bounded from below $|\delta E| > \gamma$, the amplitude of each graph is exponentially small in its length (i.e. the number of operators in the corresponding operator sequence). The number of choices of the indices $i,..., i_0$ giving rise to non-zero commutators grows factorially with n: thus, the sum is contributed by a number of graphs growing faster-than-exponential; in the perturbation theory, this growth is compensated by the $n!$ terms in the denominator of Eq.(2.100), which is present due to the fact that the expansion is performed on the generator and not on the unitary operator itself. Thus, no "problem of the factorials" arises at this level, and the sum over graphs is exponentially bounded.

Dealing with resonant regions. The exponential bounds fail in the presence of small denominators. At first order, resonant processes are just single-spin flips: small denominators are accounted for by identifying the set S_1 of resonant sites (such that the corresponding denominator in $\tilde{A}^{(1)}(i)$ is smaller than an energy cutoff ϵ for some choice

of ρ, τ) and setting

$$V^{(res)} = \sum_{i \in S_1} \gamma_i \sigma_i^x, \quad V^{(per)} = \sum_{i \notin S_1} \gamma_i \sigma_i^x, \quad A^{(1)} = \sum_{i \notin S_1} \tilde{A}^{(1)}(i). \tag{2.102}$$

The modified rotation $\Omega_1 = e^{A^{(1)}}$ implements the perturbation theory on the non-resonant sites, in such a way that the transformed Hamiltonian

$$e^{A^{(1)}} H e^{-A^{(1)}} = H_0 + V^{(res)} + \sum_{n=1}^{\infty} \frac{\mathrm{Ad}^n_{A^{(1)}}}{n!} \left\{ \frac{n}{n+1} V^{(per)} + V^{(res)} \right\} = H_0 + V^{(res)} + V^{(1)} \tag{2.103}$$

is quasilocal except for the resonant term $V^{(res)}$. The smallest connected components in S_1 (at this stage, isolated sites) are diagonalized exactly with a local rotation O_1. The composition $U_1 = O_1 \Omega_1$ defines the first partial rotation in the iterative scheme. At this step, the deviation of the expectation value (1.31) from the classical value is controlled by the probability of having resonant single-spin flips in i, that is $O(\epsilon) = O(\gamma^{1/20})$.

Fractional moments bounds. The above procedure is iterated over the sequence of length scales L_n: at any step, the terms in $V^{(n-1)}$ that are contributed by non-resonant graphs of length $|g| \in (L_{n-1}, L_n)$ defines the n-th order generator $A^{(n)}$, as in (2.97), while the couplings corresponding to graphs that are resonant (i.e., that violate exponential bounds in their length) are diagonalized exactly. The result (1.31) follows from the exponential bounds on the probability of the resonant graphs,

$$P\left(|A^{(n)}_{\sigma\sigma'}(g)| > (\gamma/\epsilon)^{|g|} \right) \leq (c\epsilon)^{s|g|}, \tag{2.104}$$

similarly to (2.34). In (2.104), s is some fixed constant and $A^{(n)}_{\sigma\sigma'}(g)$ is the contribution of a graph g to the matrix elements of the n-th step generator, between the unperturbed eigenstates $|\sigma\rangle, |\sigma'\rangle$. The graphs at the n-th scale are built from the ones at the previous scale, thus they contain energy denominators which are renormalized at any smaller scale by the rotations O_i. The bound (2.104) is derived (by means of a Markov's inequality) from the fractional moment bound on the graph-amplitude

$$\mathbb{E}|A^{(n)}_{\sigma\sigma'}(g)|^s \leq \gamma^{s|g|} \mathbb{E} \prod_{\tau,\tau' \in g} |E^{(j)}_{\tau} - E^{(j)}_{\tau'}|^{-s} \leq (c\gamma)^{s|g|}. \tag{2.105}$$

obtained in [86] for $s = 2/7$. The need for fractional moments $s < 1$, first exploited in the single particle case in [5], is due to convergence, since the amplitudes of graphs are fat-tailed distribution and have no finite mean. This is found also in our perturbative construction, reflected in the fact that the generation function (2.49) is defined only for $k > -1$. The assumption (2.96) is relevant for obtaining bounds for graphs whose amplitude is contributed by resonant regions at the smaller scale.

Beyond the forward approximation. The bound (2.105) is valid for graphs that do not contain many repeated flips of the same spins, which would correspond to non-self-

avoiding paths in the perturbative treatment. In this case, the same energy denominator appears at a large power p, and the fractional moment diverges as $|h|^{-ps}$ which is not integrable for $p > 1/s$. Bounds in the *span* (not in the length) of these non-self-avoiding graphs can however be obtained exploiting inductively the bounds on graph amplitudes at smaller scales. This allows one to solve the problem beyond the forward approximation.

Why is $d = 1$ needed? For the above procedure to work, it is necessary to control the influence of the resonant regions on the surrounding localized degrees of freedom, to prove that the local ergodic spots do not "melt" the neighboring degrees of freedom, destroying localization once the mutual interactions are accounted for. To this aim, to each resonant region of size L a "buffer zone" is associated, whose length R is chosen in such a way that the coupling of the resonant regions with the degrees of freedom outside the buffer zone is weaker than the local level spacing. While in one dimension this fixes the size of the buffer zone to be of the order of the size of the resonant spot (this follows from the constraint $\gamma^R \approx 2^{-L-R}$), in higher dimension the two quantities do not have a comparable scaling, but the buffer zones are much larger than the resonant spots. This prevents the extension of this procedure.

The results shortly summarized in this section constitute a rigorous proof (based on a reasonable assumption) of the existence of a MBL regime in which the full spectrum is localized and the system is "integrable". The proof frames the perturbative arguments in a mathematically rigorous scheme. To conclude the chapter, we finally come to the more controversial issue of the breakdown of MBL and of the occurrence of a finite temperature transition.

2.4 The fate of conserved quantities at the transition

If a many-body mobility edge does exist, it is natural to expect that the localized, low temperature phase is still governed by quasilocal conservation laws inhibiting transport, while such integrals of motion do not exist at higher temperature. Thus, one expects that (quasilocal) conserved quantities are recovered once a projection onto a portion of the Hilbert space is performed.

One step toward the formalization of this expectation has been made in [67], by considering the projection of local spin operators onto a subspace $\mathcal{H}_{1-f}$ of the total Hilbert space $\mathcal{H} = \mathcal{H}_{1-f} \oplus \mathcal{H}_f$, spanned by a finite fraction $(1 - f)$ of eigenstates. The resulting projected operators are argued to be "local" in the sense that their "weight" in compact regions of the chain remains finite in the thermodynamic limit, although there is a global dressing of the operators whose total weight scales with f [6]. Conserved quantities are obtained from this set of projected operators by time-evolving with respect to the Hamiltonian governing the dynamics in $\mathcal{H}_{1-f}$, and time-averaging the result (following the

[6] Precisely, given any such operator O and its decomposition $\mathrm{O} = \mathrm{O}^A + \mathrm{O}^\perp$, where O^A is supported on some compact interval of the spin chain of size N_A, the ratio of the Frobenius norms $\lambda = \|\mathrm{O}^A\|^2/\|\mathrm{O}\|^2$ remains finite as the thermodynamic limit is taken with N_A kept fixed (and it scales as $1 - f$). However, $\|\mathrm{O}^\perp\|$ does not decay to zero exponentially as N_A is increased, as it would be required for the operator to be quasilocal.

recipe discussed in Appendix 2.D). This analysis seems to suggest that in presence of a mobility edge, operators satisfying this weaker notion of locality might be obtained by projecting out the fraction of the Hilbert space that is delocalized (note however that in [67] only parameters corresponding to a fully MBL spectrum are considered).

The construction performed in this chapter suggests another possible formulation, namely, that in presence of a mobility edge the expansion (2.15) does not converge in the operator norm, but the convergence is recovered once the operators are projected on the fraction of the Hilbert space spanned by the low-energy states. For this to occur, the terms in the operator expansion that make it divergent must be annihilated by the projection. Within the forward approximation, this scenario is indeed realized, as shown in Sec. 2.2.6: the projection onto typical states at a given temperature T enhances the convergence of the series expansion, since T essentially replaces the bandwidth in the analytical estimates, reducing the effective connectivity of the problem. This leads to a larger domain of (weak) convergence of the operator expansion, suggesting the possibility of a delocalization transition at finite temperature. A similar consideration shows that the transition at $T = \infty$ takes place in a regime where the operator expansion is not convergent in the operator norm, but converges only weakly on typical high energy states, due to the Fermi blocking.

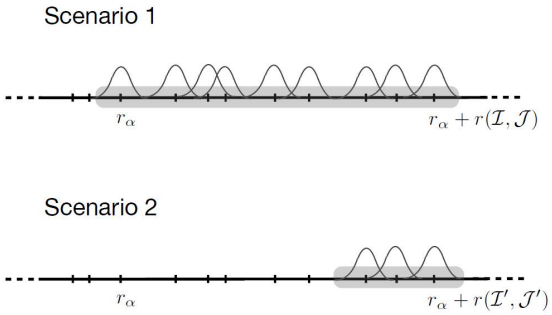

Figure 2.10: Pictorial representation of the supports of two different operators $\mathcal{O}_{\mathcal{I},\mathcal{J}}$ and $\mathcal{O}_{\mathcal{I}',\mathcal{J}'}$ contributing to the series expansion (2.15). In the pictures, the wave-functions are the single particle states contributing to $(\mathcal{I},\mathcal{J})$ and $(\mathcal{I}',\mathcal{J}')$. Both operators involve degrees of freedom whose maximal distance to the localization center r_α is the same: $r(\mathcal{I},\mathcal{J}) = r(\mathcal{I}',\mathcal{J}')$; however, the length of the support N of the operators (shaded in the picture) increases when N grows in the first case, while it remains bounded in the second case.

Beyond the forward approximation, however, the problem is more subtle. In particular, to address the question of whether or not a finite temperature transition is possible one has to inspect *how* the full operator series diverges as λ approaches the critical value (2.93). The series (2.15), or subsequences of it, can in fact diverge for two reasons: either (i) the amplitudes of terms with growing N do not decrease sufficiently fast, so that the divergence is driven by operators whose support grows indefinitely, or (ii) there are divergent subsequences of operators having bounded index level N, but supports which wander off to infinity. These two possibilities are illustrated in Fig. 2.10.

The possibility (i) is what is accounted for within the forward approximation. In this case, the fraction of terms at λ_c which survive when applied on finite T states decreases rapidly with N. The possibility (ii), instead, is not accounted for in the approximation we have made, as the operators with bounded N but increasingly far localization center are neglected. A divergence driven by this set of operators is made less likely by the largeness of the parameter $\mathcal{K}$, which is indeed invoked to neglect these terms. However, it is difficult to exclude that there is no such divergent subsequence which contributes with a relative weight which is parametrically small in $\mathcal{K}$ but finite. In that case, a projection would not affect its convergence properties: upon restricting to finite T states, the norm of the relevant operators is typically reduced by a factor which remains bounded from below. Thus, if the series diverges because of terms of this sort, it will continue to diverge despite the projection. This second scenario would thus lead to a phase diagram such as the one in Fig. 2.11 (b). Physically, it corresponds to the type of transport and delocalization driven by compact but mobile bubbles discussed in Sec.1.5.1, and would not be captured within the approximate treatment discussed in this chapter.

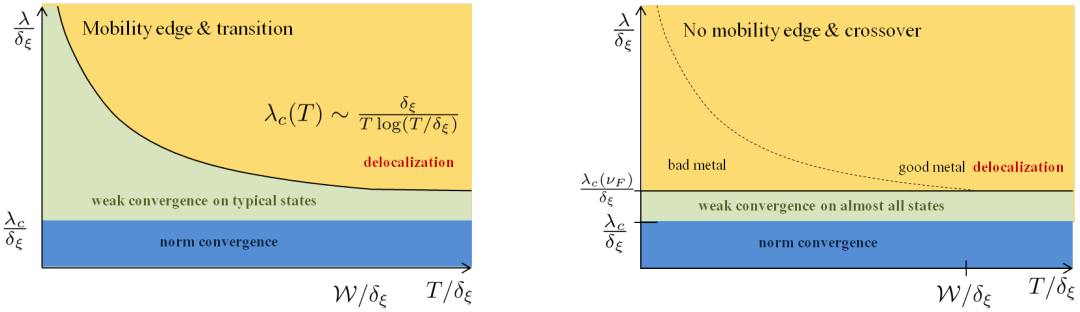

Figure 2.11: Different phase diagrams corresponding to the two scenarios discussed in the text. In both figures, the blue region corresponds to the regime of norm-convergence of the operator expansion, the green one to the regime of weak convergence on typical states at the given temperature T and the yellow one to the divergence of the series. (a) Phase diagram with a T-dependent transition line $\lambda_c(T)$ separating the regime of weak convergence from the delocalized one. This corresponds to the scenario in which the divergence is driven by a subsequence of operators with increasing support, that are annihilated by the projection onto typical states at a given T. (b) Phase diagram with a T-independent transition line $\lambda_c(\nu_F)$, obtained substituting $\mathcal{K}$ in (2.93) with $\mathcal{K}_{\text{eff}} = \nu_F(1-\nu_F)\mathcal{K}$, where ν_F the filling fraction. This corresponds to the scenario in which the divergence is driven by a subsequence of operators with bounded support. The dotted line is a crossover line.

Appendix

2.A Imposing a binary spectrum at any order (Eq. 2.11)

In this Appendix we show how the operators $\Delta K_\alpha^{(n)}$ can be fixed, order by order in λ, to guarantee that the operators $\hat{n}_\alpha$ have the spectrum of occupation numbers, i.e., $\{0, 1\}$. This is equivalent to the condition:

$$\hat{n}_\alpha^2 = \hat{n}_\alpha. \tag{2.106}$$

We work by induction on m. We set $\Delta B_\alpha^{(0)} = n_\alpha$ and we omit the index α for simplicity. We define the truncation to m-th order of $\hat{n}$:

$$\hat{n}^{\leq m} \equiv n + \sum_{i=1}^{m} \lambda^i \Delta\hat{n}^{(i)}, \tag{2.107}$$

and assume that the property (2.106) holds to order $O(\lambda^{m-1})$, namely:

$$(\hat{n}^{\leq m-1})^2 = \hat{n}^{\leq m-1} + \ o(\lambda^{m-1}). \tag{2.108}$$

Note that $\hat{n}^{\leq 0}$ is naturally binary, with $(\hat{n}^{\leq 0})^2 = \hat{n}^{\leq 0}$.

We denote with $\Delta J^{(m)}$ the solution of the equation:

$$[H_0, \Delta J^{(m)}] + [U, \Delta\hat{n}^{(m-1)}] = 0 \tag{2.109}$$

in the subspace O, cf. Eq. (2.10), and define

$$J^{\leq m} \equiv \hat{n}^{\leq m-1} + \lambda^m \Delta J^{(m)}. \tag{2.110}$$

The operator $J^{\leq m}$ is not binary to order $O(\lambda^m)$; however, we show that it is possible to add to $\Delta J^{(m)}$ a suitably chosen operator $\Delta K^{(m)}$ in the kernel K of the linear map $f(X) = [H_0, X]$, so that

$$\hat{n}^{\leq m} = J^{\leq m} + \lambda^m \Delta K^{(m)} \equiv \hat{n}^{\leq m-1} + \lambda^m \Delta\hat{n}^{(m)} \tag{2.111}$$

is binary to order $O(\lambda^m)$. To show this, it is sufficient to show that the difference

$\left(J^{\leq m}\right)^2 - J^{\leq m}$, truncated to order $O(\lambda^m)$, is an element of the subspace K, i.e.:

$$[H_0, (J^{\leq m})^2] = [H_0, J^{\leq m}] + o(\lambda^m). \tag{2.112}$$

It holds:

$$\begin{aligned}(\hat{n}^{\leq m})^2 =&[(\hat{n}^{\leq m-1})^2]_{m-1} + \lambda^m \sum_{a=0}^{m} \Delta\hat{n}^{(a)}\Delta\hat{n}^{(m-a)} + o(\lambda^m) \\ =&\hat{n}^{\leq m-1} + \lambda^m \sum_{a=0}^{m} \Delta\hat{n}^{(a)}\Delta\hat{n}^{(m-a)} + o(\lambda^m),\end{aligned} \tag{2.113}$$

where $[X]_{m-1}$ denotes the restriction of the Taylor series of $X(\lambda)$ to terms up to order λ^{m-1}. Using the inductive step $m-1$ we have from (2.113)

$$[H_0, (J^{\leq m})^2] = [H_0, \hat{n}^{\leq m-1}] + \lambda^m [H_0, \sum_{a=0}^{m} \Delta\hat{n}^{(a)}\Delta\hat{n}^{(m-a)}] + \ o(\lambda^m), \tag{2.114}$$

where in the terms with $a = 0, m$ we have replaced $\Delta J^{(m)}$ with $\Delta\hat{n}^{(m)}$, since Eq.(2.114) does not depend on the choice of $\Delta K^{(m)}$. Given that

$$\begin{aligned}[H_0, \Delta\hat{n}^{(a)}\Delta\hat{n}^{(m-a)}] &= \Delta\hat{n}^{(a)}[H_0, \Delta\hat{n}^{(m-a)}] + [H_0, \Delta\hat{n}^{(a)}]\Delta\hat{n}^{(m-a)} \\ &= -\Delta\hat{n}^{(a)}[U, \Delta\hat{n}^{(m-a-1)}] - [U, \Delta\hat{n}^{(a-1)}]\Delta\hat{n}^{(m-a)},\end{aligned}$$

summing over a we get

$$[H_0, \sum_{a=0}^{m} \Delta\hat{n}^{(a)}\Delta\hat{n}^{(m-a)}] = -[U, \sum_{a=0}^{m-1} \Delta\hat{n}^{(a)}\Delta\hat{n}^{(m-a)}]. \tag{2.115}$$

Using that (2.106) at the inductive step $m-1$ implies

$$\sum_{a=0}^{m-1} \Delta\hat{n}^{(a)}\Delta\hat{n}^{(m-a)} = \Delta\hat{n}^{(m-1)}, \tag{2.116}$$

and using (2.109), we find

$$\begin{aligned}[H_0, (J^{\leq m})^2] &= [H_0, \hat{n}^{\leq m-1}] + \lambda^m [H_0, \Delta J^{(m)}] + \ o(\lambda^m) \\ &= [H_0, J^{\leq m}] + \ o(\lambda^m),\end{aligned} \tag{2.117}$$

which proves (2.112).

By choosing:

$$\hat{n}^{\leq m} \equiv J^{\leq m} + \lambda^m \left(1 - 2\Delta\hat{n}^{(0)}\right) \left[\left(J^{\leq m}\right)^2 - J^{\leq m}\right]_m \tag{2.118}$$

the condition (2.108) is fulfilled to order $O(\lambda^m)$. Equation (2.11) follows from noticing

that:

$$\left[\left(J^{\leq m}\right)^2 - J^{\leq m}\right]_m = \sum_{i=1}^{m-1} \Delta\hat{n}^{(i)}\Delta\hat{n}^{(m-i)} + \left\{\Delta\hat{n}^{(0)} - \frac{1}{2}, \Delta J^{(m)}\right\}. \tag{2.119}$$

2.B Generating function for path weights (Eq. 2.52)

This appendix is devoted to the derivation of (2.52). We take the variables $\mathcal{E}_i/\delta_\xi$ to be Gaussian, with probability density

$$f(x) = \frac{1}{\sqrt{2\pi}} e^{-\frac{x^2}{2}}. \tag{2.120}$$

The expectation value over the joint distribution of $\mathcal{E}_i/\delta_\xi = s_i - s_{i-1}$ ($s_0 \equiv 0$) can be written as:

$$G_N(k) = \int \prod_{i=1}^{N} f(s_i - s_{i-1}) e^{k \log|s_i|} ds_i = \int \mathcal{O}_k^{N-1}[f](s_N)|s_N|^k ds_N, \tag{2.121}$$

where the integral operator $\mathcal{O}_k[\cdot]$ acting on a function g is given by:

$$\mathcal{O}_k[g](s) = \int f(s-x)|x|^k g(x) dx. \tag{2.122}$$

The integral operator conserves the parity; we consider the basis of even functions:

$$g_n(x) = \frac{e^{-\frac{x^2}{2}} x^{2n}}{\sqrt{2\pi(2n)!}}, \qquad n = 0, 1, \dots, \tag{2.123}$$

on which the linear action of $\mathcal{O}_k$ is given by:

$$\mathcal{O}_k[g_n](x) = \frac{1}{2\pi} \int e^{-\frac{1}{2}(x-y)^2} e^{-\frac{y^2}{2}} |y|^{k+2n} dy = \sum_{m \geq 0} O_{mn}(k) g_m(x), \tag{2.124}$$

with the matrix

$$O_{mn}(k) = \frac{1}{\sqrt{2\pi}} \frac{\Gamma\left(\frac{1+k}{2} + n + m\right)}{\sqrt{(2m)!(2n)!}}. \tag{2.125}$$

From (2.121) we thus readily obtain the following expression for $G_N(k)$:

$$G_N(k) = \sum_{m=0}^{\infty} \left(O(k)^{N-1}\right)_{m0} a_m, \tag{2.126}$$

with $a_m(k) = \int_{-\infty}^{\infty} g_m(s_N)|s_N|^k \, ds_N = \frac{2^{\frac{k+1}{2}+m}}{\sqrt{2\pi(2m)!}}\Gamma\left(\frac{k+1}{2}+m\right)$.

The matrix $O_{mn}(k)$ can be interpreted as a k-dependent Hamiltonian describing a particle hopping on a semi-infinite open chain with sites labeled by integers $m = 0, 1, 2, \ldots$. The large N behavior of $\log G_N(k)$ is dominated by the largest eigenvalue $\lambda_{\max}(k)$ of $\mathcal{O}$. Since for any $k > -1$, $O(k)$ is symmetric and positive definite, the Perron-Frobenius theorem ensures that $\lambda_{\max}(k)$ is positive and unique, and

$$G_N(k) \approx c(k) \left[\lambda_{\max}(k)\right]^{N-1}, \tag{2.127}$$

where $c(k) = \phi_{\max,0} \cdot \sum_{m\geq 0} a_m \phi_{\max,m}$, and $\phi_{\max}$ is the normalized eigenvector corresponding to $\lambda_{\max}$.

Numerical results for the maximal eigenvalue are shown in Fig. $2.B.1$. They are obtained by truncating the matrix O to an increasing set of basis states (or chain of sites) $m \leq L$. For k close to the singularity $k = -1$ the results rapidly converge with increasing size L. In this region, we can extract information on the limiting curve $\lambda_{\max}(k)$ from the truncated chain. In particular, we see from the plot that both the function $\log \lambda_{\max}(k)$ and its negative slope diverge at $k = -1$, which will also follow form the analysis below. We expand $\lambda_{\max}(k)$ in the vicinity of the singular point: this regime will indeed be the relevant one for the large deviation calculation.

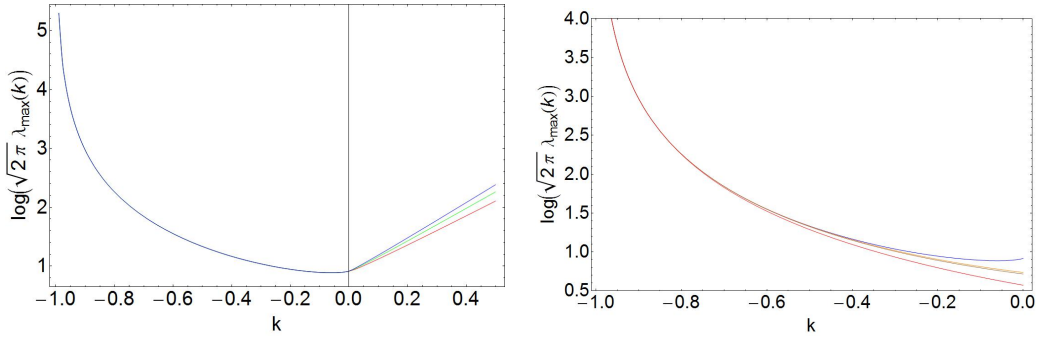

Figure 2.B.1: *Left.* Maximal eigenvalue $\log \lambda_{\max}(k)$ computed for truncated matrices $O(k)$ with basis sets of size $L = 120$ (red), $L = 200$ (green), $L = 300$ (blue). Close to the singularity $k = -1$, $\lambda_{\max}(k)$ converges rapidly with L. *Right.* Comparison between $\log \lambda_{\max}(k)$ obtained numerically for the truncated matrix (with $L = 300$ basis functions) and the analytic expression $\log[\Gamma\left(\frac{k+1}{2}\right) + g(k)]$ with $g(k)$ expanded at zeroth (red), first (brown) and second (orange) order in $(k + 1)$.

Due to the proximity to a logarithmic divergence at $k = -1$, to order $O(1 + k)$ the eigenstate $\phi_{\max}$ for $k \sim -1$ is localized on the first site ($n = 0$) of the corresponding hopping chain, $|\phi_{\max}\rangle \simeq |0\rangle$, with an eigenvalue

$$\lambda_{\max}(k) \simeq O(k)_{00} = \frac{1}{\sqrt{2\pi}}\Gamma\left(\frac{1+k}{2}\right). \tag{2.128}$$

Corrections to the maximal eigenvalue (2.128) can be evaluated perturbatively in the matrix elements $O_{ik\neq 00}$ (2.125), which yields

$$\lambda_{\max}(k) = \frac{1}{\sqrt{2\pi}}\Gamma\left(\frac{1+k}{2}\right) + \lambda^{(2)}_{\max}(k) + \lambda^{(3)}_{\max}(k) + \cdots \equiv \frac{1}{\sqrt{2\pi}}\Gamma\left(\frac{1+k}{2}\right) + \delta\lambda(k). \tag{2.129}$$

One can show that $\delta\lambda(k)$ is analytic around $k=-1$ and satisfies $\delta\lambda(k\to -1)\to 0$. This is due to the fact that in n-th order perturbation theory $\lambda^{(n)}_{\max}$ is proportional to denominators of the form $1/O_{00}^{n-1}\sim (k+1)^{n-1}$. The leading term in $\delta\lambda(k)$ results from:

$$\lambda^{(2)}_{\max}(k) = \sum_{m=1}^{\infty} \frac{(2\pi)^{-\frac{1}{2}}\left[\Gamma\left(\frac{1+k}{2}+m\right)\right]^2}{\Gamma\left(\frac{1+k}{2}\right)(2m)! - \Gamma\left(\frac{1+k}{2}+2m\right)} = \frac{1}{\sqrt{2\pi}}\frac{\pi^2}{36}(k+1)+O(k+1)^2. \tag{2.130}$$

From this it follows that

$$\phi(\tilde{y},k) := \tilde{y}k + \lim_{N\to\infty}\frac{G_N(k)}{N} = \tilde{y}k + \log\left[\Gamma\left(\frac{k+1}{2}\right) + \sqrt{2\pi}\delta\lambda(k)\right] - \frac{1}{2}\log 2\pi, \tag{2.131}$$

as given in the main text.

2.C Counting the geometries of diagrams (Eq. 2.66)

In this Appendix, we determine $\mathcal{T}_m$ in (2.66). The latter equals the number of trees with one root (of connectivity 2) and m nodes (of connectivity 4). These trees are obtained by merging two trees of branching ratio 3 at the root, and therefore

$$\mathcal{T}_n = \sum_{\substack{n_1,n_2\geq 0\\ n_1+n_2=n}} T^{(n_1)}T^{(n_2)}, \tag{2.132}$$

where $T^{(m)}$ is the number of trees with m vertices (including the root) and branching ratio 3. This number satisfies the recursion equations

$$T^{(0)} = 1, \tag{2.133}$$

$$T^{(n)} = \sum_{n_1+n_2+n_3=n-1} T^{(n_1)}T^{(n_2)}T^{(n_3)}. \tag{2.134}$$

We can define the generating function

$$T(x) = \sum_{n\geq 0} x^n T^{(n)}, \tag{2.135}$$

which in virtue of (2.134) satisfies the polynomial equation

$$T(x) = 1 + xT(x)^3. \tag{2.136}$$

Notice that the first singularity of $T(x)$ is a branch-cut at $x = 4/27$, which implies the large-n behavior $T^{(n)} \sim (27/4)^n$. However, we can find the n-th order of the expansion for small x using Lagrange's inversion theorem for the inverse function of

$$x(T) = \frac{T-1}{T^3}, \tag{2.137}$$

expanding around $T = 1$ ($x = 0$).

This yields

$$T^{(n)} = \frac{1}{n} \lim_{T\to 1} \left[\frac{1}{(n-1)!} \frac{d^{n-1}}{dT^{n-1}} \left(\frac{T-1}{x(T)} \right)^n \right] = \frac{1}{2n+1} \binom{3n}{n}. \tag{2.138}$$

In general, for k-body interactions we have $T^{(n)} = \binom{(k-1)n}{n} / ((k-2)n+1)$ diagrams. For $k = 3$ these are the numbers of binary trees with n vertices, or Catalan numbers. There are two ways to solve Eq. (2.132) and find $\mathcal{T}_n$. The first one is to notice that its generating function $\mathcal{T}(x)$ satisfies $\mathcal{T}(x) = T(x)^2$, write Eq. (2.137) in terms of $\mathcal{T}$ and use Lagrange's inversion theorem again. Alternatively, one can use the explicit form of $T^{(n)}$ and apply a summation formula for the ratio of four Γ-functions to obtain:

$$\mathcal{T}_n = \frac{3^{\frac{3}{2}+3n}}{\pi} \frac{\Gamma\left(n+\frac{2}{3}\right)\Gamma\left(n+\frac{4}{3}\right)}{\Gamma(2n+3)} \sim \frac{3}{4}\sqrt{\frac{3}{\pi}} \frac{1}{n^{\frac{3}{2}}} \left(\frac{27}{4}\right)^n. \tag{2.139}$$

2.D Comparison with the infinite-time averages of local densities

In [36], it is proposed to construct conserved quantities as the infinite-time averages of the local energy- or spin-densities of the Hamiltonian (1.10). The infinite-time averages of operators are obviously conserved; moreover, if a set of quasilocal operators I_α can be constructed, it follows that the average (1.50) of operators O with finite support is a quasilocal conserved quantity. Similarly to the operators defined by (2.15), the resulting conserved operators are not pseudospins, as the time-averaging does not preserve the spectrum [7]. To discuss the further (apparent) similarity with our operators constructed perturbatively, we consider the fermionic case. The operators I_α, corresponding to (2.10)

[7] They are nevertheless measurable in the following sense: for a chain with N spins with $\mathrm{O}_i = \sigma_i^z$, the coefficients in the expansion

$$\overline{\sigma}_i^z = \sum_{\vec{l},\vec{\kappa}} M_{\vec{l}}^{\vec{\kappa}}\, \sigma_{l_1}^{\kappa_1} \cdots \sigma_{l_n}^{\kappa_n}, \tag{2.140}$$

with $\kappa_i \in \{z, x, y\}$, can be obtained measuring multi-spin correlations on a time-averaged density matrix $\overline{\rho}$,

$$M_{\vec{l}}^{\vec{\kappa}} = 2^{-N} \mathrm{Tr}\left(\sigma_{l_1}^{\kappa_1} \cdots \sigma_{l_n}^{\kappa_n}\, \overline{\rho}\right), \tag{2.141}$$

with $\Delta K_\alpha^{(n)} = 0$, can be formally written as

$$I_\alpha = n_\alpha + \sum_{k=1}^{\infty} i^k \lim_{\eta_1 \to 0} \cdots \lim_{\eta_k \to 0} \mathscr{I}_k(\{\eta_i\}) \tag{2.142}$$

with

$$\begin{aligned}\mathscr{I}_k(\{\eta_i\}) &= \int_0^\infty dt_k \cdots \int_0^\infty dt_1 \prod_{i=1}^{k} e^{-\eta_i t_i} \, [U(t_1), [U(t_1+t_2), \cdots [U(t_1+t_2+\cdots t_k), n_\alpha]]] \\ &= \int_0^\infty dt'_k \int_0^{t'_k} dt'_{k-1} \cdots \int_0^{t'_2} dt'_1 \prod_{i=1}^{k} e^{-\eta_i (t'_i - t'_{i-1})} \, [U(t'_1), [U(t'_2), \cdots [U(t'_k), n_\alpha]]],\end{aligned} \tag{2.143}$$

where we set $t'_0 = 0$, and the time evolution of the interactions is with respect to the Hamiltonian H_0. This expression resembles the expression for the Heisenberg time evolved operator $n_\alpha(t)$ expanded perturbatively in U,

$$n_\alpha(t) = n_\alpha + \sum_m i^m \int_0^t dt_k \cdots \int_0^{t_2} dt_1 \, [U(t_1), [U(t_2), \cdots [U(t_k), n_\alpha]]], \tag{2.144}$$

when an infinite time limit is taken with the substitution

$$\int_0^t dt_k \longrightarrow \lim_{\eta \to 0} \int_0^\infty dt_k \, e^{-\eta t_k} \tag{2.145}$$

at any order in U. Despite the apparent similarity, however, the two sets of operators differ, due to the presence in (2.142) of the various regulators, whose limits have to be taken in the appropriate order. It can be checked that the role of the regulators is to project each commutator in (2.143) in the subspace O, so that at any order in the interaction (2.142) does not have any diagonal matrix elements in the basis of H_0. Instead, the operator (2.144) does. This can be checked most easily by comparing the second order terms of (2.143) with the ones of (2.144), which can be rewritten as

$$\int_0^\infty dt_2 e^{-\eta t_2} \int_0^{t_2} dt_1 \, [U(t_1), [U(t_2), n_\alpha]] = \int_0^\infty dt_2 \int_0^\infty dt_1 e^{-\eta(t_2+t_1)} \, [U(t_1), [U(t_2+t_1), n_\alpha]], \tag{2.146}$$

or by comparing the results in the single particle case, cfr. Sec. 2.2.1(B).

where ρ at $t = 0$ describes the state with magnetization one at site i and zero everywhere else, $\rho = 2^{-N}(1 + \sigma_i^z) \otimes \prod_{k \neq i} \mathbf{1}_k$. The $\overline{\sigma}_i^z$ thus provide information on the spreading of the spin through the infinite temperature ensemble.

3 MBL in antiferromagnets: remanent magnetization

The existence of extensively-many conservation laws represents a powerful tool for understanding the quantum dynamics. This is manifestly clear for ordinary integrable systems, for which the long-time limit following quantum quenches is captured by a suitable statistical ensemble taking into account the full set of conserved charges [171]. In this chapter, we aim at making a step toward the characterization of the long-time limit of an MBL system following a quantum quench, making use of the conserved operators constructed in the previous chapter. We apply the perturbative results to the study of an experimentally measurable quantity in quantum magnets, which is a magnetic analogue of the remanent density wave measured in the cold atom experiments, see Sec. 1.1.

The chapter is structured as follows: In Sec. 3.1 we propose the remanent magnetization in antiferromagnetic samples as a readily accessible order parameter for MBL. In Sec. 3.2, we explicitly show how the perturbative construction of the conserved quantities allows to make analytic predictions for this quantity of experimental relevance. In this context, we also illustrate how to explicitly account for resonances to the lowest order in the perturbation, by means of the re-summation of the divergent subsequences in the expansion. In Sec. 3.3, we comment on the non-interacting limit of the model.

3.1 A simple probe of ergodicity breaking in magnets

We aim at computing explicitly the out-of-equilibrium remanent magnetization that persists in an MBL antiferromagnetic sample after polarizing it ferromagnetically at $t = 0$. More precisely, we consider an anisotropic Heisenberg spin-$1/2$ chain

$$H = \sum_k \left(h_k \sigma_k^z - \sum_{\alpha=x,y,z} J_\alpha \sigma_k^\alpha \sigma_{k+1}^\alpha \right) \tag{3.1}$$

subject to random fields h_k along the Ising axis. In (3.1), σ_i^α are Pauli matrices. We assume $J_z < 0$, as well as $J_x \neq J_y$, to ensure the the total magnetization is not conserved. Such Hamiltonian can be realized, e.g., in Ising compounds with both exchange and dipolar interactions. However, essentially any quantum antiferromagnet with sufficiently strong disorder and non-conserved magnetization should exhibit qualitatively the same

phenomenology as the chain described here.

We assume that by applying a strong field, the antiferromagnetic chain is prepared in the fully magnetized state $|\psi_0\rangle$ with density matrix:

$$|\psi_0\rangle\langle\psi_0| = \prod_i \frac{1+\sigma_i^z}{2}. \tag{3.2}$$

After switching off the field, the dynamics is governed by (3.1). This protocol can be viewed as a quantum quench, in which a high energy eigenstate of the Hamiltonian with $J_x = 0$ is prepared, and the quantum fluctuations $J_x\sigma_k^x\sigma_{k+1}^x$ are switched on abruptly at time $t = 0$ (see Fig. 3.1 for a schematic sketch of the protocol). We are interested in the long-time behavior of the magnetization, and thus consider the time averaged magnetization at site j:

$$\hat{m}_j = \lim_{T\to\infty} \frac{1}{T}\int_0^T dt\, m_j(t);\ \ m_j(t) = \langle\psi_0|\sigma_j^z(t)|\psi_0\rangle. \tag{3.3}$$

The remanent magnetization is defined as the site average:

$$\hat{m} = \frac{1}{L}\sum_{j=1}^{L}\hat{m}_j. \tag{3.4}$$

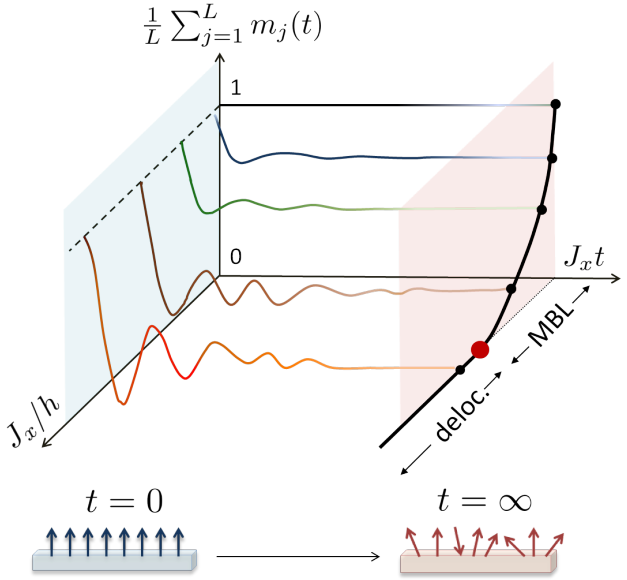

Figure 3.1: Relaxation of the total magnetization from a fully polarized initial state. The black curve is the stationary value $L^{-1}\sum_j \hat{m}_j$: it vanishes at the critical point separating the MBL and delocalized phases (red point), and it is non-analytic for $J_x/h \ll 1$, cfr. Eq. (3.31).

The quantity (3.4) serves as an order parameter for the dynamical phase transition: a finite remanence implies non-ergodicity, since an ergodic dynamics would relax the

magnetization completely. It is a magnetic analogue of the remanent density modulation measured in the cold atoms experiments [151, 29] recalled in Sec. 1.1 (see the discussion in Sec. 3.3.1). At variance with the imbalance and analogous quantities, however, (3.4) is much simpler to access experimentally, since it focuses on the total magnetization (at $q = 0$), which can be readily picked up by a squid, without requiring scattering measurements to resolve spatial patterns. Thus, the remanent magnetization is a experimentally readily observable consequence of MBL, accessible by standard experimental probes in magnets. This is of interest as direct observations of MBL in solid-state materials are still lacking (although an indirect signature of MBL in the from of strongly suppressed absorption of radiation was also found in electron-glasses [133]), mostly due to the lack of simple enough protocols or observables.

3.2 Conserved pseudo-spins: a computational tool

We consider (3.1) with random fields h_k uniformly distributed in $[-h, h]$, and assume a strong anisotropy of the couplings, $|J_y| \ll |J_x| \ll |J_z|, h$. For simplicity we restrict to $J_y = 0$. In the following, we denote with $\hat{\sigma}$ the conserved operators constructed following the perturbative recipe, to stress that they are not occupation numbers but effective spins with spectrum ± 1.

For $J_x = 0$, the spin chain (3.1) is classical and trivially localizes dynamically, as the σ_k^z form a complete set of commuting, local, conserved operators. The eigenstates are product states in this basis, and the local magnetization is trivially conserved, $m_j(t) = 1$. For finite J_x, $\sigma_j^z(t)$ has a non-trivial time dependence, which reduces $\hat{m}_j$. In the MBL regime, however, the time evolution is strongly constrained by the conservation of dressed spins $\hat{\sigma}_k = \sigma_k^z + O(J_x/h)$ with $|k - j| \lesssim \xi_{mb}$ and ξ_{mb} the length scale characterizing the decay of the operator norm. As a consequence, partial memory of the initial order $\langle \sigma_j^z \rangle = 1$ is retained for arbitrarily long time, resulting in a finite remanence of the site-averaged magnetization (3.4). To determine $\hat{m}$, we first derive an expression for it in which the conserved quantities appear explicitly.

3.2.1 Remanent magnetization in terms of conserved charges

In the absence of spectral degeneracies, (3.3) can be expressed via a Lehmann representation as

$$\hat{m}_j = \sum_\alpha \langle \psi_0 | P_\alpha \sigma_j^z P_\alpha | \psi_0 \rangle, \tag{3.5}$$

where

$$P_\alpha = |\psi_\alpha\rangle\langle\psi_\alpha| = \prod_{k=1}^{L} \left(\frac{1 + i_k^{(\alpha)} \hat{\sigma}_k}{2} \right) \tag{3.6}$$

projects onto the eigenstate labeled by the quantum numbers $i_k^{(\alpha)} \in \{\pm 1\}$ of the dressed spins $\hat{\sigma}_k$. Using the operator identity

$$\sum_\alpha P_\alpha \sigma_j^z P_\alpha = \sigma_j^z + \sum_{n=1}^{L} \sum_{k_n > k_{n-1} \cdots > k_1} \prod_{l=1}^{n} \left(\frac{\hat{\sigma}_{k_l}}{2} \right) \left[\left[\left[\sigma_j^z, \hat{\sigma}_{k_1} \right], \hat{\sigma}_{k_2} \right], \cdots, \hat{\sigma}_{k_n} \right],$$

we obtain the following expression for the remanent magnetization:

$$\hat{m}_j = 1 + \sum_{n=1}^{L} \sum_{k_n > k_{n-1} \cdots > k_1} \mathrm{Tr} \left\{ \prod_{i=1}^{n} \left(\frac{\hat{\sigma}_{k_i}}{2} \right) \left[\left[\left[\sigma_j^z, \hat{\sigma}_{k_1} \right], \hat{\sigma}_{k_2} \right], \cdots, \hat{\sigma}_{k_n} \right] \prod_{i=1}^{L} \left(\frac{1 + \sigma_i^z}{2} \right) \right\}, \tag{3.7}$$

where $\mathrm{Tr}\{\cdot\}$ denotes the trace, and an ordering among the labels of the operators $\hat{\sigma}_k$ is assumed (in the perturbative setting this ordering is natural, as there is a mapping between the set of conserved operators $\hat{\sigma}_k$ and the sites k, since $\hat{\sigma}_k$ is a perturbation of σ_k^z). We give the derivation of (3.7) in Appendix 3.A. As we illustrate in the following section, this formula is particularly suitable for perturbative calculations.

3.2.2 Conserved pseudo-spins for the anisotropic Heisenberg chain

We proceed in constructing the conserved quantities for the spin Hamiltonian (3.1) with $J_y = 0$, to lowest order in J_x. We set

$$\hat{\sigma}_k = \sigma_k^z + \Delta\hat{\sigma}_k^{(1)} + O(J_x^2) \equiv \hat{\sigma}_k^{(1)} + O(J_x^2), \tag{3.8}$$

and consider (2.10),

$$\Delta\hat{\sigma}_k^{(n)} = i \lim_{\eta \to 0} \int_0^\infty d\tau e^{-\eta\tau} e^{iH_0\tau} \left[U, \Delta\hat{\sigma}_k^{(n-1)} \right] e^{-iH_0\tau} + \Delta J_k^{(n)}, \tag{3.9}$$

with

$$\begin{aligned} H_0 &= \sum_i \left(h_i \sigma_i^z - J_z \sigma_i^z \sigma_{i+1}^z \right), \\ U &= -\sum_i J_x \sigma_i^x \sigma_{i+1}^x = -\sum_i J_x \left(\sigma_i^+ \sigma_{i+1}^+ + h.c. + \sigma_i^+ \sigma_{i+1}^- + h.c. \right), \end{aligned} \tag{3.10}$$

where we introduced $\sigma^\pm = (\sigma^x \pm i\sigma^y)/2$. In (2.10), the operator $\Delta J_k^{(n)}$ is a suitable polynomial in σ_i^z such that $\hat{\sigma}_k^2 = \mathbb{1}$ is satisfied at the given order in U. As discussed in Sec. 2.1.1, neglecting it at any order leads to a modified operator that is still conserved, although it does not have binary spectrum.

For a site k in the bulk,

$$[U, \sigma_k^z] = 2J_x \left(\sigma_k^+ \sigma_{k+1}^+ + \sigma_k^+ \sigma_{k+1}^- + \sigma_{k-1}^+ \sigma_k^+ - \sigma_{k-1}^+ \sigma_k^- - \text{h.c}\right). \tag{3.11}$$

Applying the Baker-Campbell-Hausdorff formula in (3.9), we find that $\Delta\hat{\sigma}_k^{(1)}$ is a sum of commutators of (3.11) with H_0, which are nonzero only for terms in H_0 involving spins at sites i with $|k-i| \leq 1, |k+1-i| \leq 1$. Thus, we may consider the ansatz:

$$\Delta\hat{\sigma}_k^{(1)} = \sum_{\rho,\tau=\pm 1} \left(A_{\rho\tau}^{(k)} O_{\rho\tau}^{(k)} - A_{\rho\tau}^{(k-1)} O_{\rho\tau}^{(k-1)}\right) + \sum_{\rho,\tau=\pm 1} \left(B_{\rho\tau}^{(k)} \Delta_{\rho\tau}^{(k)} + B_{\rho\tau}^{(k-1)} \Delta_{\rho\tau}^{(k-1)}\right), \tag{3.12}$$

where we define the local operators

$$\begin{aligned} O_{\rho\tau}^{(k)} &= \frac{1+\rho\,\sigma_{k-1}^z}{2} \left[\sigma_k^+ \sigma_{k+1}^- + \text{h.c.}\right] \frac{1+\tau\,\sigma_{k+2}^z}{2}, \\ \Delta_{\rho\tau}^{(k)} &= \frac{1+\rho\,\sigma_{k-1}^z}{2} \left[\sigma_k^+ \sigma_{k+1}^+ + \text{h.c.}\right] \frac{1+\tau\,\sigma_{k+2}^z}{2}. \end{aligned} \tag{3.13}$$

Using that

$$\begin{aligned} \left[\sigma_k^+ \sigma_{k+1}^- + \sigma_k^- \sigma_{k+1}^+, H_0\right] &= -2\left(h_k - h_{k+1} - J_z(\sigma_{k-1}^z - \sigma_{k+1}^z)\right)\left[\sigma_k^+ \sigma_{k+1}^- - \sigma_k^- \sigma_{k+1}^+\right] \\ \left[\sigma_k^+ \sigma_{k+1}^+ + \sigma_k^- \sigma_{k+1}^-, H_0\right] &= -2\left(h_k + h_{k+1} - J_z(\sigma_{k-1}^z + \sigma_{k+1}^z)\right)\left[\sigma_k^+ \sigma_{k+1}^+ - \sigma_k^- \sigma_{k+1}^-\right], \end{aligned} \tag{3.14}$$

we find that (3.8) with $\Delta\hat{\sigma}_k^{(1)}$ in (3.12) is conserved to first order in J_x provided that

$$\begin{aligned} A_{\rho\tau}^{(k)} &= -\frac{J_x}{h_k - h_{k+1} + J_z(\tau - \rho)}, \\ B_{\rho\tau}^{(k)} &= -\frac{J_x}{h_k + h_{k+1} - J_z(\tau + \rho)}. \end{aligned} \tag{3.15}$$

To lowest order in J_x, the operator squares to one.

3.2.3 Apparent divergences generated by resonances

At low orders, the sum over multi-indices in Eq. (3.7) reduces to the few terms involving indices sufficiently close to k, since other commutators vanish. We argue that the lowest order corrections to $\hat{m}_j$ are given by the terms with $n = 1, 2$ in (3.7): inserting (3.12) into (3.7) and (3.5), we find:

$$\hat{m}_j = 1 - \left(B_{1,1}^{(j)}\right)^2 - \left(B_{1,1}^{(j-1)}\right)^2 + O(J_x^3), \tag{3.16}$$

where the amplitudes $A_{\rho\tau}^{(j)}$ do not contribute (at this order) due to the particular choice of the initial state. We justify the result (3.16) in the following.

First, we argue that the second-order contribution to $\hat{m}_j$ is contributed only by products of conserved operators expanded at first order, so that (3.8) suffices to determine (3.16). Indeed, the zero-th order contribution to $\hat{m}_j$ is fully reproduced by the term with $n = 0$ in (3.7), since the terms with $n \geq 1$ are exactly zero for $\hat{\sigma}_i \to \sigma_i^z$. Consider now the possible first order corrections: for any $n \geq 1$, the term of $O(J_x)$ must belong to the expansion of $\hat{\sigma}_{k_1}$ (otherwise the commutator with σ_j^z would be zero). The commutator produces terms of the form $\sigma_j^+\sigma_{j+1}^-$ and similar; such terms are preserved by the commutation and by the product with other σ_i^z operators, and are annihilated by the trace. For the same reason, the second order contributions obtained expanding $\hat{\sigma}_{k_1}$ to second order in J_x is zero.

The relevant second order contributions come from terms in (3.7) in which $\hat{\sigma}_{k_1}$ and some other conserved quantity $\hat{\sigma}_{k_i}$ are both expanded to first order in J_x. To identify them, it is sufficient to consider $n = 1, 2$. With the notation:

$$\begin{aligned}\tilde{O}_{\rho\tau}^{(k)} &= \frac{1+\rho\,\sigma_{k-1}^z}{2}\left[\sigma_k^+\sigma_{k+1}^- - \text{h.c.}\right]\frac{1+\tau\,\sigma_{k+2}^z}{2},\\ \tilde{\Delta}_{\rho\tau}^{(k)} &= \frac{1+\rho\,\sigma_{k-1}^z}{2}\left[\sigma_k^+\sigma_{k+1}^+ - \text{h.c.}\right]\frac{1+\tau\,\sigma_{k+2}^z}{2},\end{aligned} \tag{3.17}$$

we find:

$$\begin{aligned}\left[\sigma_j^z, \hat{\sigma}_k^{(1)}\right] = 2\sum_{\rho,\tau}&\left(A_{\rho\tau}^{(k)}\,(\delta_{k,j}-\delta_{k+1,j})\,\tilde{O}_{\rho\tau}^{(k)} - A_{\rho\tau}^{(k-1)}\,(\delta_{k-1,j}-\delta_{k,j})\,\tilde{O}_{\rho\tau}^{(k-1)}\right)\\ + 2\sum_{\rho,\tau}&\left(B_{\rho\tau}^{(k)}\,(\delta_{k,j}+\delta_{k+1,j})\,\tilde{\Delta}_{\rho\tau}^{(k)} + B_{\rho\tau}^{(k-1)}\,(\delta_{k-1,j}+\delta_{k,j})\,\tilde{\Delta}_{\rho\tau}^{(k-1)}\right).\end{aligned} \tag{3.18}$$

For $n = 1$, only the terms in $\hat{\sigma}_k^{(1)}\left[\sigma_j^z, \hat{\sigma}_k^{(1)}\right]/2$ that are a polynomial in σ_j^z give a non-zero contributions once the trace is performed; such terms are proportional to the products:

$$\begin{aligned}\left(\sigma_k^+\sigma_{k+1}^- + \text{h.c.}\right)\left(\sigma_k^+\sigma_{k+1}^- - \text{h.c.}\right) &= \frac{1}{2}\left[\sigma_{k+1}^z - \sigma_k^z\right],\\ \left(\sigma_k^+\sigma_{k+1}^+ + \text{h.c.}\right)\left(\sigma_k^+\sigma_{k+1}^+ - \text{h.c.}\right) &= -\frac{1}{2}\left[\sigma_k^z + \sigma_{k+1}^z\right].\end{aligned} \tag{3.19}$$

The first operator in (3.19) is however annihilated when acting on the totally polarized initial state. Thus, the contribution of this term once the trace is performed reduces to:

$$-2\left[\left(B_{1,1}^{(j)}\right)^2 + \left(B_{1,1}^{(j-1)}\right)^2\right]. \tag{3.20}$$

For $n = 2$, two cases have to be considered: either the operator $\hat{\sigma}_{k_2}$ in the commutator $\left[\left[\sigma_j^z, \hat{\sigma}_{k_1}\right], \hat{\sigma}_{k_2}\right]$ is expanded to first order in J_x, or one of the two operators $\hat{\sigma}_{k_1}, \hat{\sigma}_{k_2}$ to the left of the commutators is expanded. In the first case, one needs to compute the term in the expression:

$$\frac{\sigma_{k_1}^z\sigma_{k_2}^z}{4}\left[\left[\sigma_l^z, \hat{\sigma}_{k_1}^{(1)}\right], \hat{\sigma}_{k_2}^{(1)}\right], \quad k_2 > k_1 \tag{3.21}$$

which commutes with the operators σ_i^z, and which is not annihilated once acting on the fully polarized state. Such term can be generated only for $k_2 = k_1 + 1 \equiv k + 1$, and equals

$$\frac{\sigma_k^z \sigma_{k+1}^z}{2} \left(\delta_{k,j} + \delta_{k+1,j}\right) \sum_{\rho,\tau} \left(B_{\rho\tau}^{(k)}\right)^2 \frac{1 + \rho\sigma_{k-1}^z}{2} \left[\sigma_k^+ \sigma_{k+1}^+ - \text{h.c.}, \sigma_k^+ \sigma_{k+1}^+ + \text{h.c.}\right] \frac{1 + \tau\sigma_{k+2}^z}{2} \tag{3.22}$$

Using that

$$\left[\sigma_k^+ \sigma_{k+1}^+ - \text{h.c.},\ \sigma_k^+ \sigma_{k+1}^+ + \text{h.c.}\right] = \sigma_k^z + \sigma_{k+1}^z = 2\left(P_{1,1}^{(k)} - P_{-1,-1}^{(k)}\right) \tag{3.23}$$

where we defined

$$P_{\rho,\tau}^{(k)} = \frac{1 + \rho\,\sigma_k^z}{2} \frac{1 + \tau\,\sigma_{k+1}^z}{2}, \tag{3.24}$$

and taking the trace we get the contribution

$$\left(B_{1,1}^{(j)}\right)^2 + \left(B_{1,1}^{(j-1)}\right)^2. \tag{3.25}$$

Finally, the remaining contribution is zero, as the first order term in the expansion of the product $\hat{\sigma}_k^{(1)} \hat{\sigma}_{k+1}^{(1)}$ is zero. Summing (3.20) and (3.25) we recover (3.16).

We are now in the position to understand the role of resonances: the spatial average of (3.16) is recovered performing a disorder average $\langle \hat{m}_j \rangle_{\text{dis}}$ over random fields. The latter is an analytic function of the couplings for $|J_z| > h$, while it is ill-defined for $|J_z| < h$; the apparent divergence is due to rare resonances between classical configurations differing by the flip $J_x \sigma_i^x \sigma_{i+1}^x$ of two neighboring spins, that give rise to arbitrarily small energy denominators in Eq. (3.15). Thus, the correct computation of (3.4) needs to account for the presence of these non-perturbative terms.

3.2.4 Local resummation of resonances: a concrete example

As discussed in Sec. 2.1.1, local resonances has to be treated by performing a re-summation of the divergent subsequences in the operator expansion, which is equivalent to an exact diagonalization of the resonant degrees of freedom, in the spirit of Sec. 2.3. In the present case, we re-sum the leading resonances considering the simpler Hamiltonian

$$H^{(k)} \equiv \sum_{i=1}^{L} \left(h_i \sigma_i^z - J_z \sigma_i^z \sigma_{i+1}^z\right) - J_x \sigma_k^x \sigma_{k+1}^x, \tag{3.26}$$

where only one (resonant) J_x-coupling is retained. For this Hamiltonian, a full set of exactly conserved operators $\tilde{\sigma}_i$ satisfying $\tilde{\sigma}_i^2 = \mathbb{1}$ can be constructed explicitly. It amounts to finding a local rotation that maps the $\sigma_k^z, \sigma_{k+1}^z$ to two operators $\tilde{\sigma}_k, \tilde{\sigma}_{k+1}$, and thus resums all perturbative terms containing higher powers of the resonant J_x-coupling.

The operators $\tilde{\sigma}_k, \tilde{\sigma}_{k+1}$ take the form

$$\tilde{\sigma}_k = \sigma_k^z + \sum_{\rho\tau=\pm 1} \left(\tilde{A}_{\rho\tau}^{(k)} O_{\rho\tau}^{(k)} + C_{\rho\tau}^{(k)} K_{\rho\tau}^{(k)} \right) + \sum_{\rho\tau=\pm 1} \left(\tilde{B}_{\rho\tau}^{(k)} \Delta_{\rho\tau}^{(k)} + D_{\rho\tau}^{(k)} J_{\rho\tau}^{(k)} \right), \tag{3.27}$$

where

$$\begin{aligned} K_{\rho\tau}^{(k)} &= \frac{1+\rho\,\sigma_{k-1}^z}{2} \left[P_{1,-1}^{(k)} - P_{-1,1}^{(k)} \right] \frac{1+\tau\,\sigma_{k+2}^z}{2}, \\ J_{\rho\tau}^{(k)} &= \frac{1+\rho\,\sigma_{k-1}^z}{2} \left[P_{1,1}^{(k)} - P_{-1,-1}^{(k)} \right] \frac{1+\tau\,\sigma_{k+2}^z}{2}. \end{aligned} \tag{3.28}$$

Together with the $\tilde{I}_i = \sigma_i^z$ for $i \neq k, k+1$, they serve as a new basis for the perturbation theory in the remaining, non-resonant J_x-couplings. As we show in Appendix 3.B, the amplitudes are given by

$$\begin{aligned} \tilde{A}_{\rho\tau}^{(k)} &= -\frac{J_x}{\left(\left[h_k - h_{k+1} + J_z(\tau-\rho) \right]^2 + J_x^2 \right)^{1/2}}, \\ C_{\rho\tau}^{(k)} &= -1 + \frac{h_k - h_{k+1} + J_z(\tau-\rho)}{\left(\left[h_k - h_{k+1} + J_z(\tau-\rho) \right]^2 + J_x^2 \right)^{1/2}}, \\ \tilde{B}_{\rho\tau}^{(k)} &= -\frac{J_x}{\left(\left[h_k + h_{k+1} - J_z(\rho+\tau) \right]^2 + J_x^2 \right)^{1/2}}, \\ D_{\rho\tau}^{(k)} &= -1 + \frac{h_k + h_{k+1} - J_z(\rho+\tau)}{\left(\left[h_k + h_{k+1} - J_z(\rho+\tau) \right]^2 + J_x^2 \right)^{1/2}}. \end{aligned} \tag{3.29}$$

3.2.5 The non-analyticity of the remanent magnetization

Inserting the modified coefficients (3.29) into (3.5), we find again (3.16), but with the substitution:

$$B_{\rho\tau}^{(j)} \longrightarrow -\frac{J_x}{\left(\left[h_j - h_{j+1} - J_z(\tau+\rho) \right]^2 + J_x^2 \right)^{1/2}}. \tag{3.30}$$

Computing the disorder average, we obtain the remanent magnetization

$$\langle \hat{m}_j \rangle_{\text{dis}} = 1 - \frac{\pi |J_x|}{h} \left(1 + \frac{J_z}{h} \right) + O(J_x^2). \tag{3.31}$$

Thus, for $|J_z| < h$, (3.31) is non-analytic in J_x: this feature is a signature of resonances, the non-analytic cusp at $J_x = 0$ being most pronounced in the limit of vanishing Ising interactions, $J_z \to 0$ (recall that $J_z < 0$).

3.3 Beyond the perturbative regime: possible directions

3.3.1 Atomic analogues of the remanent magnetization

The gauge transformation $\mathcal{U} = \prod_{j=1}^{L} \exp\left(i\frac{\pi}{2} j \sigma_j^x\right)$ maps the antiferromagnetic chain (3.1) into its ferromagnetic counterpart with $J_x \to J_x$, $J_{y,z} \to -J_{y,z}$, and the initial state $|\psi_0\rangle$ into a Néel state. The order parameter is mapped into the staggered magnetization. Such a quantity has been studied numerically in [175] for disordered, long-range transverse field Ising chains, modeling the ion-trap quantum simulators discussed in Sec. 1.1. The staggered magnetization is a close analogue of the particle imbalance also discussed in Sec. 1.1, see Eq. (1.2) with $|\Lambda| = L$.

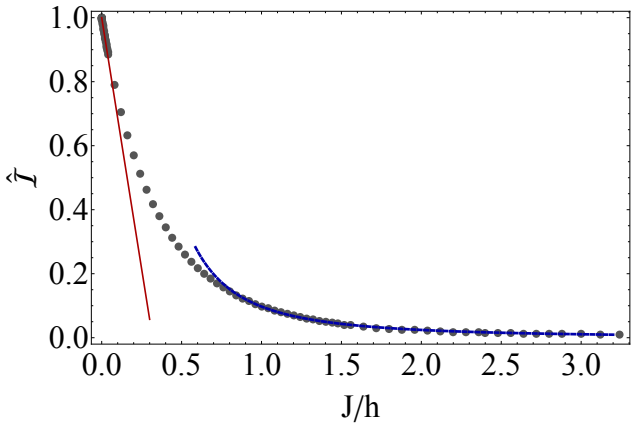

Figure 3.1: Dependence of the remanent density imbalance on the hopping strength J for a chain of non-interacting fermions ($L = 100$, $5 \cdot 10^3$ realizations). The continuous red line is the analytical estimate (3.31) with $J_x = J, J_z = 0$. The blue dashed line is a power law fit $a + c(J/h)^{-2}$, with $a = 0.003, c = 0.101$.

To make a comparison with these quantities, we exploit the fact that a ferromagnetic spin chain with $J_x = J_y$ is equivalent, via the Jordan-Wigner transformation, to a one-dimensional model of interacting spin-less fermions in a disordered potential. For $J_z = 0$ it reduces to the non-interacting Anderson model

$$H = -J \sum_{i=1}^{L-1} \left(c_i^\dagger c_{i+1} + h.c. \right) + 2 \sum_{i=1}^{L} h_i n_i \tag{3.32}$$

for which the imbalance is a sum over single particle contributions, weighted with the occupation probability of eigenstates in the initial state. A standard calculation leads to the remanent imbalance (1.2) in the form

$$\hat{\mathcal{I}} = \frac{1}{L} \sum_{\alpha=1}^{L} \sum_{l=1}^{L} \sum_{k=1}^{L} \frac{(-1)^l + (-1)^{l+k}}{2} \phi_\alpha^2(k) \phi_\alpha^2(k) = \frac{1}{L} \sum_{\alpha=1}^{L} \left(\sum_{k=1}^{L} (-1)^k \phi_\alpha^2(k) \right)^2 , \tag{3.33}$$

where $\phi_\alpha(i)$, with $1 \leq \alpha, i \leq L$ are the localized single particle eigenstates of the quadratic

Hamiltonian (3.32), and we assumed L even (so that $L^{-1}\sum_{l=1}^{L}(-1)^l = 0$). This solvable case is interesting as it can be analyzed deeper into the weak disorder limit.

Fig. 3.1 shows the imbalance as a function of J/h, as obtained by exact diagonalization. At small J/h a linear cusp with the slope predicted in (3.31) (using $J_z = 0, J_x = J$) is seen. For large J/h, $\hat{\mathcal{I}}$ decays algebraically, as $(J/h)^{-2}$. This scaling can be understood by writing

$$\phi_\alpha^2(k) = \frac{x_k^\alpha}{\xi} e^{-\frac{|k-r_\alpha|}{\xi}}, \tag{3.34}$$

where r_α denotes the localization center of ϕ_α, ξ its localization length (we are neglecting its energy dependence), and the x_k^α are positive random variables of $O(1)$ that capture the fluctuations of the squared amplitudes under the exponentially decaying envelope. Partitioning the chain into segments of length $l = \lfloor \xi \rfloor$ and approximating the x_k^α as uncorrelated variables we obtain:

$$\begin{aligned}\hat{\mathcal{I}} &\approx \frac{1}{L}\sum_{\alpha=1}^{L}\left(\sum_{R=1}^{L/l}(-1)^{Rl}\,\frac{e^{-|R-R_\alpha|}}{\xi}\sum_{k=(R-1)l}^{Rl}(-1)^k x_k^\alpha\right)^2 \\ &\approx \frac{1}{L}\sum_{\alpha=1}^{L}\left(\sum_{R=1}^{L/l}(-1)^{Rl}\,\frac{e^{-|R-R_\alpha|}}{\sqrt{\xi}}\right)^2 \sim \frac{c}{\xi} \sim c\left(\frac{J}{h}\right)^2,\end{aligned} \tag{3.35}$$

where R_α is the block containing the localization center r_α, and we have used that in the weak-disorder regime $\xi \sim (J/h)^2$ [119]. The scaling (3.35) is verified numerically in Fig. 3.1. We note that in [151] a different scaling of the form $1/\xi^2$ was obtained for the same quantity. The discrepancy with Eq. 3.35 arises because the fluctuations of the amplitudes within a correlation length were neglected in that work.

Let us finally comment on the qualitative effects of fermionic interactions. The addition of a term $U\sum_{i=1}^{L} n_i n_{i+1}$ (the equivalent of Ising interactions) to the Hamiltonian (3.32) may have opposite effects, depending on the value of J/h. For $J/h \ll 1$, the interaction broadens the distribution of the energy denominators, and thus acts as an additional source of disorder, which reduces the deviation of $\langle \hat{I} \rangle_{\text{dis}}$ from the classical limit. The same holds in the magnetic analogue as confirmed by Eq. (3.31). For larger $J/h > 1$, the single particle localization length becomes substantial. The dominant effect of interactions is then to mediate (virtual) scattering between single particle states, as discussed in Ref. [72, 20]. One expects that this suppresses the remanent imbalance, as was indeed observed in the experiments of Ref. [151]. For large enough interactions the inelastic scattering processes induce delocalization, as reflected by a breakdown of the locality of the conserved quantities $\hat{\sigma}_k$ discussed in the previous chapter. One expects the order parameter to vanish at a U-dependent critical hopping $J^*(U)/h$. The perturbative arguments in the previous chapter predict that, for $\xi \gg a$ with a the lattice constant, the localized phase is stable for $U < U^*$, where $U^* \propto \delta_\xi / \log(\mathcal{W}/\delta_\xi)$ with $\mathcal{W}$ the total bandwidth of the non-interacting Hamiltonian (3.32), $\delta_\xi = 1/\nu\xi$ and ν the density of states. In one dimension, $\xi \gg a$ corresponds to $J/h \gg 1$, implying $\mathcal{W} \sim 1/\nu \approx J$ and

$\xi \approx (J/h)^2$. This gives

$$U^*(J) \sim \frac{J}{(h/J)^2 \log\left[(J/h)^2\right]}, \tag{3.36}$$

modulo the correction due to spectral diffusion discussed in Sec. 2.2.6.

3.3.2 Exploiting numerical approaches

We conclude the chapter with a comment: since the simple formula (3.7) is derived under the sole assumption that the conserved operators have spectrum ± 1, it could be used in conjunction with the numerical recipes that have been recently devised to construct pseudo-spin operators by diagonalizing the Hamiltonian iteratively [120, 135, 145, 146], by applying RG schemes [136, 173, 121], or by variational procedures [131, 88]. This would allow one to go beyond the perturbative regime and to explore how the order parameter vanishes at the delocalization transition, or whether it exhibits a non-trivial scaling with the system size, potentially reflecting aspects of multifractality of the critical wave functions.

Appendix

3.A Expression for the local magnetization (Eq. 3.7)

In this Appendix we derive the identity (3.7). The operator in Eq. (3.5) is rewritten as

$$\sum_{\alpha} P_{\alpha}\sigma_j^z P_{\alpha} = \sum_{i_1=\pm 1}\sum_{i_2=\pm 1}\cdots\sum_{i_L=\pm 1}\prod_{k=1}^{L} P(i_k)\;\sigma_j^z\prod_{k=1}^{L} P(i_k), \tag{3.37}$$

where we introduced the projectors:

$$P(i_k) \equiv \frac{1+i_k\hat{\sigma}_k}{2}. \tag{3.38}$$

To derive Eq. (3.7), we make use of the operator identity $AB = BA + [A,B]$ together with:

$$\left[A, \prod_{k=1}^{L} B_k\right] = \sum_{k_1=1}^{L}\left(\prod_{k=1}^{k_1-1} B_k\right)[A, B_{k_1}]\left(\prod_{k=k_1+1}^{L} B_k\right). \tag{3.39}$$

For

$$A^{(1)} = \sigma_j^z, \qquad B^{(1)} = \prod_{k=1}^{L} B_k = \prod_{k=1}^{L} P(i_k), \tag{3.40}$$

the above identities imply

$$\prod_{k=1}^{L} P(i_k)\;\sigma_j^z\prod_{k=1}^{L} P(i_k) = \prod_{k=1}^{L} P(i_k)\left(\sigma_j^z + \sum_{k_1=1}^{L}\left[\sigma_j^z, \frac{i_{k_1}\hat{\sigma}_{k_1}}{2}\right]\prod_{k=k_1+1}^{L} P(i_k)\right). \tag{3.41}$$

Applying (3.39) once more with

$$A^{(2)} = \left[\sigma_j^z, \frac{i_{k_1}I_{k_1}}{2}\right], \qquad B^{(2)} = \prod_{k=k_1+1}^{L} P(i_k) \tag{3.42}$$

gives

$$\begin{aligned}&\prod_{k=1}^{L} P(i_k)\ \left[\sigma_j^z, \frac{i_{k_1}\hat{\sigma}_{k_1}}{2}\right] \prod_{k=k_1+1}^{L} P(i_k) = \\ &\prod_{k=1}^{L} P(i_k) \left(\left[\sigma_j^z, \frac{i_{k_1}\hat{\sigma}_{k_1}}{2}\right] + \sum_{k_2=k_1+1}^{L} \left[\left[\sigma_j^z, \frac{i_{k_1}\hat{\sigma}_{k_1}}{2}\right], \frac{i_{k_2}\hat{\sigma}_{k_2}}{2}\right] \prod_{k=k_2+1}^{L} P(i_k) \right).\end{aligned} \tag{3.43}$$

Further iterations with

$$A^{(n)} = \left[\left[\left[\sigma_j^z, \frac{i_{k_1} I_{k_1}}{2}\right], \cdots\right], \frac{i_{k_{n-1}} I_{k_{n-1}}}{2}\right], \qquad B^{(n)} = \prod_{k=k_{n-1}+1}^{L} P(i_k) \tag{3.44}$$

finally leads to

$$\begin{aligned}&\prod_{k=1}^{L} P(i_k)\ \sigma_j^z \prod_{k=1}^{L} P(i_k) = \\ &\prod_{k=1}^{L} P(i_k) \left(\sigma_j^z + \sum_{N=1}^{L} \sum_{k_N>\cdots>k_1} \left[\left[\left[\sigma_j^z, \frac{i_{k_1}\hat{\sigma}_{k_1}}{2}\right], \cdots\right], \frac{i_{k_N}\hat{\sigma}_{k_N}}{2}\right] \right).\end{aligned} \tag{3.45}$$

The identity (3.7) is recovered using that $i_k \in \{\pm 1\}$ and that

$$\sum_{i_k=\pm 1} P(i_k) = \mathbb{1}. \tag{3.46}$$

3.B Expression for the rotated operators (Eq. 3.27)

In this Appendix we justify the ansatz (3.27) and derive the expression for the coefficients. The ansatz (3.27) is motivated by the following considerations: the first-order truncation

$$\hat{\sigma}_k = \sigma_k^z + \delta\hat{\sigma}_k^{(1)} = \sigma_k^z + \sum_{\rho,\tau\pm 1} \left(A_{\rho\tau}^{(k)} O_{\rho\tau}^{(k)} + B_{\rho\tau}^{(k)} \Delta_{\rho\tau}^{(k)} \right) \tag{3.47}$$

with $O_{\rho\tau}^{(k)}, \Delta_{\rho\tau}^{(k)}$ given in (3.13), exactly commutes with the reduced Hamiltonian (3.26), that can be written as

$$H^{(k)} = H_0 - J_x \sigma_k^x \sigma_{k+1}^x = H_0 - J_x \sum_{\rho,\tau=\pm 1} \left(O_{\rho\tau}^{(k)} + \Delta_{\rho\tau}^{(k)} \right) \equiv H_0 + U^{(k)}. \tag{3.48}$$

This can be deduced from (3.9) setting $U \to U^{(k)}$ and $\Delta J_k^{(n)} = 0 \ \ \forall\, n$, noticing that $\left[U^{(k)}, \Delta\hat{\sigma}_k^{(1)}\right] = 0$ and thus that the perturbative expansion ends at first order. To impose the binarity of the spectrum, it is necessary to reintroduce the $\Delta J_k^{(n)}$ terms in order to

cancel the terms $\hat{I}_k^2 - \mathbb{1}$. The latter are proportional to:

$$\begin{aligned}\left(\sigma_k^+\sigma_{k+1}^+ + h.c.\right)^2 &= \frac{1+\sigma_k^z\sigma_{k+1}^z}{2} = P_{1,1}^{(k)} + P_{-1,-1}^{(k)},\\ \left(\sigma_k^+\sigma_{k+1}^- + h.c.\right)^2 &= \frac{1-\sigma_k^z\sigma_{k+1}^z}{2} = P_{1,-1}^{(k)} + P_{-1,1}^{(k)},\end{aligned} \tag{3.49}$$

where $P_{\rho,\tau}^{(k)}$ is defined in (3.24). The observation that

$$\begin{aligned}\frac{1}{2}\left\{\sigma_k^z, P_{1,-1}^{(k)} - P_{-1,1}^{(k)}\right\} &= \frac{1}{2}\left\{\sigma_k^z, \frac{\sigma_k^z - \sigma_{k+1}^z}{2}\right\} = P_{1,-1}^{(k)} + P_{-1,1}^{(k)},\\ \frac{1}{2}\left\{\sigma_k^z, P_{1,1}^{(k)} - P_{-1,-1}^{(k)}\right\} &= \frac{1}{2}\left\{\sigma_k^z, \frac{\sigma_k^z + \sigma_{k+1}^z}{2}\right\} = P_{1,1}^{(k)} + P_{-1,-1}^{(k)},\end{aligned} \tag{3.50}$$

suggests to consider the form (3.27). We now determine the coefficients in (3.27). The condition $\left[\tilde{\sigma}_k, H^{(k)}\right] = 0$ imposes:

$$\begin{aligned}\tilde{A}_{\rho\tau}^{(k)}\left(h_k - h_{k+1} + J_z(\tau-\rho)\right) + J_x\left(1 + C_{\rho\tau}^{(k)}\right) &= 0\\ \tilde{B}_{\rho\tau}^{(k)}\left(h_k + h_{k+1} - J_z(\tau+\rho)\right) + J_x\left(1 + D_{\rho\tau}^{(k)}\right) &= 0,\end{aligned} \tag{3.51}$$

from which (3.15) are recovered for $C_{\rho\tau}^{(k)} = 0 = D_{\rho\tau}^{(k)}$. This follows from:

$$\begin{aligned}\left[\tilde{\sigma}_k, H^{(k)}\right] = \left[\sigma_k^z, U^{(k)}\right] + \\ \sum_{\rho\tau=\pm1}\left(\left[C_{\rho\tau}^{(k)}K_{\rho\tau}^{(k)} + D_{\rho\tau}^{(k)}J_{\rho\tau}^{(k)}, H_1^{(k)}\right] + \left[\tilde{A}_{\rho\tau}^{(k)}O_{\rho\tau}^{(k)} + \tilde{B}_{\rho\tau}^{(k)}\Delta_{\rho\tau}^{(k)}, H_0\right]\right),\end{aligned} \tag{3.52}$$

together with:

$$\begin{aligned}\left[\sigma_k^+\sigma_{k+1}^- + \sigma_k^-\sigma_{k+1}^+, H_0\right] &= -2\left[h_k - h_{k+1} - J_z(\sigma_{k-1}^z - \sigma_{k+1}^z)\right]\left(\sigma_k^+\sigma_{k+1}^- - \sigma_k^-\sigma_{k+1}^+\right)\\ \left[\sigma_k^+\sigma_{k+1}^+ + \sigma_k^-\sigma_{k+1}^-, H_0\right] &= -2\left[h_k + h_{k+1} + J_z(\sigma_{k-1}^z - \sigma_{k+1}^z)\right]\left(\sigma_k^+\sigma_{k+1}^+ - \sigma_k^-\sigma_{k+1}^-\right)\\ \left[\sigma_k^z, U^{(k)}\right] &= -2J_x\left(\sigma_k^+\sigma_{k+1}^- - \sigma_k^-\sigma_{k+1}^+ + \sigma_k^+\sigma_{k+1}^+ - \sigma_k^-\sigma_{k+1}^-\right)\\ \left[\sigma_{k+1}^z, U^{(k)}\right] &= -2J_x\left(-\sigma_k^+\sigma_{k+1}^- + \sigma_k^-\sigma_{k+1}^+ + \sigma_k^+\sigma_{k+1}^+ - \sigma_k^-\sigma_{k+1}^-\right).\end{aligned} \tag{3.53}$$

Using (3.49) and (3.50), we obtain that $\tilde{I}_k^2 = \mathbb{1}$ is satisfied provided

$$\begin{aligned}\left(\tilde{A}_{\rho\tau}^{(k)}\right)^2 + \left(C_{\rho\tau}^{(k)}\right)^2 + 2C_{\rho\tau}^{(k)} &= 0,\\ \left(\tilde{B}_{\rho\tau}^{(k)}\right)^2 + \left(D_{\rho\tau}^{(k)}\right)^2 + 2D_{\rho\tau}^{(k)} &= 0\end{aligned} \tag{3.54}$$

for each choice of $\tau, \rho = \pm 1$. It can be checked that Eqs.(3.51), (3.54) are solved by (3.29). Similar expressions are obtained for the operator $\tilde{\sigma}_{k+1}$.

4 When a finite "bath" enhances localization: a quantum Zeno effect

Localization is a quantum phenomenon, having its root in the discreteness of the local spectrum which causes the suppression of the local hopping (or scattering) processes by making them off-shell. Such a mechanism requires the system to be isolated: in the presence of an infinite environment with continuous spectrum, the particles can draw from it the energy required to undergo on-shell transitions. This raises the following question: does the interaction of a localized systems with additional "bath-like" degrees of freedom *always* restore transport and ergodicity?

Remarkably, this is not the case: the coupling of a localized system to a finite or "small bath" (i.e. a bath with a finite number of degrees of freedom) can result in a phenomenon of bath-induced localization, in which the suppression of transport is actually enhanced by the strong coupling to the small bath. In this chapter we address an example of this phenomenon, focusing on the case of a single propagating degree of freedom.

The chapter is structured as follows: Sec. 4.1 introduces the problem and summarizes the results. In Sec. 4.2, an adaptation of the forward approximation scheme to the wave-functions is discussed, and applied in Sec. 4.3 to the estimate of the boundary of stability of the localized regime for a single particle coupled to a small bath. The mechanism by which the bath enhances the particle localization at strong coupling is discussed. A comparison of the analytics with exact diagonalization is given in Sec. 4.4. We conclude the chapter with a comment on the role of dimensionality, Sec. 4.5.

4.1 Coupling a disordered single particle to a "small bath"

4.1.1 When does a finite set of degrees of freedom act as a bath?

It is common wisdom that localization is destroyed when coupling the system to a delocalized bath with a continuous density of states, such as a phonon bath. In the single particle case, transport is restored even at very small temperatures, since phonon-assisted hopping between single particle states localized in different regions of space gives rise to a non-zero "variable range hopping" conductivity [87]. Even with phonons that are marginally localized (i.e., localized at all non-vanishing frequencies with a localization

length that diverges on approaching the zero frequency limit), a similar variable-range hopping occurs, although it involves the exchange of a number of phonons which diverges in the low temperature limit [13]. Likewise, in the many-body case it was argued in [127, 92] that, when coupling weakly a localized system to a thermodynamically large bath, the exact eigenstates of the combined system and bath immediately become thermal, while the spectral functions of local operators continue to show signatures of localization up to a crossover coupling that is independent of the size of the bath.

The question addressed in this chapter is however different, as it concerns the coupling to a *finite* number of degrees of freedom having discrete spectrum, which we refer to as a "small bath". In particular, it can be formulated in the following way: how many degrees of freedom are needed in such a small bath in order for it to delocalize the system? For this question to be meaningful, we assume that the bath is protected against localization, in such a way that the (strongly) localized system does not localize the degrees of freedom in the bath [126]. For simplicity, we restrict the discussion to a single propagating degree of freedom, without however imposing restrictions on the strength of the coupling to the bath.

4.1.2 A simple model

We now introduce a simple model for the phenomenon of "bath-induced localization". We consider the joint system of particle and finite bath to be described by an Hamiltonian of the form

$$H = H_{sys} + H_{bath} + H_{couple}. \tag{4.1}$$

We take the single particle Hamiltonian to be of the Anderson form,

$$H_{sys} = -t \sum_{\langle ij \rangle} c_i^\dagger c_j + \sum_{i \in \Lambda} \epsilon_i c_i^\dagger c_i, \tag{4.2}$$

on a d-dimensional regular lattice Λ of L^d sites, with the ϵ_i extracted from the uniform distribution $[-W, W]$. In (4.2), the tensor product with the identity operator in the Hilbert space of the bath is omitted.

The small bath is modeled as a quantum dot, or a zero-dimensional system. This guarantees that the coupling to the localized particle does not introduce any spatial disorder in it, as the system couples uniformly to the entire bath (from the system's point of view, the bath is zero dimensional). We further assume that the latter has bandwidth Ω, and can be in any one of N possible states, so that its level spacing is $\delta \approx \Omega/N$. In the limit $N \to \infty$ the spectrum might be continuum. The Hamiltonian of the bath may then be modeled simply as a properly rescaled $N \times N$ Hermitian random matrix taken from the GOE ensemble,

$$H_{bath} = \omega \sum_{\alpha', \beta'} M_{\alpha', \beta'} |\alpha'\rangle\langle\beta'| \equiv \omega M, \tag{4.3}$$

Table 4.1: Model's parameters

Particle hopping and disorder	t, W
Coupling between particle and bath	λ
Size of the bath's Hilbert space	N
Bandwidth of the bath's Hamiltonian	Ω
Rescaled bandwidth of the bath	$\omega = \Omega/(2\sqrt{2N})$
Average gap between bath's eigenstates	δ
Line broadening of bath's eigenstates	Δ

where M is a GOE matrix distributed according to: $P(M) \propto e^{-\frac{1}{2}\mathrm{Tr}M^2}$ with

$$\langle M_{\alpha,\beta}\rangle = 0, \quad \langle M^2_{\alpha,\beta}\rangle = 1/2 \text{ for } \alpha \neq \beta, \quad \langle M^2_{\alpha,\alpha}\rangle = 1. \tag{4.4}$$

For simplicity of notation, we have introduced the variable

$$\omega = \frac{\Omega}{2\sqrt{2N}}, \tag{4.5}$$

and in (4.3) the identity operator in the space of the particle is also omitted. The GOE statistics of the bath is representative of it being in a delocalized phase. The eigenstates of (4.3) are labeled by $\{\alpha\}_{\alpha=1,\ldots,N}$, with eigenvalues E_α. The density of levels E_α is given by the semicircle law [115]

$$\rho(E) = \frac{8N}{\pi\Omega^2}\sqrt{\left(\frac{\Omega}{2}\right)^2 - E^2}, \tag{4.6}$$

and hence $\delta \equiv 1/\rho(0) = \pi\omega/\sqrt{2N}$ in the middle of the spectrum.

The coupling between the system and the small bath is chosen of the following form:

$$H_{couple} = \lambda \sum_{i\in\Lambda}\sum_{\alpha,\beta} M^{(i)}_{\alpha,\beta}\, c_i^\dagger c_i \otimes |\alpha\rangle\langle\beta| = \lambda \sum_{i\in\Lambda} n_i \otimes M^{(i)}, \tag{4.7}$$

i.e. a coupling of strength λ which can scatter the bath from any eigenstate to any other eigenstate (irrespective of the energy transfer involved) with a random amplitude $M^{(i)}_{\alpha,\beta}$. This is the simplest coupling that does not introduce localization into the bath, at the same time allowing for energy to be transferred. For simplicity, we choose the amplitudes of $M^{(i)}$ to form a random GOE matrix as well. The main parameters of this model and their mutual relations are summarized in Table 4.1.

The hopping problem in the presence of a bath is represented pictorially in Fig. 4.1(a), for the case $d = 1$. For every position of the particle in Λ, there is a "tower" of N states, which differ only in the configuration of the bath. This tower of states has bandwidth $\sim \omega\sqrt{N}$ and level spacing $\sim \omega/\sqrt{N}$. A nearest neighbor hop of the particle leaving the state of the bath unchanged causes an energy shift of magnitude W in the weak λ limit.

Henceforth, we assume that

$$\frac{\omega}{\sqrt{N}} < W < \omega\sqrt{N}, \tag{4.8}$$

so that the "offset" of the tower of states on neighboring sites is bigger than the level spacing in the tower, but nonetheless adjacent towers do overlap. Right at the edge of the towers of states there are Lifshitz tails - states that are not near degenerate with any nearby states. However, we consider the properties of typical states well away from the edges of the spectrum, where the towers of states all overlap.

4.1.3 The outcome: an unexpected phase diagram

To determine the effect of the bath on the single particle, we analyze the stability of localization as a function of the coupling λ. We identify the region of parameters in which the perturbation theory in t is convergent, and compute its boundary in the various coupling regimes. The outcome of the analysis is illustrated qualitatively in Fig. 4.1 (b).

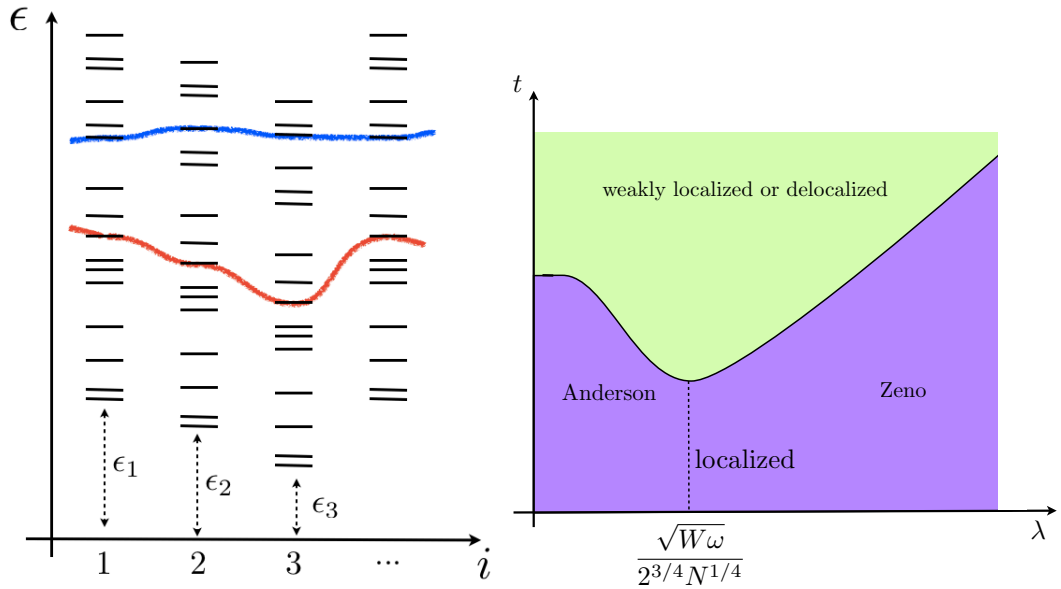

Figure 4.1: (a) Figure illustrating the basic setup: the band of states on every site i has bandwidth $\omega\sqrt{N}$ and level spacing $\omega/\sqrt{N}$. The red line indicates the hoppings between sites with no change in the state of the bath, relevant in the weak coupling regime. The blue line indicates hopping processes between states that are nearly on shell, allowed by the system-bath coupling at $\lambda = \lambda_c \sim \sqrt{\omega W}/N^{1/4}$. (b) Schematic phase diagram for the single particle, with a boundary indicating the stability of the locator expansion. The locator expansion is maximally unstable around λ_c, corresponding to the crossover (for small t) from Anderson localization to quantum Zeno localization. For $\lambda > \lambda_c$, the phase boundary is approximately linear in λ, whereas for $\lambda < \lambda_c$ is scales as $1/\lambda$.

An interesting feature emerges from the perturbative treatment: the effect of the bath on the particle's localization is non-monotonic in the coupling λ. At weak couplings, the bath facilitates transport by allowing the system to borrow from it the energy required to get on shell. Above a certain value of the coupling, however, the bath enhances localization. As we discuss in Sec. 4.3.2, the bath-induced localization originates in an orthogonality catastrophe, whereby the bath 'dresses' the system and suppresses its hopping matrix element. We refer to this regime as the "Zeno-localized" regime, due to its similarity with the quantum Zeno effect [26, 95, 118], where frequent measurements of the position of a particle impede its motion. As a result of this effect, in the localized regime (for weak hopping t) the single particle exhibits a crossover between an Anderson localized regime and the quantum-Zeno localized regime.

The detailed calculation of the "phase boundary" in Fig. 4.1(b) is performed in Sec. 4.3.3. We refer to the region of convergence of the perturbative expansion as the regime of "strong localization". When discussing one or two dimensions, we might denote the large-t region of the phase diagram as the regime of "weak localization", following the considerations in Secs. 1.4.6 and 4.5. We point out that it is essential, for the arguments given in the following sections, that the system contains a single particle. The many-body case is much harder to discuss, as indirect couplings of the particles through the bath can occur.

4.2 A perturbative expansion for the eigenstates

The phase diagram discussed in the previous section is determined examining the localization properties of the particle's eigenfunctions within a forward-approximation scheme. To this aim, we formulate in this section a criterion for localization, which is given in terms of the convergence of the perturbative expansion of the wave-function amplitudes themselves, rather than of the self energies as in Sec. 1.4.1. This connects also to the content of Chapter 2.

To keep the discussion as general as possible, we consider a generic graph $\mathcal{G}$ with N sites labeled by i, and define an effective single particle problem on it, with a disordered Hamiltonian

$$H = \sum_{i\in\mathcal{G}} \mathscr{E}_i \; c_i^\dagger c_i + \mathscr{V} \sum_{\langle i,j\rangle} \left(c_i^\dagger c_j + c_j^\dagger c_i \right). \tag{4.9}$$

The edges $\langle i,j\rangle$ define the geometry of the graph $\mathcal{G}$. We define the distance $d(a,b)$ between two arbitrary sites $a,b\in\mathcal{G}$ as the minimum number of edges in the graph connecting them, and refer to it as the graph distance in the following. For N finite, we denote with ψ_α the eigenfunctions of the Hamiltonian (4.9), with eigenvalues E_α. We derive a perturbative expansion for the eigenfunctions' amplitudes within the *Lowest Order* Forward Approximation, henceforth LOFA, which amounts to expanding the amplitude at each site to lowest order in the hopping $\mathscr{V}$.

Similarly to the self energies discussed in Sec. 1.4.1, the matrix elements of the resolvent

between two states associated to the sites $a, b \in \mathcal{G}$ admit an expansion in terms of self-avoiding paths $p \in \text{spaths}(a,b)$ in the graph $\mathcal{G}$ connecting the sites a and b, $p = (a, 1, 2, ..., b)$:

$$G_{ba}(E) = \langle b|\frac{1}{E-H}|a\rangle = \frac{1}{E-\mathscr{E}_a - S_a(E)} \sum_{p\in\text{spaths}(a,b)} \prod_{i\in p} \frac{\mathscr{V}}{E-\mathscr{E}_i - S_i^{(p)}(E)}, \quad (4.10)$$

where we introduced the compact notation $S_i^{(p)}(E)$ for the self-energy-like corrections obtained resumming the loops around site i, never crossing site i again, nor any of the sites $(a, 1, \cdots, i-1)$ already visited by the non-repeating path p. The local self energy $S_a(E)$ is related to the local Green function by the usual identity

$$G_a(E) \equiv \frac{1}{E-\mathscr{E}_a - S_a(E)}, \quad (4.11)$$

and it is obtained as the sum of the amplitudes of all the closed paths in which site a appears only as starting and ending point. To lowest order in $\mathscr{V}$,

$$S_a(E) = \sum_{j\in\partial a} \frac{\mathscr{V}^2}{E-\mathscr{E}_j} + O(\mathscr{V}^3), \quad (4.12)$$

where ∂a is the set of nearest neighboring sites of a. From the spectral decomposition of the resolvent it follows

$$G_{ba}(E) = \sum_\alpha \frac{\psi_\alpha(b)\psi_\alpha^*(a)}{E-E_\alpha}, \quad (4.13)$$

so that, assuming no degeneracy of the eigenvalues, the residue at $E = E_\alpha$ gives

$$\lim_{E\to E_\alpha} (E-E_\alpha)G_{ba}(E) = \psi_\alpha(b)\psi_\alpha^*(a), \quad (4.14)$$

The expression for the eigenfunction is obtained as follows: the eigenenergy E_α satisfies $E_\alpha = \mathscr{E}_a + S_a(E_\alpha)$, thus the first factor of (4.10) has a pole at E_α with residue $|\psi_\alpha(a)|^2$, as it follows from (4.11) and (4.14). Then:

$$\lim_{E\to E_\alpha} (E-E_\alpha)G_{ba}(E) = |\psi_\alpha(a)|^2 \lim_{E\to E_\alpha} \sum_{p\in\text{spaths}(a,b)} \prod_{i\in p} \frac{\mathscr{V}}{E-\mathscr{E}_i - S_i^{(p)}(E)}, \quad (4.15)$$

which gives

$$\psi_\alpha(b) = \psi_\alpha(a) \sum_{p\in\text{spaths}(a,b)} \prod_{i\in p} \frac{\mathscr{V}}{E_\alpha - \mathscr{E}_i - S_i^{(p)}(E_\alpha)}, \quad (4.16)$$

with $\psi_\alpha(a)$ obtained from $S_a(E_\alpha)$ using (4.14). From (4.16), it is possible to obtain the wave function amplitudes (more precisely, the ratio $\psi_\alpha(b)/\psi_\alpha(a)$ between the amplitudes) in forward approximation, by neglecting the self-energy-like corrections. The lowest order expansion in $\mathscr{V}$ is easily obtained: assume that α labels an eigenstate localized

at site a for $\mathscr{V} \to 0$. Since $S_\alpha = O(\mathscr{V}^2)$, to lowest order $E_\alpha \to \mathscr{E}_a$, $\psi_\alpha(a) \to 1$, $S_i \to 0$, giving

$$\psi_\alpha(b) = \sum_{p \in \text{spaths}^*(a,b)} \prod_{i \in p} \frac{\mathscr{V}}{\mathscr{E}_a - \mathscr{E}_i}, \tag{4.17}$$

where the set spaths$^*(a,b) \subset$ spaths(a,b) contains only the *shortest* paths from a to b, of length $d(a,b)$.

It is immediate to realize that this expansion is analogous to the one exploited in Sec. 2.2.2 for the coefficients $\mathcal{A}^{(\alpha)}_{\mathcal{I},\mathcal{J}}$ of the conserved operators (or, equivalently, for the wave-function amplitude of the effective single-particle problem). Indeed, in that case, neglecting the second term in Eq. 2.30 is equivalent to restricting only to the shortest paths connecting the root (α,α) to a given site $(\mathcal{I},\mathcal{J})$, since the latter are the paths that jump from one generation to the next, without "excursions" within the same generation[1].

When the single particle problem on $\mathcal{G}$ is localized, the wave functions are expected to be exponentially decaying at large distance. More precisely, for a state ψ_α with localization center a, it is expected that there exists a $\xi > 0$ such that:

$$\mathbb{P}\left(\frac{\log|\psi_r|^2}{r} \leq -\frac{1}{\xi}\right) \to 1 \text{ for } r \to \infty, \tag{4.18}$$

where

$$\psi_r \equiv \max_{b:\, d(b,a)=r} |\psi_\alpha(b)|, \tag{4.19}$$

the probability is over the disorder realizations, and a limit of infinite size of the graph is assumed.

When the amplitudes in (4.19) are expanded as in (4.17), the condition (4.18) reduces to the statement that the lowest order FA series is asymptotically exponentially bounded, and thus convergent. Thus, one recovers the criterion (2.34), with $z = \exp[1/(2\xi)]$. A "lowest order" estimate of the localization length of ψ_α is obtained identifying the minimum value of ξ for which Eq. (4.18) holds true. Moreover, in this approximation the criterion (4.18) can be interpreted as the requirement that resonances do not proliferate at asymptotically large distances. Indeed, an amplitude of $O(1)$ at a site b at distance r from the localization center a corresponds to a resonance between the two sites a, b. As a matter of fact, the corresponding two sites problem can be considered as a two-level system with reduced Hamiltonian

$$h = \begin{pmatrix} 0 & h_r \\ h_r & \Delta \end{pmatrix}, \tag{4.20}$$

[1]Note however that in the operator setting, the "forward approximation" introduces a further simplification, that is that certain sites that are reachable from the root only through hops within the same generation are completely neglected.

where $\Delta = \mathscr{E}_a - \mathscr{E}_b$, and

$$h_r = \mathscr{V} \sum_{p \in \text{spaths}(a,b)} \prod_{i \in p} \frac{\mathscr{V}}{\mathscr{E}_a - \mathscr{E}_i - S_i^{(p)}(\mathscr{E}_a)}, \tag{4.21}$$

where the products are taken over all sites in the path, excluding a, b. The sites are resonant when $|\Delta| < h_r$. Considering h_r to lowest order in $\mathscr{V}$, one finds that this is equivalent to $|\psi(b)| \gtrsim 1$, with $\psi(b)$ computed in the LOFA. Thus, with (4.18) one is probing the statistics of resonances within this approximation, and requiring that the probability to find at least a resonant site at *any* sufficiently large distance r from the localization center decays to zero in the localized phase.

4.3 The forward approximation analysis

We set up the analysis of the single particle problem in the perturbative framework discussed in 4.2, suitably modified to account for the presence of the small bath.

In the absence of coupling ($\lambda = 0$) the usual perturbation theory is recovered: for $t = 0$, the bands of states in Fig. 4.1(a) are decoupled for different sites. Although the statistics of the bath alone are Wigner-Dyson, the overall spectral statistics are Poisson, due to the presence of the L^d local integrals of motion n_i: the spectrum is the superposition of L^d copies of H_{bath} spectra, shifted by the random energies ϵ_i. Meanwhile, the eigenstates take the form $|\Psi\rangle = |i\rangle \otimes |\alpha\rangle$, where $|\alpha\rangle$ is an eigenstate of the bath Hamiltonian (4.3) with energy E_α. On turning on non-zero t (but still at $\lambda = 0$), the system becomes able to execute hoppings, which however do not involve any change in the state of the bath. A nearest neighbor hop thus typically involves an energy change of order W, so that strong localization occurs for $t \lesssim W$, up to logarithmic corrections (see Sec. 1.4.4) As long as the particle is localized, there remain L^d local integrals of motion (the occupation numbers of the localized eigenfunctions), and the spectral statistics thus remain Poisson.

To discuss the effect of a non-zero coupling λ, we move from the following observation: for the model (4.3), (4.7), it is possible to define a local bath Hamiltonian

$$H_{bath}^{(i)} = \omega M + \lambda M^{(i)}, \tag{4.22}$$

with eigenstates $|\alpha_{(i)}\rangle$ satisfying

$$H_{bath}^{(i)} |\alpha_{(i)}\rangle = E_{\alpha_{(i)}} |\alpha_{(i)}\rangle, \tag{4.23}$$

and some average energy gap between the eigenvalues that we denote with $\hat{\delta}(\lambda, \omega)$. In the following, we shall use the simplified notation $|\alpha_i\rangle$ to denote eigenstates of the Hamiltonian (4.22): in this notation, the index i labels the site-dependent Hamiltonian, and not its various eigenstates that are instead labeled by the running index α.

For $t = 0$ in (4.2), the sites $i \in \Lambda$ are decoupled, and the eigenstates of the joint particle

and bath system are of the form

$$|\Psi_{t=0}\rangle = |i\rangle \otimes |\alpha_i\rangle. \tag{4.24}$$

When switching on the hopping t, the expansion in the lowest order forward approximation in t of a wave-function $|\Psi\rangle$ with localization center at a site $i = 0$ reads:

$$\begin{aligned} |\Psi\rangle = |0\rangle \otimes |\alpha_0\rangle + \sum_{\alpha_1} A_{1,\alpha_1} |1\rangle \otimes |\alpha_1\rangle + \sum_{\alpha_2} A_{2,\alpha_2} |2\rangle \otimes |\alpha_2\rangle + ... + \\ \cdots \sum_{\alpha_n} A_{n,\alpha_n} |n\rangle \otimes |\alpha_n\rangle + ... \,, \end{aligned} \tag{4.25}$$

where for simplicity we assumed $d = 1$. The amplitudes A_{n,α_n} in (4.25) are of order t^n, and can be written as

$$A_{n,\alpha_n} = \sum_{p \in \text{paths}(\alpha_0, \alpha_n)} A_p, \tag{4.26}$$

where

$$A_p = \prod_{i=1}^{n} \frac{t \langle \alpha_{i-1} | \alpha_i \rangle}{\epsilon_i + E_{\alpha_i} - \epsilon_0 - E_{\alpha_0}} \tag{4.27}$$

is the amplitude of one particular path from $\alpha_0 \to \alpha_n$, described by a particular sequence $p = (\alpha_1, \alpha_2, ..., \alpha_n)$ of eigenstates of the bath Hamiltonians $H^{(i)}_{bath}$. The amplitude for the *particle* to be at site n equals $\sum_{\alpha_n} A_{n,\alpha_n}$.

The perturbative expansion in the hopping t thus requires to compare the matrix element of a transition $|i\rangle \otimes |\alpha_i\rangle \to |j\rangle \otimes |\beta_j\rangle$, that is $t|\langle \alpha_i | \beta_j \rangle|$, with the energy difference $\Delta E = \epsilon_i - \epsilon_j + E_{\alpha_i} - E_{\beta_j}$. The bath induces a site-dependent renormalization of the hopping,

$$t \to t^{\alpha\beta}_{ij} = t|\langle \alpha_i | \beta_j \rangle|, \tag{4.28}$$

which now depends on the overlap between eigenstates of the bath Hamiltonians (4.22) at different sites. The effective energy gap is also dominated by the bath: the latter allows to optimize the energy denominator over the states $|\alpha_j\rangle$, in such a way that $|E_{\alpha_i} - E_{\beta_j}| \sim W + \hat{\delta}(\lambda, \omega)$, provided that the corresponding matrix element is not suppressed.

In the following, we discuss this modified locator expansion, focusing separately on the different regimes of perturbatively weak coupling $\lambda < \omega/\sqrt{N}$, of strong coupling $\lambda > \omega$ and of intermediate coupling $\omega/\sqrt{N} < \lambda < \omega$.

4.3.1 Weak coupling: the Anderson localized regime

Let us consider the bath Hamiltonians (4.22): the eigenstates of the bare Hamiltonian (4.3) start to mix with each other when λ becomes comparable to the level spacing $\sim \omega/\sqrt{N}$; for $\lambda < \omega/\sqrt{N}$, the eigenstates of (4.22) are only slightly deformed from site to site. In this case, the hopping between neighboring sites is not enhanced by the presence of the bath. Indeed, consider the first order term in the amplitude (4.27). The optimal locator is associated to hopping processes leaving the bath untouched, i.e., such that the states $|\alpha_0\rangle$ and $|\alpha_1\rangle$ are perturbatively closed, being a perturbation of the same eigenstate $|\alpha\rangle$ of ωM. In this case the first order correction to the localized eigenstate (4.25) reads:

$$\delta\Psi \sim \frac{t}{W}\left(1 - \frac{\lambda^2}{2\delta^2}\right), \tag{4.29}$$

as it follows from computing the overlap $\langle\alpha_0|\alpha_1\rangle$ perturbatively in λ/δ. The locator associated to hopping processes changing the state of the bath, $|\alpha_0\rangle \to |\beta_1\rangle$ with $E_{\alpha_0} - E_{\beta_1} \sim W$, is at most:

$$\delta\Psi = \frac{t}{\epsilon_1 - \epsilon_0}\max_{\beta_1}\frac{\lambda}{\epsilon_0 - \epsilon_1 + E_{\alpha_0} - E_{\beta_1}} \sim \frac{t\lambda}{W\delta} < \frac{t}{W}.$$

So in this regime, the bath is typically not excited by the particle traveling. This is illustrated in Fig. 4.1(a): the solid red lines indicate the trajectory followed by a particle hopping without changing the state of the bath. The criterion for breakdown of the locator expansion derived imposing that the optimal locator (4.29) is $O(1)$ reads $t_c \sim W(1 - \lambda^2/(2\delta^2))$, and it is thus only slightly altered by a non-zero λ. For $t < t_c$ strong localization occurs, the exact eigenstates are effectively product states of system and bath, and the entropy of entanglement of the system with the bath is close to zero.

4.3.2 Strong coupling: the quantum Zeno regime

Consider now the opposite limit of strong λ. At $t = 0$, a $\lambda > \delta$ causes the hybridization of the levels in the bath. For $\lambda \gg \omega$, the Hamiltonian of the bath is dominated by the coupling $M^{(i)}$ to the particle, and the bath levels are hybridized in a radically different way for each position i of the particle. The eigenstates of the different $H^{(i)}_{bath}$ in (4.22) have overlap:

$$\langle\alpha_i|\beta_j\rangle = \delta_{\alpha,\beta}\delta_{i,j} + (1 - \delta_{i,j})x_{ij}/\sqrt{N}, \tag{4.30}$$

where the $\delta_{i,j}$ is a Kronecker delta function and x_{ij} is a Gaussian random variable $< x_{ij} >= 0$ and $< x^2_{ij} >= 1$.

We turn on a small hopping t and consider the problem (4.25). Any hop in the system $|i\rangle\otimes|\alpha_i\rangle \to |j\rangle\otimes|\beta_j\rangle$ strongly modifies the state in the bath. By inspecting (4.28) together with (4.30), one realizes that in this regime a direct hopping (blue line in Fig. 4.1(a)),

which stays on shell to a precision $\delta \sim \omega/\sqrt{N}$ is suppressed because the corresponding matrix element is.

This can be formalized realizing that the large coupling problem can be mapped to an equivalent Bethe lattice problem with connectivity $\kappa \sim N$ (counting the possible states $|\beta_j\rangle$: in higher dimension, a factor of d has to be added), effective hopping

$$\tau = t\frac{1}{\sqrt{N}} \tag{4.31}$$

and effective disorder

$$\mathcal{W} = \lambda\sqrt{N}. \tag{4.32}$$

The effective disorder $\mathcal{W}$ is determined from the bandwidth of the local bath Hamiltonians $H^{(i)}_{bath}$: the latter equals $\sqrt{2N\omega^2\left(1+\lambda^2/\omega^2\right)} \sim \lambda\sqrt{N}$ for $\lambda > \omega$. The known Bethe lattice results, see Eq. 1.66, imply that the eigenstates are localized for

$$t \lesssim \lambda/\ln N. \tag{4.33}$$

Thus, at large λ a very large hopping is needed for the perturbative expansion to breakdown.

The effect of the bath in this regime is twofold: on one hand, it enlarges the effective bandwidth of the single particle problem; on the other hand, it suppresses the hopping because the overlap between bath states corresponding to the particle being on different sites is itself suppressed. This can be viewed as an orthogonality catastrophe, where the particle is "dressed" by the bath in a different way depending on which site it is on. In the limit $\lambda \to \infty$ the hopping is completely ineffective. This bears some similarities with the Quantum Zeno effect, namely the fact that a small system coupled with a large quantum system, possibly a detection apparatus, does not evolve or evolves only into a given subspace whenever the coupling is too large [58, 56]. In this limit, the exact eigenstates are simply product states $|\Psi\rangle = |i\rangle|\alpha_i\rangle$, which, however, are exact eigenstates of the system-bath coupling. The entropy of entanglement of system and bath in an eigenstate is again zero as for λ small, and the particle is localized on a single site.

4.3.3 The intermediate regime

In the intermediate regime, the coupling λ has to be treated non-perturbatively. This requires to compute the overlap between bath states in (4.28) as λ is varied. We do this as a first step in the analysis. Turning on a coupling $\lambda > \omega/\sqrt{N}$ causes the eigenstates of ωM within an energy window Δ to hybridize. The width of this energy window may be determined by calculating the decay rate of an eigenstate $|\alpha\rangle$ of ωM due to the perturbation $V = \lambda M^{(i)}$ using Fermi's golden rule. Given a density of final states $\delta^{-1} = \sqrt{2N}/\pi\omega$ the calculation indicates that the decay rate is

$$\Delta \simeq 2\pi\lambda^2\frac{\sqrt{2N}}{\pi\omega}, \tag{4.34}$$

and suggests that the broadened spectral line is a Lorentzian with width Δ. Thus, the eigenstates $|\beta_i\rangle$ of $\omega M + \lambda M^{(i)}$ should be wave packets of eigenstates $|\alpha\rangle$ of ωM, with

$$|\langle\beta_i|\alpha\rangle| = \sqrt{\frac{\delta\Delta/\pi}{(E_{\beta_{(i)}} - E_\alpha)^2 + \Delta^2}}. \tag{4.35}$$

As $\lambda \to \omega$, $\Delta \to 2\omega\sqrt{2N} = \Omega$ indicating complete hybridization of all states. For $\lambda \to \delta/\sqrt{2\pi}$, the decay of $|\alpha\rangle$ is no longer to a continuum of states, and $\Delta \to \delta$, indicating no hybridization. Thus, at its boundaries of validity the Fermi's golden rule correctly matches on the weak and strong λ limits.

The overlap between the eigenstates of the $H^{(i)}_{bath}$ for different sites i can be computed in a similar fashion, with an analogous result. We report this short calculation in the following.

Consider an eigenstate $|\alpha_{(i)}\rangle$ of $H^{(i)}_{bath}$, and the perturbation $\lambda(M^{(i+1)} - M^{(i)}) \equiv \lambda V$. The new $H^{(i)}_{bath} + \lambda V = H^{(i+1)}_{bath}$ has eigenstates $|\alpha_{(i+1)}\rangle$. We exploit once more a simplified notation, using $|\alpha_i\rangle$ and $|\alpha_{i+1}\rangle$ for the two states, and E_i, E_{i+1} for their energies. The overlap is derived from the identities:

$$\langle\alpha_i|\frac{1}{E - H^{(i+1)}_{bath}}|\alpha_i\rangle = \int dE'\rho(E')\frac{1}{E - E'}|\langle\alpha_i|\alpha'\rangle|^2 = \frac{1}{E - E_i - S_{\alpha_i}(E)}, \tag{4.36}$$

where S_{α_i} is the self-energy function on the state $|\alpha_i\rangle$, ρ is the density of states of $H^{(i+1)}_{bath}$ and $|\alpha'\rangle$ denotes a state in the spectrum with energy E'. We take $E \to E_{i+1} + i0^+$, and take the $\Im$ part of (4.36) which gives:

$$\pi\rho(E_{i+1})|\langle\alpha_i|\alpha_{i+1}\rangle|^2 = \frac{\Delta}{(E_{i+1} - E_i)^2 + \Delta^2}, \tag{4.37}$$

where $\Delta = \Im S_{\alpha_i}(E_{i+1})$ and we have assumed that $\langle\alpha_i|\alpha'\rangle$ is some smooth function of the energy (this is true on average). At second order in the perturbation it holds

$$S_{\alpha_i}(E) \approx \lambda^2 \int dE'\rho(E')\frac{|\langle\alpha|V|\alpha'\rangle|^2}{E - E_\beta}, \tag{4.38}$$

and thus

$$\Delta = \Im S_{\alpha_i}(E_{i+1}) \approx 2\lambda^2\pi\rho(E_{i+1}) \tag{4.39}$$

using that $|\langle\alpha|V|\alpha'\rangle|^2 = 2$, again true on average. Setting $\rho(E) \equiv 1/\delta$ we obtain

$$P(E_i, E_{i+1}) \equiv |\langle\alpha_i|\alpha_{i+1}\rangle|^2 \sim \frac{\Delta\delta/\pi}{(E_i - E_{i+1})^2 + \Delta^2}, \tag{4.40}$$

in analogy with (4.35).

To get an intuition on the non-monotonic dependence of localization on λ, we first analyze the magnitude of the first order term in t in (4.25), postponing the analysis of the full expansion to Sec. 4.3.3.

Non-monotonicity from the first order term

Since $|\epsilon_i - \epsilon_{i+1}| = O(W)$, a direct hopping (blue line in Fig. 4.1(a)) which stays on shell to a precision $\delta \sim \omega/\sqrt{N}$ must involve transitions between bath states with $|E_i - E_{i+1}| \sim W$. The amplitude of the overlap between these states may be estimated by inserting $(E_i - E_{i+1}) \sim W$ into Eq. (4.40). In this way, one finds that the correction to the wave function from direct hopping processes is, at leading order in t,

$$\delta\Psi \sim \sum_{\alpha_1} \frac{t|\langle\alpha_0|\alpha_1\rangle|}{\epsilon_1 - \epsilon_0 + E_{\alpha_1} - E_{\alpha_0}} \sim \left(\frac{t}{\delta}\frac{\sqrt{\Delta\delta}}{\sqrt{W^2+\Delta^2}}\right). \tag{4.41}$$

The non-monotonic behavior in λ is already encoded in (4.41). Indeed, the line broadening Δ in (4.34) becomes comparable to W for

$$\lambda_c = \sqrt{\frac{W\omega}{2\sqrt{2N}}}. \tag{4.42}$$

Two distinct regimes can be identified:

(i) For $\lambda < \lambda_c$, it holds $\Delta < W$, and (4.41) can be approximated by $t\lambda/W\delta$: thus, the locator is enhanced by a factor $\lambda/\delta > 1$ with respect to its typical value in the absence of a bath. This expression may be understood as follows: since $\Delta < W$, a direct hop via the blue line in Fig. 4.1(a) is forbidden, as the two bath states involved have vanishing overlap. Instead, the particle first hops without changing the state of the bath, going off shell by an amount W, and then the bath relaxes to bring the system back on shell, to a precision δ. The matrix element for this two-step process is $t\lambda/W$.

(ii) For $\lambda > \lambda_c$, it holds $\Delta > W$ and the expression (4.41) can be approximated by t/λ, using that $\Delta \sim \lambda^2/\delta$. This preludes to the Zeno regime, as the locator is suppressed for large λ. The same result is obtained by reasoning that for $\lambda > \lambda_c$, a direct hopping is not forbidden, since bath states are hybridized over an energy window $\Delta > W$. However, the matrix elements are suppressed by a factor of $\sqrt{\tilde{N}}$, where $\tilde{N} = \Delta/\delta \sim (\lambda/\omega)^2 N$ is equal to the number of states involved in the hybridization. For $\lambda > \omega$, i.e. in the Zeno regime, $\tilde{N} = N$.

These considerations illustrate that, when performing a locator expansion in small t, the successive corrections to the wave function are suppressed by powers of t/λ if $\lambda > \lambda_c$, and by powers of $t\lambda/W\delta$ if $\delta/\sqrt{2\pi} < \lambda < \lambda_c$. This suggests that the boundary of stability of the perturbative expansion is given by $t \simeq \lambda$ and $t \simeq W\delta/\lambda$ for large and small λ,

respectively. In the next section, we discuss the more refined calculation accounting for all orders in t, which reproduces the first order results up to logarithmic corrections.

Non-monotonicity at any order

For simplicity of notation, we restrict in the following to the case of a single particle in one dimension, and remark what has to be adapted in case of higher dimension. Following the reasoning outlined in Sec. 4.2, we determine the probability to have a significant amplitude at a large distance n from the localization center $i = 0$ of the eigenstate (4.25). More precisely, we identify the region of parameters where:

$$\mathbb{P}\left(\left|\sum_{\alpha_n} A_{n,\alpha_n}\right| < z^n\right) \overset{n\to\infty}{\longrightarrow} 1 \tag{4.43}$$

for some $z < 1$. The convergence radius of the lowest order forward approximation is determined setting $z \to 1$.

The calculation is similar to the one performed in Chapter 2: the expansion converges whenever the exponential growth with n of the number of paths (having the particle in position n in the final state) is compensated by the exponential decay of the probability of having a single path with atypically large weight of $O(1)$. This is essentially the same mechanism driving the transition on a Bethe lattice, and occurs in this setting due to the domination of the sum in (4.43) by a single term. More precisely, the distribution of the amplitude A_p of a particular path weight (4.27) is fat-tailed. As a consequence, both the sums (4.26) and $\sum_{\alpha_n} A_{n,\alpha_n}$ are very well approximated by their maximum term:

$$\left|\sum_{\alpha_n} A_{n,\alpha_n}\right| \simeq |\max_{\alpha_n} A_{n,\alpha_n}| \simeq \max_{\alpha_n} \max_{p\in\text{paths}(\alpha_0,\ldots,\alpha_n)} |A_p|, \tag{4.44}$$

which is effectively the maximum over all the paths of length n emanating from α_0, irrespective of the final state of the bath α_n. We call this set of paths paths$^*(\alpha_0)$. Since each bath state $|\alpha_i\rangle$ along the path can be chosen among N possible states, the size of paths$^*(\alpha_0)$ is N^n. Treating the different paths as independent, one recovers:

$$\mathbb{P}\left(\max_{p\in\text{paths}^*(\alpha_0)} |A_p| < z^n\right) \approx \exp\left[-N^n P\left(|A_p| > z^n\right)\right]. \tag{4.45}$$

For a particle in a higher dimensional lattice, the sum (4.26) has to be modified to account for the fact that two lattice sites at distance n can be connected by multiple lattice paths of shortest length n, whose number is approximately equal to d^n. For each of these paths the sequence of bath states can be chosen among N^n possibilities. Thus (4.45) remains valid with the substitution $N \to Nd$.

The estimate of (4.45) requires to compute the large deviations of the random variables (4.27), taking into account the dependence of the renormalized hopping (4.28) on the coupling λ, assuming that the latter is in the intermediate regime. The large deviations

for large n are obtained from the generating function of the (4.27), by inversion of the Laplace transform within a saddle point approximation, following the same scheme as in Sec. 2.2.4. The generating function at large n is dominated by the maximal eigenvalue of an integral operator, whose kernel depends explicitly on the parameter

$$q \equiv \frac{W}{\Delta} = \left(\frac{\lambda_c}{\lambda}\right)^2, \tag{4.46}$$

with λ_c introduced in (4.42). Analytic calculations can be performed in the two limits $q \ll 1$ and $q \gg 1$, see Appendix 4.A. In the first case, from (4.43) for $z \to 1$ one obtains the approximate convergence criterion:

$$\frac{\sqrt{2}e}{\pi}\frac{td}{\lambda}\log\left(\frac{2W}{\omega}\frac{\lambda\sqrt{N}}{t}\right) \lesssim 1, \tag{4.47}$$

which is in agreement with the condition $t/\lambda \lesssim 1$ obtained in Sec. 4.3.3 (ii). In the second case, one finds the approximate criterion

$$\frac{4e}{\pi}\frac{td}{W}\frac{\lambda\sqrt{N}}{\omega}\log\left(\frac{2W\omega}{\lambda^2\sqrt{2N}}\right)\log\left(\frac{W}{t}\sqrt{\frac{W\sqrt{2N}}{\omega}}\right) \lesssim 1, \tag{4.48}$$

which is again in agreement with the condition $t\lambda/W\delta \lesssim 1$ obtained in Sec. 4.3.3(i).

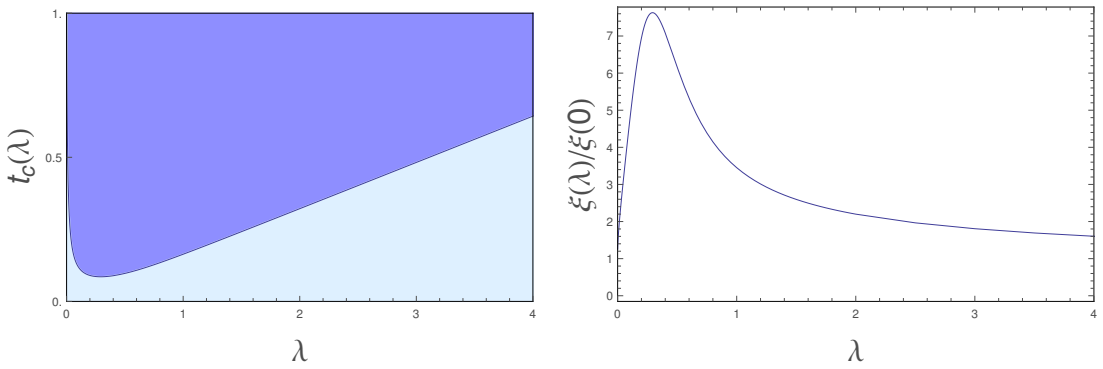

(a) (b)

Figure 4.1: Results of analytic calculations in the forward approximation for fixed $W = 3$, $N = 300$, $\omega = 4$ (substitution into Eq. (4.42) gives $\lambda_c = 0.5$). (a) The $t - \lambda$ phase diagram; the light region is the regime of convergence of the lowest order forward approximation. The calculation assumes that states in the bath are hybridized according to Eq. (4.35), and is thus not applicable at $\lambda < \delta/\sqrt{2\pi}$. (b) Localization length as a function of λ, along a horizontal slice through the top diagram that stays always on the "strongly localized" side of the phase boundary. The maximum is close to $\lambda \approx 0.3$, which indicates that the system is least localized at this intermediate value of λ. Due to the nature of the forward approximation, $t(\lambda)$ and $\xi(\lambda)$ are underestimated, while the ratio $\xi(\lambda)/\xi(0)$ is overestimated.

For intermediate values of q, the saddle point calculation can be performed numerically, the result being the phase diagram illustrated in Fig. 4.1. The latter confirms that strong localization is least stable when $\lambda \approx \lambda_c$, and becomes more stable both for weak λ (the Anderson localization limit), and for strong λ (the quantum Zeno limit). The minimum value of t that can cause breakdown of the locator expansion is $t_c(\lambda_c) = \sqrt{\omega W/(2\sqrt{2N})}$. Thus, for any t the localization length should peak at this value of λ. This is observed in the analytic calculations (Fig. 4.1), where the localization length at fixed λ is obtained computing the minimum value $z_{\min}$ for which (4.43) holds true. The same effect is found also in the numerics discussed in the following section, see Fig. 4.1. We report the saddle point calculation in Appendix 4.A.

4.4 The exact diagonalization results

To estimate numerically the localization properties of the particle we perform exact diagonalization in $d = 1$ and look at the probability distribution of the position of the particle in the eigenstates $|\Psi\rangle$ of the coupled system and bath,

$$p_i = \sum_{\alpha_i=1}^{N} |\langle i, \alpha_i|\Psi\rangle|^2. \tag{4.49}$$

We consider the inverse participation ratios of p,

$$I_q = \left(\sum_i p_i^q\right)^{-1}. \tag{4.50}$$

and extract the localization length from $I_2 \sim \xi^d$. Additional information is contained in the entropy of entanglement of the particle with the bath, $S = -\mathrm{Tr}\,(\rho \ln \rho)$, where ρ is the reduced density matrix of the particle, $\rho = \mathrm{Tr}_{\,\mathrm{bath}}|\Psi\rangle\langle\Psi|$ with $|\Psi\rangle$ an exact eigenstate of the coupled system and bath. In the present problem the entanglement entropy and the inverse participation ratios are correlated, since the less the particle is localized, the more it is entangled with the bath.

The numerical results for a one-dimensional system are presented in Fig. 4.1, and show the evolution of the inverse participation ratio and entanglement entropy along horizontal slices taken through the phase diagram in Fig. 4.1(b). The numerics are for $t = 1$, which is kept fixed, while the disorder W varies. Note that for $W \gtrsim 2\sqrt{2N}/\omega \approx 12$ we are entirely in the strongly localized regime, for any value of λ. The first panel of Fig. 4.1 shows how the inverse participation ratio I_2 varies for an infinite size system coupled to a bath with coupling λ. We have extrapolated the finite size numerics to infinite L by using a fit of the form

$$I_q(L) = I_q(\infty) + a_I/L, \tag{4.51}$$

which turns out to be a very good fitting form for the data. We observe as expected a non-monotonic behavior, with weak λ increasing the inverse participation ratio and

strong λ suppressing it.

The second panel on Fig. 4.1 shows the evolution of the entanglement entropy with coupling λ, extrapolated from the finite size system, analogously to the inverse participation ratio, using a fit of the form

$$S(L) = S(\infty) + a_S/L. \tag{4.52}$$

We show this finite size scaling in the inset; the results for the finite size scaling of I_2 are very similar. At weak λ, the particle becomes more entangled with the bath as λ is increased, but for larger λ the entanglement entropy becomes a decreasing function of the coupling, and in the extreme $\lambda \to \infty$ limit one recovers an unentangled product state. The entanglement entropy is maximized at the same value of $\lambda = \lambda_c$ that maximizes the inverse participation ratio.

Fig. 4.2 shows how the value of λ_c, which maximizes both the participation ratio and the entanglement entropy, varies with W. We compare the numerical result with our analytic estimate of Eq. (4.42), obtaining a good agreement.

4.5 A comment on the role of dimensionality

The calculation in Sec. 4.3 identifies the regime of strong localization, in which the perturbative expansion in t is convergent. What happens outside such a regime, i.e. in the large t region of the phase diagram, is highly sensitive to dimensionality. Indeed, the same results as for the conventional Anderson problem (see Sec. 1.4.6) are expected: this follows from the fact that even in the presence of the bath the hopping problem may be viewed as a (multi band) problem of a fermion moving in a random potential in the orthogonal symmetry class, and thus he scaling theory results should extend to this context as well. Based on this, we conclude that in one or two dimensions the divergence of the locator expansion signals the crossover to weak localization, while in higher dimension the boundary shown in Fig. 4.1(b) is a true phase boundary separating localized and delocalized phases.

The arguments in [3] may be used to estimate the dependence of the localization length on the parameters of the problem, in $d = 1, 2$. The localization length is simply the length scale on which g becomes of order one, i.e. $g(\xi) = 1$. In one dimension the solution of the scaling equation (Eq. (1.78) with $\beta(g) = d - 2 = -1$) gives $g(L) \sim g_0/L$, where g_0 is the bare conductance at the scale l_0. Thus, $g = 1$ happens on length scales that are only power law large in g_0. In two dimensions the localization length is exponentially large in g_0, $g(L) \sim g_0 - c\log(L/l_0)$, giving $\xi \sim l_0 \exp(g_0/c)$). The dependence on the parameters in (4.1) is obtained identifying the bare conductance g_0 with the ratio of matrix element to level spacing. This parameter takes value $g_0 \approx t/W$ for $\lambda < \omega/\sqrt{N}$, $g_0 \approx t\lambda\sqrt{N}/W\omega$ for $\omega/\sqrt{N} < \lambda < \lambda_c$, and $g_0 \approx t/\lambda$ for $\lambda > \lambda_c$ according to the analysis developed in Sec. 4.3.

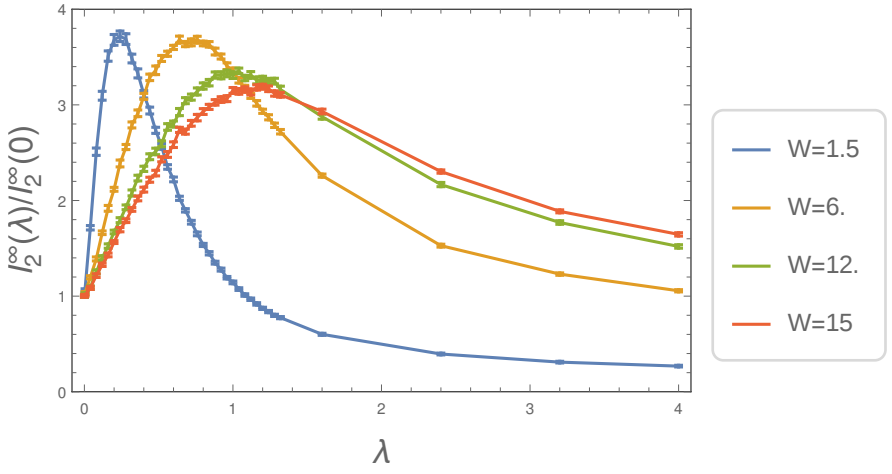

(a)

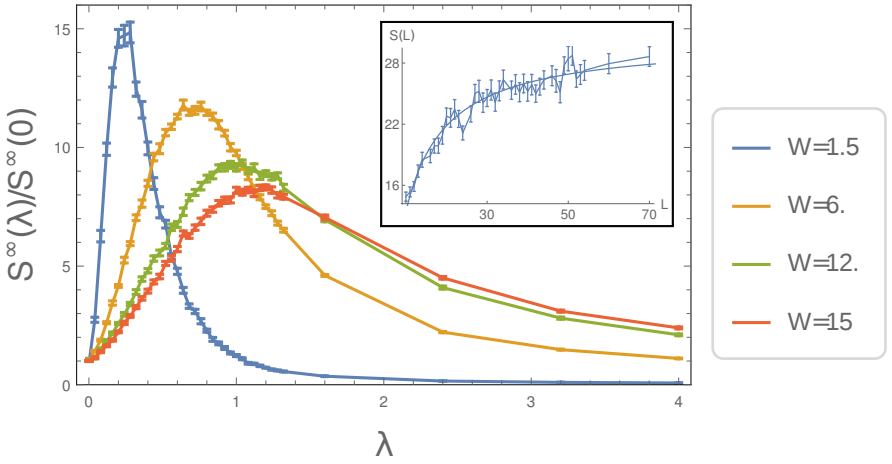

(b)

Figure 4.1: Results of exact diagonalization performed for about 50 states in the center of the band for the parameters $t = 1$, $\omega = 4$, $N = 300$, and varying W. The values of W are chosen so that we span the phase diagram in Fig. 4.1(b). For $W < 12$, we slice through the "weak localization" region, whereas for $W > 12$ we stay always in the strong localization regime. The entanglement entropy and the participation ratios have a pronounced maximum close to the (same) hybridization threshold λ_c. The peak is sharper when we go through the weak localization regime. *Inset.* Example of the finite size scaling of S^L for a given value of $\lambda = 0.8$ and $W = 6$. To extrapolate the infinite size S^∞ we used (4.52) with L ranging from 10 through 70, taking around 50 disorder realizations for each system size.

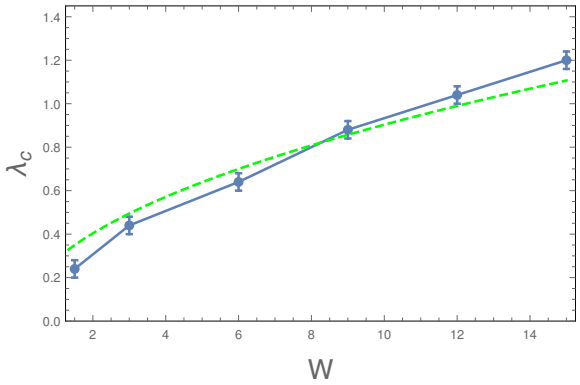

Figure 4.2: Value of λ_c for $t = 1$ and the different disorders W. In blue we plot the numerical data, with their errors coming from the resolution in λ at which the plots in Fig. 4.1 are computed. In dashed green we plot the analytic estimate of Eq. (4.42). We note that the exact diagonalization data agree well with the analytic prediction.

Appendix

4.A Derivation of the phase diagram (Fig. 4.1)

To get the distribution of $|A_p|$, it is convenient to extract all energy scales and to write the amplitude in terms of a new variable $Z_n > 0$ defined from:

$$|A_p| = \left(\frac{t}{W}\sqrt{\frac{\delta}{\pi\Delta}}\right)^n e^{Z_n}. \tag{4.53}$$

The Laplace transform of the probability distribution $P_n(Z)$ of the variable Z_n reads:

$$g(s) = \int_0^\infty dZ P_n(Z) e^{-sZ}. \tag{4.54}$$

Assuming $\epsilon_0 + E_{\alpha_0} = 0$ (this gives the transition at the center of the band), we find

$$g(s) = \frac{1}{(s+1)^n}\left(\frac{8W}{\pi\Omega}\right)^n \tilde{g}(s), \tag{4.55}$$

where

$$\tilde{g}(s) = \prod_{i=1}^{n} \frac{\Delta}{4W} \int_{-\frac{\Omega}{2\Delta}}^{\frac{\Omega}{2\Delta}} dE_i \left[1 - \left(\frac{2\Delta}{\Omega}E_i\right)^2\right]^{\frac{1}{2}} \Xi_{\frac{W}{\Delta}}(E_i, s) \exp\left\{\frac{s}{2}\log\left(1 + (E_i - E_{i-1})^2\right)\right\} \tag{4.56}$$

where the variables $E_i \equiv E_{\alpha_i}/\Delta$ are dimensionless and

$$\Xi_w(x,s) = \left|1 + \frac{x}{w}\right|^{s+1} \mathrm{sgn}\,(w+x) + \left|1 - \frac{x}{w}\right|^{s+1} \mathrm{sgn}\,(w-x \tag{4.57}$$

The inversion of the Laplace transform gives

$$P_n(Z) = \frac{1}{2\pi i}\left(\frac{8W}{\pi\Omega}\right)^n \int_{\mathcal{B}} ds\, \frac{e^{sZ}\tilde{g}(s)}{(s+1)^n}. \tag{4.58}$$

The Bromwich path is to the right of the n-pole $s = -1$. For the purpose of computing the large deviations giving rise to a resonance, we consider $Z = O(n)$ for large n, so

$Z = n\zeta$; then

$$P_n(Z) = \frac{1}{2\pi i}\int_{\mathcal{B}} ds\; e^{nf(s)}, \tag{4.59}$$

with

$$f(s) = s\zeta - \log(s+1) + \log\frac{8W}{\pi\Omega} + \frac{1}{n}\log\tilde{g}(s). \tag{4.60}$$

The distribution can be computed within the saddle point approximation, assuming $n \ll 1$.

To compute (4.56), we make some approximation. In the intermediate regime $\lambda < \omega$ it holds that $\Delta < \Omega$; thus, we approximate $1 - \left(\frac{2\Delta}{\Omega}E_i\right)^2 \to 1$; moreover, since the saddle point is dominated by the region with $s \to -1$, we set $\Xi(x,s) \simeq \Xi(x,-1) = 2\Theta(W/\Delta - |x|)$, so that

$$\begin{aligned}\tilde{g}(s) &\approx \prod_{i=1}^{n}\frac{\Delta}{2W}\int_{-\frac{W}{\Delta}}^{\frac{W}{\Delta}} dE_i\; e^{\frac{s}{2}\log\left(1+(E_i-E_{i-1})^2\right)} \\ &= \prod_{i=1}^{n}\frac{\Delta}{2W}\int_{-\frac{W}{\Delta}}^{\frac{W}{\Delta}} dE_i\; \left[1+(E_n-E_{n-1})^2\right]^{\frac{s}{2}}\cdots\left[1+(E_2-E_1)^2\right]^{\frac{s}{2}}\left(1+E_1^2\right)^{\frac{s}{2}}.\end{aligned} \tag{4.61}$$

This function is regular at $s=-1$ and it can be seen as the $n-$th application of an integral Kernel:

$$K(x',x) = \left(1+q^2(x'-x)^2\right)^{\frac{s}{2}}, \tag{4.62}$$

with measure $d\mu(x) = dx/2$, to the function $\phi = (1+q^2x^2)^{s/2}$. The parameter q is defined in (4.46). Denoting with $\alpha(s,q)$ the largest eigenvalue of the integral operator K, we have:

$$\tilde{g}(s) = c\;\alpha(s,q)^n \tag{4.63}$$

to leading exponential order in n (c does not scale with n). As K is a positive Kernel, by the Perron-Frobenius theorem, the largest eigenvalue is positive and corresponds to a positive eigenfunction $\mathcal{F}$ without any node on the interval $[-1,1]$ solving the equation

$$\int_{-1}^{1}\frac{dx}{2}(1+q^2(x'-x)^2)^{s/2}\,\mathcal{F}(x) = \alpha(s,q)\,\mathcal{F}(x'). \tag{4.64}$$

In the following, we consider separately the limits of large and small q.

The small q limit. For small q it holds

$$K(x',x) \simeq 1 + \frac{sq^2}{2}(x'-x)^2 + O(q^4). \tag{4.65}$$

Then the eigenvalue problem can be solved exactly with an ansatz of the form $\mathcal{F}(x) =$

$a + bx^2$ which for small q gives

$$\alpha = 1 + \frac{q^2 s}{3} + \frac{q^4 s^2}{45} + O(q^6), \tag{4.66}$$

so to lowest order

$$\frac{1}{n} \log \tilde{g}(s) = q^2 \frac{s}{3} + O(q^4). \tag{4.67}$$

Inserting (4.67) into (4.60), we get that $df(s)/ds$ equals zero at the point

$$s^*_{q \ll 1} = -1 + \frac{1}{\zeta + q^2/3}, \tag{4.68}$$

where

$$f(s^*_{q \ll 1}) = -\zeta + 1 + \log\left(\frac{8W}{\pi\Omega}(\zeta + q^2/3)\right) - \frac{q^2}{3}. \tag{4.69}$$

Taking (4.53) into account we obtain:

$$\mathbb{P}(|A_p| > z^n) \approx C_n \left[\frac{\sqrt{2}e}{\pi z} \frac{t}{\lambda N} e^{-\frac{q^2}{3}} \log\left(\frac{2zW}{t} \frac{\sqrt{N}\lambda}{\omega} e^{\frac{q^2}{3}}\right)\right]^n, \tag{4.70}$$

where C_n scales sub-exponentially in n. The criterion $NP\left(|A_p| > z^n\right)^{1/n} < 1$, see (4.45), is equivalent in dimension d to:

$$\frac{\sqrt{2}e}{\pi} \frac{td}{\lambda} e^{-\frac{1}{24}\left(\frac{W\omega}{\lambda^2\sqrt{N}}\right)^2} \log\left(\frac{2W}{\omega} \frac{\lambda\sqrt{N}}{t} e^{\frac{1}{24}\left(\frac{W\omega}{\lambda^2\sqrt{N}}\right)^2}\right) = 1, \tag{4.71}$$

where we have taken the limit $z \to 1$. Since $W\omega/\lambda^2\sqrt{N} = 2\sqrt{2}(\lambda_c/\lambda)^2$ is small in the small q regime the exponential factors in (4.71) can be neglected. Then the criterion for localization reduces to:

$$\frac{\sqrt{2}e}{\pi} \frac{\tau\kappa}{\mathcal{W}} \log\left(\frac{2W}{\omega\sqrt{N}} \frac{\mathcal{W}}{\tau}\right) < 1, \tag{4.72}$$

which equals the critical condition for localization on a Bethe lattice with the effective parameters $\mathcal{W} = \lambda\sqrt{N}, \kappa = Nd$ and $\tau = t/\sqrt{N}$, up to an additional factor $W/\omega\sqrt{N} \sim W/\delta > 1$ in the logarithmic correction. Thus, the extrapolation to the Zeno regime is consistent with Eq. (4.33) in the main text.

The large q limit. For generic q the integral equation is not easy to solve but the point $s = -1$ to which the saddle point is going to be very close, is regular. An approximation to the largest eigenvalue which works remarkably well for all values of q and $s < 0$ is obtained by taking the simple trial function $\mathcal{F} = 1$.

The double integral $\alpha = \langle\mathcal{F}|K|\mathcal{F}\rangle$ can then be transformed into a single integral (since it

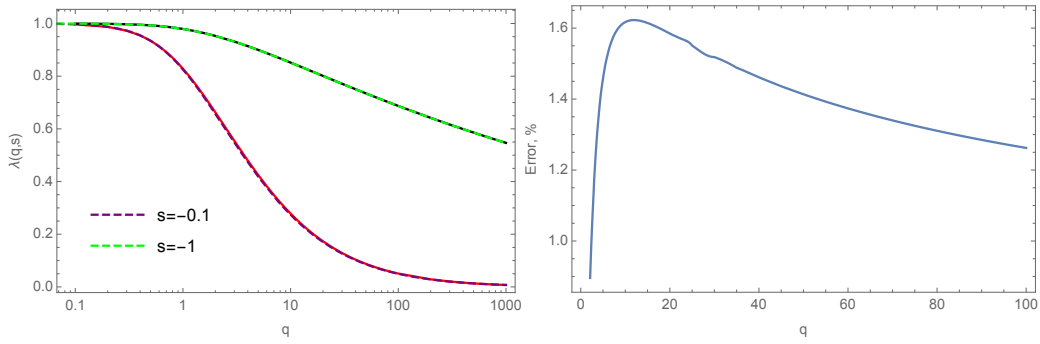

(a) (a) (b) (b)

Figure 4.A.1: Comparisons of the largest eigenvalue of the kernel in (4.64) and its approximate form (4.74). (a) Continuous line is the exact numerical results, dashed lines are analytical approximations. (b) Relative error, in percent for $s = -1$.

depends only on $x' - x$)

$$\alpha(q,s) = 2\int_0^1 (1-x)(1+q^2x^2)^{s/2}dx \tag{4.73}$$

and from this one gets:

$$\alpha(q,s) = \frac{1}{2q^2(s+2)}\left(4q^2(s+2)F\left(\frac{1}{2},-\frac{s}{2};\frac{3}{2};-4q^2\right) - \left(4q^2+1\right)^{\frac{s}{2}+1}+1\right), \tag{4.74}$$

where $F(a,b;c;x)$ is the hypergeometric function. The comparison with the numerics is in Fig. 4.A.1, the error never exceeds 1.6% and is exact both in the large-q and in the small-q limit. For small q one recovers (4.66). We derive an analytic estimate of the critical hopping in the regime of large q exploiting the approximate expression (4.74). At large q it holds

$$\alpha(s,q) = q^s\tilde{\alpha}(s,q) + \mathcal{O}\left(\frac{1}{q^2}\right) \tag{4.75}$$

with

$$\tilde{\alpha}(s,q) = \left[\frac{2^{s+1}}{(s+1)(s+2)} + \frac{1}{q^{1+s}}\frac{\sqrt{\pi}\Gamma(-(s+1)/2)}{2\Gamma(-s/2)}\right]. \tag{4.76}$$

Neglecting higher order terms in $1/q$, the saddle point is attained at the point $s^*_{q\gg1}$ satisfying:

$$s^*_{q\gg1} = -1 + \frac{1}{\zeta + \log q + \frac{d}{ds}\log\tilde{\alpha}(s^*_{q\gg1},q)}. \tag{4.77}$$

The function $\log\tilde{\alpha}(s,q)$ has the expansion:

$$\log\tilde{\alpha}(s,q) = \alpha_0(q) + \alpha_1(q)(s+1) + \mathcal{O}((s+1)^2), \tag{4.78}$$

with

$$\alpha_0(q) = \log\left[\log(4q) - 1\right], \quad \alpha_1(q) = -\frac{\log q}{2} - \frac{1}{2} + \mathcal{O}\left(\frac{1}{\log q}\right). \tag{4.79}$$

For q large, the saddle point $s^*_{q\gg 1}$ approaches the point $s=-1$; in this regime one can therefore set

$$s^*_{q\gg 1} \approx -1 + \frac{1}{\zeta + \log q + \frac{d}{ds}\log\tilde{\alpha}(-1,q)} = -1 + \frac{1}{\zeta + \log q + \alpha_1(q)}. \tag{4.80}$$

Substitution into (4.60) gives:

$$f(s^*_{q\gg 1}) = -\zeta + 1 + \log\left[\zeta + \log q + \alpha_1(q)\right] + \log\left(\frac{8W}{\pi\Omega}\frac{\log(4q)}{q}\right) + \mathcal{O}\left(\frac{1}{\log q}\right), \tag{4.81}$$

from which one gets

$$\mathbb{P}(|A_p| > z^n) \approx D_n \left[\frac{4e}{\pi z}\frac{t\lambda}{W\omega\sqrt{N}}\log\left(\frac{2W\omega}{\lambda^2\sqrt{2N}}\right)\right]^n \log^n\left(\frac{W}{t}\sqrt{\frac{W\sqrt{2N}}{\omega}}\right), \tag{4.82}$$

with D_n scaling sub-exponentially with n. In this limit, the locator expansion converges (in d dimensions) for:

$$\frac{4e}{\pi}\frac{td}{W}\frac{\lambda\sqrt{N}}{\omega}\log\left(\frac{2W\omega}{\lambda^2\sqrt{2N}}\right)\log\left(\frac{W}{t}\sqrt{\frac{W\sqrt{2N}}{\omega}}\right) < 1. \tag{4.83}$$

Arbitrary q. For arbitrary q the saddle point equation in s has to be solved numerically. The estimate of the critical value of the hopping is obtained solving numerically the equation

$$NP_n\left(n\log\left[\frac{W(\Delta\pi)^{1/2}}{t\delta^{1/2}}\right]\right)^{1/n} = 1 \tag{4.84}$$

with P_n defined in (4.59), which is equivalent to $N\mathbb{P}\left(|A_p| > z^n\right)^{1/n} = 1$ with $z \to 1$.

5 Numerical tests on the forward approximation

Most estimates derived in the previous chapters are obtained within the forward approximation, which consists in resumming only the amplitudes associated to the self-avoiding (shortest) paths in the perturbative expansion, or equivalently in neglecting the self-energy corrections. We devote this chapter to a numerical test of the performance of this approximation.

The (Lowest Order) Forward Approximation (LOFA) can be efficiently implemented numerically using transfer matrix techniques. We test it by computing the critical values for the localization-delocalization transition for both an Anderson problem in high dimensions d and for a disordered XXZ spin chain, and compare with the most precise exact diagonalization results that are available.

The chapter is structured as follows: In Sec. 5.1 we introduce the numerical implementation of the LOFA, and discuss the criterion for the transition given in terms of the statistics of resonances. In Secs. 5.2 and 5.3 we report the numerical results for the Anderson model in high d and for the XXZ chain, respectively. We conclude the chapter with some comments on the connection of the Lowest Order Forward Approximation approach with the problem of directed polymers in random media, and with a comparison with exact results on the Bethe lattice.

5.1 Computing numerically the probability of resonances

The derivation of the LOFA for the eigenstates in Sec. 4.2 does not rely on the particular structure of the graph $\mathcal{G}$ nor on the independence of the on-site energies, and thus it can be applied to hopping problems of graphs with different geometries or correlated local energies. In particular, its extension to the many-body setting is straightforward, once the many-body problem is interpreted as a single particle hopping problem in some "configuration space" (or Fock space), as discussed in Secs. 1.2.4 and 2.2.1. In this chapter, we focus on the following two cases:

(1) *Anderson model in* $3 \leq d \leq 6$. In this case, the graph $\mathcal{G}$ in (4.9) is a cube of side L, and we rewrite the Hamiltonian (4.9) with the conventional notation $\mathscr{E}_i \to \epsilon_i$ and

$\mathscr{V} \to t$,

$$H = \sum_i \epsilon_i n_i + t \sum_{\langle i,j \rangle} \left(c_i^\dagger c_j + c_j^\dagger c_i \right). \tag{5.1}$$

The on-site variables are independent from site to site, and uniformly distributed in $[-W/2, W/2]$. We label with a the site at one corner of the cube, which we treat as the origin. Given any other site b, the orientation of the non-repeating, shortest paths from a to b induces a natural orientation of the edges of the cube, which is thus directed, see Fig. 5.1(a). We denote with $r(b)$ the lattice distance of the site b to the origin a; assuming that a is the localization center of a wave function ψ_α, its amplitude at a given site b in the LOFA reads:

$$\psi_\alpha(b) = \sum_{p \in \text{spaths}^*(a,b)} \prod_{i=1}^{r(n)} \frac{t}{\epsilon_a - \epsilon_i}. \tag{5.2}$$

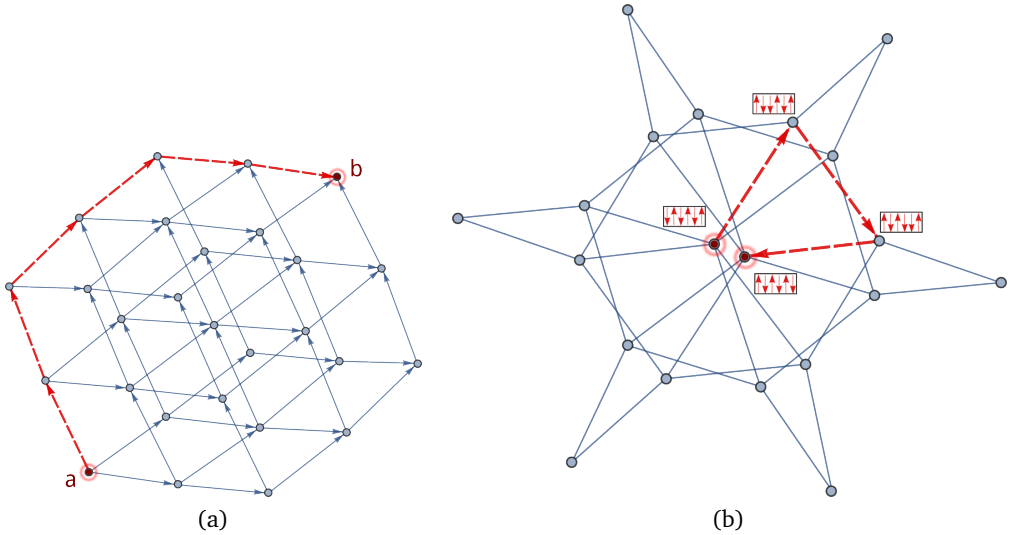

(a) (b)

Figure 5.1: (a) Anderson model on a cube of side $L = 3$. The red, dashed edges form one of the non-repeating paths connecting the sites a and b, of length $r = (L-1)d = 6$. The other elements in the set of shortest paths spaths$^*(a, b)$ are obtained following the arrows. (b) Graph corresponding to the configuration space of the chain (5.3) with $L = 6$. Each site in the graph is associated to a classical basis state with zero z-component of the total spin. The initial Néel state $|\downarrow\uparrow\ldots\rangle$ and the final, totally flipped state $|\uparrow\downarrow\ldots\rangle$ are highlighted with circles. The red, dashed edges form one of the shortest paths connecting the two states, of length $L/2 = 3$.

(2) *An XXZ spin-1/2 chain.* We consider the an XXZ spin-1/2 chain in random magnetic

field,

$$H(t) = -\sum_{i=1}^{L} h_i s_i^z - \Delta \sum_{i=1}^{L} s_i^z s_{i+1}^z - t \sum_{i=1}^{L} (s_i^x s_{i+1}^x + s_i^y s_{i+1}^y), \tag{5.3}$$

where periodic boundary conditions are assumed ($s_1^\alpha = s_{L+1}^\alpha$), and the random fields h_i are uniformly distributed in $[-h, h]$. The many body problem given by (5.3) can be seen as a single particle hopping problem in the space of the 2^L product states in the basis of the operators s_i^z, which span the full Hilbert space and diagonalize $H(0)$. We denote these classical basis states with $|n\rangle$. The mapping to the hopping problem is obtained by interpreting each $|n\rangle$ as a vertex n of a graph $\mathcal{G}$, with associated random energy E_n defined by $H(0)|n\rangle = E_n|n\rangle$. We thus set $\mathscr{E}_n \to E_n$, $\mathscr{V} \to t$ in (4.9). The third term in (5.3) provides the hopping between different sites, thus defining the geometry of the graph. Due to spin conservation, the full configuration space, and consequently the graph, are partitioned into disjoint sectors corresponding to different values of the z-component of the total spin; we restrict to the sector of total spin equal to zero, corresponding to a connected graph with $\binom{L}{L/2}$ vertices (a pictorial representation of the graph for $L = 6$ is given in Fig. 5.1(b)). We fix as the origin of the graph the site corresponding to the Néel state $|n_1\rangle = |\downarrow\uparrow \dots\rangle$, which we assume to be the localization center of a wave function Ψ_α whose amplitude on some other site $n_2 \in \mathcal{G}$ reads:

$$\Psi_\alpha(n_2) = \sum_{p \in \text{spaths}^*(n_1,n_2)} \prod_{n \in p} \frac{t}{E_{n_1} - E_n}. \tag{5.4}$$

5.1.1 A criterion for the transition within the LOFA

For a general Hamiltonian of the form (4.9), the localized phase can be characterized by the validity of the condition (4.18) which imposes the exponential decay of the eigenfunctions on $\mathcal{G}$,

$$\mathbb{P}\left(\frac{\log|\psi_r|^2}{2r} \leq -\frac{1}{2\xi}\right) \to 1 \text{ for } r \to \infty. \tag{5.5}$$

In the delocalized phase on the other hand, exponential bounds of the form (5.5) cease to hold for any finite ξ, indicating that for any arbitrarily small, positive $\epsilon = \xi^{-1}$ and at arbitrarily large distances r from the localization center a of ψ_α, there exist sites $b \in \mathcal{G}$ such that the ratio $\log|\psi_\alpha(b)|^2/2r$ exceeds the constant $-\epsilon$ with some finite probability. One might expect that the following stronger condition holds for any arbitrarily small, strictly positive value of ϵ:

$$P\left(\frac{\log|\psi_r|^2}{2r} \geq -\epsilon\right) \to 1 \text{ for } r \to \infty. \tag{5.6}$$

Within the LOFA scheme, this condition is equivalent to the statement that resonances *do* occur at any arbitrary large distance from the localization center of ψ_α. The transition to

delocalization can thus be detected by inspecting the statistics of the resonances within the LOFA. In the following, we compute the quantities (5.2) and (5.4) numerically by means of a transfer matrix scheme, and use their statistical distribution to determine the values of disorder W, h at which (5.6) holds, choosing ϵ of the order of the numerical precision. We choose b in (5.2) to be the site at the opposite corner of the cube with respect to a, and increase the system size L to inspect the scaling of the probability of resonances with the distance. Similarly, in the many-body case we compute (5.4) on the fully flipped Néel state $|n_2\rangle = |\uparrow\downarrow \dots\rangle$, varying the size L of the chain. We discuss in the following section how these quantities are obtained numerically.

5.1.2 Transfer matrix implementation of the LOFA

The amplitudes (5.2) and (5.4) are difficult to determine analytically, as they are sums of a number of correlated random variables that scales exponentially in the single-particle case (as $\sim d^r$ where $r = r(b) = (L-1)d$) and faster than exponential in the many-body case (as $\sim 2(L/2)!$, as the sites n_1, n_2 are connected by as many paths of length $r = L/2$ each). To account for the correlations between the path weights, we compute the amplitudes numerically by means of a transfer matrix technique. The transfer matrix method is convenient as it takes only polynomial time in r, as it was realized by Medina and Kardar[113] in their treatment of the Nguyen, Spivak, and Shklovskii [129, 130] (NSS) model. [1] The numerical computation is as follows: We fix $t = 1$ and introduce the matrix $\mathcal{T}$ defined as

$$\mathcal{T} = \mathcal{W} A_f, \tag{5.7}$$

where A_f is the adjacency matrix of the directed graphs in Fig. 5.1, and $\mathcal{W}$ is a diagonal matrix whose components are in the single particle case:

$$\mathcal{W} = \text{diag}\left(\frac{1}{\epsilon_a - \epsilon_k}\right)_{k=1,..,L^d}, \tag{5.8}$$

and analogously with $\epsilon_k \to E_k$ in the many-body case. For the Anderson case, we initialize the system in the state $|\psi^{(0)}\rangle = |a\rangle$ completely localized in the origin a of the directed cube, and iteratively apply the transfer matrix $\mathcal{T}$. A single iteration gives

$$|\psi^{(1)}\rangle \equiv \mathcal{T}|\psi^{(0)}\rangle = \frac{1}{\epsilon_a - \epsilon_{l_1}}|l_1\rangle + \frac{1}{\epsilon_a - \epsilon_{l_2}}|l_2\rangle + \dots, \tag{5.9}$$

where $l_1, \cdots, l_d$ are the forward neighbors of site a. The value of $\psi_\alpha(b)$ equals $\psi_\alpha(b) = \langle b|\psi^{(r)}\rangle$, where $|b\rangle$ is the state completely localized in the site b and r is the lattice distance between a and b. In the following, we set $\epsilon_a = 0$ for simplicity. In the many-body case

[1] A major difference between the present case and the NSS model is in the statistics of energy denominators: in the NSS model the binary disorder $\epsilon_i = \pm W$ (with probability p or $1-p$) does not allow for resonances due to a single site. Rather, the resonances arise from contributions of different paths. This led to a body of work following [113], on the presence of a sign transition, where effects from different paths accumulate in order to break the sign symmetry. In the LOFA for the Anderson case, the energy denominators can be arbitrarily small with finite probability, generating path weights that are fat tailed distributed.

the framework is identical, but the calculation is not: The energies associated to the different vertices are a linear combination of the independent random fields (and are thus correlated), and moreover the paths connecting two sites are much strongly correlated with respect to the Anderson problem, see the following section.

5.1.3 Domination by the optimal path and Dijkstra algorithm

Throughout the previous chapters, analytic estimates are derived under the assumption that the sums of the type (5.2) are dominated by the largest among the exponentially many summands. If the different path weights were independent, this would be justified in the light of the fact that the distribution of the summands is fat-tailed, implying that the central limit theorem scaling is violated and that rare realizations dominate the averages. However this assumption neglects the correlations between the different path weights. In order to test it numerically, we determine for each disorder realization the "optimal path" p^* in (5.2) having the largest absolute weight, which we denote with $|\omega_p^*|$. The latter is determined by means of the Dijkstra algorithm [54], a graph-search algorithm that determines the path minimizing a given cost function. We consider the directed cube in Figure 5.1(a) with $\epsilon_a = 0$, and assign a positive cost χ to each directed edge $\langle i, j\rangle$:

$$\chi(i,j) \equiv \log|\epsilon_j| - \min_k \{\log|\epsilon_k|\}\,. \tag{5.10}$$

The total cost of a path p is the sum of the costs of the edges belonging to it, and the path p^* with maximal amplitude is the one minimizing the total cost function.

In the Anderson case, the results obtained with the transfer matrix technique are faithfully reproduced by analyzing the statistics of the dominant path alone (see Sec. 5.2.4). This allows us to carry out the numerical analysis on much bigger system sizes with respect to the ones accessible with the transfer matrix technique, since the Dijkstra algorithm runs in time linear in the number of edges of the underlying graph, and it is not as memory-demanding as either the transfer matrix of shift-invert exact diagonalization. The results presented in the following section for the Anderson model in $d = 6, 7$, as well as for the higher values of r in $d = 3 - 5$, are obtained with this procedure.

In the many body case this procedure can not be applied, as the sum (5.4) is no longer dominated by a single path. Instead, most of the paths have comparable amplitude. It can be however shown that the much stronger correlation between the paths gives rise to non-negligible interference effects resulting in strong cancellations, see also Sec. 5.3.3. This is the analog, in the present setting, of the cancellation between the graphs amplitudes discussed in Sec. 2.2.3.

5.2 Anderson model in high d: numerical results

In the single particle case, the dependence of (5.2) on the disorder amplitude W can be simplified:

$$\psi_\alpha(b) \equiv \left(\frac{t}{W}\right)^r \psi'_\alpha(b) = \left(\frac{t}{W}\right)^r \sum_{p \in \text{spaths}^*(a,b)} \prod_{i=1}^{r} \frac{1}{\epsilon'_a - \epsilon'_i}, \tag{5.11}$$

with ϵ'_i uniformly distributed in $[-1/2, 1/2]$. We consider the distribution of the random variable

$$Z_r \equiv \frac{\log |\psi'_r|^2}{2r}, \tag{5.12}$$

where ψ'_r denotes the maximum among all the rescaled amplitudes ψ'_α (5.11) at sites that are at lattice distance r with respect to the origin of the hypercube a. The probability of resonances for arbitrary values of t and W, see Eq. (5.6), is easily recovered from the cumulative distribution function of Z_r as:

$$P\left(\frac{\log |\psi_r|^2}{2r} \geq -\epsilon\right) = P\left(Z_r \geq \log\left(\frac{W}{t}\right) - \epsilon\right), \tag{5.13}$$

with ϵ arbitrarily close to zero. According to Eqs. (5.5) and (5.6), if a transition to delocalization occurs at disorder $W = W_c$, the density of Z_r becomes asymptotically peaked at $\log(W_c/t)$ for $r \to \infty$, with width going to zero with r. Thus, the critical value of disorder can be estimated inspecting the scaling with r of the probability density of Z_r. We perform the numerical analysis as follows: We fix $\epsilon'_a = 0$ and compute the rescaled amplitude in (5.11) for all the points b on a shell at the same lattice distance $r = r_{max} - c$ from the origin of a hypercube of side L. Here $c \sim O(1)$ is fixed so as to have about 20 points per each size of the hypercube. We determine the maximal among the wave function amplitudes on those sites. We repeat the procedure for hypercubes of different sizes, with $O(10^5)$ disorder realizations for most system sizes, decreasing to $O(10^3)$ realizations only for the biggest system sizes that we consider (e.g. in $d = 3$ we take system sizes $r = 10$ through 292, with $1.5 \cdot 10^5$ disorder realizations up to $r = 202$ and $2.5 \cdot 10^3$ realizations up to $r = 292$). We report the results in the next sections.

5.2.1 Fluctuations of the wave function amplitudes

Fig. 5.1 shows the probability density of (5.12), for different values of r in $d = 3$. The plot shows a drift of the position of the peaks with increasing r, together with the shrinking of the width of the distribution, in agreement with the conditions (5.5), (5.6). Plots of the r-dependence of the variance $\sigma^2_{Z_r}$ of (5.12) are given in Fig. 5.2, in log-log scale for $d = 3 - 6$. The linear behavior indicates that the fluctuations of Z_r decay to zero as a power law in r, with a coefficient that depends on the dimensionality. The higher cumulants of the distribution exhibit a similar linear behavior in log-log scale. Moreover, the numerical computation indicates that for fixed d the probability densities of the

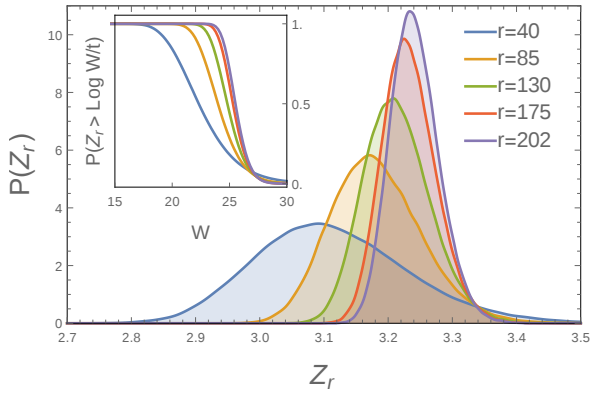

Figure 5.1: Probability density of the variable Z_r defined in Eq. (5.12), for different r and $d = 3$. For $r \to \infty$, the curves become peaked around the critical value $\log(W_c/t)$. Inset: cumulative distribution function. Each curve is obtained with $1.5 \cdot 10^5$ disorder realizations. Very similar results are obtained for higher dimensionality.

Table 5.1: Values of the exponent $\omega_{FA}(d)$ governing the decay of the fluctuations of Z_r with r, see Eq. (5.15). A comparison is made with the values of the droplet exponents $\omega_{DP}(D)$ obtained numerically for the directed polymer in dimension $1 + (d - 1)$. The numerical values are taken from Appendix A in [123].

d=D+1	$\omega_{FA}(d)$	$\omega_{DP}(D)$
3	0.278 ± 0.005	0.244
4	0.23 ± 0.01	0.186
5	0.191 ± 0.007	0.153
6	0.168 ± 0.006	0.130

variable

$$\tilde{Z}_r = \frac{Z_r - \langle Z_r \rangle}{\sigma_{Z_r}} \tag{5.14}$$

collapse to a limiting curve for increasing r, see Fig. 5.3. As shown in the same plot, for fixed r and varying dimensionality, the distribution of $\tilde{Z}_r$ does not change significantly, except for a weak d-dependence of the tails.

These numerical observations are compatible with the following large r scaling form for Z_r:

$$r Z_r \underset{r\to\infty}{\sim} r \log\left(\frac{W_c}{t}\right) + r^{\omega(d)} u, \tag{5.15}$$

where u is a random variable of $O(1)$ with a distribution which depends weakly on the dimensionality. According to (5.15), for large r the fluctuations $\sigma^2_{Z_r}$ decay to zero with

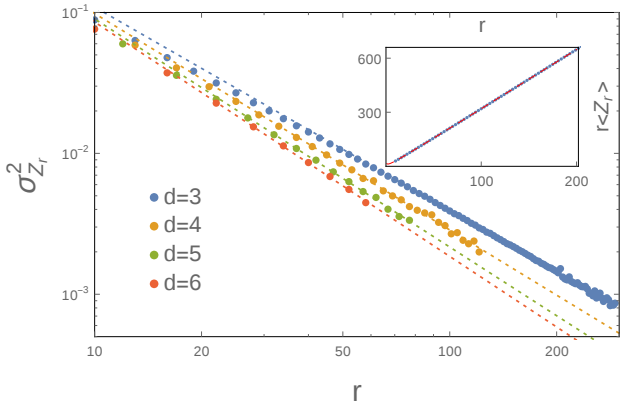

Figure 5.2: Variance $\sigma^2_{Z_r}$ of Z_r in log-log scale. The points corresponding to larger r are fitted linearly, according to the scaling form Eq. (5.15), and the values of the exponents $\omega_{FA}(d)$ reported in Table 5.1 are extracted from the coefficient of the linear term in the fit. The number of realizations is $1.5 \cdot 10^5$ for r smaller than 202, 53, 52, 40 for $d = 3$, 4, 5, and 6, respectively, and $2 \cdot 10^3$ for larger values of r. *Inset* Mean value of rZ_r for $d = 3$. The fit is linear with a correction $\propto r^{\omega_{FA}(3)}$, in agreement with Eq. (5.15), with the value of $\omega_{FA}(3)$ given in Table 5.1. The results of the fit are, with reference to Eq. (5.17): $c_1 = -18.2 \pm 0.3$, $W_c = 27.03 \pm 0.02$, $c_2 = 29.6 \pm 0.8$. The same behavior holds for higher dimensionality and results in the estimates of the critical disorder values in Table 5.2.

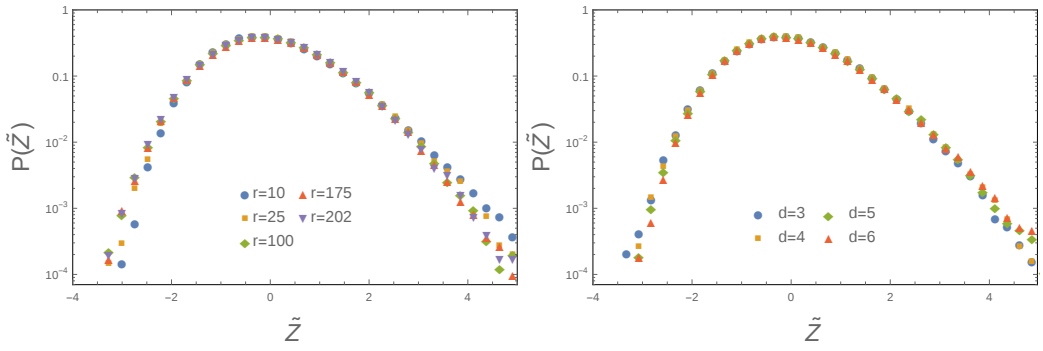

(a) (b)

Figure 5.3: (a) Density of $\tilde{Z}_r$ for different values r and $d = 3$. The curves seem to converge to a unique limiting distribution with increasing r. (b) Density of $\tilde{Z}_r$ for fixed $r = 52$ and different dimensionality. Each curve is obtained with $1.5 \cdot 10^5$ realizations.

the power $r^{2(\omega(d)-1)}$. From the linear fit of $\log\left(\sigma^2_{Z_r}\right)$ we extract the numerical estimate of the exponent in (5.15), which we denote with $\omega_{FA}(d)$. The results are reported in Table 5.1.

In order to characterize the limiting distribution in Fig. 5.3, we compute the skewness

Table 5.2: Comparison between the critical value for localization in the Anderson model in d dimensions predicted by the forward approximation (W_c^{FA}) and the numerical results ($W_c^{\rm num}$) of [157]. The relative error decreases faster than d^{-6}, presumably exponentially. For $d = 6$ the transition value $W_c^{FA} = 77.0 \pm 0.3$ can be compared with the result of [66], $W_c^{d=6} = 74.5 \pm 0.7$. This number is however an underestimation of the transition due to the choice of boundary conditions. For 7 dimensions there is no available numerics to compare with.

d	W_c^{FA}	$W_c^{\rm num}$	Error
3	27.03 ± 0.03	16.536 ± 0.007	39%
4	41.4 ± 0.1	34.62 ± 0.03	16%
5	57.8 ± 0.2	57.30 ± 0.05	0.9%
6	77.0 ± 0.3	-	-
7	93.8 ± 0.3	-	-

Sk $= \kappa_3/\kappa_2^{3/2}$ and the kurtosis Kur $= \kappa_4/\kappa_2^2$ of the density of $\tilde{Z}_r$ (here κ_i denotes the i-th cumulant of the distribution). From (5.15) it follows that these parameters approach the ones corresponding to the variable u in the limit of large r. We restrict to $d = 3$, for which we have the largest statistics available; the asymptotic values are estimated to be Sk $= 0.34 \pm 0.02$ and Kur $= 3.24 \pm 0.04$.

5.2.2 Estimate of the critical disorder

To determine the critical value of disorder for $t = 1$, we extrapolate the asymptotic limit of the typical value of Z_r. Since the distribution is not fat-tailed, we can equivalently consider the averages of Z_r and set:

$$\langle Z_\infty \rangle \equiv \lim_{r\to\infty} \langle Z_r \rangle = \log\left(W_c\right). \tag{5.16}$$

The inset in Fig. 5.2 shows the scaling with r of $r\langle Z_r\rangle$. The average grows linearly in r, in agreement with Eq. (5.15). We fit the data with the form

$$\langle r Z_r \rangle = c_1 + \log(W_c)\, r + c_2\, r^{\omega(d)}, \tag{5.17}$$

with the numerical values $\omega(d) = \omega_{FA}(d)$ reported in Table 5.1. The resulting estimates of the critical disorder, which we denote with W_c^{FA}, are displayed in Table 5.2. For the smallest dimensions, a comparison is made with the critical values $W_c^{\rm num}$ determined in Refs. [157, 169] by means of a combination of exact diagonalization and transfer matrix techniques.

The data in Table 5.2 clearly show that the FA, even in its 'lowest order' form, gives an upper bound to the critical disorder, since the renormalization of the energy denominators provided by the (modified) self-energy corrections are neglected, and the effects of resonances are thus enhanced (see the discussion in Sec.1.4.4). However, increasing the

dimensionality the discrepancy between the numerical estimates of W_c is significantly reduced.

5.2.3 Divergent length scales and critical exponents

For fixed values of W and for finite r, the probability of resonances (5.13) is determined by the tails of the distribution of Z_r. For increasing r, the asymptotic limit is approached in a different way at the two sides of the transition. In the approximation in which the correlations between the paths are neglected, for $W > W_c$ the probability of resonances goes to zero exponentially with r, while below the transition it converges to one much faster, with corrections that are only double-exponential in r. We report this calculation in Appendix 5.A. Following such estimate, to extract a W-dependent length scale $l(W)$ from the curves in Fig. 5.4(a) we perform an exponential fit for $W > W_c$,

$$P\left(\frac{\log|\psi_r|^2}{2r} > 0\right) = a_1(W)\text{exp}\left[-\frac{r}{l(W)}\right], \tag{5.18}$$

while for $W < W_c$ we determine $l(W)$ by means of the linear fit:

$$\log\left|\log\left[1 - P\left(\frac{\log|\psi_r|^2}{2r} > 0\right)\right]\right| = a_2(W) - \frac{r}{l(W)}. \tag{5.19}$$

The length scale $l(W)$ is plotted in Fig. 5.4(b) for $d = 3$. We expect it to diverge in the same way as the localization length/correlation length does in the localized/delocalized phase, respectively. We find that $l(W)$ diverges as a power-law at a critical disorder compatible with the values of W_c^{FA} listed in Table 5.2. A fit of the form $\log(l(W)) = \log c - \nu \log|W - W_c^{FA}|$ results in an exponent that is compatible with $\nu \approx 1$ for all dimensions.

5.2.4 Domination by the optimal path

To compare the statistics of the wave function amplitudes in the LOFA with that of the path with maximal amplitude ω_r^*, we compute the ratio between ω_r^* and the full sum (5.2) computed via the transfer matrix technique, for the same given disorder realization. The distribution of the ratios turns out to be very narrowly peaked around one. Figure 5.5(a) displays its average as a function of the length of the paths r for $d = 3$, which is extremely close to one, uniformly in the path length. As a further check of the agreement between the values computed with the two methods, we plot in Fig. 5.4(a) the r-dependence of the probability (5.6) with $\delta = 0$, determined with the substitution $|\psi_r| \to \omega_r^*$. The data are plotted as points, which are almost indistinguishable from the transfer matrix results (squares). This indicates that the statistics of distant resonances is fully captured by the optimal path. Thus, in the single particle case the correlation between different paths does not play a relevant role, in the sense that the sum is dominated by the maximal term as it would happen for independent random variables with fat-tailed distribution.

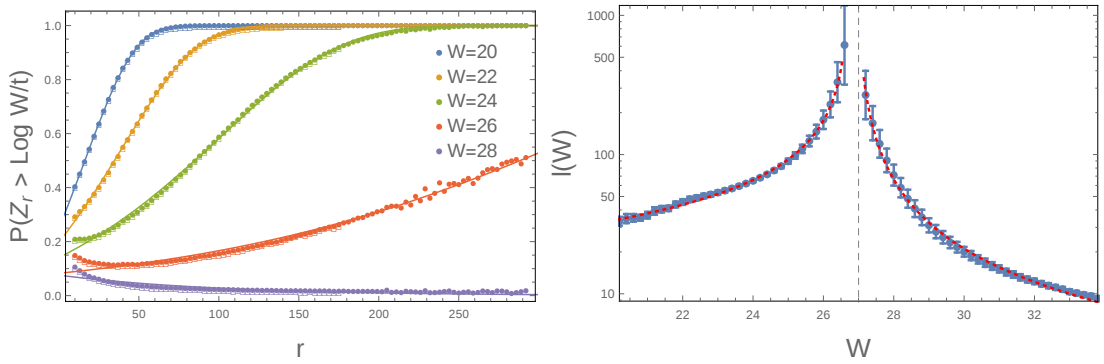

(a) (b)

Figure 5.4: (a) Probability of resonances $P\left(Z_r > \log(W/t)\right)$ for Z_r defined in (5.14) and $d = 3$. The squares are the results of the transfer matrix calculation, the points of the optimal path (see Sec. 5.2.4) while the continuous lines are the exponential or double exponential fits. Very similar results are obtained for higher dimensionality. (b) Power law divergence of the length scale $l(W)$ defined in Eqs. (5.18) and (5.19) for $d = 3$; the power law fit produces a critical exponent $\nu \simeq 1$ and a critical value W_c compatible with the ones listed in Table 5.2. In the delocalized phase the distance to observe a resonance is typically larger (for the same $|W - W_c|$) than the localization length in the localized phase.

To characterize the optimal path, we compute the inverse participation ratio (IPR) of the edge weights contributing to its amplitude, for the case $\epsilon_i \in [-1, 1]$ (i.e. $W = 2$). We define

$$\text{IPR} = \frac{(\sum_i \log|\epsilon_i|)^2}{\sum_i (\log|\epsilon_i|)^2}, \tag{5.20}$$

where i labels the sites belonging to the optimal path p^*. We find that the disorder-averaged IPR scales linearly with the length of the path r, indicating that an extensive (in r) number of edges contributes to the total path weight, and cooperate to produce the atypically big path weights dominating (5.2). Fig. 5.5(b) shows the distribution of the absolute value of the energies along the optimal path for $W = 2$, $d = 3$, $r = 210$ and $\epsilon_a = 0$. The fitting function has the form

$$\rho_r(\epsilon) = c_r + b_r|\epsilon|^{a_r}. \tag{5.21}$$

The power law behavior is consistent with the considerations in [176]: adapting their reasoning to the finite dimensional case, one can argue that asymptotically in r (and under the hypothesis of independent paths) the biased energy distribution along the optimal path has the form

$$\rho(\epsilon) = \frac{1 - 2x}{|\epsilon|^{2x}}, \tag{5.22}$$

with x solving the d-dependent equation

$$\log\left(\frac{d}{1-2x}\right) - \frac{2x}{1-2x} = 0. \tag{5.23}$$

Fitting the r-dependence of the coefficients c_r, b_r, a_r one finds that the asymptotic limits are in agreement with (5.22); for details see the inset of Fig. 5.5(b).

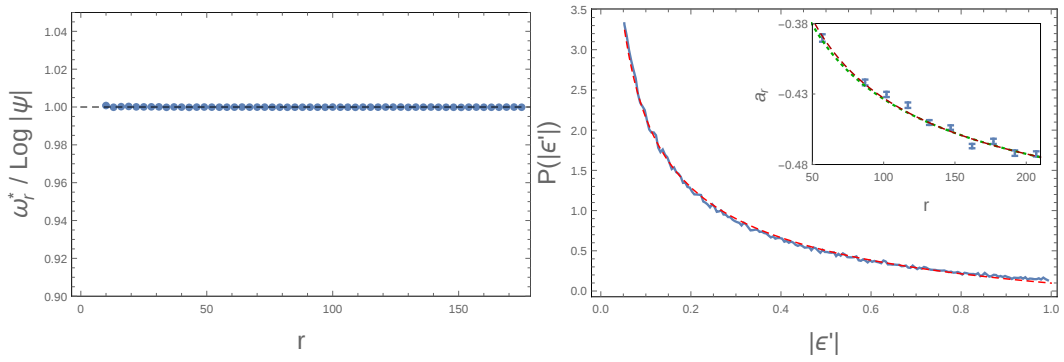

Figure 5.5: (a) Average ratio between the dominating path weight ω_r^* and the sum (5.2) for $d = 3$. Each point is averaged over $3 \cdot 10^4$ disorder realizations, and the standard deviation error bars are within the point size. (b)Probability distribution $\rho(\epsilon)$ of the energy denominators along the optimal path, see Eq. (5.22), for $d = 3$ and $r = 210$. The dashed red line is the fitting function of Eq. (5.21), with parameters $c_r = -0.95 \pm 0.04$, $b_r = 1.04 \pm 0.03$ and $a_r = 0.472 \pm 0.005$. *Inset.* Plot of the exponents a_r in the fitting function of Eq. (5.21), as a function of r. Due to the absence of a theoretical reasoning for the finite size scaling, we fit the curve considering logarithmic and $1/\sqrt{r}$ corrections. The green small-dashed curve is a fitting function of the form $a + c/\log(r)$, with fit parameters $a = -0.73 \pm 0.05$ and $c = -1.4 \pm 0.3$; the red large-dashed curve is a fitting function of the form $a + c/\sqrt{r}$, with fit parameters $a = -0.57 \pm 0.02$ and $c = -1.4 \pm 0.3$. The asymptotic value a obtained with the logarithmic fitting function is compatible with the solution of (5.23) for $d = 3$.

5.3 Heisenberg model with random fields

For the many-body Hamiltonian (5.3), the dependence on the field strength h can not be simplified. We thus compute by means of the transfer matrix the h-dependent variable

$$Z_r(h) \equiv \frac{\log |\Psi_r|^2}{2r}, \tag{5.24}$$

with Ψ_r given by (5.4). We consider spin chains of size $6-20$ with hopping and interaction constants respectively $t = 1$ and $\Delta = 1$, and $h = 1 - 6$. For these parameters, the critical disorder is estimated [108] to be $h_c \simeq 3.72(6)$ for states in the middle of the energy band.

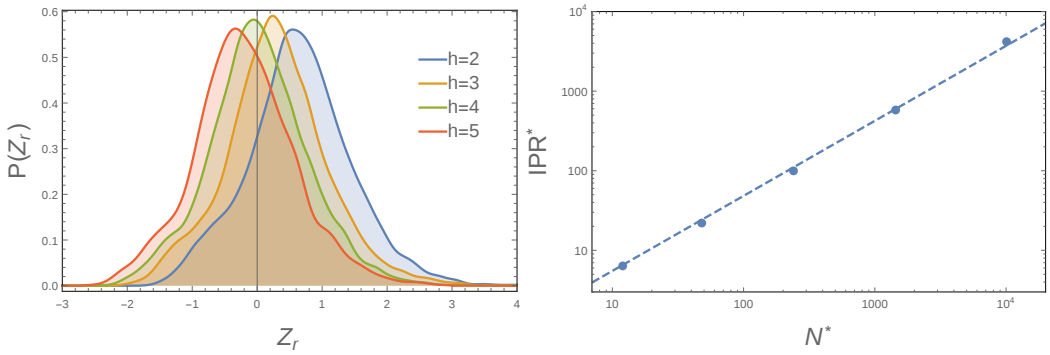

Figure 5.1: (a) Probability density of $Z_r(h)$ defined in (5.24), for chain of length $L = 20$ (corresponding to $r = 10$) and different values of h. Each curve is obtained with $3 \cdot 10^3$ realizations. (b) Linear fit of the average IPR* of the paths, Eq. (5.29), as a function of the number of paths $N^* = 2(L/2)!$ for random spin chains of different lengths L.

5.3.1 Distribution of the wave function amplitudes and critical disorder

In Fig. 5.1(a) we show the probability density of $Z_r(h)$ for a chain of length $L = 20$ and different values of h. The criterion for the transition reads

$$\langle Z_\infty(h_c)\rangle = -\log t, \tag{5.25}$$

where $\langle Z_\infty(h)\rangle$ is the extrapolated value of the average of (5.24) for fixed h. Plots of $\langle Z_\infty(h)\rangle$ are given in Fig. 5.2, with $\langle Z_\infty(h)\rangle$ extrapolated from the finite size values using the fitting function

$$r\,\langle Z_r(h)\rangle = c_1 + \langle Z_\infty(h)\rangle\, r + c_2\, r^{-1}, \tag{5.26}$$

where the corrections $\propto r^{-1}$ are consistent with the expectation that the Bethe lattice exponent $\omega_{FA} = 0$ gives the correct scaling for MBL.

For $t = 1$, the critical point h_c is estimated from the condition $\langle Z_\infty(h_c)\rangle = 0$. The resulting value is $h_c = 4.0 \pm 0.3$, which is, as expected, larger than the result $h_c \simeq 3.72(6)$ derived with exact diagonalization, but still very close.

5.3.2 Divergent length scales and critical exponents

Fig. 5.3(a) shows the behavior of the probability of resonances $P\left(Z_r(h) > -\log t\right)$ as function of the distance between the Néel states. As expected, the r-dependence changes with the disorder: the probability decays to zero at large h, and increases towards one for the smaller h. We expect the convergence to be exponential in r on both sides of the transition. In the localized phase we perform an exponential fit of the curves in

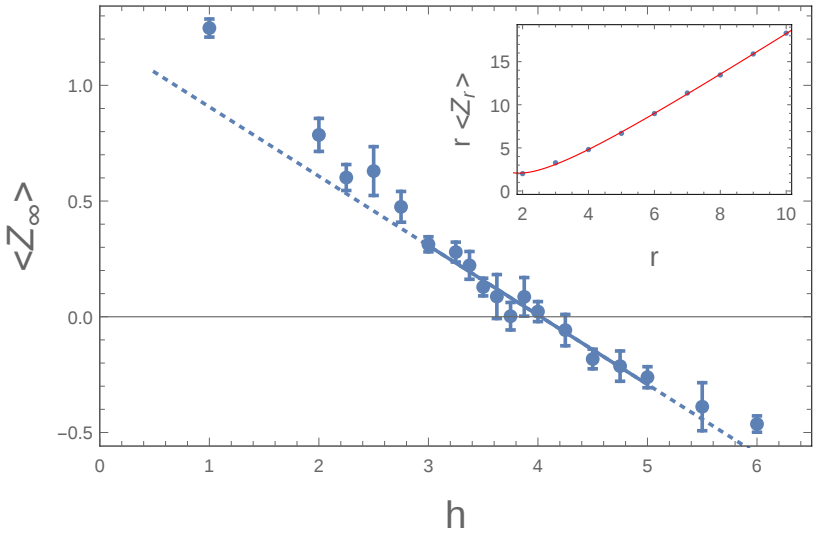

Figure 5.2: Extrapolated value of the mean $\langle Z_\infty \rangle$ of the variable (5.24). The crossing with 0 signals the many body localization/delocalization transition for $t = 1$, see (5.25). The error bars are obtained from the fitting procedure (see Inset). The resulting transition value is $h_c = 4.0 \pm 0.3$. *Inset.* Finite size scaling of $\langle r\, Z_r \rangle$ with the distance r between the Néel states n_1 and n_2. The plot corresponds to $h = 1$. The fit is linear with an r^{-1} correction, see (5.26), with parameters $c_1 = -7.2 \pm 0.4$, $\langle Z_\infty(2) \rangle = 1.23 \pm 0.02$ and $c_2 = 8.8 \pm 0.7$. The finite-r values for the mean are obtained over at least 10^4 realizations for $r < 7$ and at least $2 \cdot 10^3$ realizations for $r \geq 7$.

Fig. 5.3(a) of the form:

$$P\left(Z_r(h) > -\log t\right) = a_1(h) \exp\left(-\frac{r}{l(h)}\right). \tag{5.27}$$

In the delocalized phase, the exponential behavior is not clearly detectable due to the few accessible system sizes; for $h < h_c$ we extract a length scale $l(h)$ by fitting with the function:

$$P\left(Z_r(h) > 0\right) = a_2(h) + \frac{r}{l(h)} + \frac{b(h)}{r}. \tag{5.28}$$

The length scales $l(h)$ extracted with this procedure are shown in Fig. 5.3(b), together with the power law fit $l(h) = c|h - h_c|^{-\nu}$. The fit is performed separately for $h < h_c$ and $h > h_c$, resulting in an exponent close to 1 in both cases (see Fig. 5.3(b) for details). Note the asymmetry of the curve with respect to h_c, which indicates that at fixed $|h - h_c|$ the typical distance to find a resonance in the delocalized phase is larger than the localization length at the corresponding value of disorder in the localized phase. A possible consequence of this phenomenon, which occurs also in the Anderson model (see Fig. 5.4), could be a large "critical region" in the dynamics in the delocalized phase.

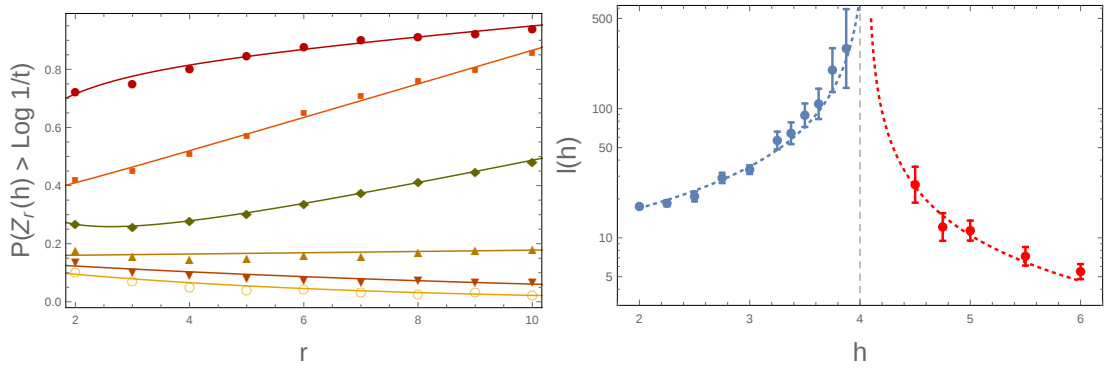

(a) (b)

Figure 5.3: (a) Probability of resonances $P(Z_r(h) > -\log t)$ as a function of the distance r between the two Néel states n_1 and n_2, for $t = 1$. We average over 10^4, $5 \cdot 10^3$ and $3 \cdot 10^3$ realizations for $r \leq 8$, $r = 9$ and $r = 10$, respectively; the plotted values of the disorder h are: $h = 1$ (points), $h = 2$ (squares), $h = 3$ (diamonds), $h = 4$ (upward triangle), $h = 5$ (downward triangle) and $h = 6$ (circle). Linear and exponential fits in the delocalized and localized regions respectively are plotted as continuous lines, see Eqs. (5.28) and (5.27). (b) Divergence of the length scales $l(h)$ extracted from the fits of the probability of resonances. The vertical dashed line indicates the critical value h_c obtained in Fig. 5.2. The dotted curve is a power law fit of the form $c|h - h_c|^{-\nu}$, resulting in a critical exponent $\nu_L = 1.12 \pm 0.06$ for $h < h_c$ and $\nu_R = 1.1 \pm 0.2$ for $h > h_c$.

5.3.3 The absence of a dominating path

As previously mentioned, when performing the analysis of the best path weight for the XXZ chain, we find that the statistics of the sum (5.4) is not well reproduced by the optimal path alone: The distribution of the ratios between the full sum and the optimal path is very wide and peaked at values that are far from one, indicating that there is not a single path dominating, even if the latter are fat-tailed distributed. Instead, we find that the average IPR* of the paths amplitudes, which we denote with ω_p,

$$\text{IPR}^* = \frac{\left(\sum_p \omega_p\right)^2}{\sum_p \omega_p^2}, \tag{5.29}$$

scales linearly with the total number of paths $N^* = 2(L/2)!$, see Fig. 5.1(b). There are factorially-many (in the length of the chain L) paths having amplitudes that are comparable in absolute value. This is a signature of the strong correlations between the paths, which is not surprising in view of the many-body nature of the model. Following the reasoning in Sec. 2.2.3, one may argue that the strongest correlations are among those paths associated to processes in which the same spin flips occur, but in different order: The different orderings of the flips produce different energy denominators in (5.4), and thus different path amplitudes; however, the resulting terms are correlated, and one can expect that for those realizations of the random fields producing one particularly

large path weight, the other ones (related to it by permutation of the order of the spin flips) will also have a large amplitude in absolute value. However, in the sum (5.4) the paths contribute with well defined relative signs, leading to the cancellations between these factorially-many terms.

5.4 Some comments on the results

5.4.1 Connections with directed polymers in random media

In the single particle case, the energy denominators associated to different sites along the paths are independent variables. Thus, the expression for the wave function amplitude in the LOFA resembles the expression for the partition function of a directed polymer (DP) in a random potential [50, 51, 77], see Sec. 6.3.1, with the thermal weights for the polymer configurations given by the amplitudes of the different paths. This analogy is not straightforward, as negative contributions occur in (4.17), and moreover the weight associated to the polymer in the LOFA is not bounded from above (as the energy denominators in (5.11) are not bounded from below). Nevertheless, the analogy has been fruitfully exploited both for the single particle problem [160, 144, 159, 122], and for problems of interacting spins on the Bethe lattice [59, 89, 124, 176].

Motivated by this analogy, the authors of [144] have proposed a scaling form analogous to (5.15) for the logarithm $\log g$ of the conductance of an Anderson model. There, the conductance in $d = 2$ is obtained from the Green functions, which are computed numerically within a modified FA, the modification consisting in taking energy denominators that are not arbitrarily small but are bounded from below. [2] It is shown that the fluctuations of $\log g$ scale with an exponent $\omega(d = 2) = 1/3$, and that the distribution of the variable u is compatible with a Tracy-Widom distribution. These results are consistent with the conjecture [114, 113] that in the strongly localized phase, where the expansion in non-repeating paths is best controlled, the Anderson model in dimension d belongs to the same universality class of the directed polymer in dimension $1 + D$, with $D = d - 1$. In particular, the conjecture implies that in the limit of large r the distribution of $\log g$ has the scaling form (5.15), with $\omega(d)$ coinciding with the droplet exponent [61] in $1+(d-1)$ dimensions (which is exactly known [78] to be equal to $1/3$ for $D = 1$), and u having the same distribution of the fluctuations of the free energy in the disordered phase of the polymer (distributed according to the Tracy-Widom distribution [91, 141, 142, 143] in $D = 1$).

In higher dimension, the values of the scaling exponents extracted from the LOFA data do not compare well with the droplet exponents $\omega(D = d - 1)$ of the DP, see Table 5.1. Moreover, the limiting distribution of the rescaled wave functions seems to depend weakly on the dimensionality. The discrepancies with respect to the directed polymer results are presumably generated by the fat-tail of the distribution of the paths amplitudes in (5.11), produced by the arbitrarily small energy denominators. It might be that the

[2] Note that if this constraint is relaxed and the energy denominators are allowed to be arbitrarily small, $\log g$ is found to be proportional to the quantity rZ_r that we are considering.

finite size effect are more pronounced in the case of unbounded denominators; also, it is quite natural to expect that the models of non-repeating paths with bounded amplitude considered in [144] exhibit a stronger dependence on the dimensionality, due to the fact that the domination by one single path is less pronounced in that case [3].

5.4.2 The asymptotic limit of infinite d

The numerical results in Table 5.2 seem to indicate that the LOFA becomes increasingly accurate when the dimensionality is increased, suggesting that this approximate scheme could be considered as a candidate for a mean field theory of the Anderson model. The LOFA in finite d involves two simplifications: only shortest paths are considered, and the self-energy corrections in the denominators of the locators are neglected. The second simplification is presumably the more severe. As a matter of fact, on the Bethe lattice, which is the setting that is expected to be recovered in the high dimensional limit [4], the self-energy corrections are relevant even in the large-connectivity limit, as they lead to a correction of the criterion obtained in FA (on the Bethe lattice the FA and the LOFA coincide) by a factor $e/2$ [2, 14]. This suggests that the optimal route to improve the above numerical results consists in incorporating the self-energy corrections (at the lowest orders) within a transfer matrix scheme involving only shortest paths. This might significantly affect the critical exponents discussed in the previous section and mitigate the discrepancy with the DP results. Similarly, in the analytic estimates of the Bethe-lattice type (such as the one performed in Appendix 5.A), the large deviations of individual path weights should be estimated accounting for the (anti-)correlations among the consecutive locators in the paths. On the other hand, neglecting the correlations among different paths of the same length might be a less subtle approximation in the high-dimensional limit, as suggested also by the optimal path analysis.

[3] Indeed, when performing the same analysis as in Sec. 5.2.4 for the modified forward approximation discussed in [144], i.e. taking the energy denominators uniformly distributed in $\left[-1,-W^{-1}\right]\cup\left[W^{-1},1\right]$ in $d=3$ with some cutoff W, we find that the ratio between the maximal path and the transfer matrix result departs from one for increasing r (the numerics is done for two values of the cutoff, $W=25$ and $W=35$). This suggests that more than one path dominates the transfer matrix result. It is natural to expect that in this case the number of dominating paths depends on the geometry of the system, thus introducing a stronger dependence on the dimensionality.

[4] It is reasonable to expect that the 'long' self-avoiding loops around a given site a that involve different neighboring sites b_1, b_2 of a (for instance the ones having the structure $a\to b_1\to\cdots\to b_2\to a$) become less relevant in higher dimension, since when the connectivity is high it is less likely to return to the initial site. This implies that in the limit of large dimensionality the correlation between the sites b_1, b_2 becomes weaker, and the Bethe-lattice framework (1.63) should be recovered.

Appendix

5.A Analytic estimate of the probability of resonances (Eqs. 5.18 and 5.19)

In this Appendix, we justify the fitting forms (5.18) and (5.19) by means of an approximate calculation. If the correlations between the different path weights in (5.11) are neglected, the calculation of the probability density of Z_r is analogous to the one performed in Sec. 1.4.4. In particular, one finds for the cumulative function of Z_r the following expression:

$$P\left(Z_r < a\right) = \exp\left[N_r \log\left(1 - \frac{1}{(r-1)!}\int_{r(a-\log 2)}^{\infty} t^{r-1}e^{-t}dt\right)\right], \tag{5.30}$$

where $N_r \sim d^r$ is the total number of paths on which the maximum is taken. This implies the following form for the probability density of $Z'_r = Z_r - \log 2$:

$$p_r(z') = \frac{N_r r^r}{(r-1)!}\frac{e^{-r(z'-\log z')}}{z'\left[1 - I_r(z')\right]}\exp\left[N_r \log\left(1 - I_r(z')\right)\right], \tag{5.31}$$

where we introduced the monotone decreasing function

$$I_r(z') = \frac{1}{(r-1)!}\int_{rz'}^{\infty} t^{r-1}e^{-t}dt. \tag{5.32}$$

The typical value of Z'_r, denoted z^*_r, is defined by the equation

$$N_r\, I_r(z^*_r) = N_r \frac{r^{r-1}}{(r-1)!}\int_{z^*_r}^{\infty} t^{r-1}e^{-rt}dt = 1. \tag{5.33}$$

The solutions of (5.33) approach a finite limit z^* for $r \to \infty$, which is related to the critical value of disorder by $z^* = \log(W_c/(2t))$, as previously discussed. The Bethe lattice critical condition with $K \to d$ is recovered using that $N_r \sim d^r$ and computing the integral in (5.33) with a saddle point calculation (assuming $z^* > 1$).

For increasing r the probability density of Z'_r peaks at the typical value, with tails that approach zero in the limit $r \to \infty$. In particular, for $z' > z^*_r$ the decay of the tail is exponential in r. Indeed, in this regime the product $N_r\, I_r(z)$ is itself exponentially

decreasing with r; thus, the rightmost exponential in (5.31) rapidly converges to one, and the distribution $p_r(z')$ approaches zero with a tail of the form

$$p_r(z') \sim e^{-r(z'-\log z'-\log(de))+o(r)}. \tag{5.34}$$

When z' becomes smaller than the typical value z_r^*, the product $N_r\, I_r(z')$ increases exponentially. Since for large r the integral $I_r(z')$ is still exponentially small for all $z' > 1 + O(1/r)$, one can still set $\log\left[1 - I_r(z')\right] \sim -I_r(z') \sim \exp\left(-rz' + r\log(ez') + o(r)\right)$. Thus, in this regime the probability density of Z_r' decays to zero much faster, double-exponentially with r

$$p_r(z') \sim \exp\left(-d^r\, e^{-rz'+r\log(ez')} + O(r)\right). \tag{5.35}$$

Note that (for r large enough) the interval in which $1 < z' < z_r^*$ does not shrink to zero for $d \geq 3$, given that the value z^* obtained from the condition (5.33) is always bigger than one. When z' approaches one, the probability in (5.32) is no longer a large deviation probability, i.e. it is no longer exponentially small in r: the term $\log\left[1 - I_r(z')\right]$ approaches a constant function of z', and the main scaling is given by the factor d^r. Finally, exactly at $z' = z_r^*$, using (5.33) and performing the integral with an integration by parts, one finds that the probability density can be written as

$$p_r(z_r^*) = \frac{r}{1-d^{-r}}\left[1 + \sum_{n=1}^{r-1} \frac{(r-1)!}{(r-1-n)!r^n}(z_r^*)^{-n}\right]^{-1} \exp\left(-1 - \frac{1}{2d^r} - \frac{1}{3d^{2r}} + \cdots\right), \tag{5.36}$$

which diverges like r when $r \to \infty$.

Given the tails of the distribution of Z_r computed in this approximation, it is immediate to derive the asymptotic decay of the probability of resonances in the localized phase. Indeed, for $W > W_c$, the probability (5.13) is is a large deviation for Z_r. Making use of (5.34) we find

$$P\left(Z_r > \log\frac{W}{t}\right) = \int_{\log\left(\frac{W}{2t}\right)}^{\infty} e^{-r(z'-\log z'-\log(de))+o(r)} dz' = \exp\left(-\frac{r}{l(W)} + o(r)\right) \tag{5.37}$$

with $1/l(W) = \log\left[W/(2tde\log\left(W/2t\right))\right]$. Thus, within this approximation for W approaching W_c from above one finds

$$l(W) \sim \frac{W_c}{W - W_c}, \tag{5.38}$$

thus the length scale diverges at the transition with a critical exponent equal to 1. Similarly, for $2te < W < W_c$, making use of (5.30) and of (5.35) we find:

$$P\left(Z_r < \log\left(\frac{W}{t}\right)\right) \approx \exp\left(-\left[\frac{2tde}{W}\log\left(\frac{W}{2t}\right)\right]^r + O(r)\right) = \exp\left(-e^{-r/l(W)} + O(r)\right). \tag{5.39}$$

6 On the temperature dependence of effective mobility edges

Throughout the previous chapters, we analyzed aspects of the localized phase making almost no reference to temperature: In Chapters 2 and 3, we assumed the full many-body spectrum to be localized irrespectively of the energy density, while in Chapters 4 and 5 we considered only single-particle states corresponding to infinite temperature[1]. As commented in Chapter 1, however, in the many-body case the role of temperature is not completely settled: on the one hand, approximate perturbative arguments and the numerical analysis based on exact diagonalization of small systems suggest an extensive mobility edge associated with a finite T transition; on the other hand, in the presence of delocalized portions of the many-body spectrum, rare thermal fluctuations within putative localized states were argued to restore ergodicity in the long time limit.

In this final chapter, we discuss possible effects of thermal fluctuations on the spatial localization of excitations in interacting many-body states, without taking a definite stance as to whether T drives a genuine transition or merely a crossover. The discussion is partly inspired by the theoretical argument given in Ref. [42] in favor of the finite T transition, which we recall in Sec. 6.1. This argument identified a precise mechanism by which the mobility of individual excitations must be enhanced by thermal fluctuations (or, more generally, fluctuations of "environmental" degrees of freedom interacting with the excitation). We revisit this mechanism and set up a self-consistent scheme to describe both the delocalized and localized phase. In Sec. 6.1.1, we recast the mechanism into the self-consistent framework, which we justify phenomenologically in Sec. 6.2 by analyzing a simple toy model containing all the relevant ingredients. We analyze the mobility of the excitations within this framework in Sec. 6.1.3, and conclude that, for the class of models that we consider, the mechanism is ineffective in enhancing mobility. In Sec. 6.3, making use of the framework introduced in these first sections, we discuss an alternative effect by which an increase in T does enhance mobility and lowers the (effective) mobility edge of the excitations. In the light of the considerations in Sec. 1.5.1, this mobility edge is effective, marking a crossover between a regime of extremely slow (activated) transport and a regime in which the individual excitations decay fast into the environment.

[1] In those chapters we considered states at zero energy, lying in the middle of the single-particle spectrum of the Anderson model, where the density of states has its maximum. These states are typical with respect to the uniform measure, meaning that they are typically selected when sampling the spectrum according to the thermal distribution at infinite temperature.

6.1 T-induced delocalization: a possible mechanism

We consider the spin Hamiltonian on a Bethe lattice with connectivity $k+1$:

$$H = -W \sum_i \xi_i \sigma_i^z - \sum_{\langle i,j \rangle} J_z \sigma_i^z \sigma_j^z - \sum_{\langle i,j \rangle} J_{xy} \left(\sigma_i^+ \sigma_j^- + \sigma_i^- \sigma_j^+ \right), \tag{6.1}$$

with ξ_i independent random variables of order $O(1)$. The Hamiltonian (6.1) is equivalent to a model of interacting hard-core bosons in a disordered potential, as it follows from the isomorphism $b_i = \sigma_i^-$, $b_i^\dagger = \sigma_i^+$ and $n_i = (\sigma_i^z + 1)/2$. It arises in several contexts ranging from quantum magnets, strongly disordered superconductors [111], or cold atomic systems. Together with its finite dimensional counterpart, (6.1) has been extensively investigated in the $J_z \to 0$ limit as a theoretical model for the quantum phase transition between a superconducting/superfluid phase at large J_{xy}/W, and an insulating one at strong disorder W/J_{xy}, conventionally referred to as the "Bose glass" [68, 62, 75]. The mobility of excitations in the Bose glass has been analyzed as well, both in the ground state [59, 89] and at finite temperature [42, 7]. In Refs. [59, 89], a mapping to the problem of the directed polymer in random medium has been exploited to address the localization properties of low-energy excitations of the spin model (6.1) with $J_z = 0$. The conclusion reached in those works, namely that an intensive mobility edge exists in the vicinity of the quantum critical point (vanishing simultaneously with the onset of long range order) has been criticized in [176], where a revisited (and amended) calculation was shown to imply the absence of any mobility edge at intensive energies.

At finite temperature, it was argued in [7] that an extensive mobility edge exists in presence of weak interactions in the Bose glass phase. An analogous statement about the occurrence of a finite temperature transition was made in [42] for the spin model (6.1), based on a phase diagram obtained analyzing the statistics of the r parameter introduced in Sec. 1.2.7. This claim is motivated in [42] with an argument which exploits the following approximate expression for the level width Γ_i of a single-spin excitation of energy ω:

$$\Gamma_i = J_{xy}^2 \sum_{l=1}^{k} \sum_{\sigma^z_{n(l)}} \frac{e^{\xi_n \sigma^z_{n(l)}/T}}{Z_l} \frac{\Gamma_l}{(\omega - W|\xi_l| + J_z \sum_{n(l)} \sigma_n^z)^2 + \Gamma_l^2}. \tag{6.2}$$

The level width Γ_i is the imaginary part of a cavity self energy on the subtree rooted at site i; due to the structure of the lattice, the expression is of the same form as (1.64). The second sum in (6.2) is over the possible configurations $\sigma_n^z = \pm 1$ of the spins $n(l)$ on neighboring sites of l (excluding the site i). Each such configuration is weighted thermally, with normalization $Z_l = \sum_{\sigma^z_{n(l)}} e^{\xi_n \sigma^z_{n(l)}/T}$. The expression (6.2) is approximate, as the shifts in the denominators generated by the real parts of the cavity self energies are neglected. Following the considerations in [176], we consider in the following the corrected form of (6.2) obtained with the substitution $|\xi_l| \to \xi_l$. The Ising interaction in

(6.1) enters in the energy denominators of (6.2), that contain the local "shifts":

$$\tau_l = J_z \sum_{n(l)} \sigma_n^z. \tag{6.3}$$

At the core of the argument in [42] lies the following consideration: in the strong-disorder regime $W \gg J_{xy}, J_z$, the statistics of the energy denominators in (6.2) is altered by the presence of the interactions (and thus by the terms (6.3)) in a way that depends strongly on T. More precisely, at low temperatures the z-components σ_n^z of the neighboring spins σ_n^z are essentially frozen in the direction of the local fields ξ_n; thus, (6.3) acts as an effective quenched variable that weakly shifts the local field $W\xi_l$, without affecting significantly the statistics of the denominators. In contrast, at higher energy density the z-components of the surrounding spins σ_n^z are fluctuating degrees of freedom which can be in various different configurations. Among such configurations, there shall be optimal ones that are more resonant with the decaying degree of freedom. Thus, by *optimizing* over the thermal configuration of the neighboring spins, the probability of occurrence of resonant denominators in (6.2) increases: in this sense, thermal fluctuations open more efficient decay channels for the excitation, thus enhancing its mobility. This scenario suggests a simple mechanism for a finite temperature transition, as it implies that a non-zero J_z term enhances the mobility of single-spin excitations on top of highly energetic states more strongly as compared to states of low energy-density, introducing a temperature dependence of the critical point on single-particle-like excitations. Note that this effect of temperature is different from the one discussed within the perturbative framework in Sec. 2.2.6. In that case, the focus is on the decay of an excitation by means of inelastic *scattering* processes, and the increase of T results in an increase of the phase space available for the excitation to undergo scattering processes. Here instead the focus is on elastic processes, i.e. on the *propagation* of the excitation to the boundary: the number of decay paths is fixed by the geometry of the lattice, while the thermal fluctuations affect the amplitude associated to each path, which explicitly depends on the thermal configuration of the neighboring degrees of freedom.

The above mechanism can be rephrased in the following terms: the decay rate of single-spin excitations on a background of surrounding spins appears to depend on whether the neighboring spins are treated as frozen, quenched variables (which corresponds to the low T scenario) or as annealed ones (corresponding to higher T). In particular, a fluctuating environment of spins appears to favor the decay of the individual excitation, by increasing the abundance of resonant denominators. This suggests an analytical approach to describe self-consistently localized and delocalized states, by focusing on the indirect effect of an ergodic -or frozen- environment on the decay channels for individual degrees of freedom. A self-consistent scheme of the following sort can be developed: (i) an assumption is made on the nature of the state and thus on the environmental spins (ii) the decay rate of the individual degree of freedom is computed treating the surrounding spins accordingly, as either fluctuating -or frozen- variables (iii) the self-consistency of the assumption is checked by showing that the decay is indeed possible -or not. Such a scheme is reasonable whenever the local potentials which determine the efficiency of the decay channels (i.e., the energy denominators in the expression for the decay rate),

depend significantly on regions of the sample that are not themselves part of the decay path under consideration. This occurs in high dimensions, on Bethe lattices with high connectivity, or in systems with sufficiently long range interactions.

Motivated by these considerations, in the remainder of the section we revisit the above argument: We set up a formalism for the description of the decay of an excitation in a fluctuating (henceforth "liquid") and a frozen environment of spins, respectively. We investigate the possibility of obtaining two different critical values of $\lambda_c = (J_{xy}/W)_c$ for the delocalization transition (at the same $T = \infty$ temperature) depending on the hypothesis made on the environment, in which case one might have self-consistently localized or delocalized states at the same parameters. However, we will see that this is not the case. Rather, both approaches give the same λ_c.

6.1.1 The setup for a self-consistent approach

As discussed in Sec. 1.4.3, the stability of the localized phase can be determined by linearizing the expression for the level width around $\Gamma = 0 \; \forall \; k$ and iterating the resulting expression up to the boundary. The latter is assumed to be at distance L from the bulk site i, and associated to an infinitesimal level width γ_L. The iteration results in a sum over all paths p connecting the site i to any of the sites at the boundary, which we write in full generality as:

$$\Gamma_i \approx \left(\sum_{\text{paths: } i \to \partial L} \omega_p \right) \gamma_L. \tag{6.4}$$

In the following, we refer to the typical value of (6.4) as[2] the decay rate of the excitation , and denote it simply by Γ. The localized phase is stable as long as the typical value of the sum (6.4) decays exponentially in L, the critical point being the one at which the typical value of Γ becomes of $O(1)$.

Due to the presence of the interactions, the weights ω_p in (6.4) depend explicitly on the configuration of all the $(k-1)L$ neighboring spins σ_n^z along the path, which we treat as independent random variables. The distinction between frozen and liquid environment translates into different weights ω_p, the difference being whether the neighboring spins are averaged over or not. In case of a frozen environment, we consider:

$$\Gamma^{(f)} = \gamma_L \sum_{\text{paths}(i;L)} \prod_{s \in p} \left(\frac{J_{xy}}{\omega - W\xi_s + \tau_s} \right)^2 = \Gamma^{(f)} \left(\{\xi_i, \tau_i\} \right), \tag{6.5}$$

where the product is over all sites s along the given path, $\xi = (\xi_1, \cdots, \xi_L)$ and $\tau = (\tau_1, \cdots, \tau_L)$ the corresponding fields and shifts (6.3). In this case, the τ_i are quenched variables on which the decay rate depends explicitly. Their distribution $P(\{\tau_i\})$ is assumed to be a "thermal" one obtained from the Gibbs distribution of the variables σ_n^z.

[2] Strictly speaking, the two coincide within the Weisskopf-Wigner approximation, whereby the self-energy function is substituted with a constant, that is its value at the dominant pole [57].

In the case of a liquid environment, we set instead:

$$\Gamma^{(l)} = \gamma_L \sum_{\text{paths}(i;L)} \sum_{\tau} P(\tau) \ \min\left\{1, \ \prod_{s\in p}\left(\frac{J_{xy}}{\omega - W\xi_s + \tau_s}\right)^2\right\} \ = \Gamma^{(l)}(\{\xi_i\}). \qquad (6.6)$$

In (6.6), the contribution of each decay path is obtained performing a thermal average over all possible configurations of the environmental spins (and thus of the local shifts τ_s) at fixed quenched disorder. As a result, $\Gamma^{(l)}$ depends explicitly only on the quenched fields. The minimum constraint of the product in (6.6) prevents atypical configurations to contribute with an exponentially large weight. The latter can be generated as a consequence of the fact that we neglected the real parts of the self energies when iterating the linearized equations for the level width. By neglecting the renormalization effect of the self energies, one might get unphysical, exponentially large decay rates that would dominate the thermal average in (6.6), leading to an erroneous estimate of the typical value of the sum. A cutoff is thus introduced, that reproduces the renormalization effect of the self-energy corrections on the rare, large amplitudes.

6.1.2 A potential scenario for fluctuation-induced delocalization

The mechanism that is singled out in [42], namely that the fluctuations of the environmental spins enhance the mobility of the individual excitations, can be tested in the simple framework developed above. In particular, one might consider the decay of a single-spin excitation on top of an infinite temperature state (meaning that each neighboring spin has equal probability to be $\sigma_n^z = \pm 1$), and ask at which critical value of $\lambda = J_{xy}/W$ the typical values of (6.5) and (6.6) become of order $O(1)$. If a liquid environment indeed opens more favorable channels for the propagation of the excitation, one should find that (6.6) becomes of order $O(1)$ at a smaller value of the hopping, i.e. $\lambda_c^{(l)} < \lambda_c^{(f)}$.

In the self-consistent treatment, this would correspond to a regime of coexistence $\lambda_c^{(l)} < \lambda < \lambda_c^{(f)}$ in which both assumptions on the environment are consistent, see Fig. 6.1. Such a scenario [3] is conceivable, based on the general expectation that the thermal averaging in (6.6) favors different decay paths than (6.5). In particular, one might expect that at $\lambda_c^{(l)}$, $\Gamma^{(l)}$ is dominated by some thermal configuration of the environment (i.e., some configuration of the local shifts) that is too rare to appear in typical instances of $\Gamma^{(f)}$, but is present in $\Gamma^{(l)}$ by virtue of the thermal average. In the following, we however rule out this scenario, arguing that the typical values of (6.5) and (6.6) become of order $O(1)$ at the *same* value of $\lambda_c^{(f)} = \lambda_c^{(l)}$, irrespectively of how the path weights are averaged.

[3] This scenario would have several implications; for instance, it would make it possible for a given system at fixed energy density to end up in states that are very different in nature (either localized or delocalized) depending on how the system is prepared [150]. We note, however, that arguments along the same lines as the ones given in Sec. 1.5.1 suggest that what (possibly) appears as a coexistence within a self-consistent treatment might actually correspond to a regime in which the localized state is long-lived but metastable, and eventually decays into the diffusive one at very large time scales.

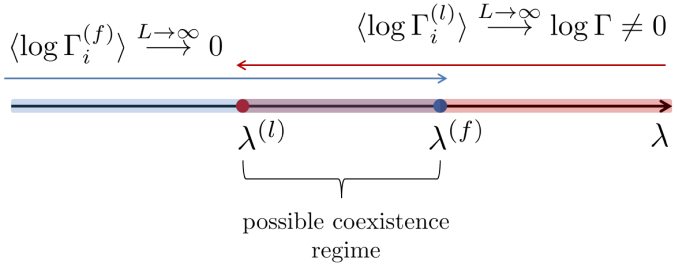

Figure 6.1: Schematic representation of a coexistence regime in which both assumptions on the environment (liquid or frozen) are consistent.

6.1.3 Ineffectiveness of rare thermal fluctuations in enhancing delocalization

To simplify the notation, we assume that the random fields ξ_i take values only within a discrete set $\xi = \{\xi_1, \cdots, \xi_N\}$. Since the possible values of the shifts τ_l are also finite, we may write:

$$\Gamma^{(f)} = \gamma_L \sum_{\xi,\tau} \mathcal{N}(\xi,\tau)\ \Gamma(\xi,\tau) \tag{6.7}$$

where the sum is over all possible sequences ξ, τ of length L of shifts and fields, $\Gamma(\xi,\tau)$ the corresponding weight, and $\mathcal{N}(\xi,\tau)$ the number of paths (out of the total k^L) having such a sequence of fields and shifts. The quantity $\mathcal{N}(\xi,\tau)$ is the random variable in (6.7). Similarly, (6.6) can be written as

$$\Gamma^{(l)} = \gamma_L \sum_{\xi} \mathcal{N}(\xi)\ \Gamma_{th}(\xi), \tag{6.8}$$

where $\mathcal{N}(\xi)$ is the number of paths with fields ξ, and $\Gamma_{th}(\xi)$ is their deterministic weight, obtained performing the thermal average over all the possible thermal shifts:

$$\Gamma_{th}(\xi) = \sum_{\tau} P(\tau) \min\{1, \Gamma(\xi,\tau)\}\,. \tag{6.9}$$

The probability for a configuration (ξ,τ) to occur equals $P(\xi)P(\tau) = \prod_{s=1}^{L} p(\xi_s)p(\tau_s)$, with $p(\xi), p(\tau)$ the distributions of the quenched fields and of the thermal shifts at a given site. When sampling k^L paths independently, there typically are $\mathcal{N}_{typ}(\xi,\tau) = k^L P(\xi)P(\tau)$ paths with such a configuration of denominators. Whenever this number is smaller than one, the configuration is rare. The same holds true for paths with a given sequence of fields ξ.

In the following we assume that whenever the typical values of the sums (6.7), (6.8) are of order $O(1)$, they are dominated by one optimal configuration (ξ^*, τ^*). For the two expressions to give two different critical conditions, it must be that the dominating configurations giving a contribution of order $O(1)$ are different in the two cases. In particular,

the scenario in Sec. 6.1.2 would occur if at $\lambda_c^{(l)}$ the rate (6.8) is dominated by a configuration (ξ^*, τ^*) such that $\mathcal{N}_{typ}(\xi^*) = k^L P(\xi^*) \geq 1$, but $\mathcal{N}_{typ}(\xi^*, \tau^*) = k^L P(\xi^*) P(\tau^*) < 1$. This would make it possible that at $\lambda_c^{(l)}$, $\Gamma^{(l)} = O(1)$ holds, but still $\Gamma^{(f)} < 1$, so that $\lambda_c^{(l)} < \lambda_c^{(f)}$. However, this scenario is not possible for the following reasons:

(i) Assume that at $\lambda = \lambda_c^{(l)}$, the sum (6.8) is dominated by a configuration (ξ^*, τ^*). Then:

$$\Gamma_{typ}^{(l)} \sim \mathcal{N}_{typ}(\xi^*) \left[P(\tau^*) \min \left\{ 1,\ \Gamma(\xi^*, \tau^*) \right\} \right] = 1, \tag{6.10}$$

which implies $\mathcal{N}_{typ}(\xi^*) P(\tau^*) \geq 1$ due to the presence of the constraint on the path weight. Since $\mathcal{N}_{typ}(\xi^*) P(\tau^*) = \mathcal{N}_{typ}(\xi^*, \tau^*)$, the configuration (ξ^*, τ^*) is not rare, and it occurs in typical realizations of $\Gamma^{(f)}$ with multiplicity $\mathcal{N}_{typ}(\xi^*, \tau^*)$, implying $\Gamma^{(f)} \geq 1$. Thus, $\lambda_c^{(f)} \leq \lambda_c^{(l)}$.

(ii) On the other hand, assume that at $\lambda = \lambda_c^{(f)}$, the typical value of the sum (6.7) is dominated by:

$$\Gamma_{typ}^{(f)} \sim \mathcal{N}_{typ}(\xi^*, \tau^*)\ \Gamma(\xi^*) = 1. \tag{6.11}$$

Then it must hold that $\mathcal{N}_{typ}(\xi^*, \tau^*) \geq 1$, which implies that $\mathcal{N}_{typ}(\xi^*) \geq 1$, meaning that typical realizations of $\Gamma^{(l)}$ receive $k^L P(\xi^*)$ path contributions with fields ξ^*. Then, in the thermal average, for each such path there is a contribution with shifts τ^*, which produces a total term of order $O(1)$. Thus, $\Gamma^{(l)} \geq 1$, implying $\lambda_c^{(l)} \leq \lambda_c^{(f)}$.

The argument (i) corresponds to the following physical picture: for $\Gamma^{(l)}$ to be of order $O(1)$, at *any time* the instantaneous decay rate must be of order $O(1)$, meaning that the *typical* thermal configurations of the environment give a decay rate of order $O(1)$. Such typical thermal configuration will also appear in the frozen case, implying that $\Gamma^{(f)} = 1$ also. For this argument to hold, the cutoff imposed on the weights in (6.6) is crucial, as it forbids that $\Gamma^{(l)} = O(1)$ due to *rare* instances of time in which the instantaneous decay rate is extremely large.

The above reasoning implies that $\lambda_c^{(l)} = \lambda_c^{(f)}$, thus ruling out the scenario of Sec. 6.1.2. We conclude that a mechanism based on thermally enhanced small denominators does not work. Moreover, it follows from this reasoning that for this class of models, *at the transition*, considering the environment as frozen or considering it as liquid (in the sense of Eqs. (6.8) and (6.7)) produces the same result for λ_c; we make use of this observation when performing the computation in Sec. 6.3. We conclude this section with a few comments:

– In the case discussed in this section, the local fields appearing in each of the energy denominators in (6.6) are a sum of *uncorrelated* contribution from the environment. The equivalence of the critical conditions given by the two different formalism is then not too surprising: indeed, the formula (6.6) entails that, while the excitation decays in a liquid environment, it experiences at any site a local

field corresponding to a *fixed* configuration of the neighbors. In this sense, the environment appears as effectively frozen at any instance of time, although in a different thermal configuration at any site. However, since the contributions of different configurations at different sites are independent, the outcome of the calculation is the same as for the frozen case. This leaves open the possibility that more complex models, in which correlations are present among the environmental spins, might indeed display a regime of coexistence when analyzed within the self-consistent scheme sketched in Sec. 6.1.

– If the constraint in (6.6) is removed, one would erroneously obtain that $\lambda_c^{(l)} < \lambda_c^{(f)}$. Indeed, in this case the typical value of (6.10) *can* reach the value 1 due to rare configurations having negative entropy (i.e., $k^L P(\xi^*)P(\tau^*) < 1$), that as such do not contribute to typical realizations of the frozen decay rate. For such rare configurations to give a contribution of order $O(1)$ in the liquid case, their instantaneous decay rate has to be large enough to compensate for the negative entropy. This can happen if the instantaneous decay rate is allowed to grow exponentially with L (which is the case in [42]). As previously discussed, this situation is however unphysical, as decay rates are physically bounded by quantities of order $O(1)$.

– The equality $\Gamma_{typ}^{(l)} = \Gamma_{typ}^{(f)}$ holds at the critical value λ_c, when both the typical values are of order $O(1)$. Deep in the localized phase however, the constraint in (6.6) is essentially ineffective due to the fact that the energy denominators are typically bounded from below. In the absence of the constraint, the inequality $\Gamma^{(l)} \geq \Gamma^{(f)}$ holds at fixed λ, as it follows from interpreting the two quantities as an annealed and quenched partition functions, respectively. Then, the calculation of the typical decay rate indicates that a liquid environment enhances the localization length of the individual excitation.

6.2 A toy model for the decay in a liquid environment

The framework developed in the previous sections naturally raises the question of when it is permitted to treat the surrounding spins as frozen or annealed. In particular, it is important to ask under which circumstances it is justified to consider a decay rate of the form (6.6), and more generally (6.2).

These two expressions correspond to the following dynamical picture: the excitation propagates on a background of spins that is not static, but nevertheless, at any site it experiences the field generated by an environment that is frozen in some thermal configuration. In this setting, the decay rate is obtained by averaging the individual decay rates at fixed thermal configurations. On general grounds, we expect this picture to be meaningful as long as the time scale associated to the fluctuations in the environment, i.e. the typical time scale of fluctuation of the effective local fields (6.3), is not "too fast" (with respect to a time scale to be established below). Indeed, very fast oscillations should result in local effective fields that are themselves averages over all possible configurations of the environment.

To make this statement concrete, we consider a simple toy model describing the decay of a single particle subject to a fluctuating local potential, which mimics the effect of the neighboring spins. More precisely, we consider a two-site system with Hamiltonian:

$$H^{(s)}(t) = h_1 n_1 + h_2(t) n_2 - J(c_1^\dagger c_2 + c_1 c_2^\dagger), \tag{6.12}$$

with $h_2(t)$ a periodically-modulated field with period Ω^{-1}, of the general form

$$h_2(t) = h + \tilde{h} f(\Omega t). \tag{6.13}$$

The total Hamiltonian reads $H(t) = H^{(s)}(t) \otimes \mathbb{1} + \mathbb{1} \otimes H^{(b)} + H^{(sb)}$, where the Hamiltonian of the (fermionic) bath reads

$$H^{(b)} = \sum_\alpha \omega_\alpha b_\alpha^\dagger b_\alpha, \tag{6.14}$$

and the coupling is chosen to be

$$H^{(sb)} = \sum_\alpha \lambda_\alpha \left(b_\alpha^\dagger c_2 + c_2^\dagger b_\alpha \right). \tag{6.15}$$

The spectral function of the bath is given by $\Gamma(\omega) = \pi \sum_\alpha \lambda_\alpha^2 \delta(\omega - \omega_\alpha)$. For simplicity, we consider a uniform coupling of all the modes $\lambda_\alpha = \lambda_0$, and a uniform density of states γ of the bath, so that $\Gamma(\omega) \to \pi \lambda_0^2 \gamma = \Gamma$.

For $h_1 = 0$, this toy-model contains four different energy scales ($J, h, \tilde{h}$ and Ω). In the following, we assume that the hopping amplitude J is the smallest scale in the problem. The constant $\tilde{h}$ can be loosely identified with the coupling J_z setting the size of the fluctuating local shifts in the model (6.1), while h corresponds to the gap between the two neighboring local fields along a path of propagation; the situation considered in the previous sections corresponds to $\tilde{h} \lesssim h$. Within this simplified setting, the analogue of the formula (6.2) would prescribe a decay rate for the particle that is an average (in this case over time) of the individual rates associated to a fixed configuration of the local field $h_2(t)$.

To check whether this is indeed correct, we determine the effective field that the particle experiences at the second site while decaying to the bath. We consider the particle's retarded Green function

$$G_{ij}^R(t, t') = -i\theta(t - t') \langle \left\{ c_i(t), c_j^\dagger(t') \right\} \rangle, \tag{6.16}$$

with $i, j \in \{1, 2\}$ labeling the sites in the lattice. The Green function (6.16) is not time-translation invariant, due to the time-dependence in the system's Hamiltonian. To lowest order in the hopping J, the following expansion holds for the component at the first site

of the lattice:

$$G^R_{11}(t,t') = \sum_{n=-\infty}^{\infty} \int \frac{d\omega}{2\pi} \frac{e^{i\frac{\Omega}{2}n(t+t')} e^{-i\omega(t-t')}}{\omega - \frac{\Omega}{2}n - h_1} \times \\ \times \left[\delta_{n,0} + \frac{J^2}{\omega + \frac{\Omega}{2}n - h_1} \sum_m \frac{u_{n+m} u^*_m}{\omega - h_0 + i\frac{\Gamma}{2} + \frac{\Omega}{2}(n+2m)} + \cdots \right], \tag{6.17}$$

where the u_n are the Floquet modes associated with the solution of the Schrödinger equation$(i\partial_t - h_2(t))\,\psi(t) = 0$,

$$\psi(t) = e^{-ih_0 t} u(t) = e^{-ih_0 t} \sum_{k=-\infty}^{\infty} e^{i\Omega k t} u_k. \tag{6.18}$$

In (6.18), we assumed the Fourier decomposition $h_2(t) = h_0 + \sum_{k\neq 0} h_k\, e^{ik\Omega t}$, with

$$h_0 = \frac{1}{T} \int_0^T dt\; h_2(t) \tag{6.19}$$

the Floquet quasienergy. The coefficients u_n are the solutions of the tight-binding problem in frequency space:

$$\sum_{k\neq 0} h_k u_{n-k} + \Omega n u_n = 0. \tag{6.20}$$

Note that the same physical state (6.18) is obtained shifting $h_0 \to h_0 + \Omega j$, $u(t) \to e^{i\Omega j t} u(t) = u^{(j)}(t)$. The Fourier coefficients of $u^{(j)}(t)$ satisfy the equivalent tight-binding problem:

$$\sum_{k\neq 0} h_k u^{(j)}_{n-k} + \Omega(n-j) u^{(j)}_n = 0. \tag{6.21}$$

We give the derivation of the expansion (6.17) in Appendix 6.A.

In the limit $\Omega \to \infty$, the problem (6.21) has solutions $u^{(j)}_n = \delta_{n,j}$. Substitution of this (for $j = 0$) into (6.17) gives:

$$G_{11}(t,t') \overset{\Omega\to\infty}{\to} \int \frac{d\omega}{2\pi} \frac{e^{-i\omega(t-t')}}{\omega - h_1} \left[1 + \frac{J^2}{\omega - h_1} \frac{1}{\omega - h_0 + i\Gamma/2} + \cdots \right]. \tag{6.22}$$

Thus, in this limit the correct locator is obtained averaging the local field in the denominator, cfr. (6.19), as expected in the limit of fast fluctuations of the environment. For a potential of the form (6.13), corrections to the solution $u_n = \delta_{n,0}$ can be obtained perturbatively in $\tilde{h}/\Omega$.

To address the opposite regime of small Ω, we neglect the terms in (6.17) oscillating at the large scale $T \sim \Omega^{-1}$ with respect to the variable $(t+t')/2$, focusing on the term with $n = 0$.

For concreteness, we specify to the discontinuous[4] potential

$$h_2(t) = \begin{cases} h & \text{for } t \in \left[0, \frac{\pi}{\Omega}\right] \\ h+\tilde{h} & \text{for } t \in \left(\frac{\pi}{\Omega}, \frac{2\pi}{\Omega}\right] \end{cases} = h + \frac{\tilde{h}}{2} + \frac{i\tilde{h}}{\pi} \sum_m \frac{e^{i(2m+1)\Omega t}}{2m+1}, \tag{6.23}$$

whose jump of amplitude $\tilde{h}$ mimics a fluctuation of the local shifts (6.3) due to the flip of a neighboring spin. In this case, the solution of the tight binding problem (6.20) is:

$$u_n = \frac{i\Omega\tilde{h}}{2\pi} \frac{e^{-i\pi n + i\tilde{h}\frac{\pi}{2\Omega}} - 1}{(\Omega n + \tilde{h}/2)(\Omega n - \tilde{h}/2)}. \tag{6.24}$$

The series needed for (6.17) with $n = 0$,

$$\mathcal{S}_\Omega(z) = \sum_m \frac{|u_m|^2}{z + \Omega m} = \left(\frac{\Omega\tilde{h}}{2\pi}\right)^2 \sum_m \frac{2 - 2\cos\left(\pi m - \tilde{h}\frac{\pi}{2\Omega}\right)}{(z+\Omega m)\left[\Omega m + \tilde{h}/2\right]^2\left[\Omega m - \tilde{h}/2\right]^2} \tag{6.25}$$

where $z = \omega - h_0 + i\Gamma/2$, can be resummed explicitly, the result being:

$$\mathcal{S}_\Omega(z) = \frac{z}{(z-\tilde{h}/2)(z+\tilde{h}/2)}\left[1 + \frac{\Omega\tilde{h}^2}{z(z-\tilde{h}/2)(z+\tilde{h}/2)}F\right]. \tag{6.26}$$

In (6.26), F is a linear combination of oscillating terms, of the form:

$$F = ie^{-\frac{\pi\Gamma}{2\Omega}}e^{\frac{i\pi(\omega-h)}{\Omega}} + \frac{2e^{-\frac{\pi\Gamma}{\Omega}}e^{\frac{2i\pi(\omega-h-\tilde{h}/2)}{\Omega}} - e^{-\frac{\pi\Gamma}{2\Omega}}e^{\frac{i\pi(\omega-h-\tilde{h})}{\Omega}} - e^{-\frac{\pi\Gamma}{2\Omega}}e^{\frac{i\pi(\omega-h)}{\Omega}}}{i(1 - e^{-\frac{\pi\Gamma}{\Omega}}e^{\frac{2i\pi(\omega-h-\tilde{h}/2)}{\Omega}})}. \tag{6.27}$$

When substituting $z \to \omega - h - \tilde{h}/2 + i\Gamma/2$, one recognizes in the first term of (6.26) the time average of the instantaneous locator, as expected:

$$\frac{1}{T}\int_0^T \frac{1}{\omega + i\frac{\Gamma}{2} - h_2(t)} = \frac{1/2}{\omega + i\frac{\Gamma}{2} - h} + \frac{1/2}{\omega + i\frac{\Gamma}{2} - h - \tilde{h}} = \frac{\omega + i\Gamma/2 - h - \tilde{h}/2}{(\omega + i\frac{\Gamma}{2} - h - \tilde{h})(\omega + i\frac{\Gamma}{2} - h)}. \tag{6.28}$$

For $\omega = 0$ and neglecting Γ, one finds that the correction to this term is small provided that

$$\Omega \ll \frac{(h + \tilde{h}/2)h(h+\tilde{h})}{\tilde{h}^2}. \tag{6.29}$$

For $\tilde{h} \lesssim h$, the condition (6.29) can be written as $\Omega \ll h(h/\tilde{h})^2$ up to corrections of order $\tilde{h}/h$. Thus, for $h \gg \tilde{h}$ the expression (6.28) is a good approximation for a wide range of frequencies, although in this regime the resulting locator is essentially equivalent to the time averaged one in (6.22), since the two differ by a term of the order of $(\tilde{h}/h)^2/4 \ll 1$.

[4]The choice of a discontinuous field implies that no Landau-Zener transitions have to be considered in this discussion.

The decay rate containing the locator (6.28) is most different from the case (6.22) whenever the fields satisfy $h < \tilde{h}/4$. In this case it holds

$$\frac{1}{h+\tilde{h}/2} = \frac{2}{\tilde{h}}\left(1 - 2\frac{h}{\tilde{h}} + \cdots\right) < \frac{1}{2h}\left(1 + \frac{h}{\tilde{h}} + \cdots\right) = \frac{h+\tilde{h}/2}{(h+\tilde{h})h}. \tag{6.30}$$

When $(\tilde{h}/h)^2/4 \ll 1$, the condition (6.29) reads $\Omega \lesssim h/2$. In this case, an intermediate regime $h \lesssim \Omega \lesssim \tilde{h}$ occurs in which neither of the approximations considered above is valid.

In general, we conclude from (6.29) that in this toy-model the expression for the decay rate exploited in Sec. 6.1.2 is justified when the fluctuating effective field varies at a rate Ω that is smaller than the timescale for the local precession of the spins, set by the static local field.

6.3 T-induced delocalization: an effective mechanism

Following the considerations above, we conclude that the annealed average over thermally distributed configurations is ineffective in enhancing the mobility of the excitations. However, the effective mobility edge might nevertheless display a dependence on T, if it arises from a T-dependence of the distribution of the effective local fields (irrespectively of whether they are treated as frozen or annealed), which was not the case in the simple case treated above. We discuss this mechanism in this section. We consider the same setup as above, namely a single-spin-flip excitation of energy ω propagating from the root to the boundary of a Bethe lattice with connectivity $k+1$. We consider the rescaled hopping $\lambda = J_{xy}/W$ to be fixed, and focus on the dependence on temperature of the mobility edge of such excitations, $\omega_c(\lambda, k, T)$. Assuming a slowly fluctuating environment, an expression as (6.6) for the decay rate can be exploited. Moreover, it follows from the discussion in Sec. 6.1.1 that the configuration of the neighboring spins can be considered as frozen for the purpose of estimating the critical hopping or mobility edge, as the two averaging procedures result in the same estimate. This allows us to bypass the technical difficulties that arise in the computation of (6.6) due to the constraint. Instead, the typical value of the "forward approximation" decay rate (6.5) can be computed exploiting the formalism of directed polymers in random media, which we recall in the following.

6.3.1 Quenched free energy of directed polymers on Bethe lattices

The directed polymer problem on the Bethe lattice was solved exactly in [51], where a recipe to compute the typical value of the partition function is given. The latter can be generically written as

$$\mathcal{Z}(\beta, \alpha) = \sum_{\text{paths}} \prod_{i \in p} \left[f_i(\xi, \alpha)\right]^{\beta}, \tag{6.31}$$

where the sum is over all k^L paths of length L, whose weight is a product over L independent, positive terms $f_i(\alpha, \xi)$ depending on some set of quenched random variables ξ with distribution $p(\xi)$. Here β is the inverse temperature, and α is a set of parameters on which the problem might depend. The quenched free energy of the polymer is given in terms of the convex function:

$$g(x, \alpha) = \frac{1}{x} \log \left(k \int d\xi p(\xi) \left[f(\xi, \alpha) \right]^x \right) \tag{6.32}$$

as

$$\frac{1}{L\beta} \mathbb{E} \left[\log \mathcal{Z}(\beta, \alpha) \right] = \begin{cases} g(x_c(\alpha), \alpha), & \text{if } \beta > x_c(\alpha) \\ g(\beta, \alpha), & \text{if } \beta \leq x_c(\alpha), \end{cases} \tag{6.33}$$

where $x_c(\alpha)$ is the stationary point of (6.32),

$$\frac{d}{dx} g(x, \alpha) \Big|_{x = x_c(\alpha)} = 0. \tag{6.34}$$

For those parameters α for which $x_c(\alpha) < \beta$, the polymer is in its frozen phase. The annealed partition function $\mathbb{E}[\mathcal{Z}]$ is dominated by rare paths with negative entropy, and thus one has $\log \mathbb{E}[\mathcal{Z}] > \mathbb{E}[\log \mathcal{Z}]$.

Within the forward approximation, a sum of the form (6.5) is a polymer partition function at $\beta = 2$, since the path weights are products of independent variables. Moreover, due to the unboundedness of the denominators from below, the integral in (6.32) converges only for $x < 1/\beta = 1/2$, and thus the polymer is always in its frozen phase. This implies that the sum over all paths contributing to the partition function is dominated by the path with maximal amplitude, a fact that we have made use of in Sec. 6.1.3. For those parameters α for which the sum in (6.8) does not decay exponentially with L, the decay rate is not vanishing in the thermodynamic limit. The critical parameters α_l at which (6.8) becomes of order $O(1)$ are fixed by the coupled set of equations:

$$\frac{d}{dx} g(x_c(\alpha_l), \alpha_l) = 0, \quad g(x_c(\alpha_l), \alpha_l) = 0. \tag{6.35}$$

6.3.2 The dependence on temperature of the mobility edge

Let us denote with $P_T(h)$ the distribution of the effective local fields which appear in the denominators of the locators, at a given temperature T. For interacting models, it is a very general expectation that the density of soft excitations $P_{T=0}(0)$ is suppressed in the zero temperature regime. This follows from stability arguments, and it occurs in a variety of models ranging from the Edward-Anderson and Sherrington-Kirkpatrick models, to the extreme case of the gapped Mott insulator. As temperature is increased, the suppression of $P_T(0)$ is typically softened. To capture this effect qualitatively, we assume the local

effective fields to be distributed according to the following simple form:

$$P_T(h) = \int dz \, \frac{|z|}{2} e^{-\frac{z^2}{2}} \frac{1}{\sqrt{2\pi}T} e^{-\frac{(z-h)^2}{2T^2}}. \tag{6.36}$$

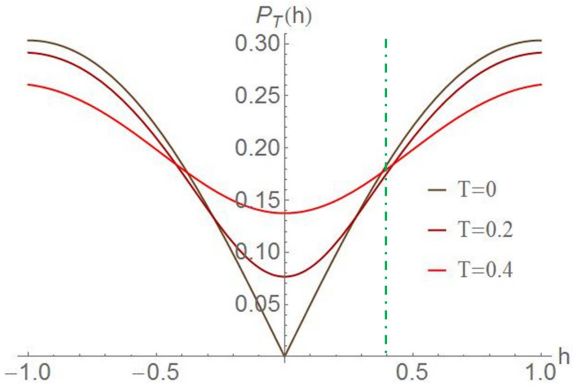

Figure 6.1: Temperature dependence of the toy-distribution of effective fields, see Eq. 6.36. The vertical dashed line identifies a point within the pseudo-gapped region, where the distribution depends weakly on temperature.

Eq. (6.36) is the simplest form of a pseudo-gapped distribution smeared out at the scale of the temperature T. This is precisely the local-field distribution derived in [167] for the fully-connected Sherrington-Kirkpatrick model, which is determined self-consistently by averaging over both disorder and thermal fluctuations. Although the pseudo-gap is distinctive feature of models with long-range interactions, this specific example optimizes the generic behavior of realistic $P_T(h)$ in a large set of models, having the advantage of being easily-tractable.

We compute the decay rate of an excitation along paths whose local fields are distributed according to (6.36), under the assumption that the quantum fluctuations are weak enough not to spoil the features of the effective field distribution derived in the classical limit. By inspecting its form, see Fig. 6.1, one realizes that the density of states of low-energy excitations increases with temperature, as the pseudo-gap gets filled. Again, this trend is rather generic. For values of λ for which ω_c lies in the region where the density of states is suppressed, an increase in temperature should result in a lowering of the effective mobility edge, as smaller denominators become more probable. We now show that this is indeed the case.

Following the recipe for the directed polymer, the typical value of the decay rate of the spin excitation is obtained by means of the function (6.32), which reads:

$$g(x; \{\omega, \lambda, k\}) = \frac{1}{x} \log \left[k I_1(x, \omega) \right] + 2 \log \lambda, \tag{6.37}$$

where $x < 1/2$ and

$$I_1(x,\omega) = \int dh \frac{P_T(h)}{(h-\omega)^{2x}}. \tag{6.38}$$

The critical values x_c, ω_c are fixed by the conditions (6.35), which are equivalent to:

$$\begin{aligned} I_2(x,\omega) + I_1(x,\omega)\frac{1}{x}\log\left[kI_1(x,\omega)\right] = 0, \\ \frac{1}{x}\log\left[kI_1(x,\omega)\right] + 2\log\lambda = 0, \end{aligned} \tag{6.39}$$

where

$$I_2(x,\omega) = \int dh \log\left[(h-\omega)^2\right] \frac{P_T(h)}{(h-\omega)^{2x}}, \tag{6.40}$$

and the condition for the minimum of (6.37) is rewritten as:

$$\begin{aligned} 0 &= (-x^2) I_1(x,\omega)\frac{d}{dx} g(x,\omega;\lambda,k) \\ &= I_1(x,\omega)\log\left[kI_1(x,\omega)\right] - x\frac{d}{dx} I_1(x,\omega) \\ &= I_1(x,\omega)\log\left[kI_1(x,\omega)\right] + xI_2(x,\omega). \end{aligned} \tag{6.41}$$

This system of equations is solved numerically for different values of the parameters k, T. A frequency-dependent critical value $x_c(\omega)$ is obtained by solving the first equation in (6.39). The effective mobility edge $\omega_c(\lambda, k, T)$ is then derived by solving:

$$F(\omega) = -\frac{I_2(x_c(\omega),\omega)}{I_1(x_c(\omega),\omega)} = -2\log\lambda. \tag{6.42}$$

Fig. 6.2 shows the dependence of $\omega_c(\lambda(k), k, T)$ on T for different values of the connectivity k and of the hopping λ. For any k, the value of the hopping $\lambda(k)$ is chosen in such a way that the location of the mobility edge at small temperatures $T = 0.05$ coincides for all curves. As temperature is increased, the position of the mobility edge is shown to decrease for any fixed k. This reflects the effect of thermal fluctuations on the density of local fields, which increases the density of small denominators producing an effective temperature-induced delocalization. As illustrated in the inset of Fig. 6.2, the effective mobility edge $\omega_c(T)$ decreases in a way that depends on T^2, which is the fraction of thermally active degrees of freedom[5] in the toy-distribution (6.36).

We conclude the chapter with a comment about the dependence on the connectivity k. First, the local-field distribution does not depend on k: this choice of energy units corresponds to the standard scaling of the interaction couplings in the mean-field limit,

[5] As for the exact mean field distribution derived in [167], the toy distribution (6.36) satisfies the scaling $P_T(h) = Tp(h/T)$, with $p(x)$ a function increasing linearly for $x \gg 1$ (as it follows from the change of variable $z \to z/T$).

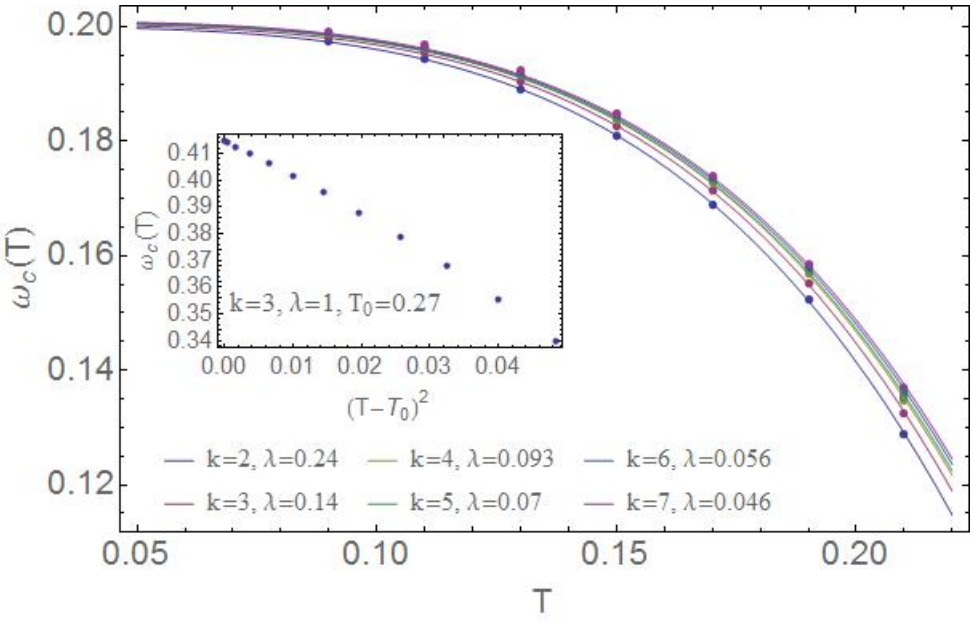

Figure 6.2: Temperature-dependence of the effective mobility edge $\omega_c(T, k, \lambda(k))$ for different values of k. The dimensionless hopping $\lambda = \lambda(k)$ is chosen in such a way that $\omega_c(T = 0.05, k, \lambda(k))$ coincides for all curves. The continuous lines are interpolating functions. *Inset.* Linear dependence of the effective mobility edge $\omega_c(T, k, \lambda(k))$ on T^2, for $k = 2, \lambda = 1$ and values of temperature larger than $T_0 = 0.27$.

$\langle J_{ij}^2 \rangle \sim k^{-1}$. This description is expected to be accurate for quantum systems on Bethe lattices with finite but large connectivity. For larger k, the decrease of $\omega_c(T)$ with T is less pronounced, see Fig. 6.2. This is a consequence of the fact the mobility edge on a Bethe lattice in the large connectivity limit is determined by the distribution of local fields only, as a solution of

$$P_T(\omega_c) = \frac{1}{4\lambda k \log k}, \tag{6.43}$$

as proved in [14]. Since within the pseudo-gapped region the shape of $P_T(h)$ is not strongly affected by T (see Fig. 6.1), it follows that the T-dependence of the mobility edge becomes weaker as the connectivity increases, as described by the asymptotic formula (6.43).

Appendix

6.A Green functions expansion (Eq. 6.17)

Let $\hat{G}(t,t')$ denote the 2x2 matrix with components (6.16). The equations of motion are:

$$\begin{aligned}\left\{i\overrightarrow{\partial_t} - \hat{H}^{(s)}(t)\right\}\hat{G}(t,t') - i\frac{\Gamma}{2}\hat{G}(t,t') &= \hat{\mathbb{I}}\delta(t-t'),\\ \hat{G}(t,t')\left\{-i\overleftarrow{\partial_{t'}} - \hat{H}^{(s)}(t')\right\} - i\frac{\Gamma}{2}\hat{G}(t,t') &= \hat{\mathbb{I}}\delta(t-t'),\end{aligned} \tag{6.44}$$

where we used $\hat{\Sigma}_{ij}(t,t') = -i\Gamma\delta(t-t')\delta_{1,2}\delta_{j,2}$. For $J=0$, the matrix $\hat{G}^{(0)}(t,t')$ is diagonal in the position basis and given by

$$\hat{G}^{(0)}(t,t') = -i\theta(t-t')\begin{pmatrix} e^{-ih_1(t-t')} & 0 \\ 0 & e^{-\frac{\Gamma}{2}(t-t')}\psi(t)\psi^*(t')\end{pmatrix} \tag{6.45}$$

where $\psi(t)$ admits the decomposition (6.18). The second component of (6.45) thus reads:

$$G^{(0)}_{22}(t,t') = -i\theta(t-t')e^{-i\left(h_0 - i\frac{\Gamma}{2}\right)(t-t')}u(t)u^*(t') = -i\theta(t_r)\sum_{n,m} e^{i\Omega n t_a}e^{-iX_{nm}t_r}u_{n+m}u^*_m, \tag{6.46}$$

where $t_a = (t+t')/2$ and $t_r = t-t'$, and $X_{nm} = h_0 - i\frac{\Gamma}{2} - \frac{\Omega}{2}(n+2m)$. The above can be written as

$$G^{(0)}_{22}(t,t') = \sum_{n=-\infty}^{\infty} e^{i\frac{\Omega}{2}n(t+t')}\int_{\mathcal{C}}\frac{d\omega}{2\pi}e^{-i\omega(t-t')}G^{(0)}_{22}(\omega,n), \tag{6.47}$$

where $\mathcal{C} = \{\Im\omega = \epsilon > 0\}$ and

$$\begin{aligned}G^{(0)}_{22}(\omega,n) &= -i\int_0^\infty dt\; e^{i(\omega - h_0 + i\frac{\Gamma}{2} + \frac{\Omega}{2}n)t}\left(\sum_m e^{i\Omega m t}u_{n+m}u^*_m\right)\\ &= \sum_m \frac{u_{n+m}u^*_m}{\omega - h_0 + i\frac{\Gamma}{2} - \frac{\Omega}{2}(n+2m)},\end{aligned} \tag{6.48}$$

where in the last equality we assumed that integral and series expansion commute. We now determine the lowest order corrections in J, assuming $G_{ij}(t,t') = \sum_n J^n G_{ij}^{(n)}$. The equations (6.44) give to first order in J:

$$\{i\partial_t - h_1\}\, G_{12}^{(1)}(t,t') + JG_{22}^{(0)}(t,t') = 0\,\{-i\partial_{t'} - h_1\}\, G_{21}^{(1)}(t,t') + JG_{22}^{(0)}(t,t'), \quad (6.49)$$

which are solved in frequency space by:

$$\begin{aligned} G_{12}^{(1)}(\omega,n) &= \frac{-J}{\omega - \frac{\Omega}{2}n - h_1} G_{22}^{(0)}(\omega,n), \\ G_{21}^{(1)}(\omega,n) &= \frac{-J}{\omega + \frac{\Omega}{2}n - h_1} G_{22}^{(0)}(\omega,n). \end{aligned} \quad (6.50)$$

Using these solutions one finds to second order:

$$G_{11}^{(2)}(\omega,n) = \frac{J^2}{\left(\omega - \frac{\Omega}{2}n - h_1\right)\left(\omega + \frac{\Omega}{2}n - h_1\right)} G_{22}^{(0)}(\omega,n), \quad (6.51)$$

thus recovering (6.17) once (6.48) is substituted.

Conclusive remarks

We have devoted this thesis to the investigation of several aspects of the localized phase in quantum systems with quenched disorder. Particular focus has been put on the characterization of the Many-Body Localized phase in terms of its "integrability". We have argued that non-trivial conservation laws exist, adapting at the operator level the theoretical framework developed in the seminal works [10, 2]. Our treatment involves several approximations, which can, however, be improved upon [86], as we discussed in Sec. 2.3. Although approximate, this approach has the advantage of making contact with the diagrammatic formalism in [20, 72]: some of the tools that we have used (for instance the re-summation of diagrams described in Sec. 2.3) can be exploited in other contexts in which diagrammatic expansions are considered [73]. Moreover, it has the advantage of being constructive: the calculation in Chapter 3 illustrates the practical usefulness of the perturbative recipe, which, being explicit, allows one to obtain analytic expressions for relevant quantities characterizing the MBL phase, such as the remanent magnetization after a quench. Our formalism also allowed us to reformulate the debate on the existence of a finite-temperature transition at the operator level, and to illustrate why this controversy cannot be settled within the approximations made in our treatment, as well as in [20, 72].

The theoretical arguments for the existence of integrals of motion and, more generally, of the localized phase rely on probabilistic estimates of the occurrence of resonances, generated by rare fluctuations of the randomness. In the analytical computations throughout the whole thesis, the probability of resonances is argued to decay fast enough with the distance between the degrees of freedom involved. This is done exploiting a set of approximations, which we have always referred to as "the forward approximation". It is probably worth to comment at this point about the various versions of this approximation. In its single-particle formulation [10], the approximation consists in restricting the sum over all processes (or paths) contributing to the propagator to only those processes that do not contain repetitions of the intermediate states, i.e., to the self-avoiding paths; this amounts to neglecting the renormalization of the bare energy levels produced by the self-energy corrections, as pointed out in Sec. 1.4.1. In Chapter 4 and 5, we have exploited this approximation to its lowest order in the hopping, considering only the *shortest* among the self-avoiding paths. The forward approximation performed on the effective hopping problem in Chapter 2 contains an additional simplification, that is the fact that some processes (the hopping "within the same generation") are neglected. Let us briefly recall the main results obtained within these approximations, and mention possible directions for improving such results.

The treatment of the "small bath problem" in Chapter 4 illustrates how the lowest order forward approximation captures the basic features of the phase diagram, such as the non-monotonic dependence of localization on the coupling to the finite bath, in agreement with exact diagonalization results. The "Zeno regime" discussed in this context provides an example of localization induced by coupling to further degrees of freedom. Although we focused on the simplified setting of non-interacting particles, it is possible that an analogous phenomenon occurs in more general frameworks (it was for instance taken into account in [49] in an interacting setting, with the purpose of ensuring that the mobility of the bubbles is not hindered once the coupling to configurations without bubbles is taken into account). Broadly speaking, the problem in Chapter 4 can be related to the discussion about how "bath-like" regions, having "ergodic" features, affect the the surrounding localized degrees of freedom. This problem is of central relevance, as any analytic treatment of the localized phase, and possibly of the transition, requires to control the effect of such regions (be they the "resonant blocks" in [86], or the "ergodic grains" in [47], or the "bubbles" in [49]).

Besides being analytically tractable, the lowest order forward approximation can be easily implemented numerically via transfer matrix techniques, as discussed in Chapter 5. In general, we expect that restricting to the shortest paths is a good approximation deeply in the localized phase and, in high dimension d, even up to a relatively close vicinity of the transition point: as a matter of fact, the criterion (1.66) states that the transition occurs for a value of the hopping V that is parametrically smaller than the disorder W by a factor of $\kappa(d)$, κ being an effective connectivity increasing with d. This approximate approach may however be improved staying within the transfer matrix scheme, by retaining only the shortest paths but incorporating the self-energy corrections in their denominators (at least to the lowest orders). Such corrections may affect substantially the large deviations of individual path weights, due to the mechanism of compensation of small denominators discussed in Sec. 1.4.4: it would be interesting to revisit the discussion in Sec. 5.4.1 accounting for the correlations among the locators that the self-energies induce.

For what concerns the treatment in Chapter 2, it is clear that restoring the neglected processes in the vicinity of the transition is relevant in the light of the discussion on the delocalizing bubbles in Sec. 1.5.1. Understanding which type of processes leads to the breakdown of the quasilocality of the conserved operators is undoubtedly a physically relevant problem.

As already mentioned, in this thesis we focused primarily on the localized phase, touching the topic of the transition only in Chapter 6. There, we investigated the possibility of coexistence between the two types of states within a self-consistent scheme, and we showed that such a coexistence is not realized in the model that we considered. This allowed us to rule out a possible argument in favor of a finite temperature transition, based on the expectation that the decay of individual excitations is enhanced by rare thermal fluctuations of the surrounding spins. The framework developed in this chapter enabled us to discuss an alternative mechanism by which temperature affects the (effective) mobility edge of the individual excitations, by filling the pseudogapped region in the distribution of effective local fields, thus increasing the abundance of small denominators. The self-consistent approach exploited in Chapter 6 was introduced in a heuristic way, by

choosing to treat the thermal fluctuations of the environmental spins as either annealed or quenched variables. It should be possible to frame this into a more rigorous scheme: intuitively, one might expect that two different expressions for the decay rate of individual excitations on top of a given many-body eigenstate (involving two different types of averages over the environmental spins) can be derived exploiting two different parameterizations of the eigenstate. In particular, a parametrization of the "ETH form" (a uniform superposition of classical states within the same energy shell, the classical states being product states in the basis of the z-components of the local spin operators) is expected to lead to an "annealed" average over classical states. In contrast, a parametrization of the MBL form (a "weak deformation" of a classical state) should lead to a decay rate in which the configurations of the neighboring spins are quenched. Such a formal derivation would allow to recast our heuristic self-consistent scheme into a well-defined program, which could be applied to more complex models for which a coexistence is in principle possible. It is worth to point out that the realization of the coexistence scenario in more complex models would be interesting even if true coexistence turns out to be absent in the thermodynamic limit, and the localized state is metastable: in that case, it would raise the question of how metastable states eventually decay into the liquid phase.

The above remarks concern the content of this thesis. There are certainly many other issues regarding the localized phase that need to be addressed, among which the role of dimensionality, the nature of the critical points found within the MBL phase [81, 136], the possible occurrence of localization in systems with long-range interactions, or in continuum space, or with an unbounded local spectrum, the detailed characterization of the dynamics within this phase. Moreover, a field theoretical description of MBL has only just started to be developed [8]. The possibility that MBL systems might serve as platforms for quantum information technologies is one of the compelling reasons to keep investigating this phase, with the aim of clarifying in which setting these systems can actually be used as quantum memories in which to store quantum information and preserve its quantum coherence.
Despite plenty of open problems, the recent years have produced a fair amount of insight into the localized phase. We hope that our work gives a valuable contribution to this insight. On the other hand, understanding the breakdown of localization and the dynamical transition to the delocalized, thermal phase is an issue whose resolution is still in its infancy. This is a tough problem, which requires to deal simultaneously with out-of-equilibrium quantum physics, interactions, quenched randomness and highly-energetic states: capturing this physics remains an open theoretical challenge.

Bibliography

[1] D. A. Abanin, W. D. Roeck, and F. Huveneers. Theory of many-body localization in periodically driven systems. *Annals of Physics*, 372:1 – 11, 2016.

[2] R. Abou-Chacra, D. Thouless, and P. Anderson. A selfconsistent theory of localization. *J. Phys. C*, 6:1734, 1973.

[3] E. Abrahams, P. Anderson, D. Licciardello, and T. Ramakrishnan. Scaling theory of localization: Absence of quantum diffusion in two dimensions. *Physical Review Letters*, 42(10):673, 1979.

[4] K. Agarwal, S. Gopalakrishnan, M. Knap, M. Müller, and E. Demler. Anomalous diffusion and griffiths effects near the many-body localization transition. *Phys. Rev. Lett.*, 114:160401, Apr 2015.

[5] M. Aizenman and S. Molchanov. Localization at large disorder and at extreme energies: an elementary derivation. *Comm. Math. Phys.*, 157(2):245–278, 1993.

[6] M. Aizenman and S. Warzel. Resonant delocalization for random schrödinger operators on tree graphs. *Journal of the European Mathematical Society*, 15(4):1167–1222, 2013.

[7] I. Aleiner, B. Altshuler, and G. Shlyapnikov. A finite-temperature phase transition for disordered weakly interacting bosons in one dimension. *Nature Physics*, 6:900, 2010.

[8] A. Altland and T. Micklitz. Effective field theory approach to many-body localization. *arXiv:1609.00877 [cond-mat.dis-nn]*.

[9] B. L. Altshuler, Y. Gefen, A. Kamenev, and L. S. Levitov. Quasiparticle lifetime in a finite system: A nonperturbative approach. *Phys. Rev. Lett.*, 78:2803, 1997.

[10] P. W. Anderson. Absence of diffusion in certain random lattices. *Phys. Rev.*, 109:1492, 1958.

[11] P. W. Anderson. Local moments and localized states. *Reviews of Modern Physics*, 50(2):191, 1978.

[12] Y. Avishai, J. Richert, and R. Berkovits. Level statistics in a heisenberg chain with random magnetic field. *Phys. Rev. B*, 66:052416, Aug 2002.

[13] S. Banerjee and E. Altman. Variable-range hopping through marginally localized phonons. *Phys. Rev. Lett.*, 116:116601, 2016.

[14] V. Bapst. The large connectivity limit of the anderson model on tree graphs. *Journal of Mathematical Physics*, 55(9), 2014.

[15] Y. Bar Lev, G. Cohen, and D. R. Reichman. Absence of diffusion in an interacting system of spinless fermions on a one-dimensional disordered lattice. *Phys. Rev. Lett.*, 114:100601, Mar 2015.

[16] Y. Bar Lev and D. R. Reichman. Dynamics of Many-Body Localization. *Physical Review B*, 89(22):220201, 2014.

[17] J. H. Bardarson, F. Pollmann, and J. E. Moore. Unbounded growth of entanglement in models of many-body localization. *Phys. Rev. Lett.*, 109:017202, Jul 2012.

[18] O. S. Barišić, J. Kokalj, I. Balog, and P. Prelovšek. Dynamical conductivity and its fluctuations along the crossover to many-body localization. *arXiv preprint arXiv:1603.01526*, 2016.

[19] T. Barthel and U. Schollwöck. Dephasing and the steady state in quantum many-particle systems. *Physical Review Letters*, 100:100601, 2008.

[20] D. M. Basko, I. L. Aleiner, and B. L. Altshuler. Metal–insulator transition in a weakly interacting many-electron system with localized single-particle states. *Annals of Physics*, 321:1126, May 2006.

[21] B. Bauer and C. Nayak. Area laws in a many-body localized state and its implications for topological order. *J. Stat. Mech*, 2013:P09005, 2013.

[22] T. C. Berkelbach and D. R. Reichman. Conductivity of disordered quantum lattice models at infinite temperature: Many-body localization. *Physical Review B*, 81(22):224429, 2010.

[23] R. Berkovits and B. I. Shklovskii. Statistics of energy spectra of a strongly disordered system of interacting electrons. *Journal of Physics: Condensed Matter*, 11(3):779, 1999.

[24] M. V. Berry. Regular and irregular semiclassical wavefunctions. *Journal of Physics A: Mathematical and General*, 10(12):2083, 1977.

[25] M. V. Berry and M. Tabor. Level clustering in the regular spectrum. *Proceedings of the Royal Society of London A: Mathematical, Physical and Engineering Sciences*, 356(1686):375–394, 1977.

[26] A. Beskow and J. Nilsson. The concept of wave function and the irreducible representations of the Poincare group, II. Unstable systems and the exponential decay law. *Ark. Fys.*, 34:561, 1967.

[27] J. Billy, V. Josse, Z. Zuo, A. Bernard, B. Hambrecht, P. Lugan, D. Clément, L. Sanchez-Palencia, P. Bouyer, and A. Aspect. Direct observation of anderson localization of matter waves in a controlled disorder. *Nature*, 453(7197):891–894, 2008.

[28] O. Bohigas, M. J. Giannoni, and C. Schmit. Characterization of chaotic quantum spectra and universality of level fluctuation laws. *Phys. Rev. Lett.*, 52:1–4, Jan 1984.

[29] P. Bordia, H. P. Lüschen, S. S. Hodgman, M. Schreiber, I. Bloch, and U. Schneider. Coupling Identical 1D Many-Body Localized Systems. *arXiv:1508.07026 [cond-mat.quant-gas]*.

[30] A. Burin, I. Gornyi, A. Mirlin, D. Polyakov, and I. Protopopov. *unpublished*.

[31] A. Burin and Y. Kagan. Low-energy collective excitations in glasses. new relaxation mechanism for ultralow temperatures. *J. Exp. Theor. Phys.*, 80:761, 2005.

[32] P. Calabrese and J. Cardy. Evolution of entanglement entropy in one-dimensional systems. *Journal of Statistical Mechanics: Theory and Experiment*, 2005(04):P04010, 2005.

[33] E. Canovi, D. Rossini, R. Fazio, G. E. Santoro, and A. Silva. Quantum quenches, thermalization, and many-body localization. *Physical Review B*, 83(9):094431, 2011.

[34] A. Chandran, J. Carrasquilla, I. H. Kim, D. A. Abanin, and G. Vidal. Spectral tensor networks for many-body localization. *Phys. Rev. B*, 92:024201, Jul 2015.

[35] A. Chandran, V. Khemani, C. R. Laumann, and S. L. Sondhi. Many-body localization and symmetry-protected topological order. *Phys. Rev. B*, 89:144201, Apr 2014.

[36] A. Chandran, I. H. Kim, G. Vidal, and D. A. Abanin. Constructing local integrals of motion in the many-body localized phase. *Physical Review B*, 91(8):085425, 2015.

[37] A. Chandran, C. Laumann, and V. Oganesyan. Finite size scaling bounds on many-body localized phase transitions. *arXiv: 1509.04285 [cond-mat.dis-nn]*, 2015.

[38] A. Chandran, A. Pal, C. R. Laumann, and A. Scardicchio. Many-body localization beyond eigenstates in all dimensions. *arXiv: 1605.006556 [cond-mat.dis-nn]*.

[39] G. D. Chiara, S. Montangero, P. Calabrese, and R. Fazio. Entanglement entropy dynamics of heisenberg chains. *Journal of Statistical Mechanics: Theory and Experiment*, 2006(03):P03001, 2006.

[40] J.-y. Choi, S. Hild, J. Zeiher, P. Schauß, A. Rubio-Abadal, T. Yefsah, V. Khemani, D. A. Huse, I. Bloch, and C. Gross. Exploring the many-body localization transition in two dimensions. *arXiv preprint arXiv:1604.04178*, 2016.

[41] M. Cramer, C. M. Dawson, J. Eisert, and T. J. Osborne. Exact relaxation in a class of nonequilibrium quantum lattice systems. *Physical Review Letters*, 100:03062, 2008.

[42] E. Cuevas, M. Feigel'Man, L. Ioffe, and M. Mezard. Level statistics of disordered spin-1/2 systems and materials with localized cooper pairs. *Nature communications*, 3:1128, 2012.

[43] H. L. Cycon, R. G. Froese, W. Kirsch, and B. Simon. *Schrödinger operators: With application to quantum mechanics and global geometry*. Springer, 2009.

[44] L. D'Alessio and A. Polkovnikov. Many-body energy localization transition in periodically driven systems. *Annals of Physics*, 333:19, 2013.

[45] C. Dasgupta and S.-k. Ma. Low-temperature properties of the random heisenberg antiferromagnetic chain. *Phys. Rev. B*, 22:1305–1319, 1980.

[46] A. De Luca and A. Scardicchio. Ergodicity breaking in a model showing many-body localization. *Europhys. Lett.*, 101:37003, 2013.

[47] W. De Roeck and F. Huveneers. Stability and instability towards delocalization in MBL systems. *arXiv:1608.01815 [cond-mat.dis-nn]*.

[48] W. De Roeck and F. Huveneers. Scenario for delocalization in translation-invariant systems. *Phys. Rev. B*, 90:165137, 2014.

[49] W. De Roeck, F. Huveneers, M. Müller, and M. Schiulaz. Absence of many-body mobility edges. *Phys. Rev. B*, 93:014203, Jan 2016.

[50] B. Derrida. Directed polymers in a random medium. *Physica A Statistical Mechanics and its Applications*, 163:71–84, Feb. 1990.

[51] B. Derrida and H. Spohn. Polymers on disordered trees, spin glasses, and traveling waves. *Journal of Statistical Physics*, 51(5):817–840, 1988.

[52] J. M. Deutsch. Quantum statistical mechanics in a closed system. *Phys. Rev. A*, 43:2046, Feb 1991.

[53] T. Devakul and R. R. P. Singh. Early breakdown of area-law entanglement at the many-body delocalization transition. *Phys. Rev. Lett.*, 115:187201, Oct 2015.

[54] E. Dijkstra. A note on two problems in connexion with graphs. *Numerische Mathematik*, 1(1):269–271, 1959.

[55] J. Edwards and D. Thouless. Numerical studies of localization in disordered systems. *Journal of Physics C: Solid State Physics*, 5(8):807, 1972.

[56] P. Facchi and S. Pascazio. Quantum zeno subspaces. *Phys. Rev. Lett.*, 89:080401, 2002.

[57] P. Facchi and S. Pascazio. *Unstable systems and quantum Zeno phenomena in quantum field theory*, pages 222–246. WORLD SCIENTIFIC, 2011.

[58] P. Facchi, S. Pascazio, A. Scardicchio, and L. S. Schulman. Zeno dynamics yields ordinary constraints. *Phys. Rev. A*, 65:012108, 2001.

[59] M. V. Feigel'man, L. B. Ioffe, and M. Mézard. Superconductor-insulator transition and energy localization. *Phys. Rev. B*, 82:184534, Nov 2010.

[60] D. S. Fisher. Random transverse field ising spin chains. *Phys. Rev. Lett.*, 69:534–537, Jul 1992.

[61] D. S. Fisher and D. A. Huse. Directed paths in a random potential. *Phys. Rev. B*, 43:10728–10742, May 1991.

[62] M. P. A. Fisher, P. B. Weichman, G. Grinstein, and D. S. Fisher. Boson localization and the superfluid-insulator transition. *Phys. Rev. B*, 40:546–570, Jul 1989.

[63] L. Fleishman and P. W. Anderson. Interactions and the anderson transition. *Phys. Rev. B*, 21:2366–2377, 1980.

[64] M. Friesdorf, A. H. Werner, W. Brown, V. B. Scholz, and J. Eisert. Many-body localization implies that eigenvectors are matrix-product states. *Phys. Rev. Lett.*, 114:170505, May 2015.

[65] J. Fröhlich and T. Spencer. Absence of diffusion in the anderson tight binding model for large disorder or low energy. *Comm. Math. Phys.*, 88(2):151–184, 1983.

[66] A. M. García-García and E. Cuevas. Dimensional dependence of the metal-insulator transition. *Phys. Rev. B*, 75:174203, 2007.

[67] S. D. Geraedts, R. N. Bhatt, and R. Nandkishore. Emergent local integrals of motion without a complete set of localized eigenstates. *arXiv:1608.01328 [cond-mat.stat-mech]*.

[68] T. Giamarchi and H. J. Schulz. Anderson localization and interactions in one-dimensional metals. *Phys. Rev. B*, 37:325–340, Jan 1988.

[69] C. Gogolin and J. Eisert. Equilibration, thermalisation, and the emergence of statistical mechanics in closed quantum systems. *Reports on Progress in Physics*, 79(5):056001, 2016.

[70] J. Goold, C. Gogolin, S. R. Clark, J. Eisert, A. Scardicchio, and A. Silva. Total correlations of the diagonal ensemble herald the many-body localization transition. *Phys. Rev. B*, 92:180202, Nov 2015.

[71] S. Gopalakrishnan, K. Agarwal, E. A. Demler, D. A. Huse, and M. Knap. Griffiths effects and slow dynamics in nearly many-body localized systems. *Phys. Rev. B*, 93:134206, Apr 2016.

[72] I. Gornyi, A. Mirlin, and D. Polyakov. Interacting electrons in disordered wires: Anderson localization and low-T transport. *Phys. Rev. Lett.*, 95:206603, 2005.

[73] I. V. Gornyi, A. D. Mirlin, and D. G. Polyakov. Many-body delocalization transition and relaxation in a quantum dot. *Phys. Rev. B*, 93:125419, 2016.

[74] T. Grover. Certain general constraints on the many-body localization transition. *arXiv:1405.1471 [cond-mat.dis-nn]*.

[75] V. Gurarie, L. Pollet, N. V. Prokof'ev, B. V. Svistunov, and M. Troyer. Phase diagram of the disordered bose-hubbard model. *Phys. Rev. B*, 80:214519, Dec 2009.

[76] D. B. Gutman, I. V. Protopopov, A. L. Burin, I. V. Gornyi, R. A. Santos, and A. D. Mirlin. Energy transport in the anderson insulator. *Phys. Rev. B*, 93:245427, 2016.

[77] T. Halpin-Healy and Y.-C. Zhang. Kinetic roughening phenomena, stochastic growth, directed polymers and all that. aspects of multidisciplinary statistical mechanics. *Physics reports*, 254(4):215–414, 1995.

[78] D. A. Huse, C. L. Henley, and D. S. Fisher. Huse, henley, and fisher respond. *Phys. Rev. Lett.*, 55:2924–2924, Dec 1985.

[79] D. A. Huse, R. Nandkishore, and V. Oganesyan. Phenomenology of certain many-body-localized systems. *Physical Review B*, 90(17):174202, 2014.

[80] D. A. Huse, R. Nandkishore, and V. Oganesyan. Phenomenology of fully many-body-localized systems. *Phys. Rev. B*, 90:174202, Nov 2014.

[81] D. A. Huse, R. Nandkishore, V. Oganesyan, A. Pal, and S. Sondhi. Localization-protected quantum order. *Phys. Rev. B*, 88:014206, 2013.

[82] F. Iemini, A. Russomanno, D. Rossini, A. Scardicchio, and R. Fazio. Signatures of many-body localisation in the dynamics of two-sites entanglement. *arXiv:1608.08901 [quant-ph]*.

[83] F. Iglói and C. Monthus. Strong disorder rg approach of random systems. *Physics Reports*, 412(5–6):277 – 431, 2005.

[84] E. Ilievski, M. Medenjak, T. Prosen, and L. Zadnik. Quasilocal charges in integrable lattice systems. *Journal of Statistical Mechanics: Theory and Experiment*, 2016(6):064008.

[85] J. Z. Imbrie. Multi-scale jacobi method for anderson localization. *Communications in Mathematical Physics*, 341(2):491–521, 2016.

[86] J. Z. Imbrie. On many-body localization for quantum spin chains. *Journal of Statistical Physics*, 163(5):998–1048, 2016.

[87] Y. Imry. *Introduction to Mesoscopic Physics*. Oxford University, London, 1996.

[88] S. Inglis and L. Pollet. Accessing many-body localized states through the Generalized Gibbs Ensemble. *arXiv: 1604.07056 [cond-mat.dis-nn]*.

[89] L. B. Ioffe and M. Mézard. Disorder-driven quantum phase transitions in superconductors and magnets. *Phys. Rev. Lett.*, 105:037001, 2010.

[90] R. V. Jensen and R. Shankar. Statistical behavior in deterministic quantum systems with few degrees of freedom. *Phys. Rev. Lett.*, 54:1879–1882, Apr 1985.

[91] K. Johansson. Shape fluctuations and random matrices. *Communications in Mathematical Physics*, 209(2):437–476, 2000.

[92] S. Johri, R. Nandkishore, and R. N. Bhatt. Many-body localization in imperfectly isolated quantum systems. *Phys. Rev. Lett.*, 114:117401, 2015.

[93] P. Jordan and E. Wigner. Über das paulische äquivalenzverbot. *E. Z. Phys.*, 47:631, 1928.

[94] V. Kerala Varma, A. Lerose, F. Pietracaprina, J. Goold, and A. Scardicchio. Energy diffusion in the ergodic phase of a many body localizable spin chain. *ArXiv:1511.09144[cond-mat.dis-nn]*.

[95] L. A. Khalfin. Phenomenological Theory of K^0 Mesons and the Non-exponential Character of the Decay. *Soviet Journal of Experimental and Theoretical Physics Letters*, 8:65, July 1968.

[96] V. Khemani, S. P. Lim, D. N. Sheng, and D. A. Huse. Critical Properties of the Many-Body Localization Transition. *arXiv:1607.05756 [cond-mat.dis-nn]*.

[97] V. Khemani, F. Pollmann, and S. L. Sondhi. Obtaining highly-excited eigenstates of many-body localized Hamiltonians by the density matrix renormalization group. *arXiv:1509.00483 [cond-mat.dis-nn]*.

[98] H. Kim and D. A. Huse. Ballistic spreading of entanglement in a diffusive nonintegrable system. *Phys. Rev. Lett.*, 111:127205, 2013.

[99] I. H. Kim, A. Chandran, and D. A. Abanin. Local integrals of motion and the logarithmic lightcone in many-body localized systems. *arXiv:1412.3073 [cond-mat.dis-n]*.

[100] W. Kirsch. An Invitation to Random Schroedinger operators. *arXiv: 0709.3707 [math-ph]*.

[101] J. A. Kjäll, J. H. Bardarson, and F. Pollmann. Many-body localization in a disordered quantum ising chain. *Phys. Rev. Lett.*, 113:107204, Sep 2014.

[102] B. Kramer and A. MacKinnon. Localization: theory and experiment. *Reports on Progress in Physics*, 56(12):1469, 1993.

[103] Y. B. Lev and D. R. Reichman. Dynamics of many-body localization. *Physical Review B*, 89(22):220201, 2014.

[104] E. H. Lieb and D. W. Robinson. The finite group velocity of quantum spin systems. In *Statistical Mechanics*, pages 425–431. Springer, 1972.

[105] S. P. Lim and D. N. Sheng. Many-body localization and transition by density matrix renormalization group and exact diagonalization studies. *Phys. Rev. B*, 94:045111, 2016.

[106] D. J. Luitz. Long tail distributions near the many-body localization transition. *Phys. Rev. B*, 93:134201, 2016.

[107] D. J. Luitz and Y. Bar Lev. Anomalous thermalization in ergodic systems. *arXiv:1607.01012 [cond-mat.stat-mech]*.

[108] D. J. Luitz, N. Laflorencie, and F. Alet. Many-body localization edge in the random-field heisenberg chain. *Phys. Rev. B*, 91:081103, Feb 2015.

[109] D. J. Luitz, N. Laflorencie, and F. Alet. Extended slow dynamical regime close to the many-body localization transition. *Phys. Rev. B*, 93:060201, Feb 2016.

[110] M. Lüscher. Dynamical charges in the quantized renormalized massive Thirring model. *Nuclear Physics B*, 117:475–492, Dec. 1976.

[111] M. Ma and P. A. Lee. Localized superconductors. *Phys. Rev. B*, 32:5658–5667, Nov 1985.

[112] P. Mazur. Non-ergodicity of phase functions in certain systems. *Physica*, 43(4):533 – 545, 1969.

[113] E. Medina and M. Kardar. Quantum interference effects for strongly localized electrons. *Physical Review B*, 46(16):9984, 1992.

[114] E. Medina, M. Kardar, Y. Shapir, and X. R. Wang. Interference of directed paths in disordered systems. *Phys. Rev. Lett.*, 62:941–944, 1989.

[115] M. Mehta. *Random Matrices,* 3^{rd}. Elsevier Inc., Amsterdam, 2004.

[116] N. Minami. Local fluctuation of the spectrum of a multidimensional anderson tight binding model. *Communications in mathematical physics*, 177(3):709–725, 1996.

[117] A. D. Mirlin. Statistics of energy levels and eigenfunctions in disordered systems. *Physics Reports*, 326(5):259–382, 2000.

[118] B. Misra and E. C. G. Sudarshan. The zeno's paradox in quantum theory. *Journal of Mathematical Physics*, 18(4):756–763, 1977.

[119] L. Molinari. Exact generalized Lyapounov exponents for one-dimensional disordered tight binding models. *Journal of Physics A: Mathematical and General*, 25:513, 1992.

[120] C. Monthus. Flow towards diagonalization for Many-Body-Localization models : adaptation of the Toda matrix differential flow to random quantum spin chains. *Journal of Physics A: Mathematical and Theoretical*, 49(30):305002.

[121] C. Monthus. Many-Body Localization : construction of the emergent local conserved operators via block real-space renormalization. *arXiv:1509.06258 [cond-mat.dis-nnl]*.

[122] C. Monthus and T. Garel. Statistics of low energy excitations for the directed polymer in a $1 + d$ random medium $(d = 1, 2, 3)$. *Phys. Rev. E*, 73:056106, 2006.

[123] C. Monthus and T. Garel. Random transverse field ising model in dimension $d > 1$: scaling analysis in the disordered phase from the directed polymer model. *Journal of Physics A: Mathematical and Theoretical*, 45(9):095002, 2012.

[124] M. Müller. Magnetoresistance and localization in bosonic insulators. *EPL (Europhysics Letters)*, 102(6):67008, 2013.

[125] G. Mussardo. *Statistical field theory: an introduction to exactly solved models in statistical physics*. Oxford University Press, 2010.

[126] R. Nandkishore. Many-body localization proximity effect. *Phys. Rev. B*, 92:245141, 2015.

[127] R. Nandkishore, S. Gopalakrishnan, and D. A. Huse. Spectral features of a many-body-localized system weakly coupled to a bath. *Phys. Rev. B*, 90:064203, Aug 2014.

[128] A. Nanduri, H. Kim, and D. A. Huse. Entanglement spreading in a many-body localized system. *Phys. Rev. B*, 90:064201, 2014.

[129] V. Nguyen, B. Spivak, and B. Shklovskii. Tunnel hopping in disordered systems. *Sov. Phys.—JETP*, 62:1021, 1985.

[130] V. Nguyen, B. Spivak, and B. Shklovskii. Hopping-conductivity fluctuations in small samples. *JETP Lett*, 43(1), 1986. [Pis'ma Zh. Eksp. Teor. Fiz. **43**, 35 (1986)].

[131] T. E. O'Brien, D. A. Abanin, G. Vidal, and Z. Papić. Explicit construction of local conserved operators in disordered many-body systems. *arXiv:1608.0329 [cond-mat.str-el]*.

[132] V. Oganesyan and D. A. Huse. Localization of interacting fermions at high temperature. *Phys. Rev. B*, 75:155111, 2007.

[133] Z. Ovadyahu. Suppression of inelastic electron-electron scattering in anderson insulators. *Phys. Rev. Lett.*, 108:156602, Apr 2012.

[134] A. Pal and D. A. Huse. Many-body localization phase transition. *Phys. Rev. B*, 82:174411, Nov 2010.

[135] D. Pekker, B. K. Clark, V. Oganesyan, and G. Refael. Fixed points of Wegner-Wilson flows and many-body localization. *arXiv:1607.07884 [cond-mat.dis-n]*.

[136] D. Pekker, G. Refael, E. Altman, E. Demler, and V. Oganesyan. Hilbert-glass transition: New universality of temperature-tuned many-body dynamical quantum criticality. *Phys. Rev. X*, 4:011052, 2014.

[137] D. Poilblanc, T. Ziman, J. Bellissard, F. Mila, and G. Montambaux. Poisson vs. goe statistics in integrable and non-integrable quantum hamiltonians. *EPL (Europhysics Letters)*, 22(7):537, 1993.

[138] P. Ponte, A. Chandran, Z. Papić, and D. A. Abanin. Periodically driven ergodic and many-body localized quantum systems. *Annals of Physics*, 353:196 – 204, 2015.

[139] P. Ponte, Z. Papić, F. Huveneers, and D. A. Abanin. Many-body localization in periodically driven systems. *Phys. Rev. Lett.*, 114:140401, 2015.

[140] A. C. Potter, R. Vasseur, and S. A. Parameswaran. Universal properties of many-body delocalization transitions. *Phys. Rev. X*, 5:031033, Sep 2015.

[141] M. Prähofer and H. Spohn. Universal distributions for growth processes in $1+1$ dimensions and random matrices. *Phys. Rev. Lett.*, 84:4882–4885, May 2000.

[142] M. Prähofer and H. Spohn. Scale invariance of the png droplet and the airy process. *Journal of statistical physics*, 108(5-6):1071–1106, 2002.

[143] M. Prähofer and H. Spohn. Exact scaling functions for one-dimensional stationary kpz growth. *Journal of statistical physics*, 115(1-2):255–279, 2004.

[144] J. Prior, A. M. Somoza, and M. Ortuño. Conductance distribution in two-dimensional localized systems with and without magnetic fields. *The European Physical Journal B*, 70(4):513–521, 2009.

[145] V. L. Quito, P. Titum, D. Pekker, and G. Refael. Anderson transition in one dimension using Wegner Flow Equations. *arXiv:1606.03094 [cond-mat.dis-nn]*.

[146] L. Rademaker and M. Ortuño. Explicit local integrals of motion for the many-body localized state. *Phys. Rev. Lett.*, 116:010404, 2016.

[147] Rigol Marcos, Dunjko Vanja, and Olshanii Maxim. Thermalization and its mechanism for generic isolated quantum systems. *Nature*, 452(7189):854, apr 2008.

[148] G. Roati, C. D'Errico, L. Fallani, M. Fattori, C. Fort, M. Zaccanti, G. Modugno, M. Modugno, and M. Inguscio. Anderson localization of a non-interacting bose–einstein condensate. *Nature*, 453(7197):895–898, 2008.

[149] V. Ros, M. Müller, and A. Scardicchio. Integrals of motion in the many-body localized phase. *Nuclear Physics B*, 891:420 – 465, 2015. [Corrigendum. *Nuclear Physics B*, 900:446 - 448, 2015].

[150] M. A. Schmidt, D. M. Silevitch, G. Aeppli, and T. F. Rosenbaum. Using thermal boundary conditions to engineer the quantum state of a bulk magnet. *Proceedings of the National Academy of Sciences*, 111(10):3689–3694, 2014.

[151] M. Schreiber, S. S. Hodgman, P. Bordia, H. P. Lüschen, M. H. Fischer, R. Vosk, E. Altman, U. Schneider, and I. Bloch. Observation of many-body localization of interacting fermions in a quasi-random optical lattice. *Science*, 349(6250):842–845, 2015.

[152] M. Serbyn, M. Knap, S. Gopalakrishnan, Z. Papić, N. Y. Yao, C. R. Laumann, D. A. Abanin, M. D. Lukin, and E. A. Demler. Interferometric probes of many-body localization. *Phys. Rev. Lett.*, 113:147204, Oct 2014.

[153] M. Serbyn, Z. Papić, and D. A. Abanin. Local conservation laws and the structure of the many-body localized states. *Physical review letters*, 111:127201, 2013.

[154] M. Serbyn, Z. Papić, and D. A. Abanin. Universal Slow Growth of Entanglement in Interacting Strongly Disordered Systems. *Phys. Rev. Lett.*, 110:260601, June 2013.

[155] M. Serbyn, Z. Papić, and D. A. Abanin. Quantum quenches in the many-body localized phase. *Phys. Rev. B*, 90:174302, 2014.

[156] M. Serbyn, Z. Papić, and D. A. Abanin. Criterion for many-body localization-delocalization phase transition. *Phys. Rev. X*, 5:041047, Dec 2015.

[157] K. Slevin and T. Ohtsuki. Critical exponent for the anderson transition in the three-dimensional orthogonal universality class. *New Journal of Physics*, 16(1):015012, 2014.

[158] J. Smith, A. Lee, P. Richerme, B. Neyenhuis, P. W. Hess, P. Hauke, M. Heyl, D. A. Huse, and C. Monroe. Many-body localization in a quantum simulator with programmable random disorder. *arXiv:1508.07026 [quant-ph]*.

[159] A. M. Somoza, P. Le Doussal, and M. Ortuño. Unbinding transition in semi-infinite two-dimensional localized systems. *Phys. Rev. B*, 91:155413, 2015.

[160] A. M. Somoza, M. Ortuño, and J. Prior. Universal distribution functions in two-dimensional localized systems. *Phys. Rev. Lett.*, 99:116602, Sep 2007.

[161] M. Srednicki. Chaos and quantum thermalization. *Phys. Rev. E*, 50:888, 1994.

[162] M. Srednicki. Thermal fluctuations in quantized chaotic systems. *Journal of Physics A: Mathematical and General*, 29(4):L75, 1996.

[163] H.-J. Stöckmann. *Quantum chaos: an introduction*. Cambridge university press, 2006.

[164] B. Sutherland. *Beautiful Models: 70 Years Of Exactly Solved Quantum Many-Body Problems*. Singapore: World Scientific, 2004.

[165] M. Suzuki. Ergodicity, constants of motion, and bounds for susceptibilities. *Physica*, 51(2):277 – 291, 1971.

[166] B. Swingle. A simple model of many-body localization. *arXiv:1307.0507 [cond-mat.dis-nn]*.

[167] M. Thomsen, M. F. Thorpe, T. C. Choy, D. Sherrington, and H.-J. Sommers. Local magnetic field distributions. iii. disordered systems. *Phys. Rev. B*, 33:1931–1947, Feb 1986.

[168] D. Thouless. Electrons in disordered systems and the theory of localization. *Physics Reports*, 13:93, 1974.

[169] Y. Ueoka and K. Slevin. Dimensional dependence of critical exponent of the anderson transition in the orthogonal universality class. *Journal of the Physical Society of Japan*, 83(8):084711, 2014.

[170] R. Vasseur, S. A. Parameswaran, and J. E. Moore. Quantum revivals and many-body localization. *Phys. Rev. B*, 91:140202, Apr 2015.

[171] L. Vidmar and M. Rigol. Generalized gibbs ensemble in integrable lattice models. *Journal of Statistical Mechanics: Theory and Experiment*, 2016(6):064007, 2016.

[172] R. Vosk and E. Altman. Many-body localization in one dimension as a dynamical renormalization group fixed point. *Phys. Rev. Lett.*, 110:067204, 2013.

[173] R. Vosk and E. Altman. Dynamical quantum phase transitions in random spin chains. *Phys. Rev. Lett.*, 112:217204, 2014.

[174] R. Vosk, D. A. Huse, and E. Altman. Theory of the many-body localization transition in one-dimensional systems. *Phys. Rev. X*, 5:031032, Sep 2015.

[175] Y.-L. Wu and S. Das Sarma. Understanding analog quantum simulation dynamics in coupled ion-trap qubits. *Phys. Rev. A*, 93:022332, Feb 2016.

[176] X. Yu and M. Müller. Localization of disordered bosons and magnets in random fields. *Annals of Physics*, 337:55 – 93, 2013.

[177] X. Yu, D. Pekker, and B. K. Clark. Finding matrix product state representations of highly-excited eigenstates of many-body localized Hamiltonians. *arXiv:1509.01244 [cond-mat.str-el]*, 2015.

[178] M. Žnidarič, T. Prosen, and P. Prelovšek. Many-body localization in the Heisenberg XXZ magnet in a random field. *Phys. Rev. B*, 77:064426, 2008.

[179] M. Žnidarič, A. Scardicchio, and V. K. Varma. Diffusive and subdiffusive spin transport in the ergodic phase of a many-body localizable system. *Phys. Rev. Lett.*, 117:040601, 2016.

[180] X. Zotos. Finite temperature drude weight of the one-dimensional spin- $1/2$ heisenberg model. *Phys. Rev. Lett.*, 82:1764–1767, 1999.

[181] X. Zotos, F. Naef, and P. Prelovsek. Transport and conservation laws. *Phys. Rev. B*, 55:11029–11032, May 1997.